REVIEW AND OPTIMISATION OF PUMP SUCTION REDUCER SELECTION

RM MAHAFFEY

REVIEW AND OPTIMISATION OF PUMP SUCTION REDUCER SELECTION

ROSS MICHAEL MAHAFFEY

A dissertation submitted in partial fulfilment of the requirements for the degree of

MASTER OF ENGINEERING (WATER RESOURCES ENGINEERING)

In the

FACULTY OF ENGINEERING

UNIVERSITY OF PRETORIA

September 2014

DISSERTATION SUMMARY
REVIEW AND OPTIMISATION OF PUMP SUCTION REDUCER SELECTION

RM MAHAFFEY

Supervisor: Professor SJ van Vuuren
Department: Civil Engineering
University: University of Pretoria
Degree: Master of Engineering (Water Resource Engineering)

The approach flow to a pump must be undisturbed and free from unequal velocity distributions, unequal pressure distributions, entrained air or gas bubbles, vortices and excessive pre-swirl. A reducer fitting is typically used in pump station pipe work to reduce the size of the suction pipe to match the size of the pump suction end flange. Two types of reducer fittings are commonly manufactured, namely: Eccentric Reducers and Concentric Reducers. Inlet pipework design guidelines traditionally prescribe the use of eccentric reducers, with the flat side on top. This prescription is to allow the transport of air through the fitting. The flow through an eccentric reducer accelerates along the sloped side as the flow path narrows from below, thereby causing higher velocities towards this sloped side. These flow conditions are contradictory to the recommended pump inlet approach flow conditions and pump station failures have been recorded resulting from the incorrect application of eccentric reducers.

Relationships exist to assess the hydraulic transportation of air through a pipe and these relationships can be applied to calculate the ability to transport air through a concentric reducer. It is therefore **hypothesised that a correctly designed concentric reducer will not only provide a more uniform pressure/velocity distribution in comparison to an eccentric reducer, but will allow any free air to be hydraulically transported through the reducer to the pump.**

Computational Fluid Dynamics (CFD) was utilised to assess the resulting velocity distributions through various concentric and eccentric reducer geometries at various flow rates. Six concentric reducers and six eccentric reducers were simulated with four inlet velocities. The resulting velocity

distributions were recorded with scalar scenes and velocity probes at four positions spaced at a distance of 1 x the downstream diameter starting at the downstream end of the reducer.

These velocity distributions were then compared to the pump inlet requirements typically used in the industry. These requirements require the velocity variation along a line drawn through the centre of the pipe to be less than 10% of the average velocity along that line and the velocity variation along a circle within the pipe is less than 5% of the average velocity along the circle.

It was found that the eccentric reducers with angles of 15°, 20° and 30° and the concentric reducer with an angle of 20° do not pass the requirements used in the assessment at all four velocities. From these results it was highlighted that some of the standard eccentric reducer geometries (including those specified by AWWA C208) do not pass the inlet requirements. It was then assessed if air can be hydraulically transported through the concentric reducers utilising available hydraulic air transport theory. Air can be hydraulically transported through all of the concentric reducers except for the 20° reducer (the same size that failed the velocity distribution assessment) at 1m/s for the assessed diameters.

It was therefore shown that **a correctly designed concentric reducer (angle less or equal to 15°) will not only provide a more uniform pressure/velocity distribution in comparison to an eccentric reducer, but will allow air to be hydraulically transported through the reducer to the pump.**

SAMEVATTING VAN VERHANDELING

ONDERSOEK EN OPTIMALISERING VAN POMP SUIGKANT VERLOOPSTUK SELEKSIE

RM MAHAFFEY

Promotor: Professor SJ van Vuuren
Department: Siviele Ingenieurswese
University: Universiteit van Pretoria
Degree: Magister in Ingenieurswese (Water Hulpbron Ingenieurswese)

Die inkomende vloei na n pomp moet aaneenlopend wees en vry wees van enige oneweredige snelheids verspeidings, oneweredige druk verspreidings, vasgevangde lug of gas borrels, draaikolke en oormatige “pre-swirl”. ‘n Verloopstuk word tipies gebruik in pompstasie pypwerk om die grootte van die suigpyp aan te pas by die pomp suigkant flens. Twee soorte verloopstukke word hoofsaaklik gebruik, naamlik eksentriese en konsentriese verloopstukke. Inlaat pypwerk ontwerp riglyne skryf die gebruik van eksentriese verloopstukke met die horisontale kant na bo voor. Eksentriese verloopstukke word voorgeskryf om die vervoer van lug deur die verloopstuk toe te laat. Die vloei deur n eksentriese verloopstuk versnel langs die skuins kant soos die vloei roete vernou van onder af, en sodoende word hoë snelhede langs die skuins kant gevorm. Hierdie vloei omstandighede is teenstrydig met die aanbeveelde pomp inlaat vloei omstandighede en pompstasie falings is al aangeteken wat toegeskryf kan word aan die verkeerde toepassing van eksentriese verloopstukke.

Verwantskappe om die hidrouliese vervoer van lug deur n pyp te evalueer bestaan en die verwantskappe kan toegepas word om die vermoë om lug deur ń konsentriese verloopstuk te vervoer te bereken. **Die hipotese is dat ‘n konsentriese verloopstuk wat reg ontwerp is, nie net ‘n meer uniforme druk/snelheid verspreiding sal voorsien in vergelyking met ‘n eksentriese verloopstuk nie, maar ook hidrouliese vervoer van lug deur die verloopstuk sal toelaat.**

Berekende vloei dinamika is gebruik om die snelheid verspreidings deur verskeie konsentriese en eksentriese verloopstukke vir verskeie vloei tempos te bereken. Ses konsentriese verloopstukke en ses eksentriese verloopstukke is gesimuleer met vier inlaat vloei snelhede. Die snelheid verspreidings is opgeneem met skalaar tonele en snelheid peilstewe by vier posisies, met ‘n spasiëring van 1 maal die deursnee van die pyp.

Hierdie vloei verspreidings is gevolglik vergelyk met pomp inlaat vereistes wat hoofsaklik in die industrie gebruik word. Die vereistes vereis dat die snelheidsvariasie op ń lyn wat deur die middel van die pyp, minder as 10% mag wees van die gemiddelde snelheid op die lyn en dat die snelheidsvariasie op ń sirkel binne die pyp is minder as 5% mag wees van die gemiddelde snelheid op die sirkel.

Dit was bevind dat eksentriese verloopstukke met hellings van 15°, 20° en 30° en konsentriese verloopstuk met n helling van 20° nie aan die vereistes voldoen vir enige van die vier snelhede wat ondersoek is nie. Die resultate het ook aangedui dat van die standaard eksentriese verloopstukke (soos verloopstukke voorgeskryf deur AWWA C208) nie voldoen aan die inlaat vereistes nie. Lug kan hidroulies deur al die konsentriese verloopstukke, behalwe die 20° verloopstuk, vervoer word teen 1 m/s.

Dit is **gevolglik bewys dat ‘n konsentriese verloopstuk wat reg ontwerp is (helling van 15° of minder) ‘n meer uniforme druk/snelheid verspreiding tot gevolg het as ‘n eksentriese verloopstuk en dat lug hidroulies deur die verloopstuk vervoer sal word na die pomp.**

ABSTRACT

Title: Review and optimisation of pump suction reducer selection
Author: RM Mahaffey
Supervisor: Professor SJ van Vuuren
Department: Civil Engineering
University: University of Pretoria
Degree: Master of Engineering (Water Resource Engineering)

Eccentric reducers are traditionally recommended for the pump suction reducer fitting to allow transportation of air through the fitting to the pump. It was hypothesised that a concentric reducer will provide better approach flow to the pump and allow air to be transported through the fitting. CFD was utilised to analyse six concentric and six eccentric reducer geometries at four different inlet velocities to determine the flow velocity distribution on the downstream end. It was found that eccentric reducers with angles of 15°, 20° and 30° and concentric reducer with an angle of 20° did not pass the assessment. Air could be hydraulically transported through all of the concentric reducers modelled except for the 20° reducer at 1m/s. It was found that a correctly designed concentric reducer will therefore not only provide a more uniform velocity distribution in comparison to an eccentric reducer, but will also still allow for the hydraulic transportation of air through the reducer.

DECLARATION

I, the undersigned hereby declare that:

- I understand what plagiarism is and I am aware of the University's policy in this regard;
- The work contained in this thesis is my own original work;
- I did not refer to work of current or previous students, lecture notes, handbooks or any other study material without proper referencing;
- Where other people's work has been used this has been properly acknowledged and referenced;
- I have not allowed anyone to copy any part of my thesis;
- I have not previously in its entirety or in part submitted this thesis at any university for a degree.

DISCLAIMER:

The work presented in this report is that of the student alone. Students were encouraged to take ownership of their projects and to develop and execute their experiments with limited guidance and assistance. The content of the research does not necessarily represent the views of the supervisor or any staff member of the University of Pretoria, Department of Civil Engineering. The supervisor did not read or edit the final report and is not responsible for any technical inaccuracies, statements or errors. The conclusions and recommendations given in the report are also not necessarily that of the supervisor, sponsors or companies involved in the research.

Signature of student:

Name of student: Ross Michael Mahaffey

Student number: 24202909

Date: 4 September 2014

Number of words in report: 27 162

ACKNOWLEDGEMENT

I wish to express my appreciation to the following organisations and persons who made this dissertation possible:

a) My ever supportive wife for all the patience and subtle occasional pressure.

b) Aurecon who supported this study financially and allowed for the use of their STAR-CCM+ CFD software.

c) Mr J Olivier and Mr J Mulder, true engineers, for guidance around STAR-CCM+.

d) Professor SJ van Vuuren for his technical direction.

e) My parents who taught me to aim high.

f) The Father, Son and Holy Spirit, through Grace by Faith.

TABLE OF CONTENTS

LIST OF TABLES

LIST OF FIGURES

LIST OF EQUATIONS

LIST OF SYMBOLS

ER	-	Eccentric Reducer
CR	-	Concentric Reducer
L_r	-	Reducer Length (mm)
DN	-	Nominal Bore of a Pipe (mm)
OD or D	-	Outside Diameter of a Pipe (mm)
ID	-	Inside Diameter of a Pipe (mm)
D_L or D1	-	Outside Diameter of the large end of a reducer (mm)
D_s or D2	-	Outside Diameter of the small end of a reducer (mm)
t	-	Pipe Wall Thickness (mm)
Q_c	-	Critical Flow Rate for the Hydraulic Transport of Air (m^3/s)
V_c	-	Critical Velocity for the Hydraulic Transport of Air (m/s)
g	-	Gravitational Acceleration (9.81 m^2/s)
Θ	-	Slope of a Pipeline (°) or Reducer Angle (°)

1. BACKGROUND

1.1. INTRODUCTION

There are two options available to reduce the suction pipe diameter to match the pump inlet diameter in pumping systems. The first option is the commonly recommended option where an eccentric reducer is used with its flat side positioned on top to allow for a horizontal upper surface that enables air pockets or bubbles to be freely transported through the reducer. The second option is the application of a concentric reducer. A concentric reducer is not recommended in the industry due to its apparent inability to transfer air pockets or bubbles in the manner that the eccentric reducer does.

The eccentric reducer is however asymmetrical about the horizontal axis and will result in an asymmetrical velocity distribution at its downstream end. An asymmetrical load on a pump impeller will result on radial thrust harmonics that may be detrimental to the pump. A concentric reducer is concentric about both its vertical and horizontal axes and will therefore have a symmetric velocity distribution exiting the reducer if there is a symmetrical velocity distribution entering the reducer.

Air can be transported through sloped pipelines and the capacity of air to be transported through a sloped pipeline is a function of the flow characteristics, pipeline slope and the amount of accumulated air (Pothof and Clemens 2011; Van Vuuren, Van Dijk and Steenkamp 2004). The same principles can be applied to the hydraulic transportation of air through a concentric reducer where the angle of the reducer is representative of the pipeline slope. If the air can be hydraulically transported past a concentric reducer and the velocity distribution exiting a concentric reducer is more uniform in comparison to that exiting an eccentric reducer, is the concentric reducer not superior in comparison to the eccentric reducer?

The hypothesis of this study is that a correctly designed concentric reducer will not only provide a more uniform pressure/velocity distribution in comparison to an eccentric reducer, but will allow air to be hydraulically transported through the reducer to the pump.

1.2. LOCAL AND GLOBAL APPLICATION OF PUMPS

The difference in geographic location and height above sea level of available water resources, as well as varying water demand produces the need for water to be pumped over varying distances and heads. According to Bloch and Budris (2010) pumps are used in every industry conceived by man and are installed in every country worldwide with an estimated 10, 000, 000, 000 pumps in use.

South Africa is largely a semi-arid country and according to Basson, Van Niekerk and Van Rooyen (1997) the availability of water can be a limiting factor on economic growth and social development as South Africa's water resources are, in global terms, scarce and extremely limited in magnitude. Interbasin transfers of water in South Africa are therefore present to decrease the difference in geographic location and height above sea level of available water resources and water demand. These transfer schemes often require pump stations.

An increase in water demand is directly related to population growth, industrialisation and urbanisation and is influenced by an increase in standards of living and economic growth (DWA 1986; Basson, et al 1997). An increase in population growth and standard of living will require an increase in water pumping stations as municipalities rely on elevated storage and distribution networks. According to the Hydraulic Institute (2001) pumping systems account for nearly 20% of the world's energy usage, thereby illustrating the widespread use of pumps in municipal/waste water services, commercial services and the agricultural, chemical, petrochemical and mechanical industries.

There is hence a large local and global application of pumps and pump stations and the continuous operation of these pump stations has an impact on the economy, standard of living and social and economic development, both locally and globally.

1.3. PUMP INLET DESIGN

According to Jones et al (eds. 2008) pump station designers often overlook the importance of the pump inlet conditions and these conditions are likely to be the single reason most often responsible for the success or the failure of a pump station. Jones et al (eds. 2008) also recommends that regardless of the type of intake (pressurized, sump or forebay) attention should be paid during the pump intake design to avoid poor hydraulic conditions at the pump inlet/impeller.

Piping and other components forming a pump inlet design typically include: bends, spool pipes, branches, valves and a transition fitting (reducer) that reduces the pipe diameter to match the diameter of the suction entry of the pump. This pipework together with the components is illustrated in **Figure 1.1.**

The approach flow to a pump must be undisturbed as flow disturbances in the form of unequal velocity distribution, unequal pressure distribution, entrained air or gas bubbles, vortices and excessive pre-swirl at the pump inlet are detrimental to pump performance, cavitation and smooth pump running (ANSI/HI 2000; Sulzer 2010; Jones et al eds. 2008). The ideal pump inlet piping design is a straight length of pipe leading directly into the pump with no turns or flow-disturbing fittings in near proximity to the pump. Failure of the inlet piping to deliver the liquid to the pump with a uniform velocity distribution can lead to noisy operation, random axial load oscillations, premature bearing or seal failure, cavitation damage to the impeller and inlet portions of the casing and occasional damage on the discharge side due to liquid separation (ANSI/HI 2009).

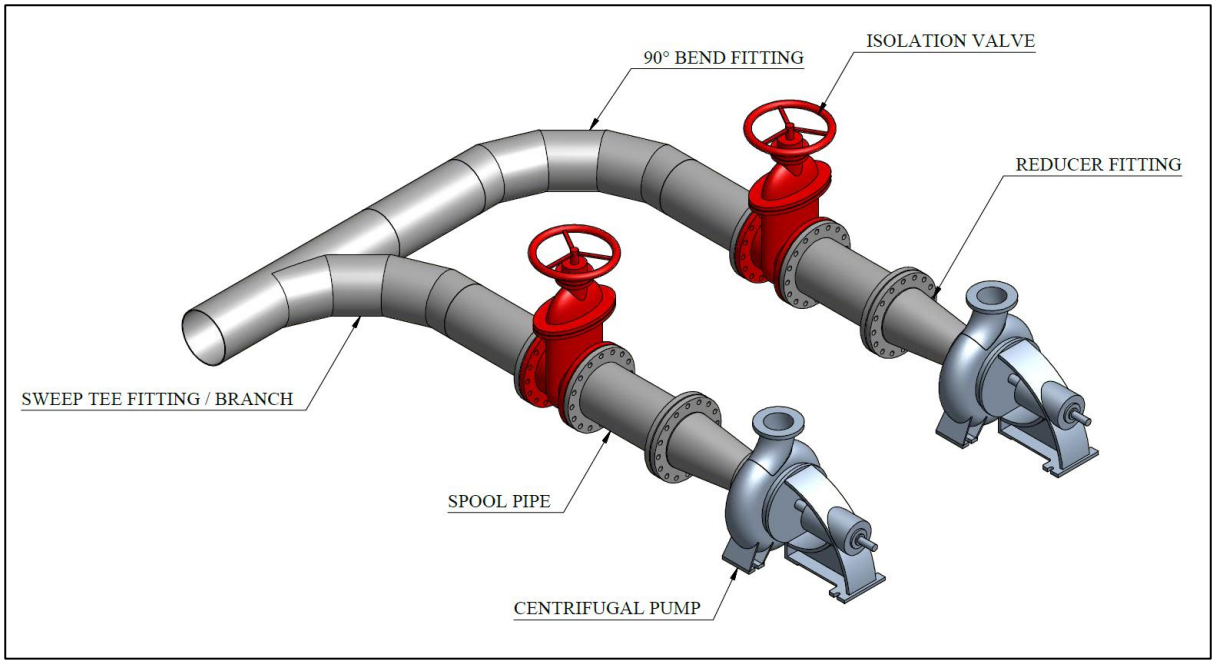

Figure 1.1: Typical pump inlet design components for parallel centrifugal pumps

Pump stations are designed to provide the following main outcomes: 1) house numerous pumps, 2) minimize construction cost by optimizing the pump station size and 3) provide desired pump inlet and discharge conditions. These design outcomes limit the pump inlet piping design not to consist of the ideal inlet piping design of a straight length of pipe leading directly to the pump. Design guidelines and design standards have been compiled to assist the designer with the inlet piping design.

A review of these design guidelines and design standards with the intention to ensure pump inlet piping designs that consistently produce ideal flow conditions at the pump inlet is presented as the central *objective* of this study.

1.4. PUMP INLET PIPING: SELECTION OF REDUCER TYPE

Two types of reducer fittings are commonly manufactured to allow for the transition from one pipe size (diameter) to another pipe size (diameter). These two reducers are:

a) **Eccentric Reducer.** The reduction of the pipe size is achieved by decreasing the diameter of the fitting at a constant rate over a specified length, maintaining one side of the fitting horizontal.
b) **Concentric Reducer.** The reduction of the pipe size is achieved by decreasing the diameter of the fitting at a constant rate over a specified length, maintaining symmetry around the center line of the fitting.

The two types of reducers are clarified in **Figure 1.2**.

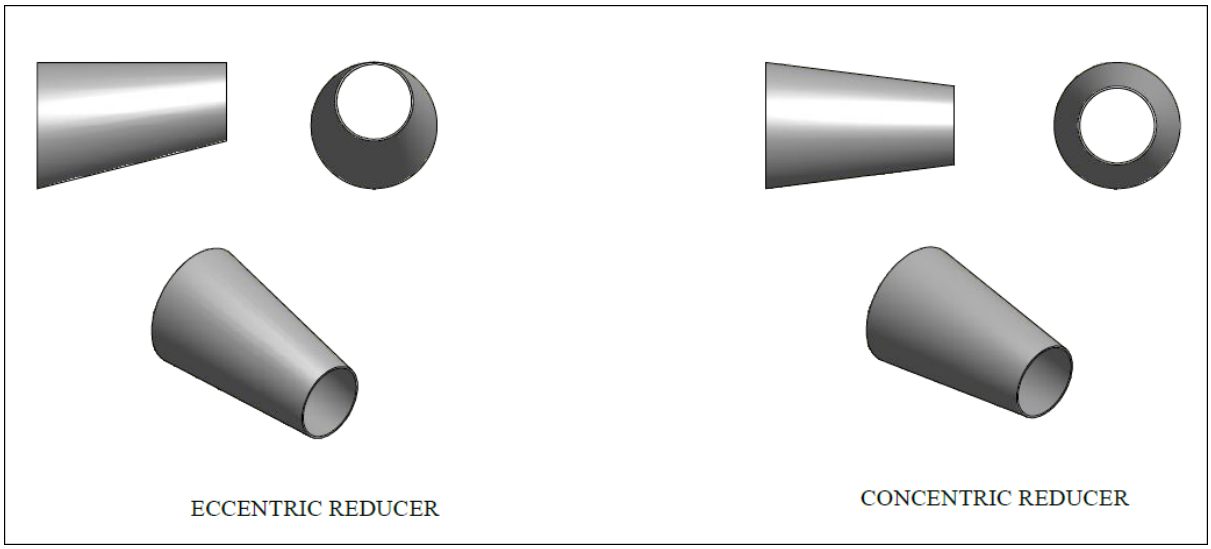

Figure 1.2: Clarification of the two types of reducers

Design guidelines such as those provided by Jones et al (eds. 2008) and installation guidelines such as those provided by KSB (2012) prescribe the use of an eccentric reducer in the pump inlet piping design. The eccentric reducer is prescribed such that air is not trapped within the pump inlet piping. This phenomenon is illustrated in **Figure 1.3**

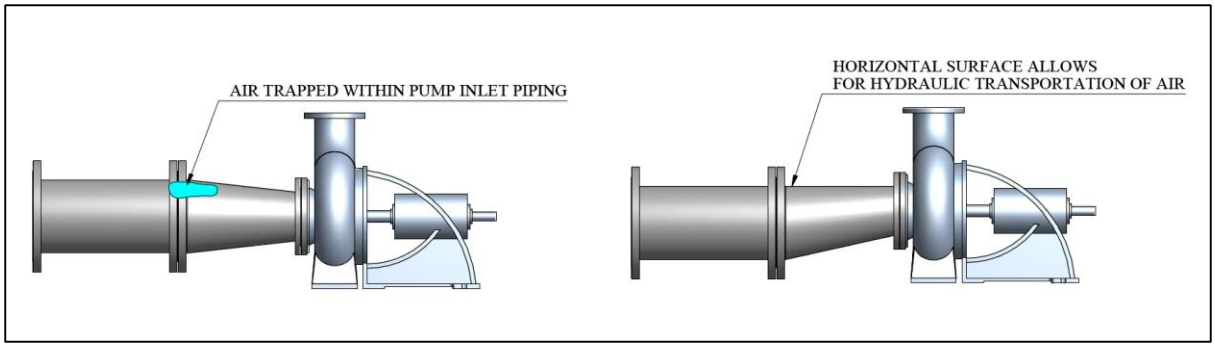

Figure 1.3: Design guidelines requiring an eccentric reducer

The design standards prescribed in ANSI/HI 9.6.6 (ANSI 2009) recommend a concentric reducer to be used for vertical inlet piping design and for horizontal inlet piping designs where there is no potential for vapor accumulation. In the case of potential for air vapor accumulation an eccentric reducer is recommended in the horizontal inlet design. Where an eccentric reducer is recommended, the flat (horizontal) side of the eccentric reducer is to be located on the top. **The concentric reducer is therefore the preferred reducer if vapor accumulation is not possible.**

Bloch (2010) indicated that the question relating to the selection of the correct reducer type has been posed for many bygone decades and also indicated that the available design guidelines and standards indicate that an eccentric reducer is to be used, but gives no indication as to whether the inlet pipe work enters the pump from above or from below. Should the inlet pipe work enter the pump from above, the eccentric reducer's flat side should be at the bottom, in order for trapped air to migrate back to the source. Should the pump inlet piping enter from below the pump or from a long straight length, the eccentric reducer's flat side should be at the top. These recommended layouts are illustrated in **Figure 1.4.** (Bloch 2010).

This philosophy presented by Bloch is correct in that it will aid the transport of air through the reducer, however three items are not addressed:

i) **The origin of air at this position in the pumping system**. If a pump station sump, forebay, intake bay, suction pipework and reservoir outlets are correctly designed and constructed where does this air originate? Pumps typically operate under positive suction pressure heads and therefore air should not be able to enter the system on the suction side. Under first time start up conditions after construction or after maintenance where air may be present in the system the air may be released with a manual bleed off valve.

ii) **The hydraulic capacity of the system to transport air**. Trapped air in pipelines can be hydraulically transported along the length of a pipeline through valves and fittings depending on the pipeline slope, flow rate and fitting geometry. For an eccentric reducer with the flat section on top the hydraulic capacity for air to be transported through it is larger than that for a concentric reducer, but with the correct flow rate and geometry of the concentric reducer air will be hydraulically transported through it.

iii) **The non-uniform velocity distribution on the impeller created by the flow through the eccentric reducer**. The geometry of an eccentric reducer is asymmetrical and flow through a fitting of this nature will produce asymmetrical flow conditions such as non-uniform velocity and pressure distributions. These flow conditions are contradictory to the recommended pump inlet designs which recommend symmetrical flow conditions with a uniform velocity and pressure distribution.

Bloch's (2010) recommendation for the case where the flow enters the pump station from below (see **Figure 1.4**) should not be limited to an eccentric reducer as a concentric reducer will produce a more uniform flow distribution and a shorter fitting (if the eccentric reducer angle is maintained) together with the hydraulic capacity to transport air through it.

The *scope* of the review of the pump inlet design guidelines and design standards is limited to selection of the correct reducer type. The remaining pump inlet piping design falls outside the scope of this study.

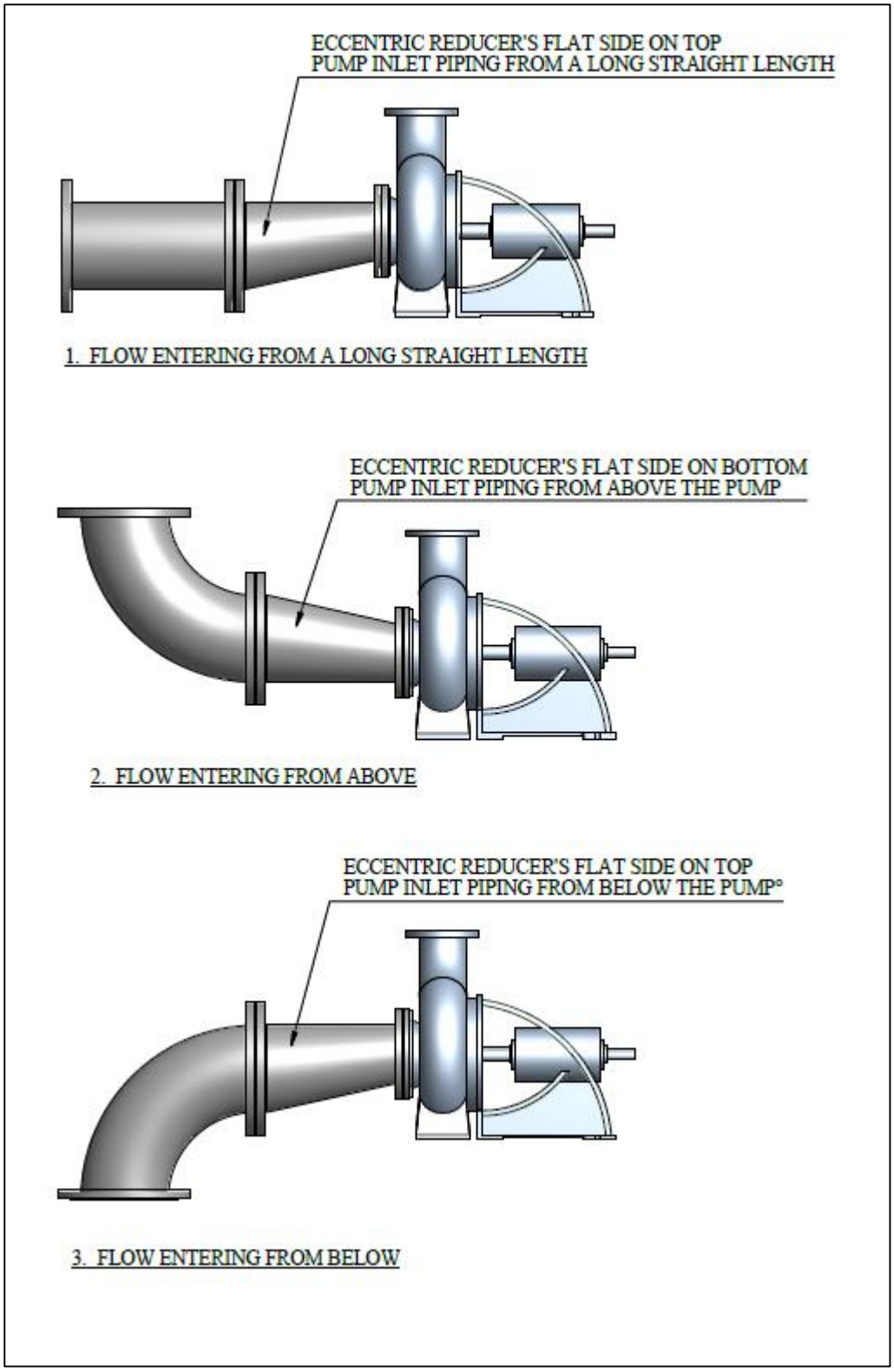

Figure 1.4: Eccentric reducer installation according to Bloch (2010)

1.5. APPLICATION OF NUMERICAL MODELS IN PUMP INLET DESIGN

According to Hirsch (2007) Computational Fluid Dynamics (CFD) is the defined set of methods that are used by a computer to solve numerically the governing laws of fluid motion in or around a material system, where its geometry is also modelled on the computer. Sturm (2010) highlighted the remarkable growth in CFD that has been elevated with the growth of computational power of parallel computer processors and that the long awaited promise of the power of CFD is beginning to be realised.

Tu, Yeoh and Liu (2008) state that CFD can be used to better understand the physical phenomena associated with boundary layers and turbulence and be utilised as a research tool to perform numerical experiments. CFD can provide detailed information and a comprehensive visual result in comparison to analytical and experimental fluid dynamics. Sturm (2010) further highlighted the use of CFD in the application of parallel experimental investigations to yield enhanced insights into these experiments.

Various CFD studies in the design of phase of pump station design have been completed on the pump inlet piping design. Such studies include:

- Eastford Pump Station (Ninham Shand Consulting Services 2007);
- Mokolo Crocodile-West Water Augmentation Project (Aerotherm 2011).

This highlights the application of CFD in pump inlet piping design. These studies are discussed as case studies in **Chapter 2.**

The *methodology* of the review is to utilise CFD to analyse the differences in flow conditions resulting from the selection of different reducers and flow velocities.

1.6. ORGANISATION OF THE REPORT

The report consists of the following chapters and appendices:

- Chapter 1 serves as an introduction to the report.
- Chapter 2 contains background literature to pump inlet piping and design guidelines, hydraulic transportability of air and case studies regarding pump inlet piping design.
- Chapter 3 describes the geometry selection and setup of the numerical models.
- Chapter 4 presents the results obtained from the numerical models.
- Chapter 5 discusses the results obtained from the numerical models.
- Chapter 6 contains the conclusions and recommendations from the study.
- Chapter 7 is the list of references.
- Appendix A – Reducer Type Selection Reference Drawings.
- Appendix B – Calculations (not CFD related).
- Appendix C – CFD Input Parameters.
- Appendix D – Criteria 2 Velocity Distribution Plots
- Supporting Digital Media containing the CFD report summaries, the CFD scalar scene images and CFD residual plots.

2. LITERATURE REVIEW

2.1. PUMP INLET DESIGN – SELECTION OF REDUCER TYPE

The concept of the reducer type selection was introduced in ***Paragraph 1.3.*** Two types of reducers are available to reduce the suction pipe diameter to match the diameter of the suction connection of the pump; namely: concentric reducers and eccentric reducers. The selection of the type of reducer has an influence on the hydraulic transportation of air within the suction pipe work and the flow conditions exiting the reducer and entering the pump. Design guidelines, standards and manufacturer installation guidelines present recommendations on the selection of reducer type. These reducer type selection recommendations are summarised in **Table 2.2**. The reference drawings noted in this table are provided in **Appendix A**.

From **Table 2.2** it is established that the eccentric reducer with the flat section on the top is prescribed in the majority of the references. **This selection of reducer type is to allow for the transportation of air to ensure undisturbed flow to the pump.** A number of references also prescribe the use of straight lengths of pipes downstream from the reducer, this requirement will promote uniform flow conditions towards the pump inlet. The required straight lengths of pipe recommended by ANSI/HI (2009) are provided in **Table 2.1**.

Table 2.1: ANSI/HI (2009) straight length of pipe requirements

	Number of pipe diameters [a]	
Reducer	**Concentric**	**Eccentric**
1 pipe size reduction	0 (<10°)[b]	0 (<20°)[b]
2 pipe size reduction	0 (<20°)	1 (<30°)
3 pipe size reduction	1 (<20°)	2 (<30°)
4 pipe size reduction	2 (<20°)	3 (<40°)
5 pipe size reduction	3 (<30°)	4 (<40°)

Notes:

[a] Minimum required straight pipe length before pump suction inlet = diameter *x* number of pipe diameters.

[b] The angles quoted reflect the maximum per side for standard commercial fittings.

Table 2.2: Summary of reducer requirements

Reference	Reference Type	Reducer Selection	Conditions for Selection	Reason for Reducer Selection	Reference Drawing
ANSI/HI (2009)	National Standard	Concentric Reducer	Vertical Inlet Pipes	Ensures no air accumulation	
			Installations where there is no potential for vapour accumulation		
			Minimum straight lengths of pipe are required	Ensures disturbance free flow	Figure A-1
		Eccentric Reducer	Horizontal installations where air accumulation is possible	Allows for transportation of air	
			Flat section on top		
			Minimum straight lengths of pipe are required	Ensures disturbance free flow	Figure A-1
Bloch (2010)	Journal Article	Eccentric Reducer	Flat section on top for suction pipe entering in a horizontal plane	Allows for transportation of air	Figure A-2
			Flat section at the bottom for suction pipe entering from above	Ensures no air accumulation	Figure A-2
			Flat section on top for suction pipe entering from below	Allows for transportation of air	Figure A-2
Mackay (2004)	Pump Station Handbook	Eccentric Reducer	Flat section on top	Eliminates the potential problem in eddy currents in a high point in the suction line that might travel into the impeller eye	Figure A-3
Bloch and Budris (2010)	Pump Station Handbook	Eccentric Reducer	Flat Section on top	Allows for transportation of air	Figure A-4
			Minimum straight pipe and reducer length required	Ensures disturbance free flow	Figure A-5
KSB (2012)	Pump Manufacturer Operating Instructions	Eccentric Reducer	Flat section on top	Allows for transportation of air	Figure A-6
Jones et al (eds. 2008)	Pump Station Handbook	Eccentric Reducer			
SAPMA (2002)	Pump Station Handbook	Eccentric Reducer			Figure A-7

2.2. PUMP INLET PIPING REQUIREMENTS

According to Jones et al (eds. 2008) piping with excessive velocities may cause unreasonable headloss and can lead to vibration problems due to turbulence in fittings and valves and that attention should be paid to the pump intake design; this concept was introduced in ***Paragraph 1.2***. Various velocity requirements were identified in the literature review and are summarised in **Table 2.3**. These velocities are related to flow velocities in suction piping and not to flow velocities in sumps and intakes. From this table it is observed that the recommended maximum velocities are of the same order of magnitude, but do however differ in the various reviewed documents. The conditions for the recommended velocities are also not constant in the reviewed documents, however the recommendations made by ANSI/HI (2009), ANSI/HI (2000) and Jones et al (eds. 2008) are supportive.

Further to the velocity requirements the approach flow to a pump must be undisturbed as flow disturbances in the form of a distorted velocity distribution, unequal pressure distribution, entrained air or gas bubbles, vortices and excessive pre-swirl at the pump inlet are detrimental to pump performance, cavitation and smooth pump running (ANSI/HI 2000; Sulzer 2010; Jones et al eds. 2008). The phenomenon of radial thrust is illustrated in **Figure 2.1**; a pressure differential between circumferential points on the impeller (P1 and P2 in this illustration) creates a radial thrust on the pump shaft that is accounted for by the radial bearing. Radial thrust occurs in all centrifugal pumps when the pump does not operate at the pump's best efficiency point (it therefore depends on flow rate, head and rotational speed). The bearings, shafts and casings are designed to resist the anticipated radial load, **pumps have however been destroyed within days or even a few hours through excessive wear in bearings, seals, shaft sleeves, and wearing rings** (Jones et al eds. 2008).

ANSI/HI (2000), Jones et al (eds. 2008) and Ninham Shand Consulting Services (2007) specify the requirement for time averaged velocities at the pump suction to be within 10% of the cross-sectional area average velocity. HR Wallingford (2001) in Sinotech CC (2005) and University of Pretoria (2011) provided the following guidelines for velocity distribution variations in suction pipework:

- Velocity variation along line ABCD is less than 10% of the average velocity (see **Figure 2.2**); and
- Maximum velocity variation along a circle AEDF is ± 5% of the average velocity (see **Figure 2.2**).

Table 2.3: Summary of pump suction velocity requirements

Reference	Reference Type	Recommended Maximum Velocity (m/s)	Conditions for Recommendation
ANSI/HI (2009)	National Standard	2.4	Suction Pipe at least as large as the pump suction connection
			Valves and other flow disturbing fittings are to be at least one pipe size larger than the pump suction nozzle
			Excludes slurries
			Values greater than 2.4 m/s are to be evaluated with respect to flow distribution, erosion, NPSH, noise, water hammer and the manufacturer's recommendations
			Maximum velocity applies to any point in the suction piping
			For fluids close to the vapor pressure velocities are to be kept low enough to avoid flashing of the liquid in the piping
ANSI/HI (2000)	National Standard	2.4	Velocities may be increased at the pump suction flange by the use of a gradual reducer
			Higher velocities are acceptable providing the piping design delivers a smooth inlet flow to pump suction (velocity distributions are specified)
			The velocity in the pump suction piping should be constant or increasing as the flow approaches the pump
			The velocity is to be large enough to prevent sedimentation in horizontal piping
			There shall be no flow disturbing fittings closer than five suction pipe diameters from the pump (fully open, non-flow disturbing valves, vaned elbows, long radius elbows and reducers are not considered flow disturbing fittings)
			The suction diameter is to be at least one size larger than the suction fitting on the pump, in such cases an eccentric or concentric reducer fitting is fitted
Mackay (2004)	Pump Station Handbook	(no velocity recomended)	The suction diameter is to be at least one size larger than the suction fitting on the pump
SAPMA (2002)	Pump Station Handbook	0.5~0.75	The suction pipe should never be smaller than the suction connection of the pump and in most cases should be at least one size larger
			Pipe velocities should be in the range of 0.5 to 0.75 m/s unless suction conditions are exceptionally good
			Elbows or tees located adjacent to the pump suction flange will result in uneven flow patterns which prevent the liquid from filling the impeller evenly
Bloch and Budris (2010)	Pump Station Handbook	2.5	Maximum velocity applies to any point in the suction piping
			Suction pipe at least as large as the pump suction nozzle
KSB (2012)	Pump Manufacturer Operating Instructions	2	For an individual suction lift pipe
			If it is for a suction manifold the flow velocity is to be kept as low as practically possible
Jones et al (eds. 2008)	Pump Station Handbook	1.8~2.4	The conditions in ANSI/HI 9.6.6 and ANSI/HI 9.8 are to be followed
			The velocity is not applicable to suction manifolds, where the recommendation is 1.8 m/s
			The velocity applies to constant speed pumps

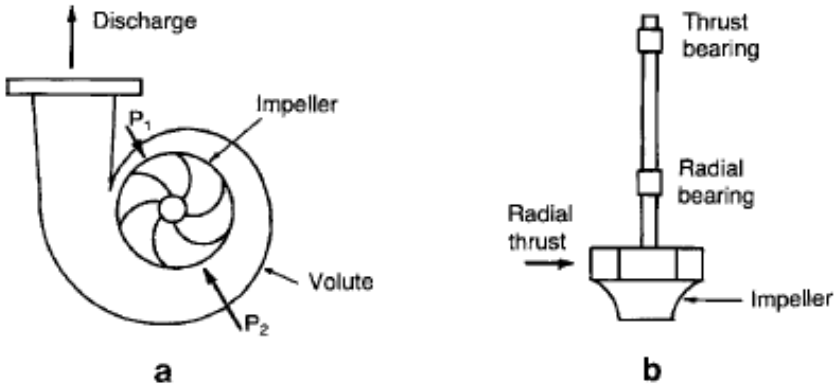

Figure 2.1: Development of Radial Thrust in a Centrifugal Pump (Jones et al eds. 2008)

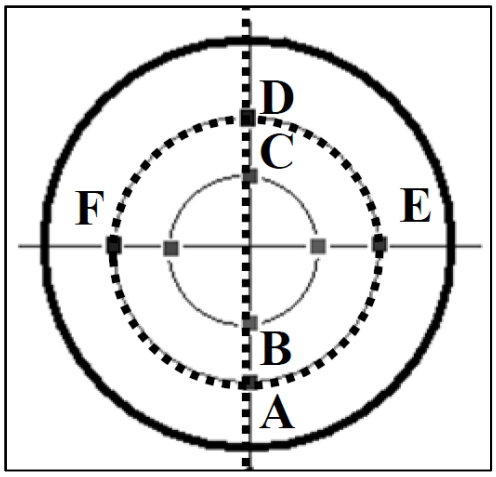

Figure 2.2: HR Walingford Suction Inlet Velocity Requirements – Section View (Sinotech CC 2005; University of Pretoria 2011)

2.3. STANDARD REDUCER FITTING DESIGN

Two methods are commonly used in South Africa for specifying the dimensions for fabricated steel water fittings, namely the standard AWWA M11 and standard fitting sizes provided by fitting manufacturers. AWWA (2004) recommends that fittings should be specified using standard methods to prevent design and construction faults. AWWA (2004) instructs the designer to reference AWWA C208 for the formulas to calculate the dimensions for fittings. Fitting manufacturers (Abeyla Trading 2008; Hall Longmore 1989; Mining Pressure Systems n.d.) provide a standard list of dimensions for various fittings of different pipe diameters.

AWWA (2008) provides a formula to calculate the length of a reducer, L_r. This formula is provided in Equation 2-1 and is illustrated in **Figure 2.3.**

$$L_r = 4(D_L - D_S) \quad (2\text{-}1)$$

Where:

L_r = Length of reducer

D_L = Outside diameter of steel cylinder of large end of a reducer

D_S = Outside diameter of steel cylinder of small end of a reducer

The fitting dimensions for reducers listed by fitting manufacturers such as: Abeyla Trading (2008), Hall Longmore (1989) and Mining Pressure Systems (n.d.) are provided in **Figure 2.4** and the variables are illustrated in **Figure 2.3**. It is noted that the dimensions are consistent for the three fitting manufacturers referenced. It is noted that the dimensions provided in AWWA C208 do not relate to the dimensions presented by the fitting manufacturers in **Figure 2.4**.

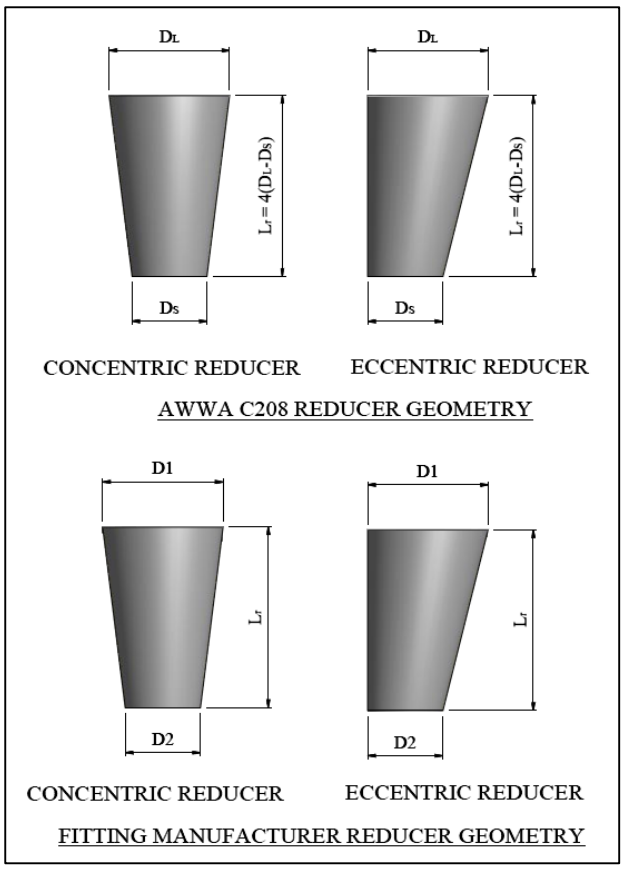

Figure 2.3: Fitting manufacturers' standard reducer size illustration

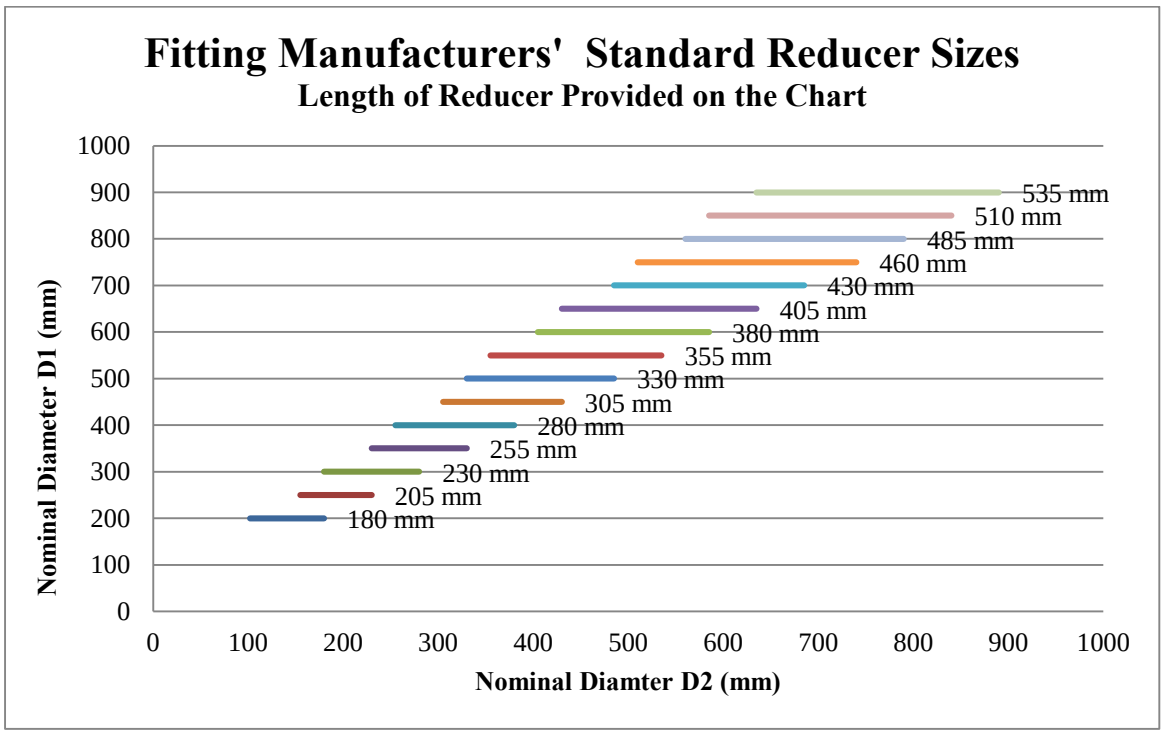

Figure 2.4: Fitting Manufacturers' Standard Reducer Sizes

SANS 62-2 (SABS 2013) and SANS 719 (SABS 2011) specify the South African National Standard for steel pipe dimensions, these dimensions are commonly used in water engineering projects and will be utilised throughout this study. The dimensions are provided below in **Table 2.4**.

Table 2.4: SANS 62-2 and SANS 719 Standard Steel Pipe Dimensions (SABS 2013, SABS 2011)

Nominal Bore (DN) (mm)	Outside Diameter (OD) (mm)	Minimum Wall Thickness (t) (mm)	Inner Diameter (ID) (mm)
25	33.4	2.8	27.8
50	59.8	3.2	53.4
80	88.1	3.5	81.1
100	113.3	3.9	105.5
125	138.7	4.2	130.3
150	165.1	4.2	156.7
200	219.1	4.5	210.1
250	273	5	263
300	323.9	6	311.9
350	355.6	6	343.6
400	406.4	6	394.4
500	508	6	496
600	609.6	6	597.6
700	711.2	8	695.2
800	812.8	8	796.8
900	914.4	10	894.4
1000	1016	10	996
1200	1220	12	1196
1400	1420	12	1396
1600	1626	14	1598
1800	1789	14	1761
2000	2032	16	2000
2200	2230	16	2198

In this review the standard reducer sizes, both from the fitting manufacturers and AWWA C208 will be compared to the final outcomes to determine if the standard sizes yield acceptable downstream velocity profiles.

2.4. HYDRAULIC TRANSPORTABILITY OF AIR

Air can enter a pipeline and specifically on the suction end of a pump in the following manners:

- Air present in the pipes due to first time start up or start up after maintenance;
- Air released from solution at sufficiently low pressures;
- Air that enters the pipe work due to inefficient seals and/or faulty connections; and
- Air entering the pipe from a free surface due to an incorrect design and/or incorrect operating conditions.

This air present in the pipeline negatively affects pumps and pumping systems. These negative effects include:

- A reduction in the water cross sectional area (Jones et al eds. 2008, ANSI/HI 2009);
- An increase to the flow resistance (Jones et al eds. 2008, ANSI/HI 2009);
- Possible loss of prime to the pump if a slug of air is swept into the pump case during a restart causing a partial or complete loss of prime (ANSI/HI 2009);
- The creation of an environment conducive to corrosion (Jones et al eds. 2008);
- Creation of turbulence and air entrainment (Mackay 2004);
- Implosion of entrained air due to increasing pressure at the eye of the impeller causing damage identical to that of cavitation (Mackay 2004);
- Noisy operation (Bloch and Budris 2010); and
- Unbalanced axial loads (Bloch and Budris 2010)

The hydraulic transportability of air refers to the ability of a fluid flowing within a conduit to transport free air in the direction of the flow. This free air is then transported within the conduit until it reaches an air valve or vent where it can be mechanically removed, until it reaches the end reservoir, or until it reaches a position within the conduit where the fluid cannot transport the free air any further. The minimum fluid velocity required to transport free air within a conduit is referred to as the clearing velocity (Pothof and Clemens 2011) or as the critical velocity (Van Vuuren, , et al 2004), it will be referred to as the critical velocity throughout this study.

The hydraulic transportability of air within a pipeline is a function of the pipe slope, amount of accumulated air and the flow characteristics of the fluid with the pipeline (i.e. Froude number, flow

velocity and flow rate) (Pothof and Clemens 2011; Van Vuuren, et al 2004). Various relationships for the assessment of the hydraulic transportability of air have been developed by various researchers.

According to Van Vuuren, et al(2004) the two most widely used relations to calculate the critical velocity are those presented by Kalinske and Bliss (Eq 2-2) and by Wisener, Mohsen and Kouwen (Eq 2-3). Van Vuuren, et al (2004) also derived their own relationship to calculate the critical velocity. This relationship is presented in Eq 2-4 and the differences in calculated critical velocities of a selection of pipe diameters for these three relationships are illustrated in **Figure 2.5**. These calculations are provided in **Table B.1** in **Appendix B.**

$$\frac{{Q_c}^2}{gD^5} = 0.707 \sin\theta \qquad (2\text{-}2)$$

Where:

Q_c = Critical Flow Rate (m^3/s)

g = Gravitational Acceleration (m^2/s)

D = Diameter of the pipe (m)

θ = Slope of the pipeline (°)

$$\frac{V_c}{\sqrt{gD}} = 0.25\sqrt{\sin\theta} + 0.825 \qquad (2\text{-}3)$$

Where:

V_c = Critical Velocity (m/s)

g = Gravitational Acceleration (m^2/s)

D = Diameter of the pipe (m)

θ = Slope of the pipeline (°)

$$V_c = a\sqrt{gD}\theta^b \quad (2\text{-}4)$$

Where:

V_c = Critical Velocity (m/s)

g = Gravitational Acceleration (m^2/s)

D = Diameter of the pipe (m)

θ = Slope of the pipeline (°)

a = Constant (0.2178)

b = Constant (0.4007)

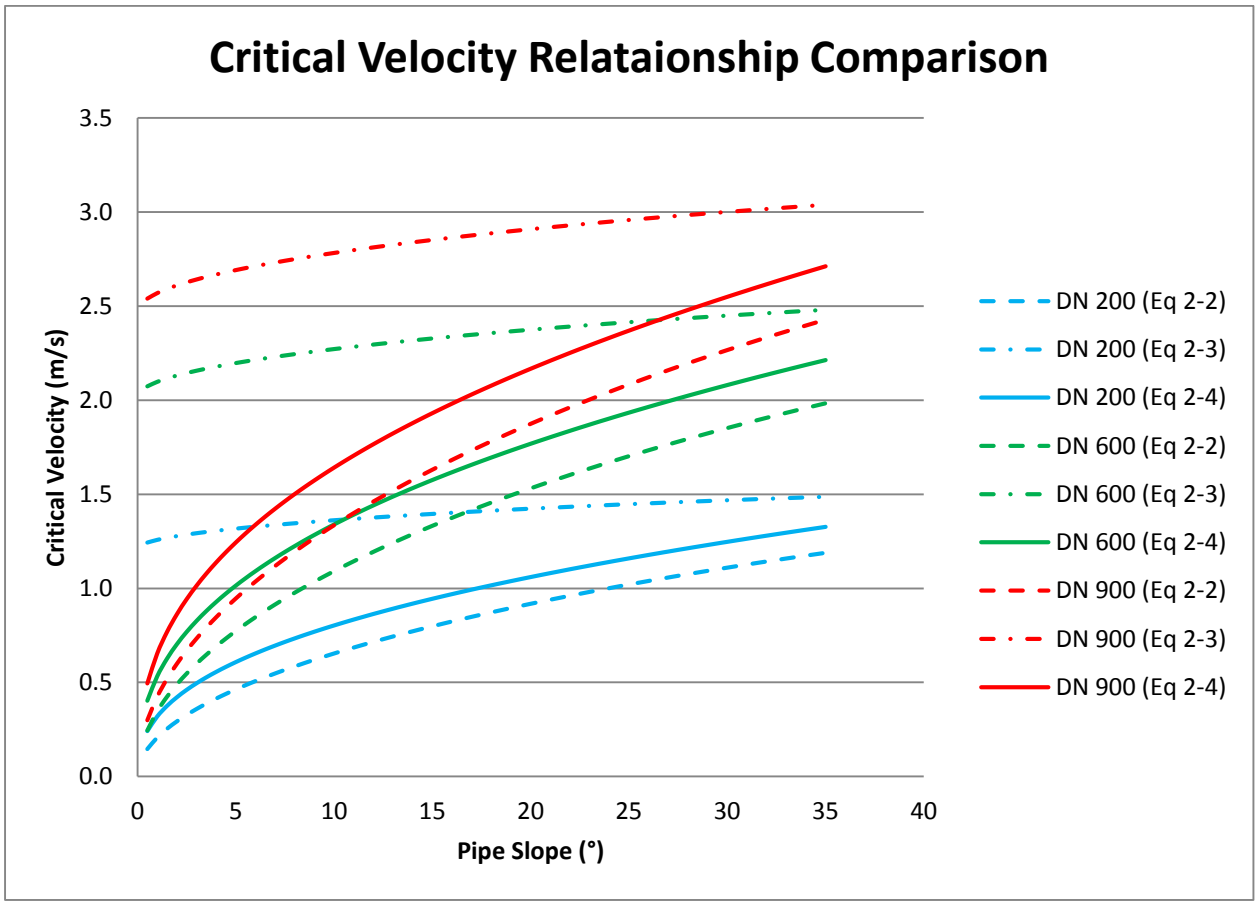

Figure 2.5: Critical Velocity Relationship Comparison

2.5. PREVIOUS PUMP STATION REDUCER SELECTION CASE STUDIES

2.5.1. Case Study: Inlet conditions leading to problems – Knysna

A pump failure in Knysna as described by Van der Westhuizen (2011) involved the incorrect selection of reducer type. The general pump station layouts are provided in **Figure 2.6** and **Figure 2.7**. The following problems were experienced with the pumps:

- High pump vibrations;
- Pump bearing failures;
- Pump shaft failures;
- Pumps "haunting";
- Pumps running at part load;
- System resistance higher than expected; and
- Pump control valves working against each other.

The problems experienced with the pumps were not constant for all the pumps. Pump 1 experienced no failures, Pump 2 experienced a few failures and Pump 3 experienced numerous failures (refer to **Figure 2.7** for pump numbers). The pump inlet piping design for the pump station is presented in **Figure 2.8**. It is noted that the suction reducer fittings used are eccentric reducers.

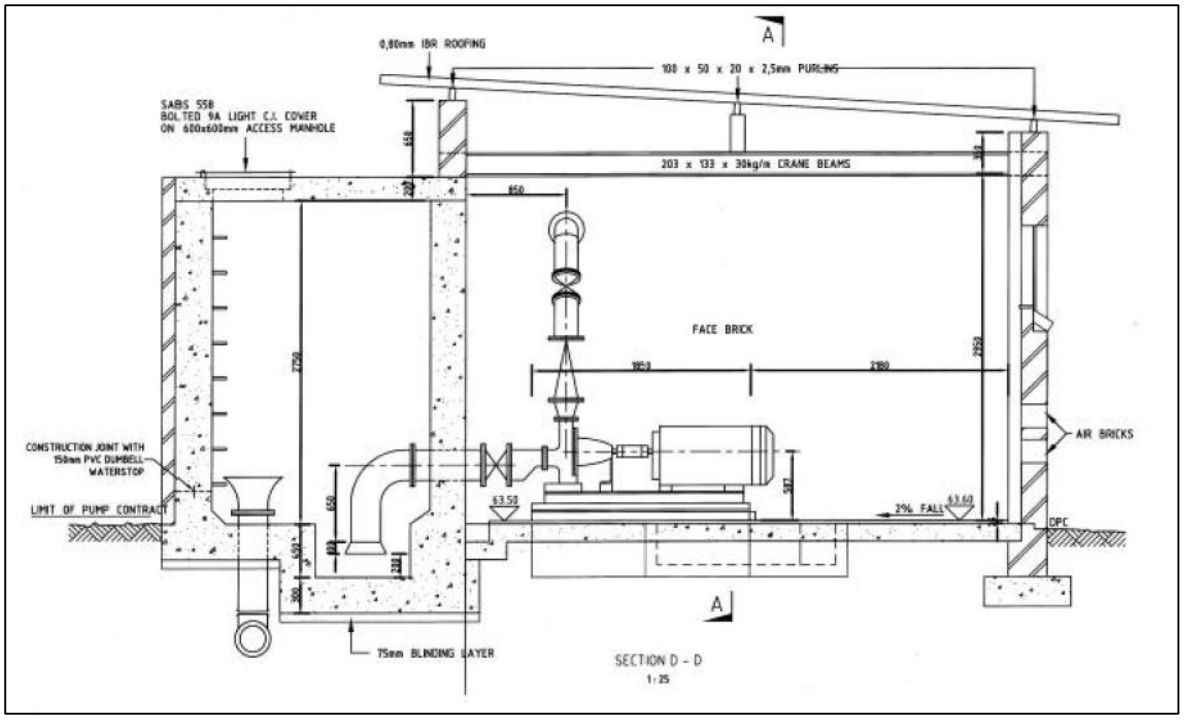

Figure 2.6: Knysna pump station section view (Van der Westhuizen 2011)

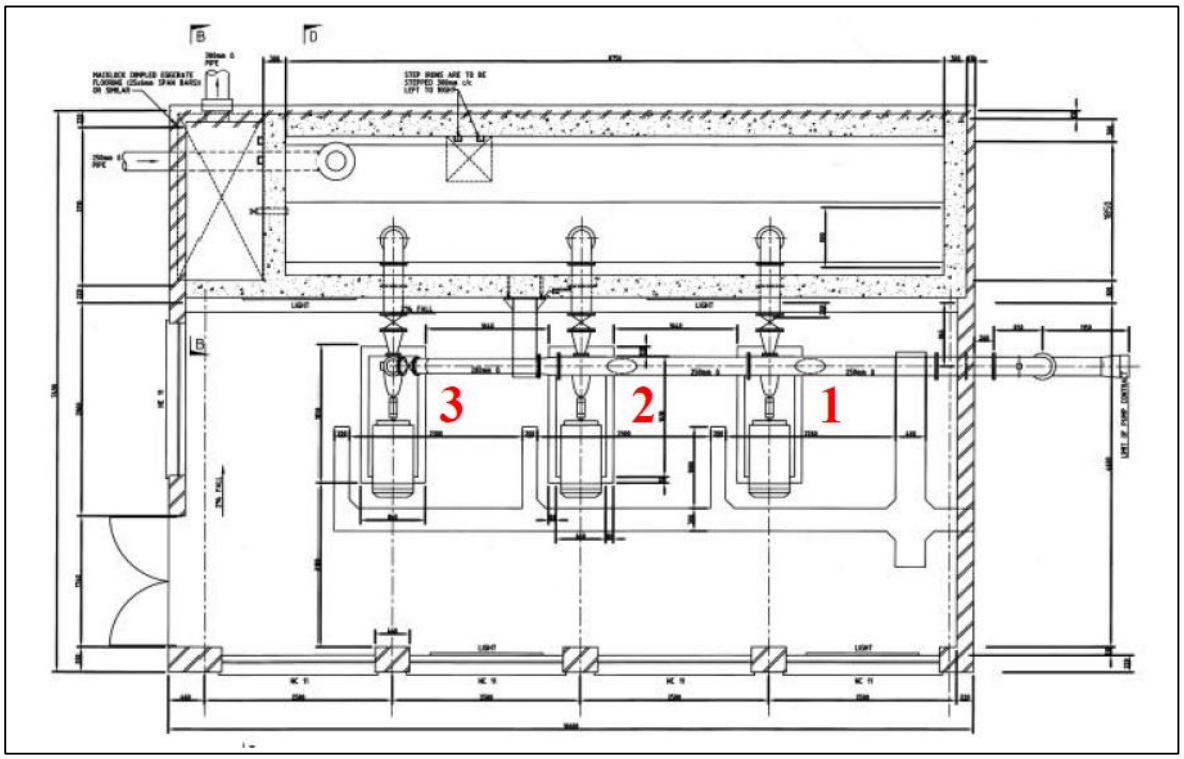

Figure 2.7: Knysna pump station plan view (Van der Westhuizen 2011)

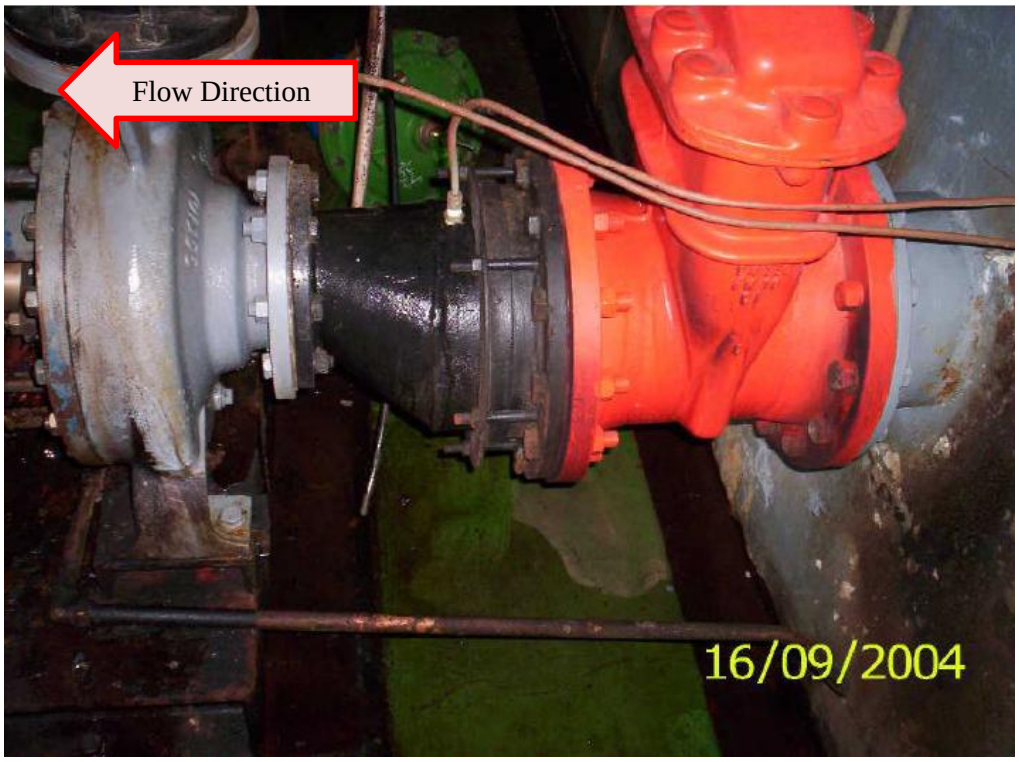

Figure 2.8: Knysna pump station pump inlet piping design together with eccentric reducer (Van der Westhuizen 2011)

An investigation as to why these various pumping problems occurred was conducted. Pressures were measured and recorded on the reducer (at various locations described in **Figure 2.9**), suction piping and the delivery piping. The results of the pressure measurements measured on the reducer are provided in **Figure 2.10**. From the results it is observed that there were considerable variances in pressure distributions in the pump inlet piping, with the greatest difference being approximately 11 kPa, 65% of the larger pressure reading. This was noted as one of the reasons for the pump failure. **The incorrect choice of reducer type therefore has an influence on pump station operation and may lead to pump station failures**.

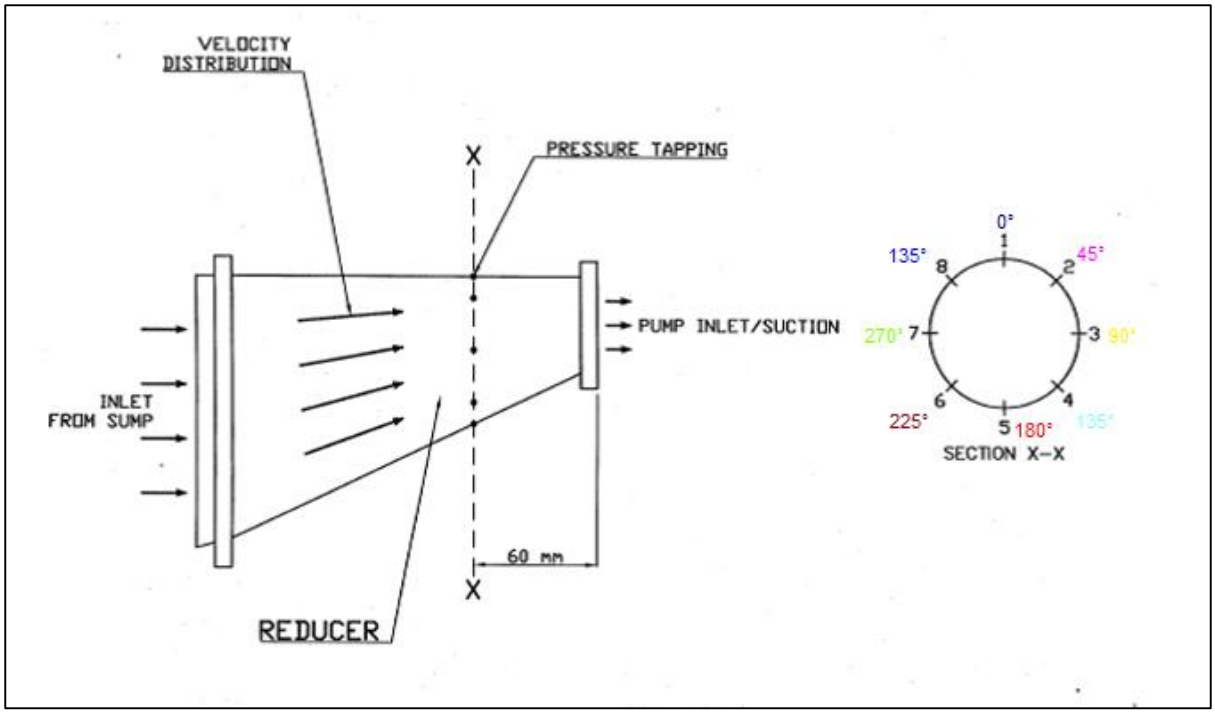

Figure 2.9: Knysna pump station position of pressure measurement on eccentric reducer (van der Westhuizen 2011)

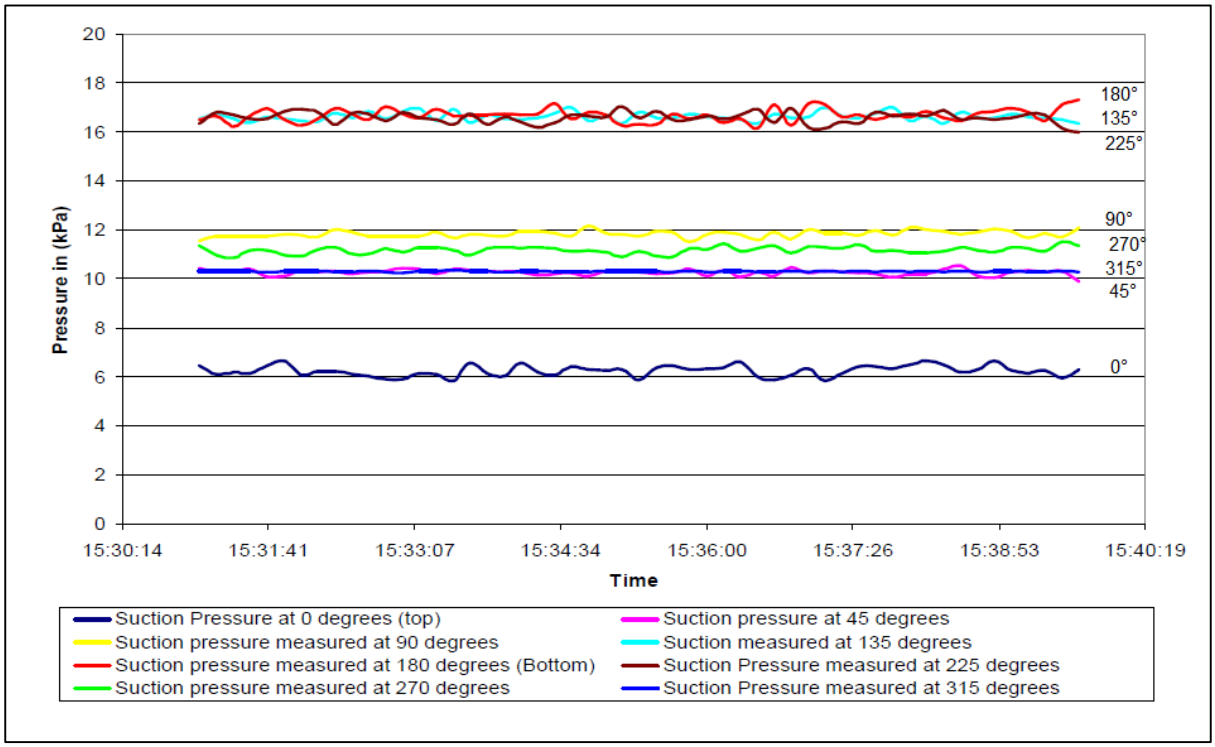

Figure 2.10: Knysna pump station pressure measurements on eccentric reducer (van der Westhuizen 2011)

2.5.2. Case Study: CFD Analysis for Eastford Pump Station

The Eastford pump station in Knysna experienced intermittent pump failures for a number of years and Ninham Shand Consulting Engineers were tasked to investigate the flow patterns in a proposed suction pipework design (Ninham Shand Consulting Services 2007). Previous investigations on the pump failures indicated that the possible causes of the failures were:

- Pumps are operating outside of the recommended operating range;
- Poor suction design; and
- "Haunting" of the pumps on the delivery side.

The poor suction design described by Ninham Shand Consulting Services (2007) included a reduction in pipe diameter that is not achieved through a reducer, but is a direct reduction in pipe diameter; i.e. two different flange hole diameters coupled directly, as is presented in **Figure 2.11**. Due to this poor suction design a new suction pipework design was proposed and a CFD analysis was performed on the new design to investigate the flow patterns in the proposed suction pipework. The flow patterns would illustrate the possibility of any significant pre-rotation that could like lead to uneven pressure distributions, which could lead to pump shaft failures. The proposed suction pipework design is provided in **Figure 2.12**. It is noted that the proposed reducer type is a **concentric reducer**.

Four operating scenarios were identified by Ninham Shand Consulting Services (2007) and all four these scenarios were analysed. The four operating scenarios were directly related to the pump station layout, i.e. a common pump sump, a single inlet pipe discharging into the sump and three pumps with individual pipework abstracting water from the sump. The four scenarios analysed are (Ninham Shand Consulting Services 2007):

- Scenario 1: The two pumps closest to the inlet in operation.
- Scenario 2: The two pumps furthest away from the inlet pipe in operation.
- Scenario 3: The pump closest to the inlet pipe in operation.
- Scenario 4: The first and last pumps in operation.

The 3-D geometry of the pump station was created in AutoCad 2000, imported into Fluent's pre-processor Gambit v2.2.30 and analysed with Fluent's steady state solver.

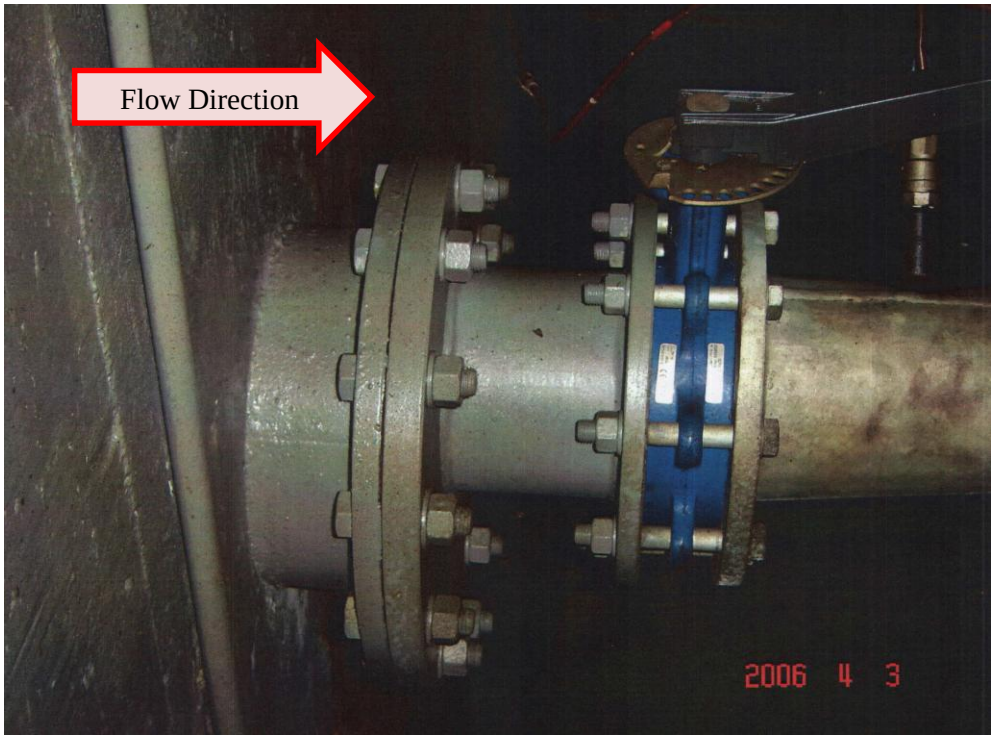

Figure 2.11: Eastford Pump Pipe Diameter Reduction Design (Ninham Shand Consulting Services 2007)

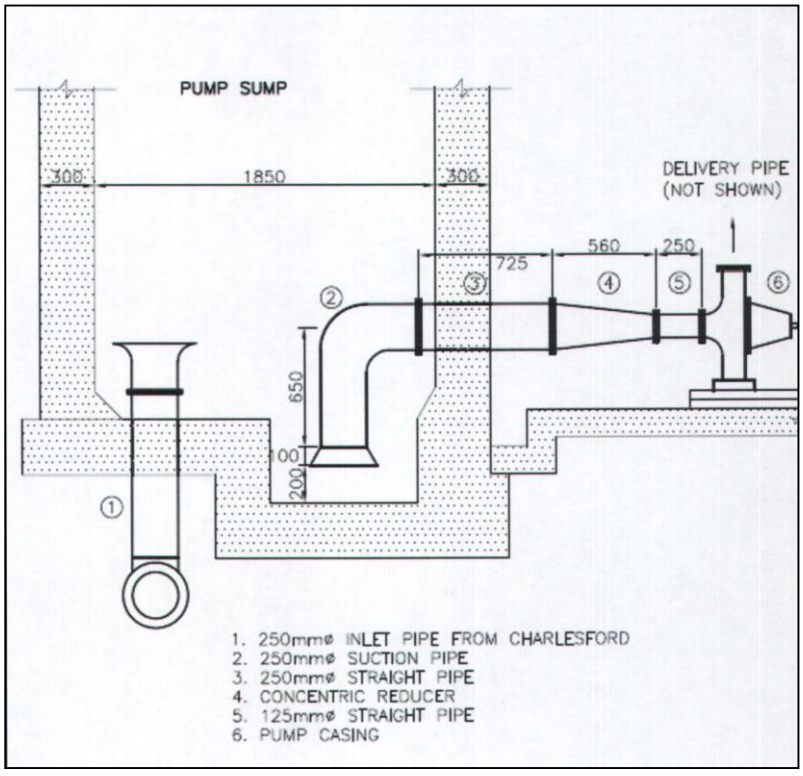

Figure 2.12: Proposed Eastford Pumpstation Inlet Pipework Design (Ninham Shand Consulting Services 2007)

The results obtained from the analysis depicted the predicted flow patterns in the inlet pipework and pressure and velocity distributions upstream of the pumps. An example of the predicted flow patterns is provided in **Figure 2.13**. The results of the pressure distributions are provided in **Figure 2.14.** The maximum pressure variations for the four scenarios as determined from the analyses were calculated to be approximately 1.5 kPa. The corresponding maximum velocity distributions across the pipe cross section were calculated to be approximately 0.2 m/s (mean velocity is 4.1 m/s). According to Ninham Shand Consulting Services (2007) the pressure and velocity distributions appear to be within the acceptable limits (within 10% of the mean velocity) and that the proposed design will therefore not impose excessive stresses on the pump shafts. Ninham Shand Consulting Services (2007) also indicated that the proposed design does not present flow patterns in the sump and pipework that would create a concern for unbalanced load on the pump impellers.

The application of a concentric reducer in this case study provided a design where the pressure and velocity distributions are within the acceptable limits. It was noted that no reference to the transportation of air was made in the report by Ninham Shand Consulting Services (2007).

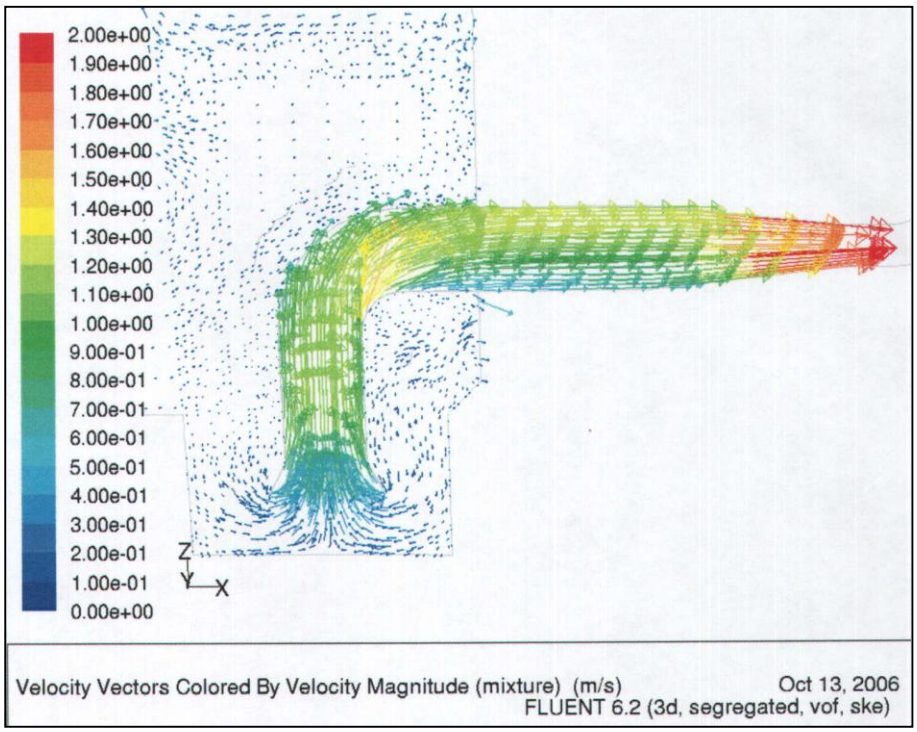

Figure 2.13: Scenario 1 - Velocity vectors in pipe closest to the inlet (Ninham Shand Consulting Services 2007)

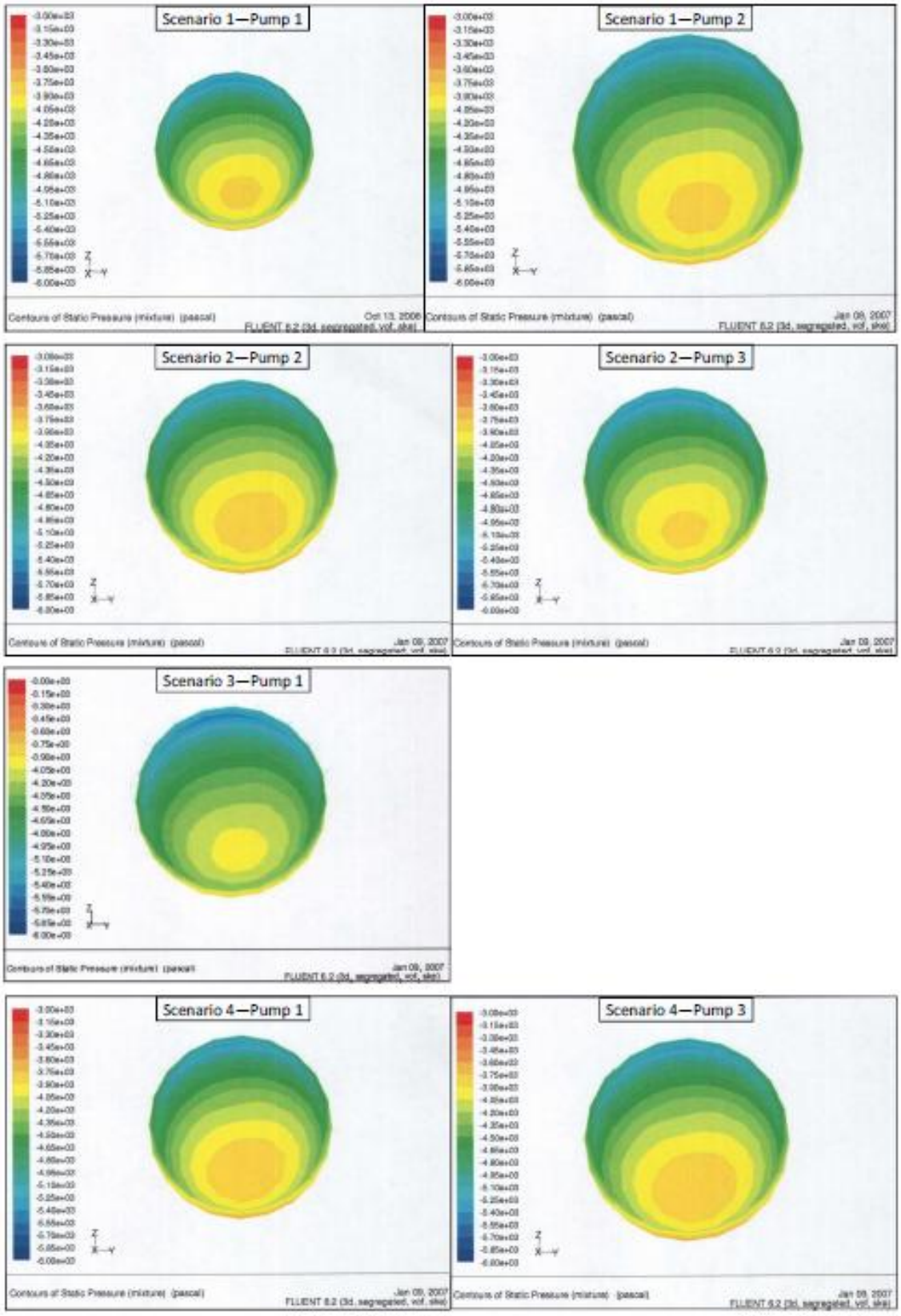

Figure 2.14: Pressure distribution in pipe closest to the inlet (Ninham Shand Consulting Services 2007)

2.5.3. Case Study: CFD Analysis for Mokolo Pump Station

The Mokolo Pump Station is situated near Lephalale in the Limpopo Province and construction of the pump station commenced in September 2011. During the design phase of the pump station a CFD study was performed on the pump station pipe work design. The study was completed by Aerotherm on behalf of Mokolo Crocodile Consultants in 2011. The study had a specific focus on the pressure and velocity distributions at the pump inlets resulting from the use of the two different reducer types.

The Mokolo Pump Station consists of two sets of pumps, each consisting of three pumps. The sets of the pumps are named: the booster pumps and the high lift pumps. A common suction manifold supplies the booster pumps and these booster pumps discharge flow into a delivery manifold. The booster pump delivery manifold transfers the flow to a common suction manifold on the high lift side. The high lift pumps discharge into a common delivery manifold. A bypass pipe is provided from the booster suction manifold to the high lift suction manifold such that the high lift pumps can be operated without the booster pumps. The pump station layout is provided in **Figure 2.15**.

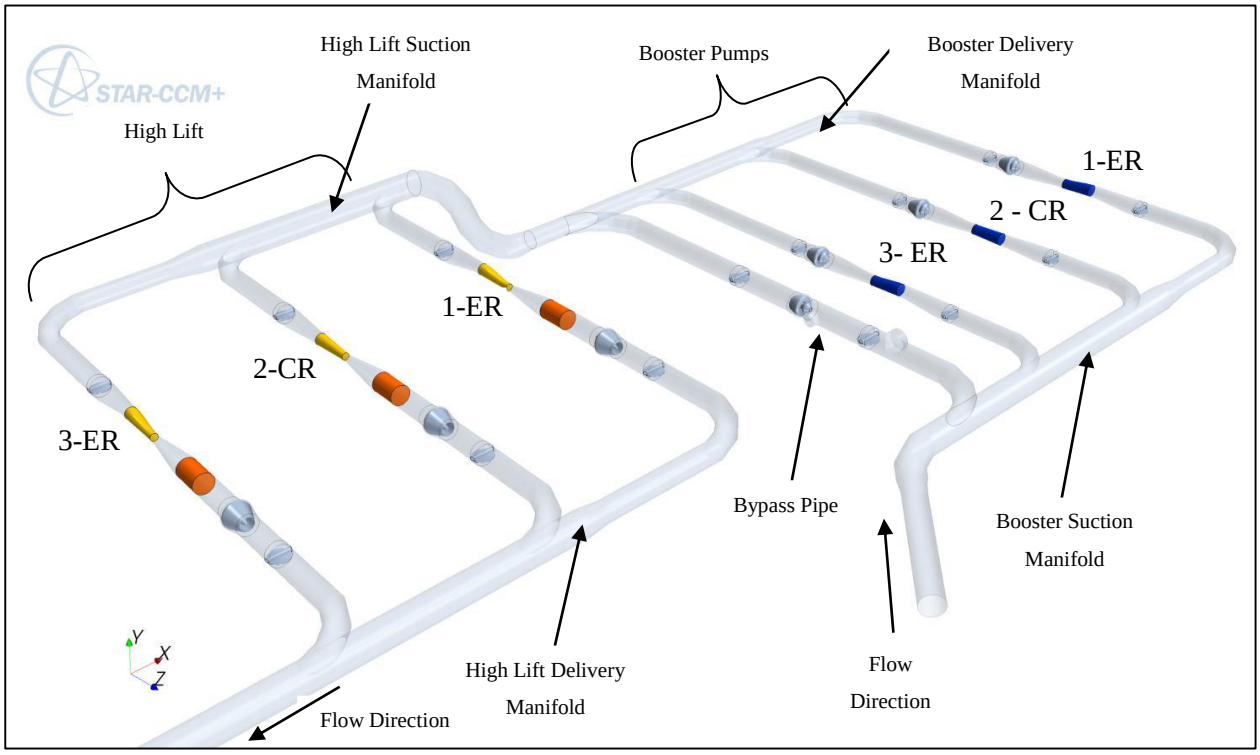

Figure 2.15: Mokolo Pump Station Layout (Aerotherm 2011)

Six operating scenarios were analysed during the study, these scenarios are summarized in **Table 2.5** (Aerotherm 2011). The 3-D geometry of the pump station was created in Inventor 2011 and analysed with STAR CCM+ steady state solver.

Table 2.5: Operating Scenarios for Mokolo Pump Station CFD Analysis (Aerotherm 2011)

Scenario 1	Booster 1	Booster 2	Booster 3	High Lift 1	High Lift 2	High Lift 3
1	Off	Off	Off	On	On	Off
2	On	On	Off	On	On	Off
3	On	On	On	On	On	On
4	Off	Off	On	Off	On	Off
5	On	On	Off	Off	On	On
6	On	Off	On	On	Off	On

It is noted that the reducers on the suction side at Booster pumps 1 and 3 and High Lift pumps 1 and 3 are eccentric reducers and the reducers on the suction side at Booster pump 2 and High Lift pump 2 are concentric reducers. Each of the six scenarios are briefly summarised below. Depending on the flow rate for the scenario being analysed the lift in pressure head for each pump was calculated based on pump performance curves and the momentum source representing the pumps in CFD (Aerotherm 2011). The minimum absolute pressures calculated for the six scenarios were comfortably larger than 2.33 kPa (the vapor pressure for water at 20 °C) therefore cavitation does not present a problem in this system (Aerotherm 2011). The velocity profiles were recorded for both the vertical direction and the horizontal direction, the orientation of profiles is explained in **Figure 2.16**. Vertical velocity profiles for all six scenarios for all the pumps are provided in **Figure 2.17** and the horizontal velocity profiles are provided in **Figure 2.18**.

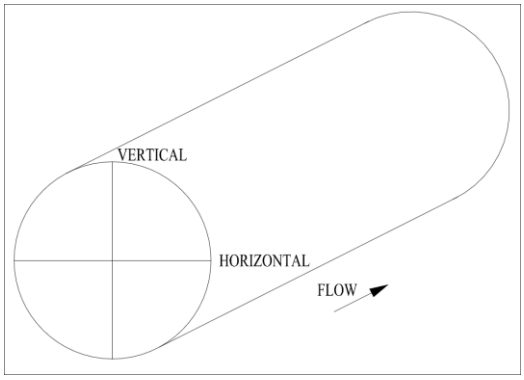

Figure 2.16: Orientation of Velocity Profiles

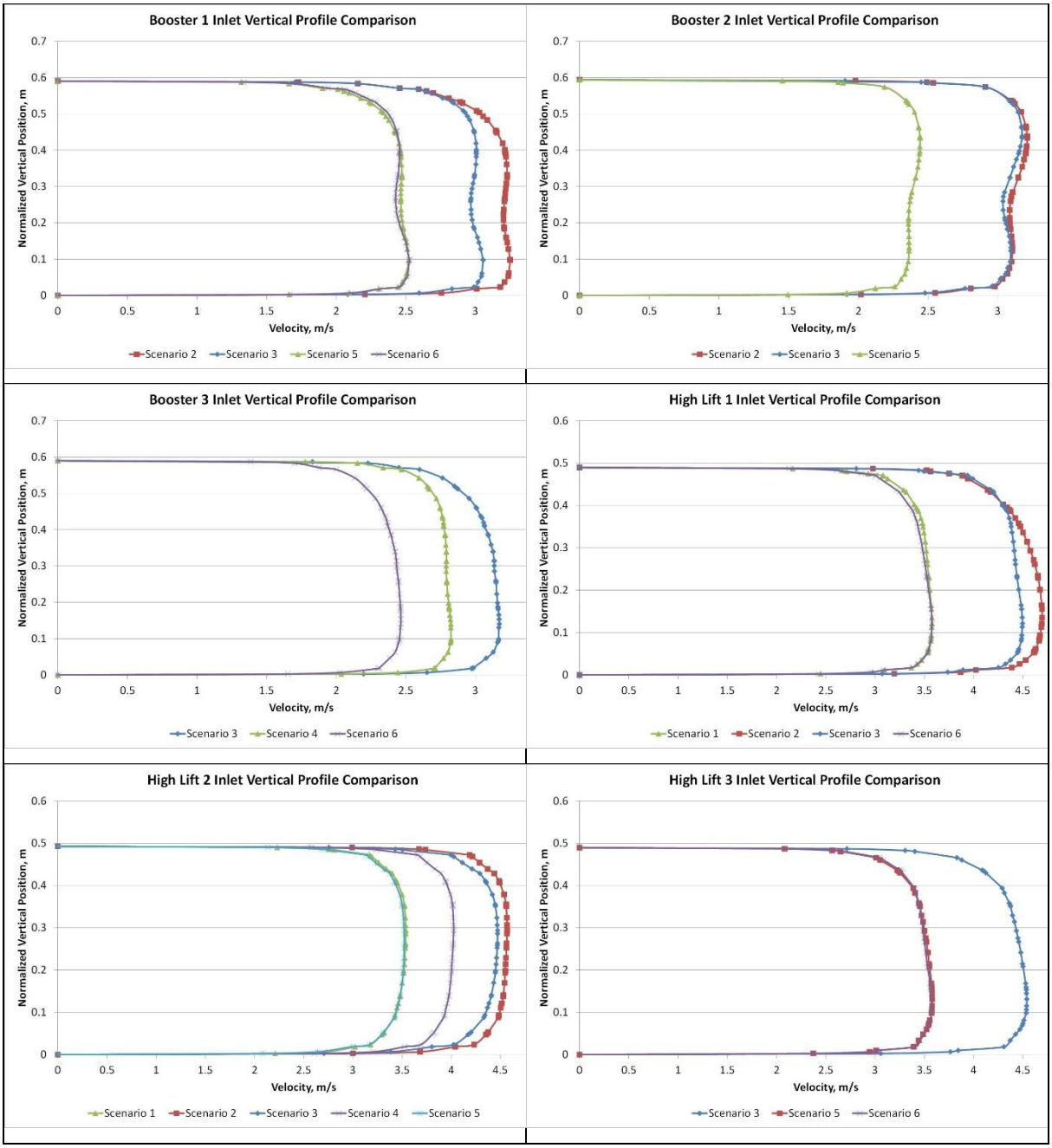

Figure 2.17: Comparison of the vertical velocity profiles at pump entry for all six scenarios (Aerotherm 2011)

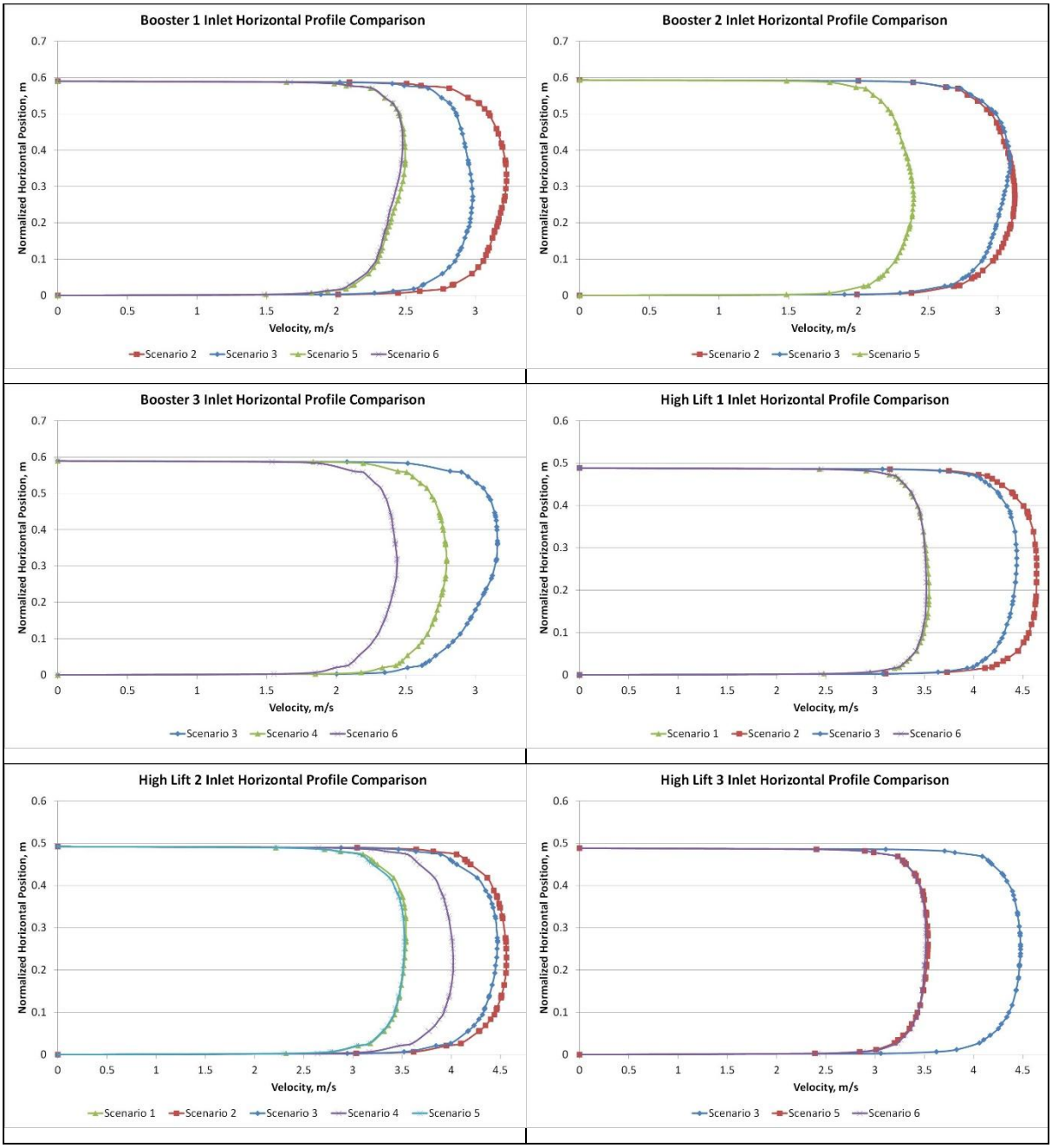

Figure 2.18: Comparison of the horizontal velocity profiles at pump entry for all six scenarios (Aerotherm 2011)

High Lift pumps. It is observed that the vertical velocity profiles for High Lift pumps 1 and 3 are more skewed compared the vertical velocity profile for High Lift pump 2 (**Figure 2.17**). **The concentric reducer configuration (High Lift pump 2) produces a more uniform velocity and pressure distribution compared to the eccentric reducer configuration (High Lift Pump 1 and 3)**. This phenomenon is caused by acceleration in velocity at the bottom edge of the eccentric reducer as the flow path narrows from below. This is further illustrated in the section views presented in **Figure 2.19**. The horizontal velocity profiles for the three High Lift pumps have uniform velocity

distributions, the choice of reducer type therefore doesn't influence the horizontal velocity distribution for the pipework design that was analysed.

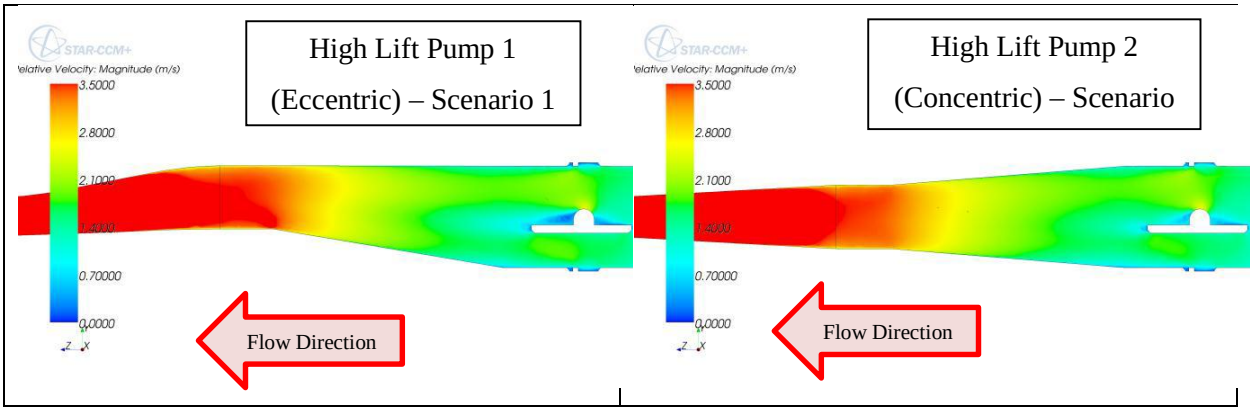

Figure 2.19: High Lift velocity profiles illustrating the vertical acceleration through the different reducer types (Aerotherm 2011)

Booster pumps. Two distinct velocity peaks are present in the vertical velocity profiles of Booster pumps 1 and 2. According to Aerotherm (2011) these peaks are caused by the wake of the upstream butterfly valve extending into the pump. The greater velocity peaks on the top side of Booster pump 2 are due to the flow following the path of the least resistance on the top side of the eccentrically offset butterfly valve. This phenomenon is illustrated in **Figure 2.20**. The different behaviour in Booster pump 3 was concluded by Aerotherm (2011) to be a result from the wake extending from the bypass branch to the pump inlet and therefore cancelling out the effect of the wake from the butterfly valve. The horizontal velocity profiles for the three High Lift pumps have uniform velocity distributions, the choice of reducer type therefore doesn't influence the horizontal velocity distribution for the pipework design that was analysed.

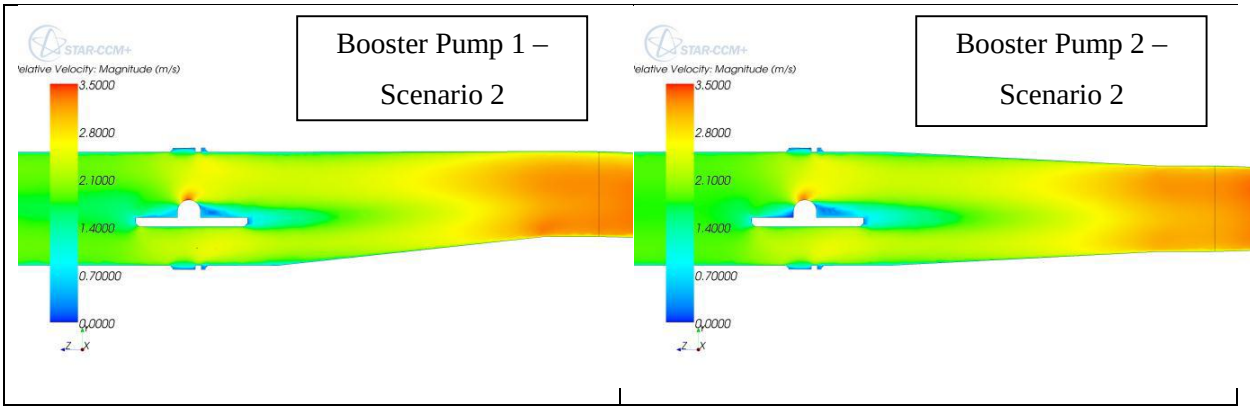

Figure 2.20: Booster velocity profiles illustrating the vertical acceleration through the different reducer types (Aerotherm 2011)

It was concluded by Aerotherm (2011) that the velocity distribution is strongly influenced by the geometry and to a lesser degree the flow rates as the profiles remain similar regardless of the flow rate. Aerotherm further concluded that the **vertical velocity profile for the High Lift pump with the concentric reducer is very evenly distributed**.

2.6. RATIONALISATION OF LITERATURE

The design standards prescribed in ANSI/HI (2009) recommend a concentric reducer to be used for vertical inlet piping design and for horizontal inlet piping designs where there is no potential for vapor accumulation. In the case of potential air vapor accumulation an eccentric reducer is recommended in the horizontal inlet design. Where an eccentric reducer is recommended the flat (horizontal) side of the eccentric reducer is to be located on the top. The concentric reducer is therefore the preferred reducer if vapor accumulation is not possible. This preference is due to the undesirable pressure and velocity differential (flow profile) caused by an eccentric reducer as described throughout this chapter. A pressure differential on a pump's impeller causes radial thrust, which in turn impacts of the pump's service life and maintenance intervals. Excessive radial thrust can cause premature pump failure. **This preference is confirmed by superior performance of the concentric reducer regarding flow profile on the downstream side of the reducer illustrated in all three case studies presented.**

Air or vapor can be hydraulically transported in a pipeline conduit and of is a function of the pipe slope, amount of accumulated air and the flow characteristics of the fluid with the pipeline (Pothof and Clemens 2011; Van Vuuren, et al 2004). Why is the air or vapor not hydraulically transported past a concentric reducer as it is in a pipeline conduit with a specific pipe slope? Air will be transported according to the relationships provided in ***Paragraph 2.4*** and if the concentric reducer's angle and the flow rate through the reducer is such that the air will be transported through the reducer, a more uniform pressure and velocity distribution will be present at the downstream end when compared to an eccentric reducer.

The air present in the pipework at first time start up or after maintenance can easily be removed with a manual bleed-off valve and the remaining sources of air entrapped in the pump suction pipework originates from improper designs or lack of maintenance.

Why do the design guidelines then require the pump suction reducer fitting to be selected to allow for transportability of air and negatively impact on the pump by creating unbalanced forces on the impeller, if there will be no or limited air in the pipework if the suction pipework and inlet structures/fittings are correctly designed and adequately maintained?

The hypothesis of this study is that a correctly designed concentric reducer will not only provide a more uniform pressure/velocity distribution in comparison to an eccentric reducer, but will allow air to be hydraulically transported through the reducer to the pump. This hypothesis is to be tested by numerically modelling a range of both eccentric and concentric reducers with a range of typical design flow rates to asses both the flow profile and the ability to transport air through the reducer.

3. NUMERICAL SIMULATION METHODOLOGY AND SETUP

3.1. BACKGROUND

A CFD simulation (numerical simulation) consists of four distinct processes that are to be completed in a specific order to solve a three dimensional flow problem. The four processes including a brief description of each process as described by Barba (2010) are:

- Mathematical Model – includes a set of partial differential equations, boundary conditions and initial conditions appropriate to describe the three dimensional flow problem;
- Discretization Method – the approximation of each differential operator by an algebraic operator (typical methods include finite difference, finite volume, finite element and spectral methods);
- Numerical Scheme Analysis – analysis of the discretization process to satisfy consistency, stability and convergence; and
- Numerical Solution – calculation of numeric values of the field variables on a set of grid points or point (may be a steady state or an unsteady state problem).

Once the four processes have been completed, the results are to be visualized and reported in a format useful for interpretation. The selection of the CFD process and the inputs into the CFD software are described in this chapter.

Numerous CFD codes are available commercially. The CFD code produced by CD-adapco: STAR-CCM+ Version 8.04.007 was utilized to complete the numerical simulations in this study. STAR-CCM+ is a software package that solves problems involving flow (fluids or solids), heat transfer and stress. The software package consists of the following components: 3D-CAD modeler, CAD embedding, surface preparation tools, automatic preparation tools, physics modeling, turbulence modeling, post processing and CAE (Computer Aided Engineering) integration (CD-adapco 2012). CD-adapco (2012) recommends following a workflow published in the STAR-CCM+ User Guide. This guideline has been linked into a flow chart, **Figure 3.1**, to provide structure to this Chapter.

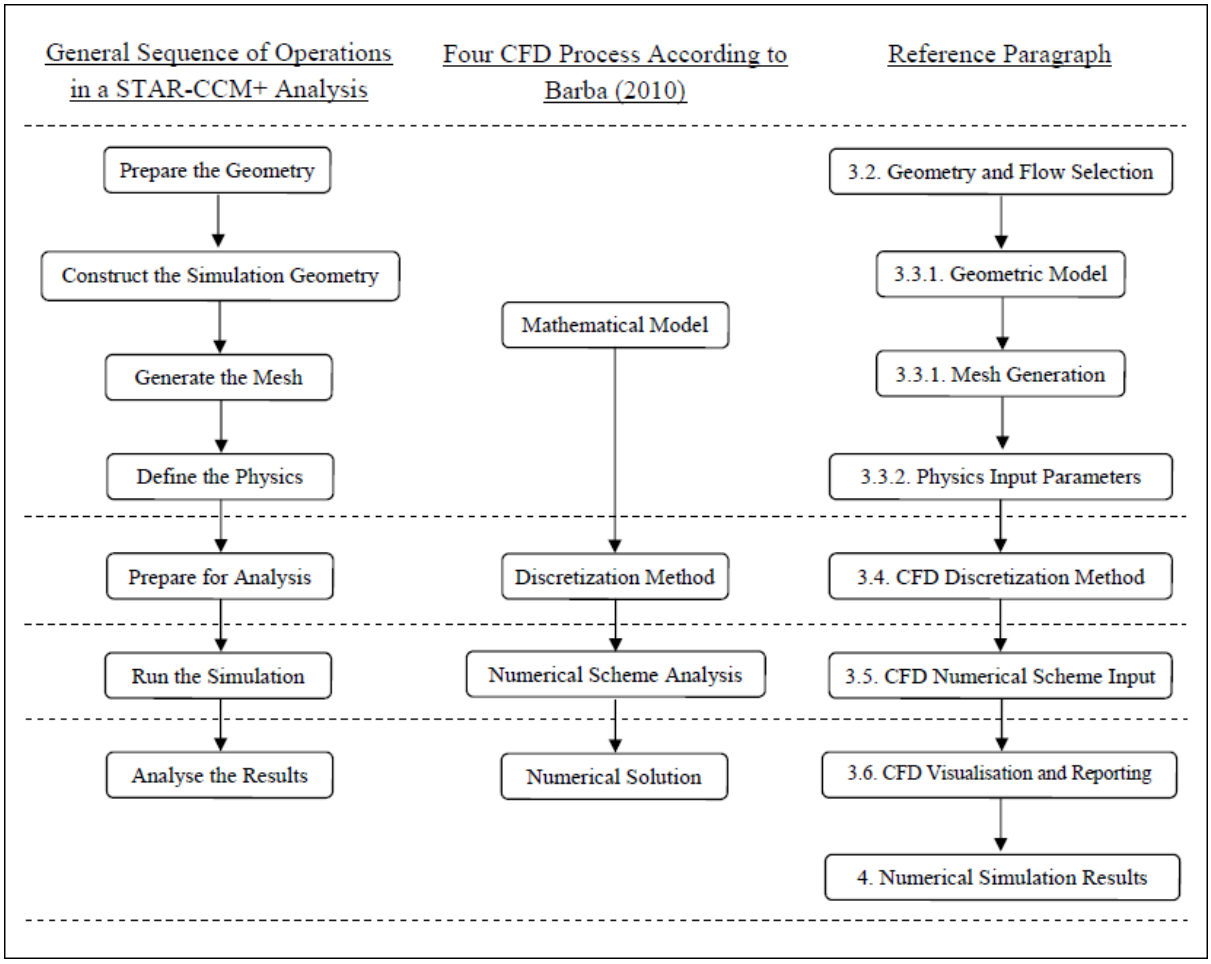

Figure 3.1. STAR-CCM+ Workflow and CFD Methodology

3.2. GEOMETRY AND FLOW SELECTION

In order to set up the mathematical models in STAR-CCM+ the geometries of the reducers are to be created in the 3D-CAD modeler. These reducer geometries are however first to be defined and selected. The principles of concentric and eccentric reducers were introduced in ***Paragraph 1.3.*** and the standard reducer fitting designs were discussed in ***Paragraph 2.3.*** The selection of reducer geometries that provide an accurate representation of the range of standard reducer geometries is required. The reducer angles (°) for the various reducer designs were calculated (**Figure 3.2** illustrates how this calculation was performed) and the results are presented graphically in **Figure 3.3** and in tabular format in **Table B.2** provided in **Appendix B.** From this figure it is observed that the angles are not constant for the fitting manufacturer's designs and that the angles remain constant for the AWWA C208 reducer. The fitting manufacturer's designs present a general trend where the angles are larger for the smaller diameters of reducers and the angles reduce as the diameters increase. The

reducer angles extend from a range of approximately 30° to 2.5° for the eccentric reducers and 20° to 1.5° for the concentric reducers.

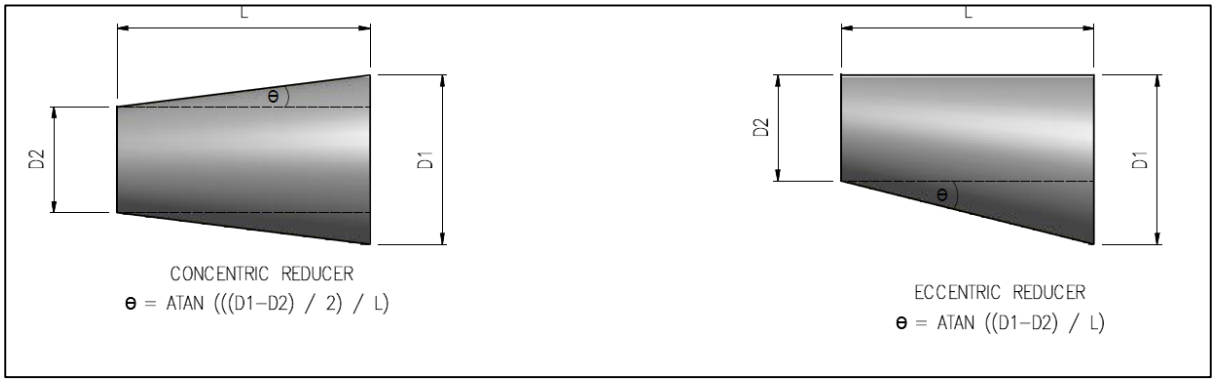

Figure 3.2: Reducer Angle Calculation

In ***Chapter*** 2 the effect of pipe slope (reducer angle) on the pressure and velocity distribution and on the hydraulic transportability of air was discussed. With an **increasing** reducer angle it is hypothesised the uniformity of the pressure and velocity distributions will decrease and the hydraulic transportability of air through the reducer will also decrease. A selection of various reducer angles for both the concentric and the eccentric reducers were modelled to define the extents of these effects that are brought about the change in reducer angle.

The application of a range of constant velocities and not flow rates as inputs in the CFD calculations allows for a single reducer dimension to be modelled, i.e. the flow patterns resulting from a 1 m/s flow rate through a DN 200 to DN 150 reducer will be representative of the flow patterns through a DN 2000 to DN 1500 reducer if the reducer angles are equal. The DN 200 (D1) to DN 150 (D2) reducer was selected as the representative size reducer to be modelled with varying reducer angles. The various reducer geometries selected for the study are summarised numerically in **Table 3.1**. The pipe properties, Outside Diameter (OD), Inside Diameter (ID) and Wall Thickness (t), used in the geometries are the geometries specified in and SANS 62-2 and SANS 719**.** In order to provide flow information resulting from the application of additional straight lengths of pipe requirements as described by ANSI/HI (2009) and to model the effect of the discontinuities at the upstream and downstream ends of the reducer, a straight pipe length of 600 mm (3 x D1) is added to the reducer geometry. Refer to **Figure 3.4** and **Figure 3.5** for illustration of the geometries used to define the mathematical models.

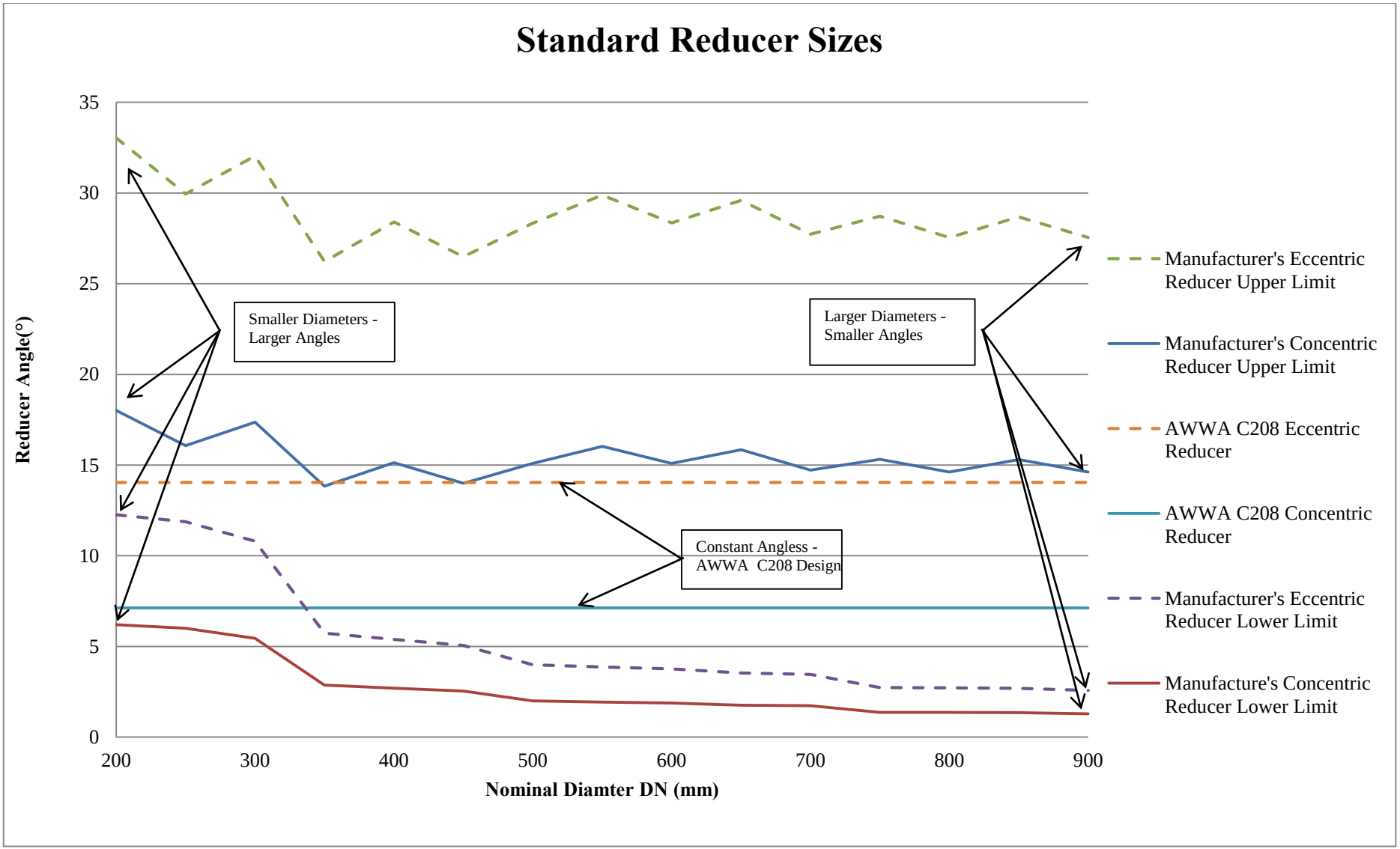

Figure 3.3: Standard Reducer Fitting Angles

Table 3.1: Model Reducer Selection Dimensions and Details

Geometry Name	Reducer Type	D1 (mm)	D2 (mm)	Angle (°)	L (mm)	t (mm)	ID D1 (mm)	ID D2(mm)
ER 30	Eccentric Reducer	219.1	165.1	30	94	4.5	210.1	156.1
ER 20	Eccentric Reducer			20	148			
ER 15	Eccentric Reducer			15	202			
ER 10	Eccentric Reducer			10	306			
ER 5	Eccentric Reducer			5	617			
ER 2.5	Eccentric Reducer			2.5	1237			
CR 20	Concentric Reducer			20	74			
CR 15	Concentric Reducer			15	101			
CR 10	Concentric Reducer			10	153			
CR 5	Concentric Reducer			5	309			
CR 2.5	Concentric Reducer			2.5	618			
CR 2	Concentric Reducer			2	773			

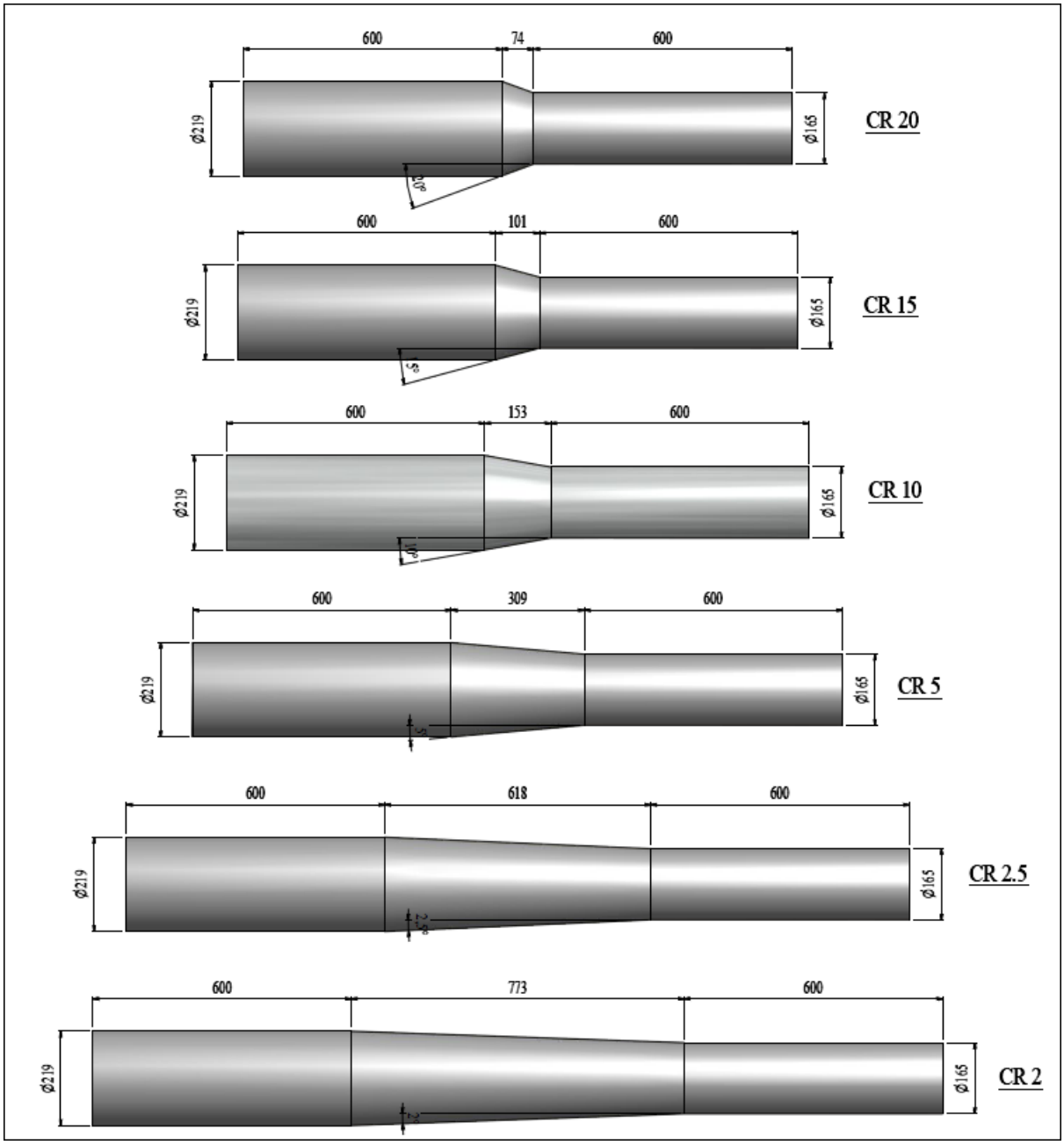

Figure 3.4: Concentric Reducers Geometries

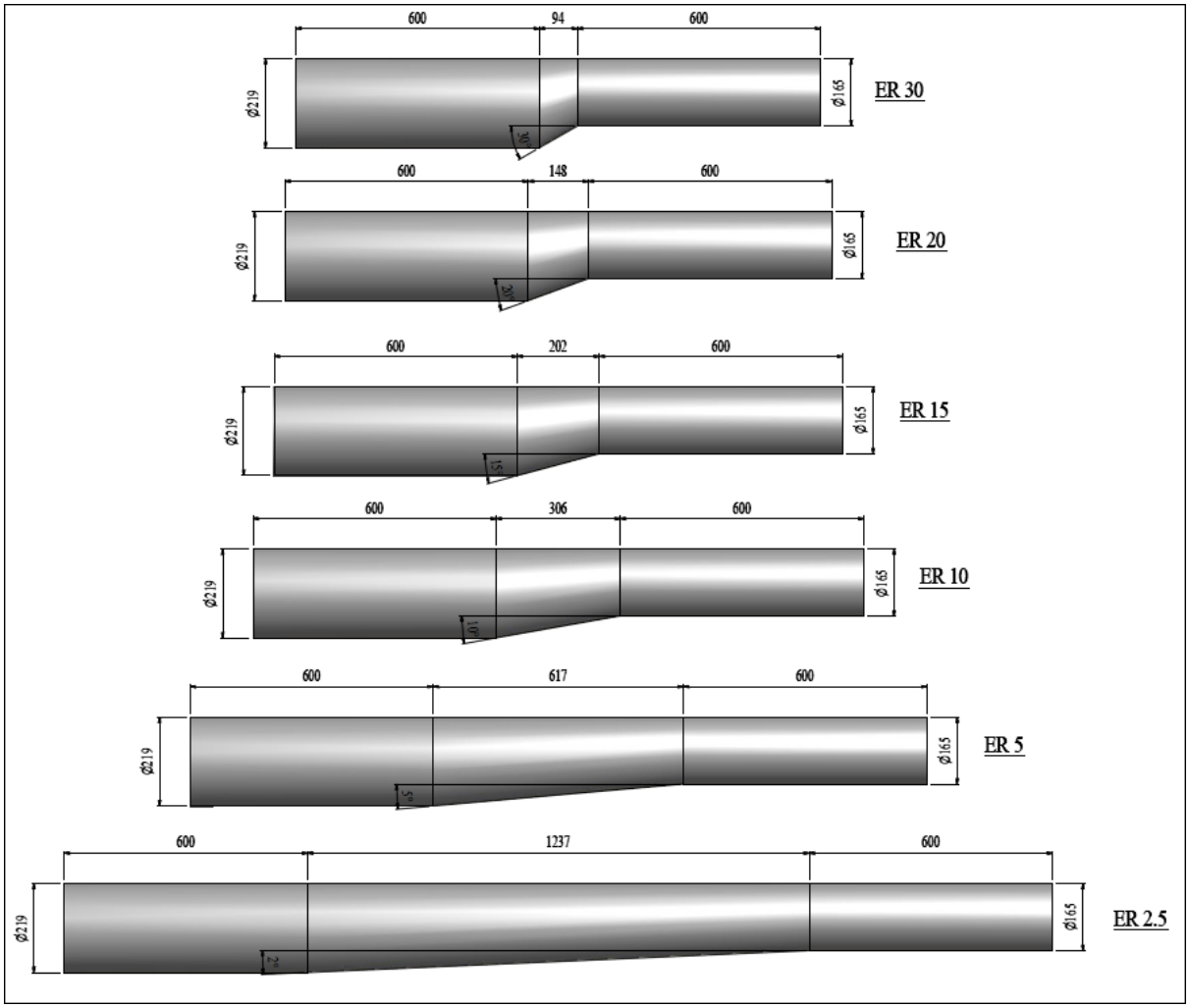

Figure 3.5: Eccentric Reducers Geometries

The flow velocities to be utilised as the velocity inlet conditions of the numerical models were selected with the maximum velocity of 2.4 m/s recommended by ANSI/HI (2009), ANSI/HI (2000) and Jones et al (2008). A maximum suction flow velocity of 2.4 m/s may be considered to be high and not typically used in the bulk water industry. By using the maximum velocity the non-uniform flow profiles will be exaggerated while the hydraulic transportability of air will be at its maximum. The other flow velocities were selected as a range extending from 1 m/s to the maximum velocity of 2.4 m/s (velocities: 1m/s, 1.5 m/s, 2 m/s and 2.4 m/s) to provide a complete result set. The flow rates for this range of velocities were calculated with the inner diameter of the upstream reducer end with the flow rate equation provided in Equation 3-1. The calculated flow rates are tabulated and provided below. Further to the flow rate calculation the Reynolds numbers for the various flow velocities were also calculated with the relationships provided in Equations 3-2 and 3-3. From the Reynolds number calculation it is observed that the flow is in the turbulent flow range (Re>2000). Turbulent flow

models are therefore utilised in the CFD models. The results of the calculations described above are presented in **Table 3.2**.

$$Q = V \times A \tag{3-1}$$

Where:

Q = Flow Rate (m^3/s)

V = Flow Velocity (m/s)

A = Flow Cross Sectional Area (m^2)

$$Re = \frac{\rho u D}{\mu} \tag{3-2}$$

Where:

Re = Reynolds Number

ρ = Density (kg/m^3)

u = Velocity (m/s)

D = Pipe diameter (m)

μ = Viscosity ($N.m^{-2}.s$) (Equation 3-3)

$$\mu = A \times 10^{B/T-C} \tag{3-3}$$

Where:

μ = Viscosity ($N.m^{-2}.s.$)

A = $2.414x10^5$

B = 247.8 (k)

C = 140 (k)

T = Fluid Temperature (K)

Table 3.2: Flow Rate to be Utilised in the Numerical Models

Upstream DN	Upstream ID (mm)	Upstream ID Area (m^2)	Flow Velocity (m/s)	Flow Rate (m^3/s)	Flow Rate (l/s)	Reynolds Number
200	210.1	0.35	1	0.034669	34.67	235951
			1.5	0.052004	52.00	353927
			2	0.069338	69.34	471902
			2.4	0.083206	83.21	566282

3.3. CFD MATHEMATICAL MODEL

3.3.1. Geometric Model

The geometric models were initially envisaged to be created utilizing the built in 3D-CAD module within STAR-CCM+. This module is a feature based parametric solid modeler that enables geometric models to be generated from scratch within STAR-CCM+. A separate geometry file would be created for the concentric reducer setup (the straight length of pipe upstream, the concentric reducer and the straight length of pipe downstream) and for the eccentric reducer (the straight length of pipe upstream, the eccentric reducer and the straight length of pipe downstream). The length of the reducer in both the geometry files was to be modeled as a "design parameter". STAR-CCM+ allows the user to change a design parameter outside of the 3D-CAD module and this enables you to solve for a particular geometry, change the length of the reducer (thereby changing the reducer angle) and re-run the case. If a solution has already been computed, this will be mapped across the modified geometry, thereby decreasing the overall run time (CD-adapco 2012). The first step in creating a geometric model is by creating a sketch. The sketches are lofted from the upstream end to downstream to model the solid body. A lofted feature is a body that is created by transitioning a body between sketches. It is noted that only the internal body of water is modeled and not the pipe, this is illustrated in **Figure 3.6**. This is done such that only the fluid domain is modeled. Once the geometries were modeled in the 3D-CAD module within STAR-CCM+ it was observed that the module does not model the reducer with a uniform angle, but rather includes transition curves; this phenomenon is illustrated in **Figure 3.7**. The built in 3D-CAD module did not provide a method to generate the geometries without the transition curves.

The geometries were alternatively modeled in Autodesk Inventor, where reducers with uniform angle can be modeled and the Autodesk Inventor bodies were exported as Parasolid Text Files (*.x_t) and directly imported in STAR-CCM+. The resultant geometry from the import is a solid part consisting of surfaces and curves. The center of the downstream reducer was modeled in the center (0,0,0) of the

XY plane and this reference point was maintained in STAR-CCM+ throughout all the analyses. The reference planes are illustrated in **Figure 3.8**.

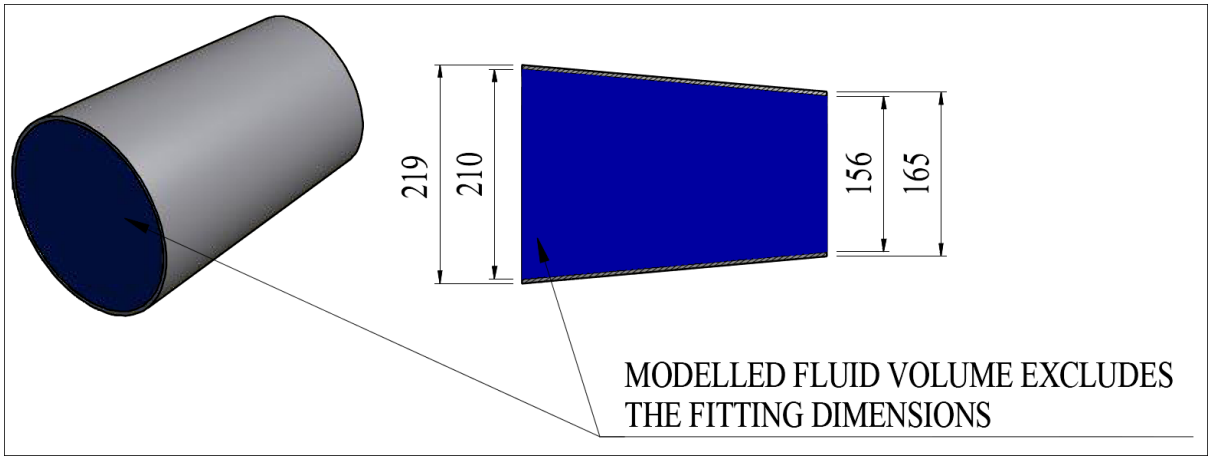

Figure 3.6: Modelled Volume

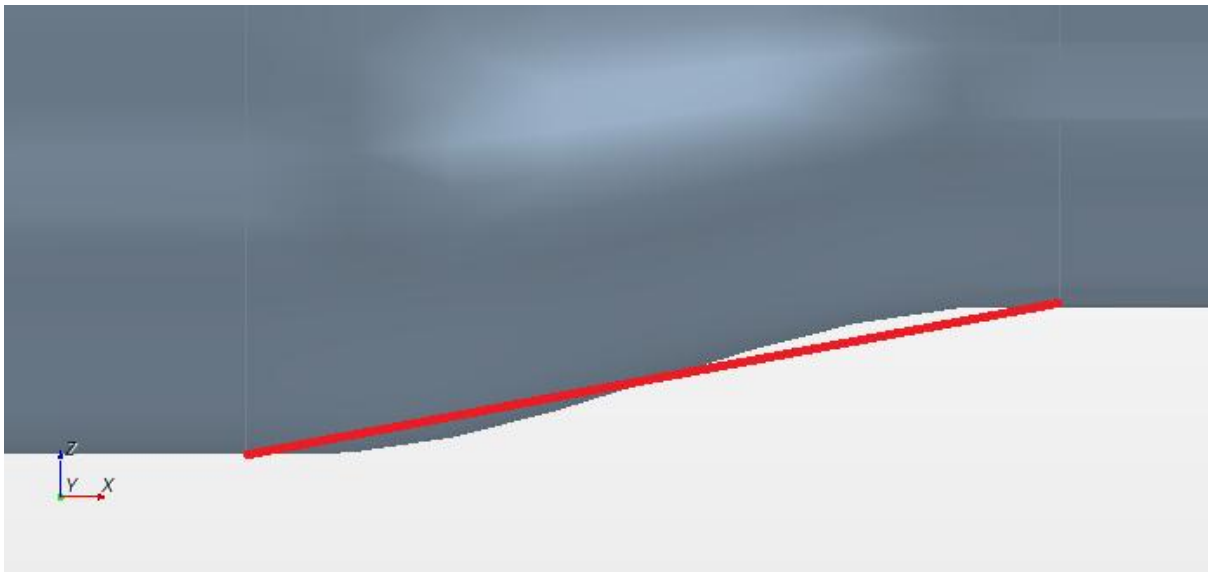

Figure 3.7: Non-uniform Slope Modelled in the Built in 3D-CAD Module

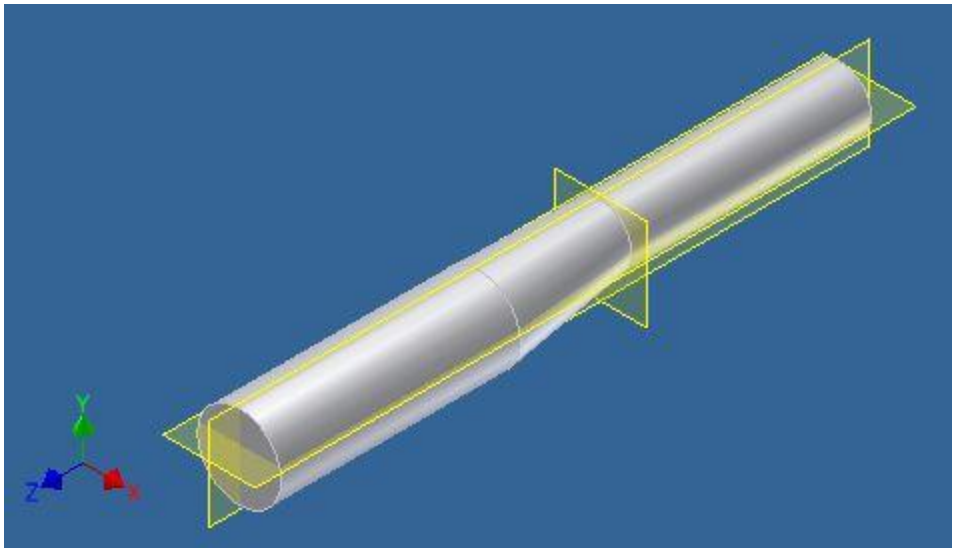

Figure 3.8: Model Together with Reference Planes

During the import process the tessellation density of the imported model was selected as fine. The tessellation density refers to the surface refinement used by STAR-CCM+ when importing geometry and affects the degree to which surface curvature is preserved in the imported model (CD-adapco 2012). The geometry that was modeled is planar and therefore the tessellation density would not have a significant effect on the triangulation of the geometry. An example of the surface tessellation is provided in **Figure 3.9** and is representative of the tessellation of the various models. According to CD-adapco (2012) it is good practice to check the validity of the geometries' surfaces before a geometry is converted to a mesh. The *Surface Preparation* tool was utilized to provide diagnostic checks for assessing the validity of the surfaces. The only diagnostic errors that were found during the surface preparation were isolated cases of *Face Quality*, but according to CD-adapco (2012) if the surface wrapper or surface remesher is utilized during meshing of the geometry, poor quality faces do not usually cause a problem. These errors were therefore disregarded.

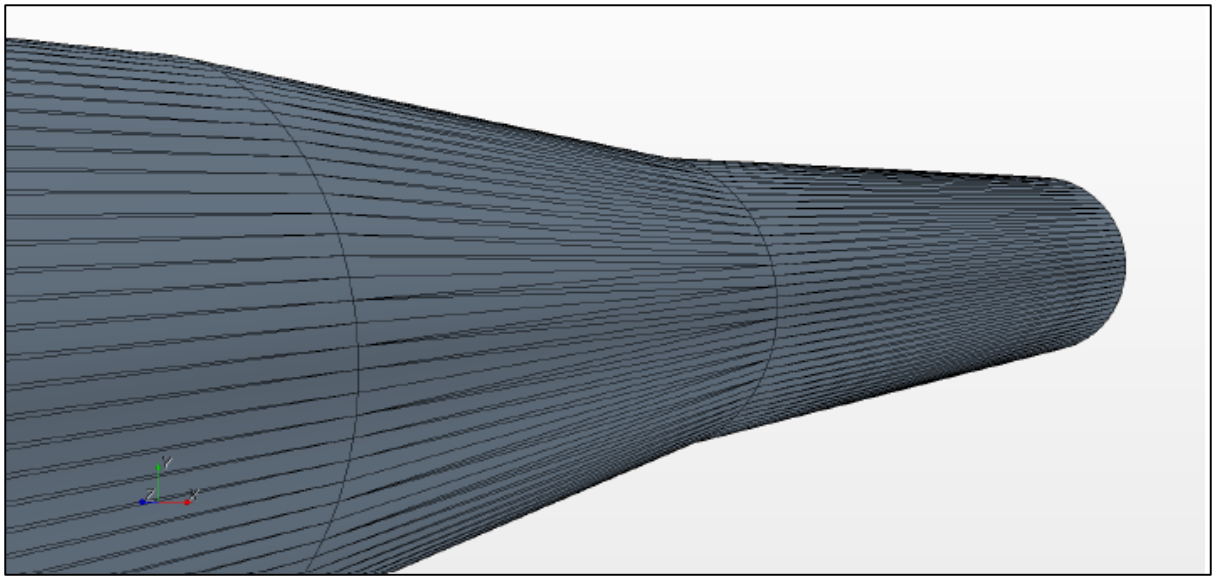

Figure 3.9: Tessellation Example

The geometries and model were named with the same naming convention used in **Table 3.1**. The geometry faces of the models were also named. The names of the various faces are:

- Upstream face: US End – Velocity Inlet;
- Downstream face: DS End – Pressure Outlet; and
- Pipe fluid: Fluid Wall.

Each named face was assigned as a boundary with an identical name to those mentioned above. Each boundary was assigned to a specific boundary type. These assignments are discussed further in ***Paragraph 3.3.3.3***.

3.3.2. Mesh Generation

3.3.2.1. Introduction

The CR 10 Model geometry was selected to be used as the model where all the CFD inputs would be tested and refined before the remainder of the models are imported and set up. This workflow is illustrated below in **Figure 3.10.** The built-in STAR-CCM+ tools were used to generate a volume mesh for the CR 10 model from the imported model's surface. This mesh was utilized to assess and refine the quality of the mesh utilizing the settings described below and then by running the CFD solver to determine if the solution converges. The computing time required to generate the mesh and to reach the CFD solution was also assessed. If required the mesh input values (e.g. Base Size) would be changed and the solver would be run again until a converged solution is obtained in a reasonable

computing time. The correct mesh settings and input values would then be used to generate the meshes for the remaining model geometries. The results from the initial run(s) of the CR 10 Model are reported in ***Paragraph 3.7***.

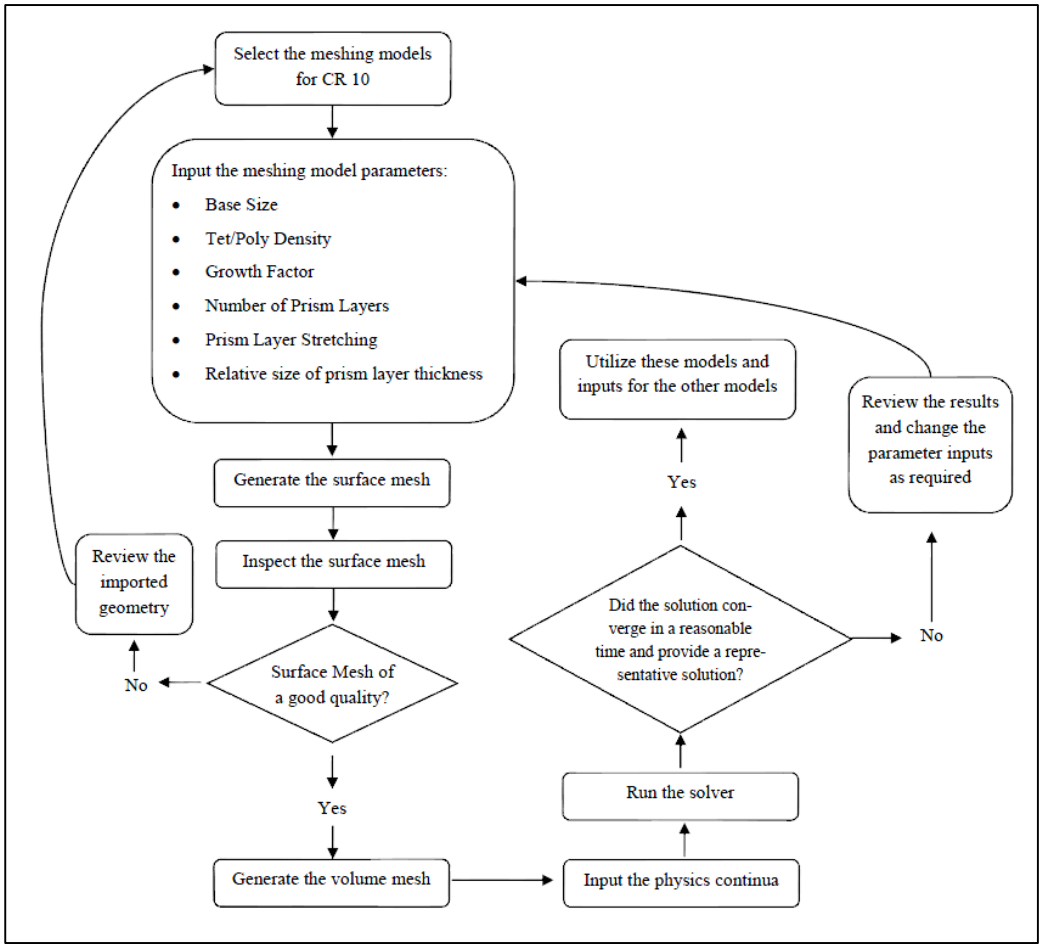

Figure 3.10: CR 10 Model Workflow Diagram

As stated in ***Paragraph 3.3.1*** the surface remesher was used to improve the surface quality and eliminate the *Face Quality* errors found in the diagnostic checks. The quality of the mesh has significant implications on the accuracy of the CFD solution and the stability and convergence of the analysis (Tu, Yeoh and Liu, 2008). Volume meshes can contain trimmed-, polyhedral- or tetrahedral-type cells for a certain mesh region (CD-adapco, 2012), but due the simplicity of this study's model geometries, only one region is defined for each geometry and therefore only one volume mesh type is used per model.

STAR-CCM+ provides various meshing models that can be selected for a CFD simulation. These models are to be selected to suit the specific problem. According to CD-adapco (2012) a polyhedral mesh generated with the generalized cylindrical mesher is suited to pipe flow. The following meshing models were therefore selected:

- Surface Remesher
- Polyhedral Mesher
- Prism Layer Mesher
- Generalized Cylindrical Mesher

Brief explanations on the selection of the various meshing models together with input parameters are provided below. Further details on the selection of these input parameters is provided in **Appendix C** where the summary report for the CR 10 model is provided. The surface mesh was created prior to the generation of the volume mesh (prism layer and the generalized cylinder). This surface mesh was inspected to determine the quality of the mesh as a high quality surface mesh is required before the volume mesh is generated.

3.3.2.2. Meshing Models

Surface Remesher. A high quality starting surface geometry will result in a high quality volume mesh. The surface remesher re-triangulates a closed starting surface in order for a higher quality surface to be obtained (CD-adapco 2012). The surface remesher is used in instances where the imported surface is of extremely poor quality. In this study this not the case, but its application will remove the *Face Quality* errors observed in the diagnostic checks. The surface mesh for CR 10 is illustrated in **Figure 3.11** below.

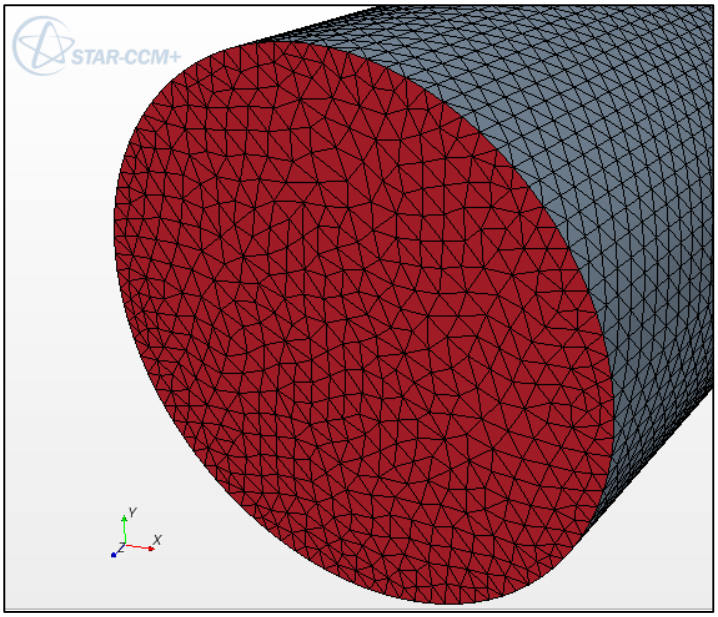

Figure 3.11: CR 10 Model Surface Mesh

Polyhedral Mesher. Polyhedral type cells (and trimmed type cells) produce a more accurate solution when compared to a tetrahedral mesh and provide a balanced solution for complex mesh generation problems (CD-adapco 2012). STAR-CCM+ utilizes an arbitrary polyhedral cell shape in order to build the *core mesh*, the polyhedral cells typically contain an average of 14 cell faces (CD-adapco 2012). When used in conjunction with the generalized cylinder mesher extruded orthogonal cells along the length of the cylinder are generated. The polyhedral cells and their position are illustrated in **Figure 3.12**. According to Tu, Yeoh and Liu (2008) the base size must be adequately small to provide an adequate resolution of flow features and the model geometry (pipe layout). The input parameters for the polyhedral mesher utilised in the CR 10 Model are provided in **Table 3.3** below.

Table 3.3: Polyhedral Mesh Model Input Parameters

Parameter	Value
Base Size	5 mm
Tet/Poly Density	1.0 (Default Value)
Growth Factor	1.0 (Default Value)

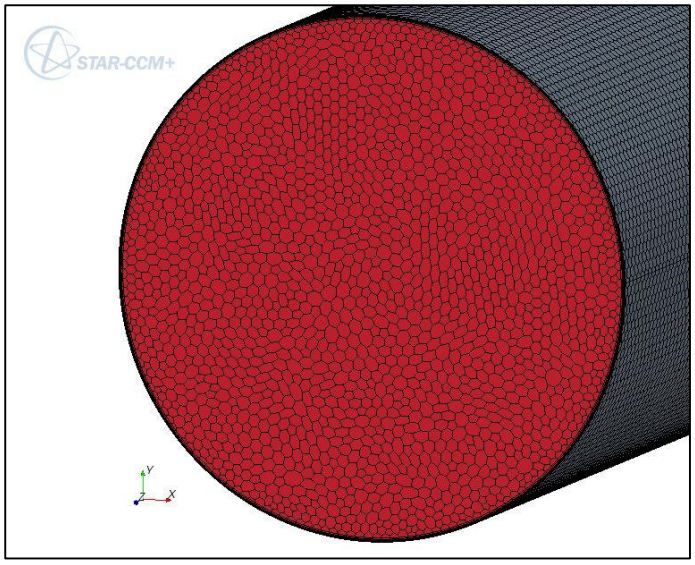

Figure 3.12: CR 10 Model Volume Mesh Showing the Polyhedral Cells and the Prism Layer

Prism Layer Mesher. Tu, Yeoh and Liu (2008) recommend that geometries with flows within bounded walls have locally refined or clustered mesh in the vicinity of the wall boundaries to ensure that the viscous boundaries are properly resolved. The prism layer mesher is used with a core volume (generated by the polyhedral mesher) to generate orthogonal prismatic cells next to wall boundaries in order to improve the accuracy of the flow solution (CD-adapco 2012). The prism layer is defined by its thickness, number of cell layers and the size distribution of the cells. According to CD-adapco (2012) the use of prism layers greatly enhances accuracy of a solution as a result of the intended consequence of aligning the flow with the mesh. The prism layer cells and their position are illustrated in **Figure 3.12**. According to CD-adapco (2012) a layer consisting of 10-20 prism layer cells (depending on the Reynolds number) in the cross-stream direction of the flow, is required for accurate resolution of the turbulent flow profile at the turbulent shear layer. The input parameters for the prism layer mesher utilised in the CR 10 Model are provided in **Table 3.4** below.

Table 3.4: Prism Layer Mesh Model Input Parameters

Parameter	Value
Number of Prism Layers	10
Prism Layer Stretching	1.5 (default)
Relative size of the prism layer thickness	33.3% of base size (default)

Generalized Cylinder Mesher. An extruded mesh is generated along the length of the parts that represents cylinder type structures. According to CD-adapco (2013) the generalized cylinder meshing model is best suited to flow conditions where the flow direction is parallel to the vessel wall and the fluid flows in roughly cylindrical sections along the geometry. This type of fluid flow represents the fluid flow in this study and therefore this particular model is selected. In order to generate the generalized cylinder mesh the boundaries for the cylinder were defined (the defined boundary is *Fluid Wall Boundary*).

3.3.3. Physics Input Parameters – Pressure Distribution Models

3.3.3.1. Introduction

The physics were modelled in the Physics Continua in STAR-CCM+, where the physics are divided into the following distinct models for the physics representing this study:

- Space
- Time
- Material
- Flow
- Equation of State
- Viscous Regime
- Reynolds – Averaged Turbulence
- Optional Models

Brief explanations on the selection of the various physics models together with input parameters are provided below. In addition to the selection and input values for the physics models, the boundaries of the geometric models are to be defined. The definitions and selection of these boundaries are discussed after the description pertaining to the physics models.

3.3.3.2. Physics Models

Space. According to CD-adapco (2012) the function of the selected space model is to provide methods for computing and accessing mesh metrics (cell volume and centroid, face area and centroid, cell and face indexes and skewness angle). The space model that would accurately model the geometry is the *Three-Dimensional* space model, as the remaining models are only suitable for two-dimensional models or where the model thickness is sufficiently small that it can be considered a surface with a single cell's thickness in the normal direction (Shell Three-Dimensional Model).

Time. The time physics model controls the iteration and/or time stepping of the solver. For the pressure distribution models there is no time step required, therefore the *Steady* time model was selected.

Material. The material model controls the definition of the substances being analyzed, liquid in the case of this study. The selected material in turn (water in the case of this study) is responsible for managing the various properties (i.e. transport properties) relative to that material. By default the *Liquid* model selects the liquid material water from the material database.

Flow. CD-adapco (2012, p. 2659) provided the following suggested flow model selection procedure:

i. Choose the Coupled Flow and Coupled Energy models for compressible flows, natural convection problems and flows with large body forces or energy sources;
ii. If computational resources are not an issue, choose the Coupled Flow model for incompressible and/or isothermal flows; and
iii. Choose the Segregated Flow model for incompressible or mildly compressible flows.

Option iii, *Segregated Flow*, was selected to represent the incompressible water flow.

Viscous Regime. The flow being modelled is viscous and is in the turbulent zone, see **Table 3.2**. Therefore the *Turbulent* viscous regime was selected. By selecting the *Turbulent* viscous regime the Reynolds-Averaged Navier-Stokes (RANS) turbulence model was auto selected by STAR-CCM+ as a recommended model. The two other available turbulence models are only applicable if the following models are selected: *Three Dimensional model*, *Implicit Unsteady model* and *Segregated Flow model*

.

Equation of State. According to CD-adapco (2012) the equation of state model is used to compute the density and density derivatives relating to temperature and pressure. Temperature does not form part of this study and the change in density of the water will be insignificant due to the pressure loss experienced in the pump inlet piping. The *Constant Density* model was selected to model the equation of state.

Reynolds-Averaged Turbulence. According to CD-adapco (2012) a model needs to be selected to provide closure to the RANS equations and it has bee indicated that it is widely recognized that the Reynolds-Averaged Turbulence models are inexact representations of the physical occurrences being modelled and that no single model is best suited for every flow problem encountered, it is therefore required to select a Reynolds-Averaged Turbulence model that is best suited to the problem presented in this study. CD-adapco (2012, pp. 3008-P3009) provided the following suggested turbulence model selection procedure:

i. **Spalart-Allmaras models –** A good selection if the applications in which boundary layers are largely attached and separation is mild if it occurs. Typical examples would be flow over a wing, fuselage or other aerospace external-flow applications.
ii. **K-Epsilon models** – provide a good robustness, computational cost and accuracy. They are generally well suited to industrial-type applications that contain complex recirculation, with or without heat transfer.
iii. **K-Omega models** – Are similar to the K-Epsilon Models and the performance differences are likely to be a result of subtle differences in the models, rather than a higher degree of complexity in the physics being captured. These models have seen most application in the application in the aerospace industry and are recommended as an alternative to the Spalart-Allmaras models.
iv. **Reynolds stress transport models** – Are the most complex models and computationally expensive models offered in STAR-CCM+. They are recommended for situations where the turbulence is strongly anisotropic, such as swirling flow in a cyclone separator.

The *K-Epsilon* model was selected for this study as it provided a lower computational cost and was well suited to the flow properties of the study. The *K-Epsilon* model is a two-equation model in which the transport equations are solved for the turbulent kinetic energy (k) and it's energy dissipation rate (Ɛ) and is the most widely used model for industrial applications (CD-adapco 2012). STAR-CCM+ provides a choice of seven different *K-Epsilon* models, the selection of these models is discussed in ***Paragraph 3.4.1.***

No further input values were entered and changed regarding the selection of the physical models and no optional models were selected to model the physics. The final selection of the physics models is illustrated in **Figure 3.13**.

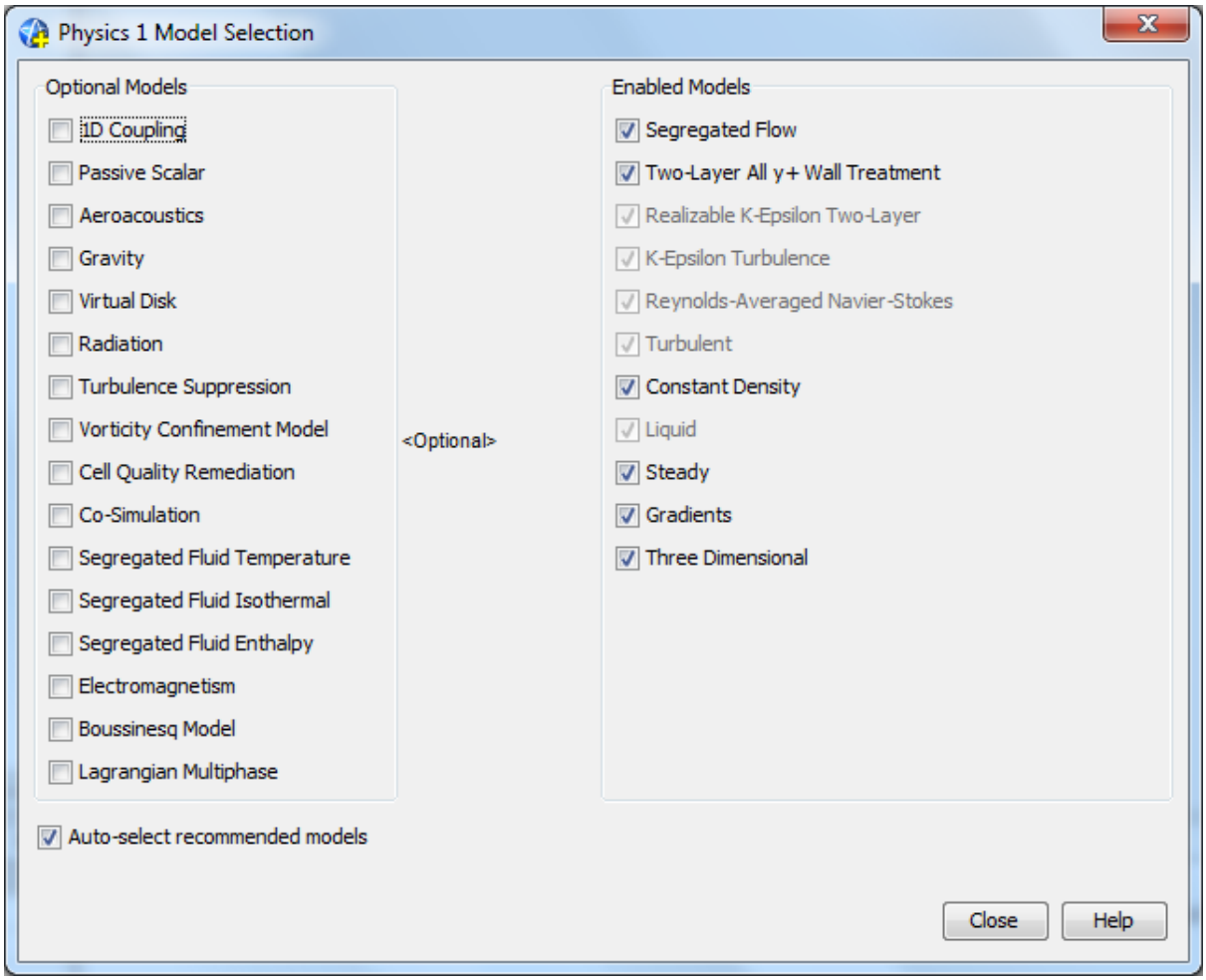

Figure 3.13: Physics Model Selection

3.3.3.3. Boundary Conditions

Appropriate boundary conditions that represent the real physical fluid flow conditions are required to be selected in the CFD software. It was previously stated that each named face was assigned to a specific boundary type identical to the name of the face. The boundary types selected to represent the fluid flow problem are: Velocity Input, Pressure Outlet and Fluid Wall. The locations of these boundary conditions are illustrated in **Figure 3.14**.

These boundary types were selected from the nine different user selectable boundary types recognized by STAR-CCM+ and the full list of available boundary conditions are:

- Axis
- Flow Split Outlet
- Free-stream
- Mass Flow Inlet
- Pressure Outlet
- Stagnation Inlet
- Symmetry Pane
- Velocity Inlet
- Fluid Wall

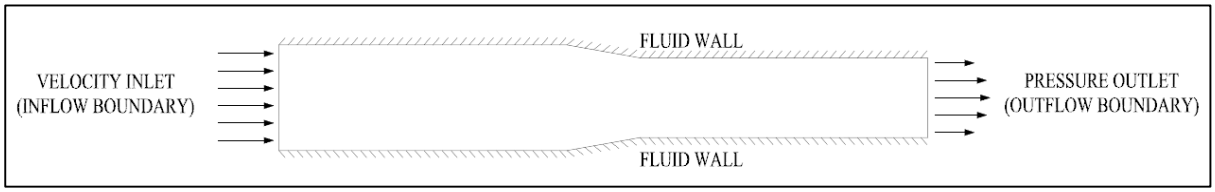

Figure 3.14: CFD Model Boundary Conditions

Descriptions and input parameters for the selected boundary types are provided below. No interface boundaries (connections between boundaries used during the meshing setup and/or analysis process that allow mass, energy and other physical quantities to pass from one region to another) were required due to the nature and shape of the geometry, as there is only one region present.

Velocity Inlet. A velocity inlet boundary represents the inlet of a duct where the flow velocity is known and is applicable to the inlet of a simulation of incompressible internal flows (CD-adapco 2012). This boundary type was selected for the inflow boundary (upstream end) of the model and represents normal flow conditions entering the pipe perpendicular with a constant velocity that is supplied as input parameter (see **Figure 3.14**). According to CD Adapco (2012) this type of boundary may be used in combination with a pressure outlet boundary. The initial flow velocity (see **Table 3.2** for velocities modelled, 1.5 m/s was utilized in the CR 10 model to assess convergence) was entered into both the Velocity Inlet Boundary Condition Physics Value – Velocity magnitude and the Physics Continuum Initial Condition – Velocity ([0.0, 0.0, -1.5] m/s). By entering the initial flow

velocity for the Physics Continuum Initial Condition – Velocity in addition to the Velocity Inlet Boundary Conditions the entire fluid domain has an initial velocity equal to the velocity at the inlet thereby assisting in the numerical solution procedure and thereby decreasing the simulation time.

Pressure Outlet. A pressure outlet boundary is a flow boundary at which the pressure is specified and is applicable to the outflows of compressible and internal flows (CD-adapco 2012). This boundary type was selected for the outflow boundary (downstream end) and represents a uniform constant pressure at the outlet that is supplied as an input parameter (see **Figure 3.14**). The constant physics value for the Boundary Condition Physics Value – Pressure and the Physic Continuum Initial Condition – Pressure was set to 150 000 Pa (150 kPa) to provide a back pressure for the model. This value was selected as it represents a typical Net Positive Suction Head (NPSH) requirement for centrifugal pumps. By entering the initial pressure for the Physics Continuum Initial Condition – Pressure in addition to the Pressure Inlet Boundary Conditions the entire fluid domain has an initial pressure equal to the pressure at the outlet thereby assisting in the numerical solution procedure and therefore decreasing the simulation time.

Fluid Wall. A wall boundary represents an impermeable surface and is applicable as an impermeable boundary for inviscid flows and as an impermeable, no-slip boundary for viscous flow simulations (CD-adapco 2012). The position of the fluid wall is provided in **Figure 3.14**. A roughness value was added to the fluid wall to enable near wall turbulence and thereby apply friction to the model in order accurately model the pipework. This was achieved by changing the default Wall Surface Specification under the Physics Conditions of the Fluid Wall to Rough and then entering a constant roughness height of 0.00 006 m for the Roughness Height under the Physics Values of the fluid wall. The remaining Wall Roughness Parameters were not altered. The value of 0.00 006 m (0.06 mm) is the roughness value provided by Wallingford and Barr (2006) for an epoxy lined steel pipe in a normal condition, which is typically the type of fitting lining used in water pump stations in South Africa.

3.4. CFD DISCRETIZATION METHOD

3.4.1. Discretization Method Selection

The CFD discretization method selection describes the selection of the *CFD solver* used to compute and solve the underlying equations describing the fluid flow problem at hand. This procedure of solving the fluid flow requires the iterative solution of to the discrete values of the fluid flow properties such as the velocity and pressure (Tu, Yeoh and Liu, 2008)

The K-Epsilon models were selected for the analysis as they provide a good robustness, computational cost and accuracy as discussed previously. Various K-Epsilon models are available and STAR-CCM+ provides a choice of seven different K-Epsilon turbulence models, namely (CD-Adapco 2012, pp. 3073-3074):

- Standard K-Epsilon
- Standard Two-Layer K-Epsilon
- Standard Low Reynolds Number
- Realizable K-Epsilon
- Realizable Two-Layer K-Epsilon
- Abe-Kondoh-Nagano Low-Reynolds Number
- V2F Low-Reynolds Number

The selection of the K-Epsilon turbulence model is determined by the wall treatment (near wall modeling assumptions), Reynolds number and the coarseness or the fineness of the mesh. CD-Adapco (2012) provide the following recommendations regarding the choice of model:

i. The **Standard K-Epsilon model** and the **Realizable K-Epsilon model** are suitable for coarse meshes, where the wall-cell y^+ values are typically 30 and above.
ii. The **Standard Two-Layer K-Epsilon model** and the **Realizable Two-Layer K-Epsilon model** offer the most mesh flexibility. They can be utilized on a wide range of y^+ values (all-y^+).
iii. The **Standard low-Reynolds number model, Abe-Kondoh-Nagano low-Reynolds number model** and the **V2F low-Reynolds number model** are recommended for truly low-Reynolds number applications.

Two-Layer All y+ Wall Treatment and ***Realizable K-Epsilon Two-Layer*** was automatically selected by STAR-CCM+ on selection of the K-Epsilon turbulence model selection. This selection corresponds to the guidelines described above and was not changed in the study.

3.4.2. Discretization Method Input Parameters

The two-layer models allow the K-Epsilon model to be applied in the viscous sublayer and in this approach the computation is divided into two layers. According to Cd-Adapco (2012) in the layer next to the wall, the turbulent dissipation rate (ε) and the turbulent viscosity (μ), are specified as functions of wall distance. The values of ε specified in the near wall layer are blended smoothly with the values

computed from solving the transport equation far from the wall. The equation for turbulent kinetic energy is solved in the entire flow.

The **Two-Layer All y+ Wall Treatment** combines the standard K-Epsilon model with the two-layer model. The coefficients in the models are matching and this model gains the flexibility of on all y^+ wall treatment when compared to the standard K-Epsilon model. The standard K-Epsilon model is the industry standard version of the two-equation model that involves the transportation equations for the turbulent kinetic energy κ and its dissipation rate ε. None of the properties (both standard and expert) were changed when setting up this discretization method of the numerical model.

The **Realizable Two-Layer K-Epsilon Model** combines the Realizable K-Epsilon Model with the two-layer approach. The coefficients in the models are matching and this model gains the flexibility of an all y+ wall treatment when compared to the standard Realizable K-Epsilon model. According to Cd-Adapco (2012) the realizable K-Epsilon model contains a new transport equation for the dissipation rate ε and a critical coefficient of the model, C_u, is expressed as a function of mean flow and turbulence properties, rather than assumed as constant as in the standard K-Epsilon model. CD-Adapco further describes the Realizable K-Epsilon model as being substantially better than the standard K-Epsilon Model for many applications and generally provides solutions that are at least as accurate as the standard K-Epsilon model. None of the properties (both standard and expert) were changed when setting up this discretization method of the numerical model.

3.5. CFD NUMERICAL SCHEME INPUT

CFD software programs solve the numerical model's transportation equations to satisfy the boundary conditions entered in the model by using iterative procedures. Knowledge of when this procedure has converged to an acceptable solution is required in order for the solver to stop iterating. STAR-CCM+ provides a residual plot while running a simulation, but CD-Adapco (2012) advises that engineering values are also to be monitored to provide an additional check on the solution progress. Residuals represent the degree to which the discretized equation is not completely satisfied, in a perfectly converged solution the residual in each cell would be equal to the machine round-off (CD-Adapco 2012). The residual monitors provided from the solutions in this study provide a gauge to measure the progress of the solution by reporting on the global quantity for each of the transport equations that is solved.

CD-Apdaco (2012) provides the following limitations on the use of residuals to judge convergence (or divergence):

- The amount a residual decreases is dependent on the particulars of the specific simulation and the acceptance of the decrease therefore also depends on the simulation (i.e. a three order of magnitude drop in residuals may be acceptable for one simulation, but not for another); and
- Residuals do not necessarily relate to quantities of interest in the simulation, velocity and pressure in the case of this study.

The use of engineering quantities and the residual plots are therefore used together to define the stopping criterion or a stopping criteria can be set to a certain number of iterations. The default stopping criteria for STAR-CCM+ is 1000 iterations. For the purpose of this study the philosophy to select a stopping criteria is based on the residual plot observed for the CR 10 model (utilizing the stopping criteria default) where the convergence was monitored and the mass flow rate at the upstream end is compared to the mass flow rate at the downstream to ensure the model is correctly balanced (flow in = flow out).

3.6. CFD VISUALISATION AND REPORTING

In order to visualize the velocity magnitude through the pump inlet pipework two scalar scenes were created. The first scene was created on the X-Y plane at the downstream end of the reducer, this scene allows for the visualization of the simulation velocity results. The second scene was created on the Y-Z plane to visualize the propagation of a velocity (pressure) differential (if any) through the reducer. The locations of the velocity scalar scenes are provided in **Figure 3.15**. All of the generated scalar scenes are provided on the ***Supporting Digital Media***.

Further to scalar scenes created to visualize the flow through the reducer, X-Y Plots of the velocity were generated along both the X Axis and Y Axis of the pipe at four different positions (probe positions). The X-Y velocity plots were generated at these four probe positions starting at the downstream end of the reducer at Probe Position 1 and then at intervals of 1xD2 (downstream diameter) ending at Probe Position 4. The locations of the four probe positions and orientation of the line probes along the X Axis and Y Axis are illustrated in **Figure 3.15** below. The X-Y Plots were created by creating a line probe derived part along the required axis at the probe position, referencing this derived in the X-Y Plot and then exporting the data where it could be utilized to produce charts outside of the STAR-CCM+ environment. Each line probe recorded the velocity at 100 positions. This

data could then be used to compare the results to the criteria provided by HR Wallingford (Sinotech CC 2005) in ***Paragraph 2.2.***

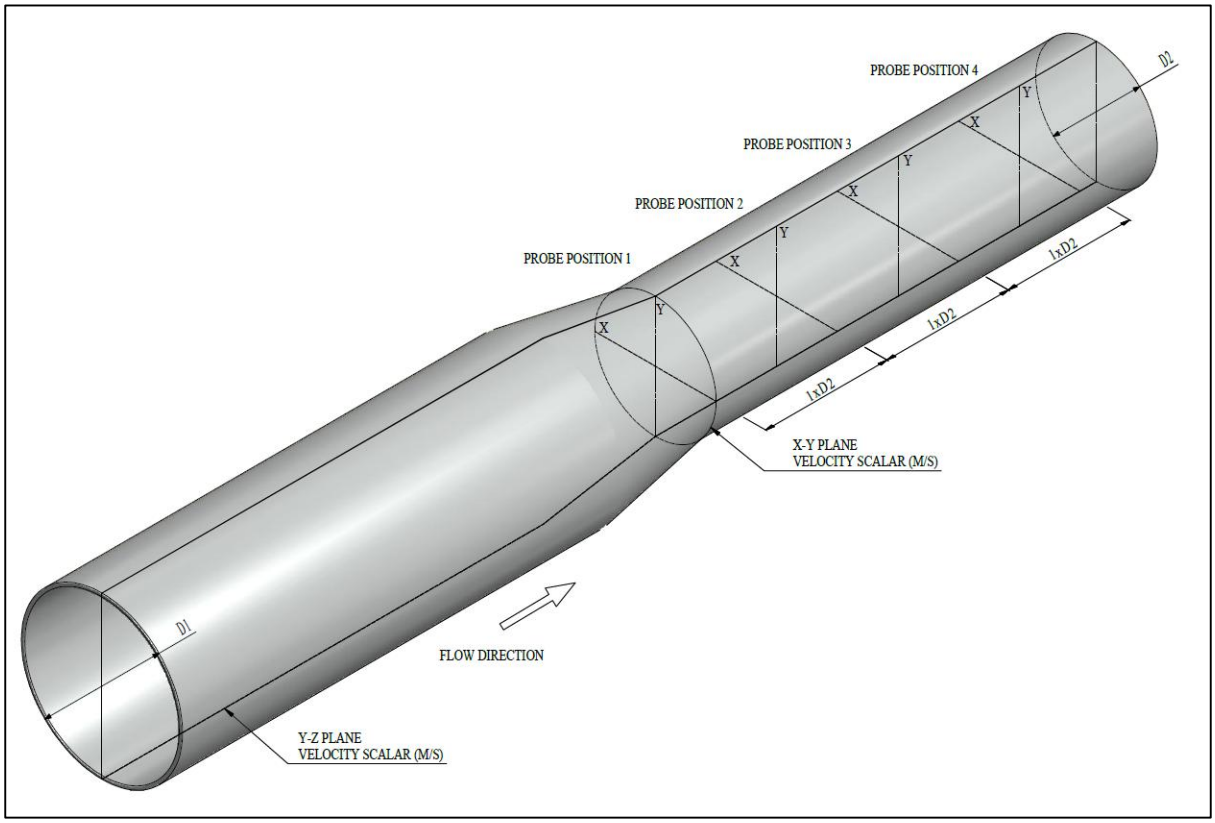

Figure 3.15: Orientation of the Scalar Scenes and Locations of the Probe Positions

Threshold plots of the Cell Centroid of the meshes were created to allow for the inspection of individual mesh cells. This plot provides a three dimensional representation of the mesh cells that allows the user to inspect the overall structure of the mesh. This type of plot was not created for all the analyses, but only those that required the in depth inspection of the mesh cells.

When a simulation is run in STAR-CCM+ a Residuals Plot is automatically generated. The Residuals Plot is useful for judging convergence (or divergence) of a solution (CD-adapco, 2012). The residual values that are plotted by STAR-CCM+ are:

- Continuity;
- X-momentum;
- Y-momentum;

- Z-momentum;
- Tke (Turbulent Kinetic Energy); and
- Tdr (Turbulent Dissipation Rate).

These Residual Plots were reviewed to assess convergence and are included in the results an all of the generated residual plots are provided on the ***Supporting Digital Media***.

A Summary Report in **.html* format containing the Session Summary, Software Summary, Hardware Summary, Simulation Properties (consisting of all the Part data, Mesh data, Physics data, Regions data, Derived Parts, Solvers data and Stopping Criteria) and Solution data was generated for each analysis. All of these Summary Reports for various analyses performed are provided on the ***Supporting Digital Media***.

3.7. REVIEW AND REFINEMENT OF INITIAL CR 10 MODEL

The CR 10 Model was set up and analyzed with all the settings and inputs as described in the paragraphs above. The Threshold Plot of the model is provided in **Figure 3.16** and **Figure 3.17** below. From these figures the length vs. width ratio of the cells is noted (cell length in direction of flow is approximately 14 mm). The generalized cylinder model generates longer type polyhedral cells when compared to the polyhedral model alone. This may affect the results closer to the wall and at discontinuities in the pipe fittings as the mesh is coarser in the flow direction than the original polyhedral base cell input size of 5 mm.

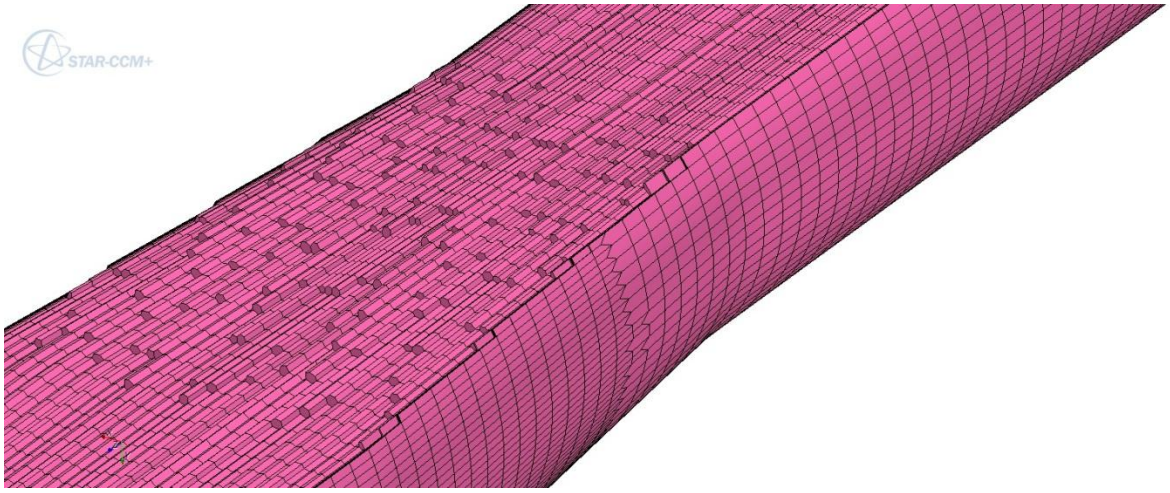

Figure 3.16: CR 10 Model Cell Centroid Threshold Plot

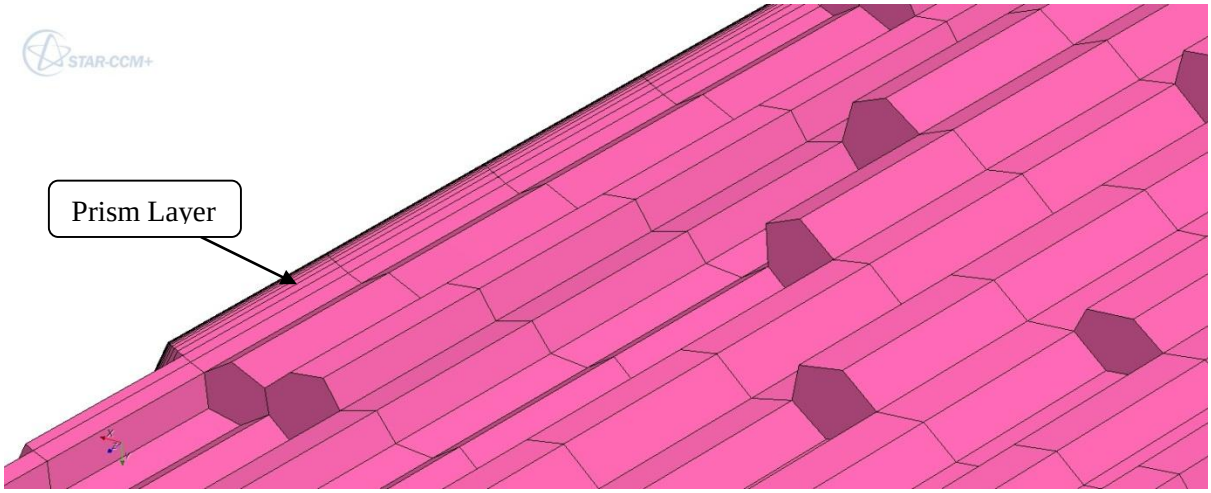

Figure 3.17: CR 10 Model Cell Centroid Threshold Plot Showing the Prism Layer

The Residuals Plot, X-Y Plane Scalar Scene and the Y-Z Plane Scalar Scene are provided below (**Figure 3.18** to **Figure 3.20**). The two Scalar Scenes illustrate the flow through the reducer and the flow corresponds to the flow patterns described by Aerotherm (2011) where flow is accelerated in uniform pattern through the concentric reducer. The flow accelerates along the sides where the pipe is reduced (all sides in this case). The residual plot does show that the residuals do decrease approximately three orders of magnitude, but the residuals tend to oscillate in the last 250 iterations.

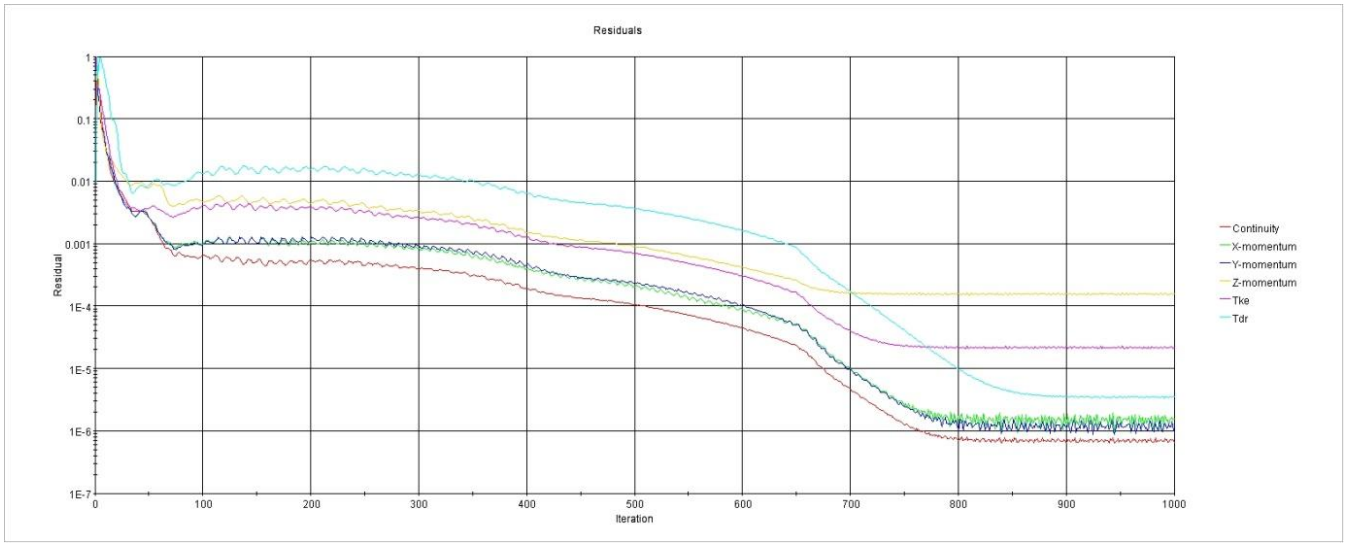

Figure 3.18: CR 10 Model Residual Plot

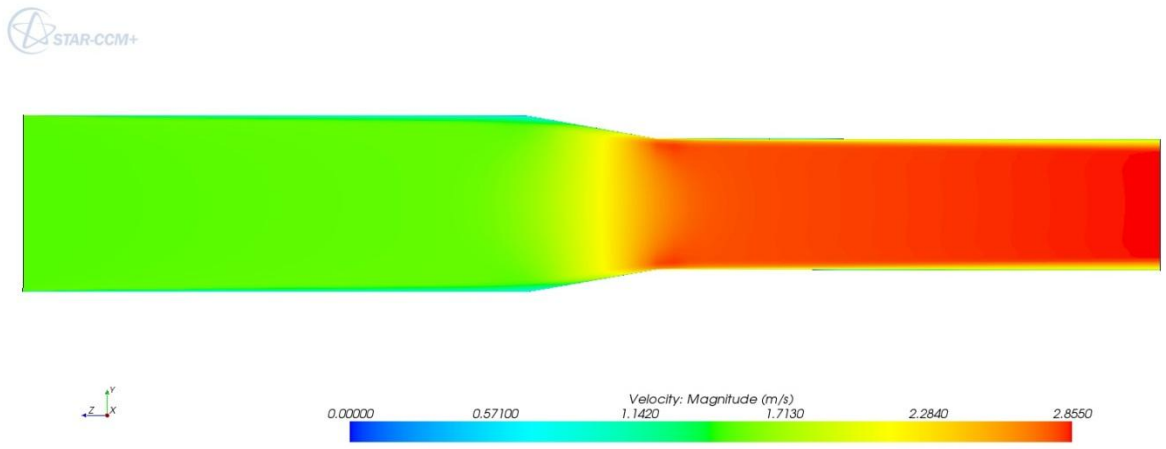

Figure 3.19: CR 10 Model YZ Plane Velocity Scalar Scene

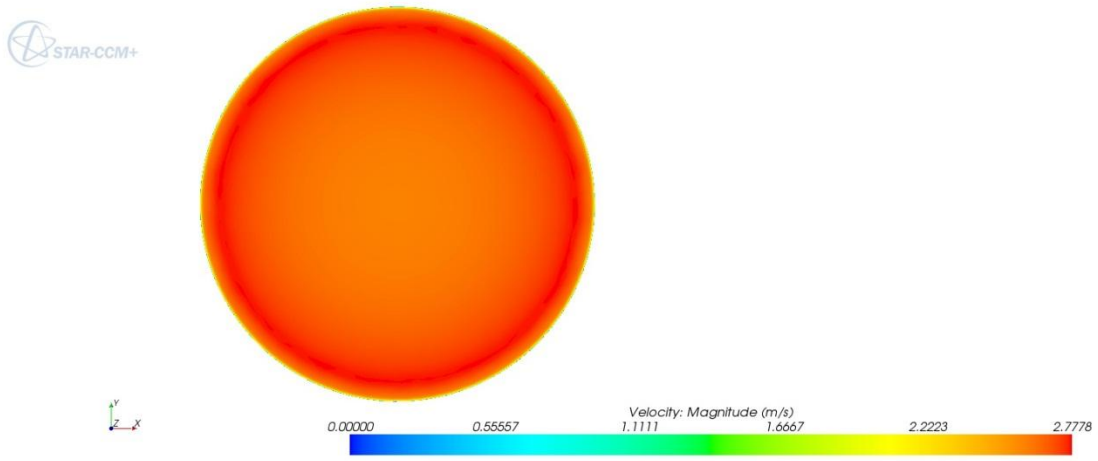

Figure 3.20: CR 10 Model XY Plane Velocity Scalar Scene

With the longer generalized cylinder model cells and the oscillating residuals it was decided to regenerate the volume mesh and re-run the model without the generalized cylinder model. This produced a mesh that consists of more compact polyhedral cells, shown in **Figure 3.21** and **Figure 3.22** below. This new volume mesh has increased the number cells from 363 067 cells to 760 013 cells and the number of faces from 1 281 624 faces to 4 054 812 faces. The implication of this change will be an increase in computational time. This model is named CR 10 – Attempt 2.

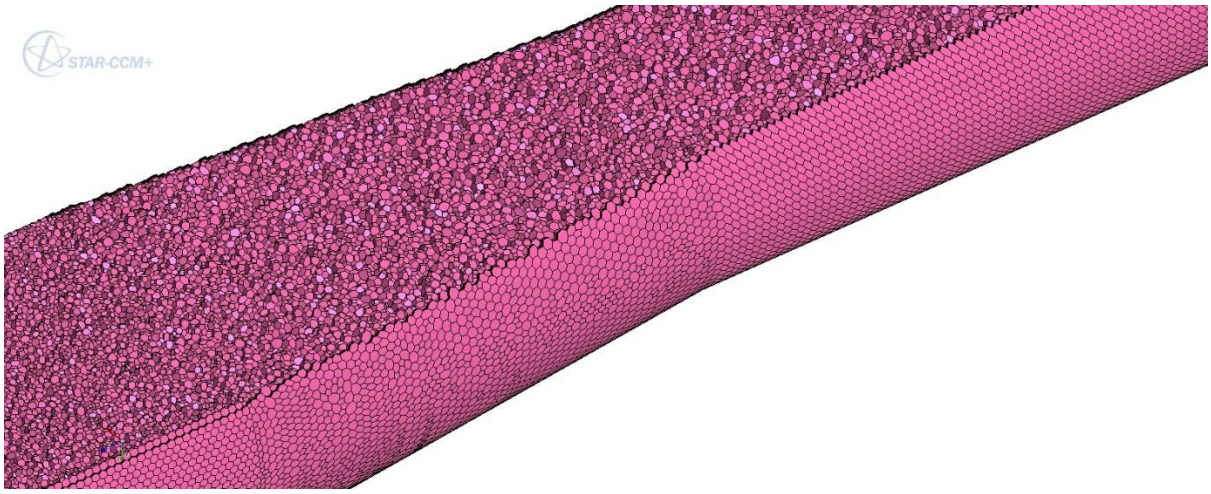

Figure 3.21: CR 10 – Attempt 2 Cell Centroid Threshold Plot

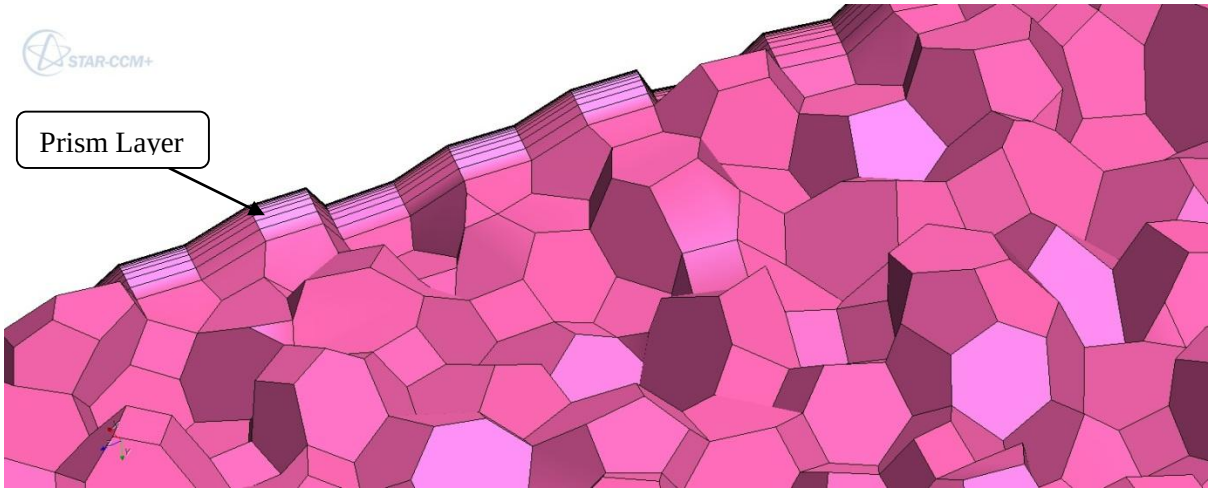

Figure 3.22: CR 10 – Attempt 2 Cell Centroid Threshold Plot

The Residual Plot, X-Y Plane Scalar Scene and the Y-Z Plane Scalar Scene for CR 10 – Attempt 2 are provided below (**Figure 3.23** to **Figure 3.25**). The two scalar scenes once again correspond to the flow patterns provided in ***Paragraph 2.5*** and to the scenes provided from the initial CR 10 Model solution. The residual plot illustrates a stable solution that converges after approximate 320 iterations where the residuals decrease approximately 5 orders of magnitude. In comparison to the initial CR 10 Model, CR 10 – Attempt 2 converges to a higher level of convergence after a fewer number of iterations without the oscillating residuals.

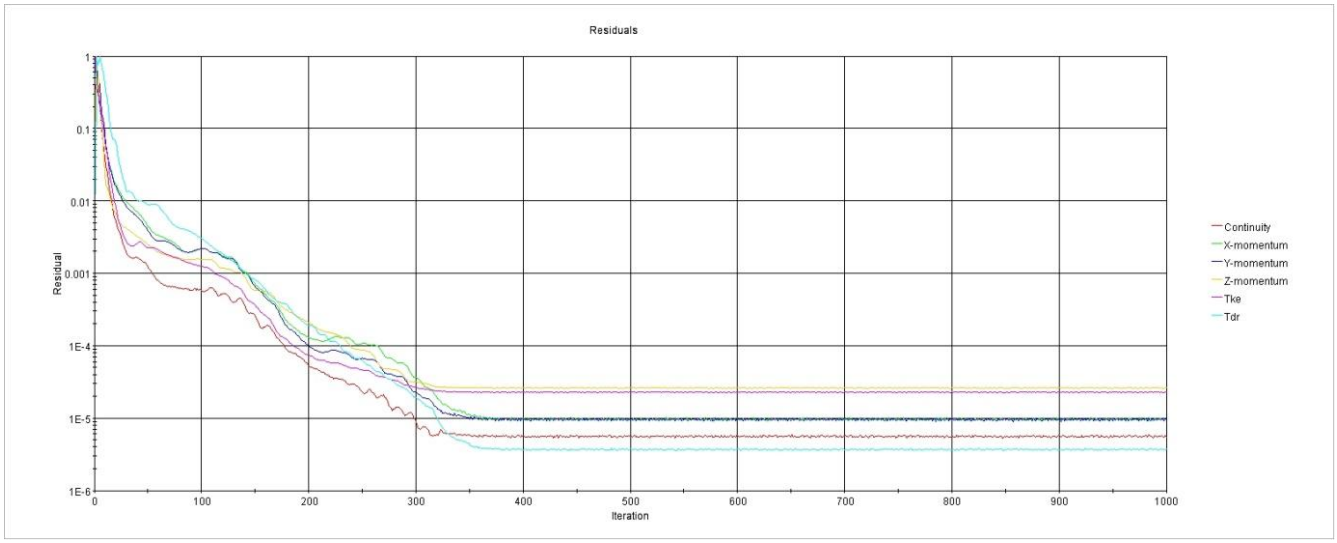

Figure 3.23: CR 10 – Attempt 2 Residuals Plot

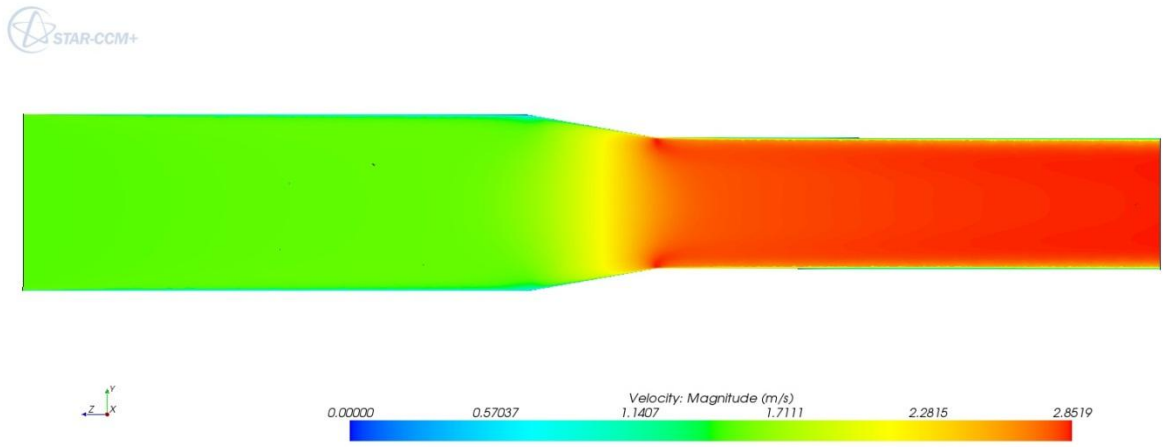

Figure 3.24: CR 10 - Attempt 2 YZ Scalar Velocity Scene

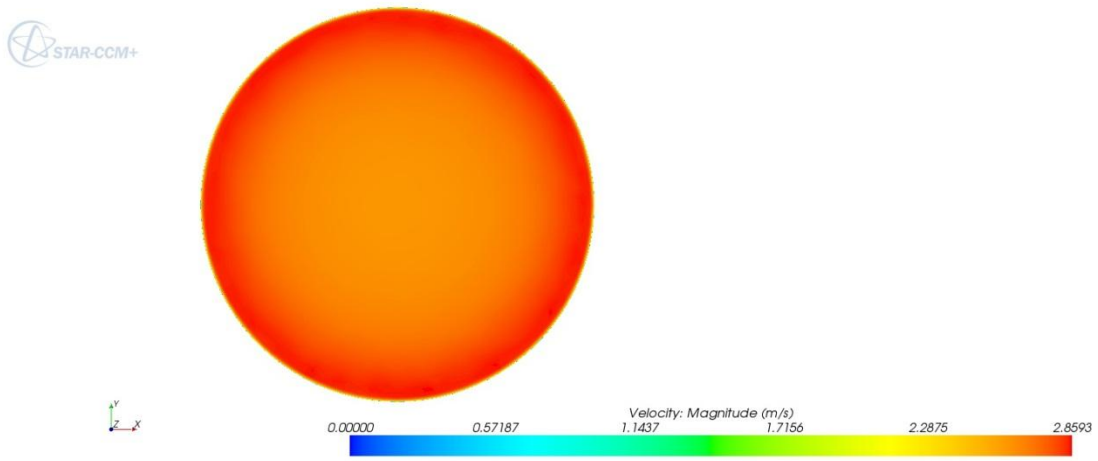

Figure 3.25: CR 10 - Attempt 2 XY Plane Velocity Scalar Scene

The X-Y Plot data for both models were plotted together for both X Axis and the Y Axis in order to evaluate the difference in simulation results between the two models. These plots are presented in **Figure 3.26** for the X Axis and **Figure 3.27** for the Y Axis. From these plots it is observed that the solutions are closely related from approximately -0.05 m to 0.05 m, this region is in the central region of the flow. The CR 10 – Attempt 2 provides a solution where the change in velocity towards the wall (between the central region of flow and the wall) is more gradual when compared to that of the initial CR 10 Model which has a steeper more sudden increase and decrease in velocity towards the pipe wall. When compared to typical near wall type flow rates reflected by Chadwick et al (2004) in **Figure 3.28** the distributions provided by both attempts represent the typical flow patterns.

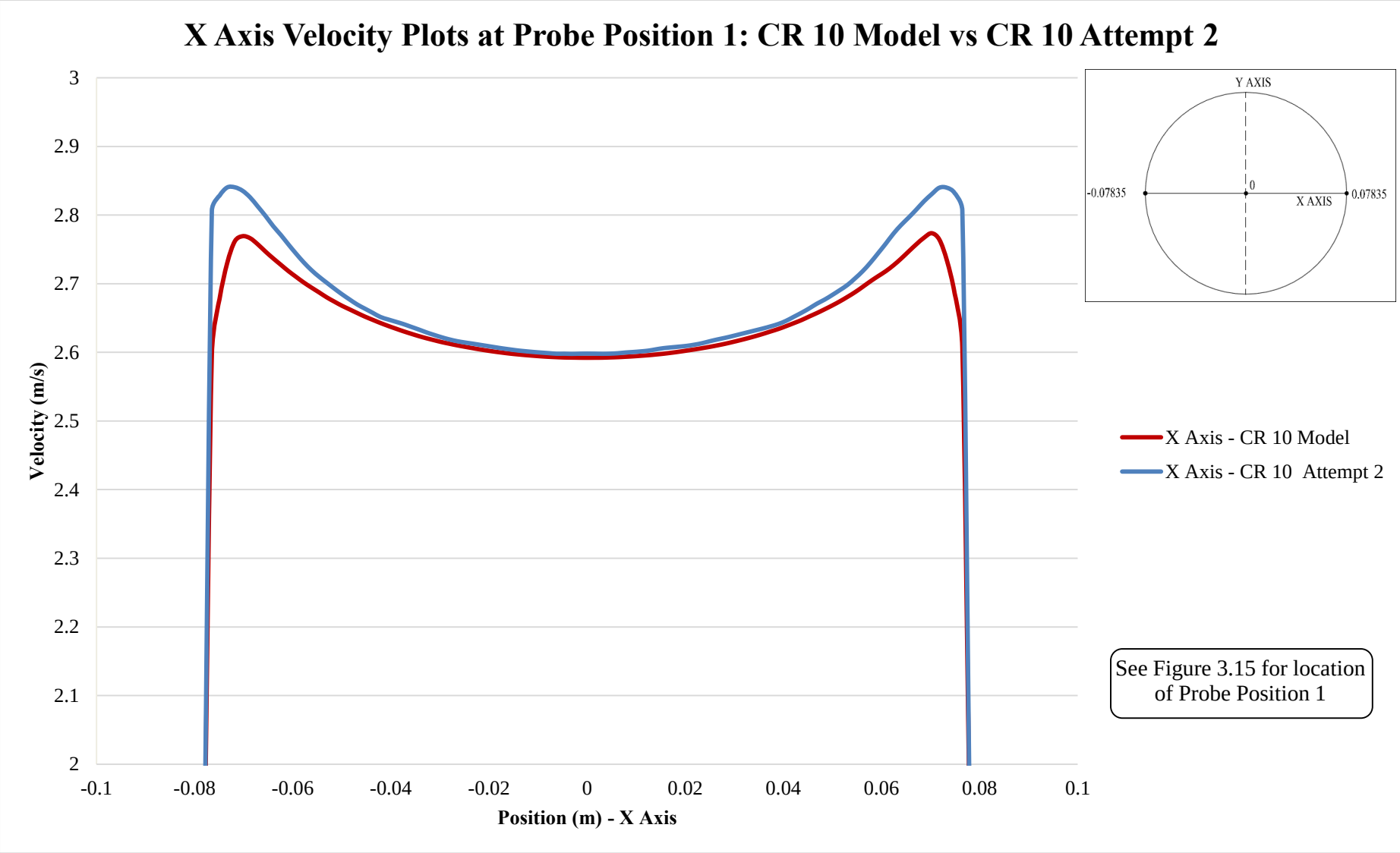

Figure 3.26: X Axis Velocity Plots at Probe Position 1: CR 10 Model vs. CR 10 – Attempt 2

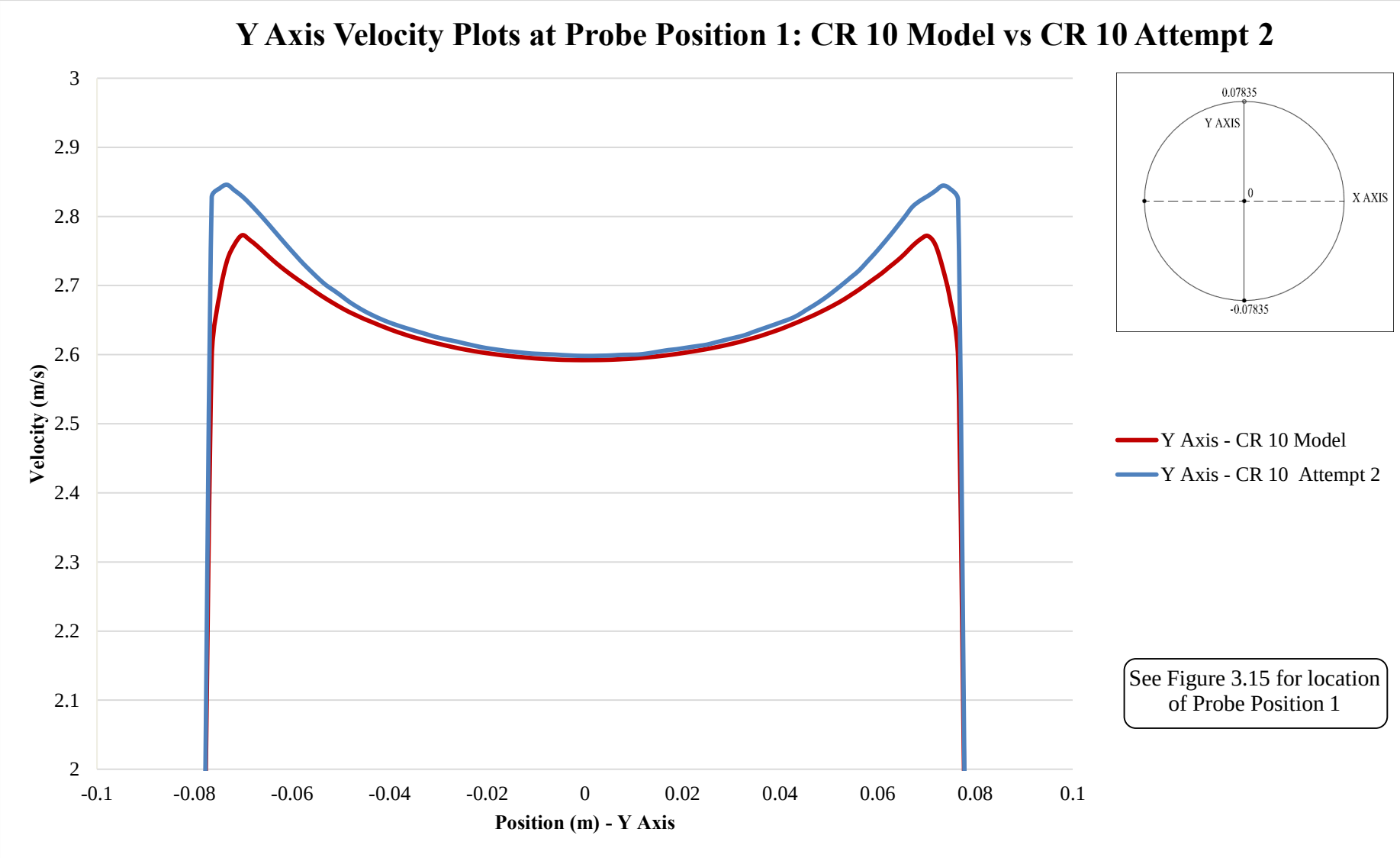

Figure 3.27: Y Axis Velocity Plots at Probe Position 1: CR 10 Model vs. CR 10 – Attempt 2

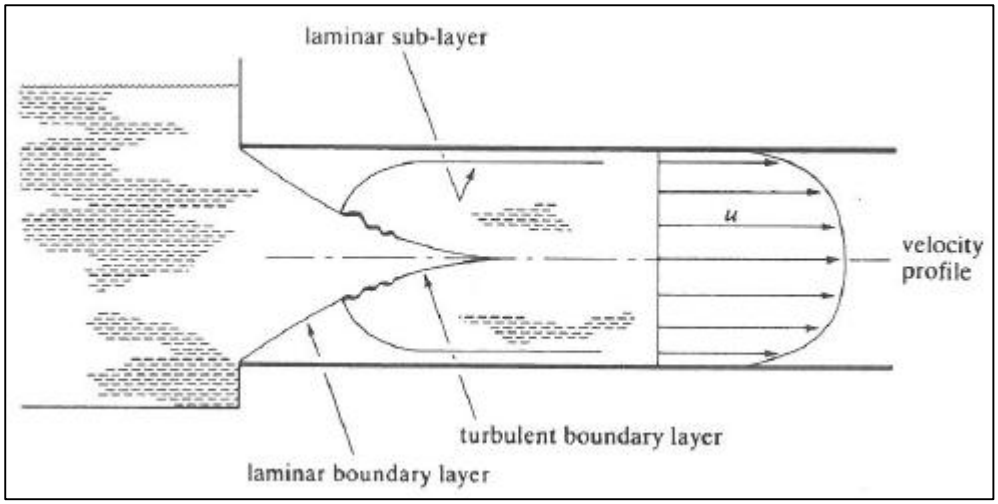

Figure 3.28: Turbulent Pipe Flow Velocity Distribution (Chadwick et al, 2004)

The longer cylindrical type cells may not accurately calculate the acceleration of the flow at the discontinuities of the reducer due to the length spanning over the discontinuity between the straight length of pipe and the reducer, where the shorter polyhedral cells will model this acceleration more accurately. Together with this phenomenon and the increased level of stability, decreased number of iterations required and higher order of magnitude decrease in residuals it was decided to remove the generalized cylinder model from the meshing models selected to be utilized in this study and only use the polyhedral mesh cells. Confirmation of the numerical convergence of the model is however required.

In order to assess the numerical convergence a mass flow plot illustrating the mass flow into the reducer versus the mass flow exiting the reducer provides a mechanism to assess the numerical convergence of the analysis. Once the mass flow is balanced the model has numerically converged. The mass flow plot for CR 10 Attempt 2 is provided in **Figure 3.29** and in **Figure 3.30** where only first 100 iterations are shown. It is observed that after the 40'th iteration the mass flow in is equal to the mass flow out and the model has therefore numerically converged.

Convergence and meshing are closely related and the mesh parameters have a direct impact on both the numerical convergence and computational time. The increase in number of cells has increased the computation time, but this increased computational time is still acceptable for the computational time available for this study. Therefor the only change that was made from the settings and inputs listed earlier in this chapter is the removal of the generalized cylinder model. The remaining models

together with the various flow rates were analyzed to 500 iterations. The results are provided in the following chapter and are discussed in Chapter 5.

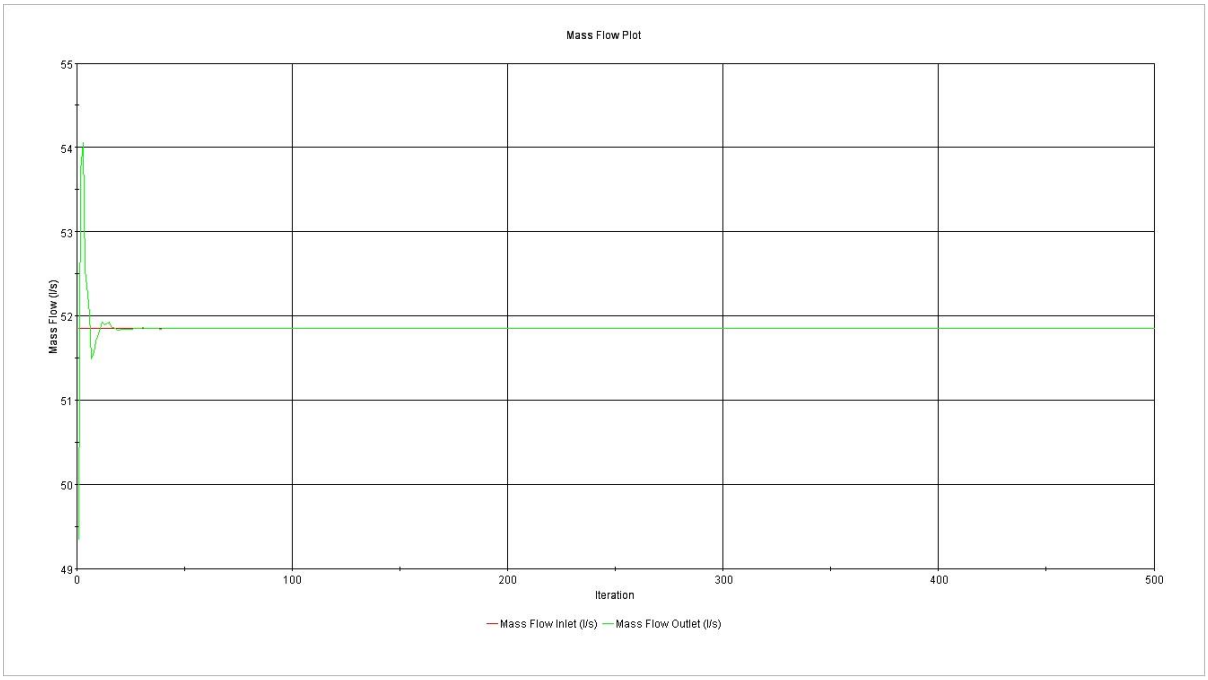

Figure 3.29: CR 10 Attempt 2 Mass Flow Plot

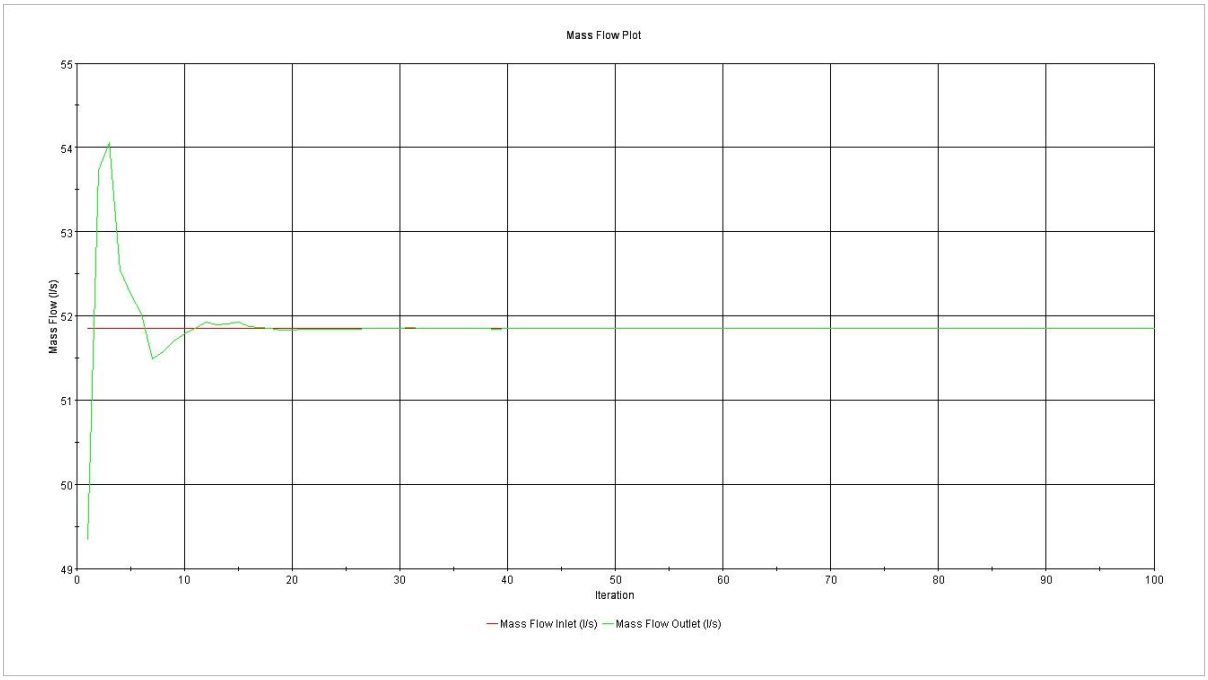

Figure 3.30: CR 10 Attempt 2 Mass Flow Plot First 100 Iterations Only

4. NUMERICAL SIMULATION RESULTS

4.1. RESULTS PRESENTED

All the models described in ***Paragraph 3.4*** (six concentric geometries and six eccentric geometries) were modelled with inlet velocities of 1 m/s, 1.5 m/s, 2.0 m/s and 2.4 m/s. A total of 48 simulations were therefore run. The results are presented for each geometry with the scalar scenes described in ***Paragraph 3.6*** for each inlet velocity modelled. The residual plots for the 1 m/s simulations are provided, to confirm the convergence and the remainder of the residual plots (1.5 m/s, 2 m/s and 2.4 m/s) are provided on the ***Supporting Digital Media***. In addition to these results, the summary reports and scalar scenes are also provided on the ***Supporting Digital Media***.

One of the benefits of CFD analyses is that the solution at every point in the mesh is known. However it was observed in the ***Chapter*** 2 that the velocity distribution resulting from an eccentric reducer with its flat surface on top results in a non-uniform velocity distribution along the vertical axis of the reducer. It was also observed in ***Chapter 2*** that the pump inlet requirements provided by HR Wallingford (2001) in Sinotech CC (2005) require the velocity distributions to be assessed along the X (horizontal) Axis and the Y (vertical) Axis. Therefore under the paragraph headings for each model geometry, XY plots of the position in the pipe cross section versus velocity (one for the X Axis velocities and one for the Y Axis velocities) for each flow velocity modelled, at the four probe positions, were created (i.e. an X Axis probe line and a Y Axis probe line at each probe position). The numerical orientation of the axes in the XY plots is clarified in **Figure 4.1**. The locations of the probe positions and the orientation of the axes and scalar scenes are illustrated in **Figure 4.2** and are the positions and locations described in ***Paragraph 3.6***.

These XY plots illustrate the difference in flow patterns resulting from the different flow velocities and also reflect the dissipation of the non-uniform flow patterns in the downstream direction. Brief comments are provided for each simulation under each model heading and observations regarding the results are provided at the end of this chapter and are discussed further in the following chapter.

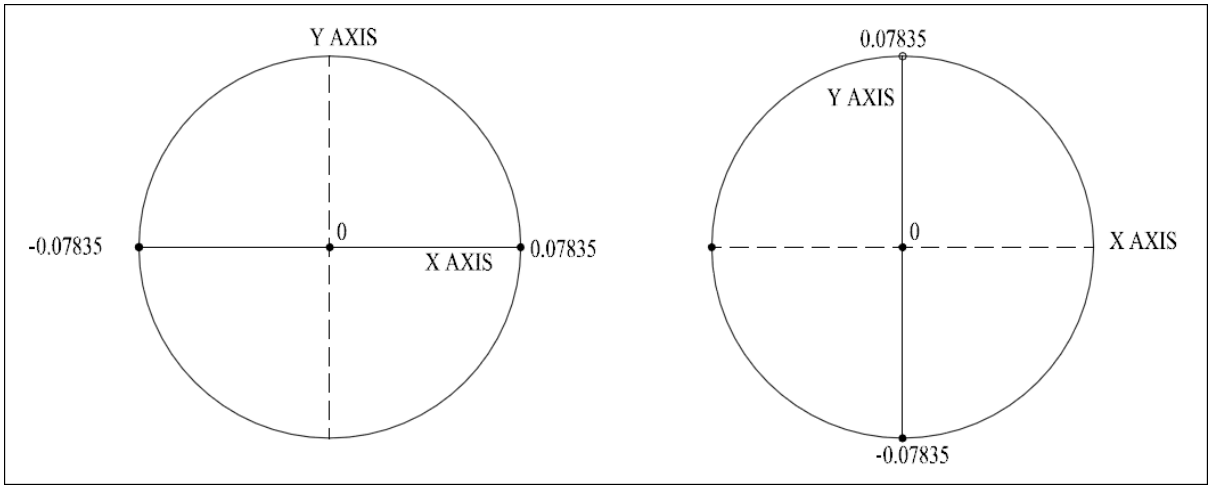

Figure 4.1: Numerical Orientation of the Axes for the XY Plots

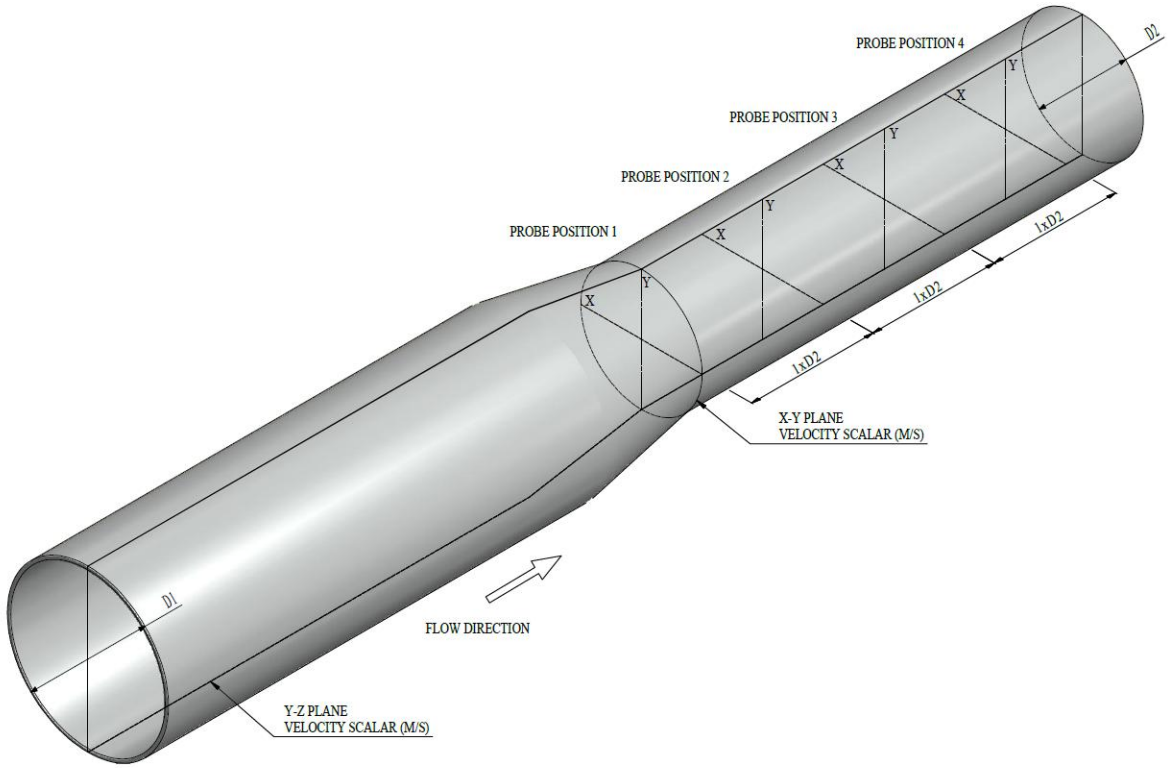

Figure 4.2: Orientation of the Scalar Scenes and Locations of the Probe Positions

4.2. CONCENTRIC REDUCER MODELS SIMULATION RESULTS

4.2.1. CR 2 Model Results

The results for the CR 2 Model are provided in **Figure 4.3** to **Figure 4.7**. The four flow velocities were applied to the CR 2 Model and all four simulations were completed with acceptable results within the stopping criteria of 500 iteration steps. The residual plot for the 1 m/s simulation is provided in **Figure 4.7.** The velocity distribution on the downstream end of the reducer is fairly uniform with no significant velocity gradient present in all four of the simulations as reflected in **Figure 4.3** and **Figure 4.4**. **Figure 4.5** and **Figure 4.6** illustrate that the acceleration of flow creates a velocity distribution with acceleration towards the sides of the pipe at Probe Position 1, but this velocity distribution is evened out into a uniform distribution typical of pipe flow at a distance of 1xD2 downstream from the reducer (Probe Position 2). The two XY plots reflect the same velocity distributions due to the concentric nature of the reducer and the flow accelerating evenly from all directions.

1 m/s

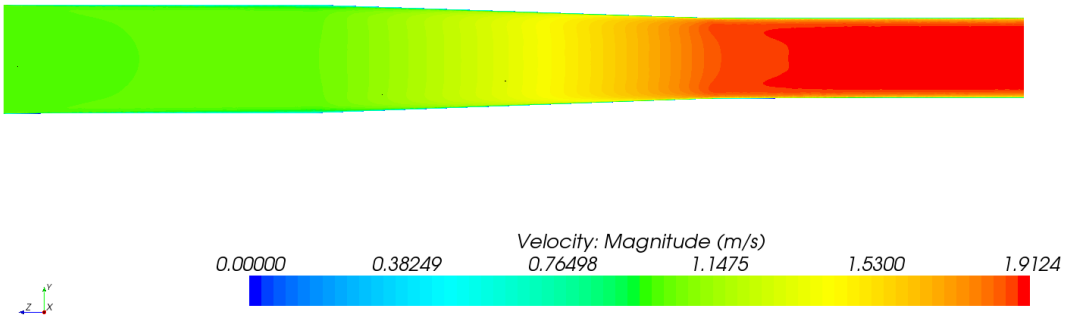

1.5 m/s

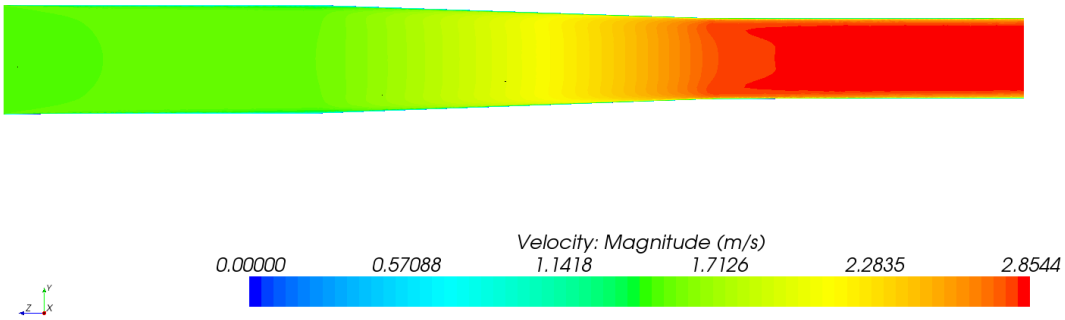

2 m/s

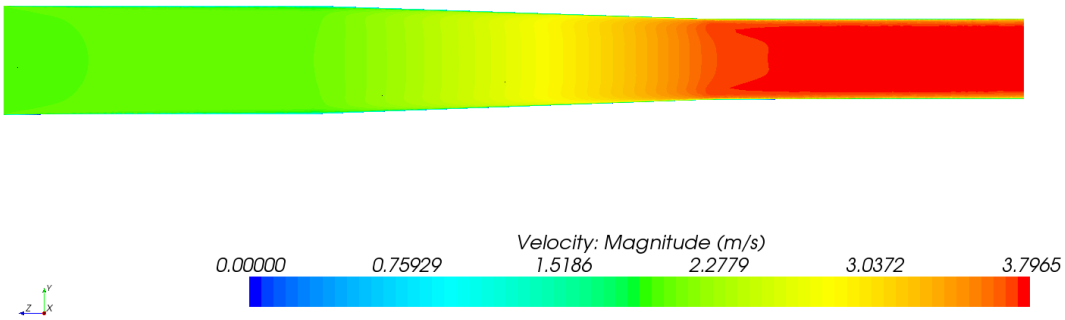

2.4 m/s

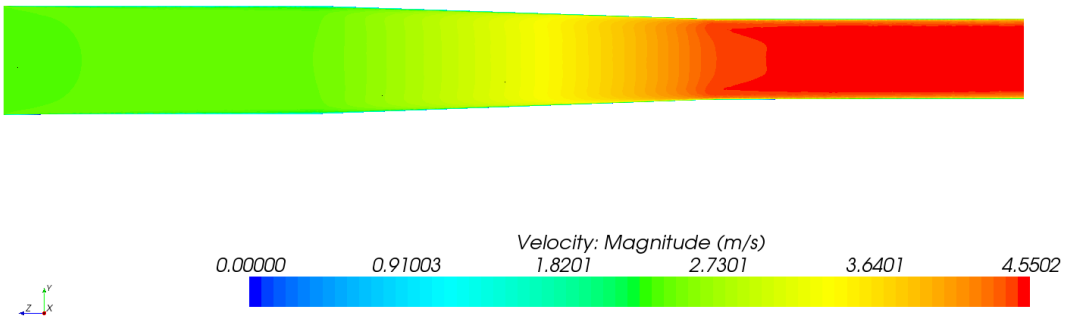

Figure 4.3: CR 2 Model YZ Plane Velocity Scalars

1 m/s

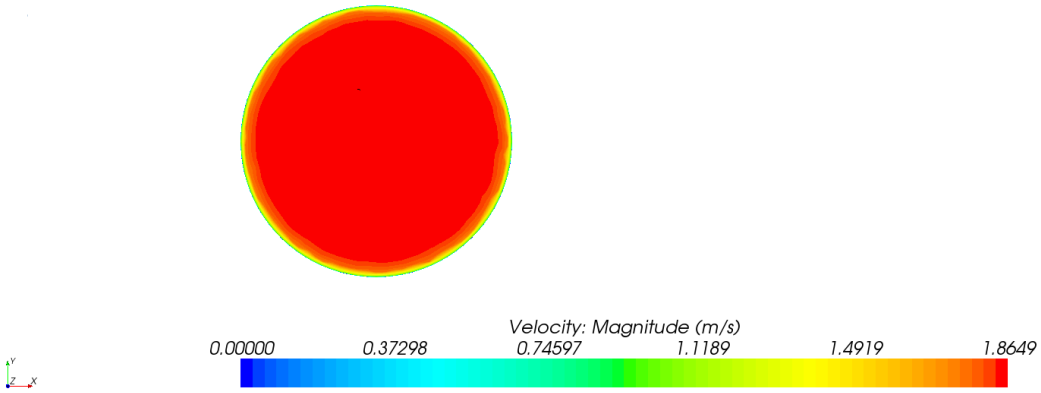

1.5 m/s

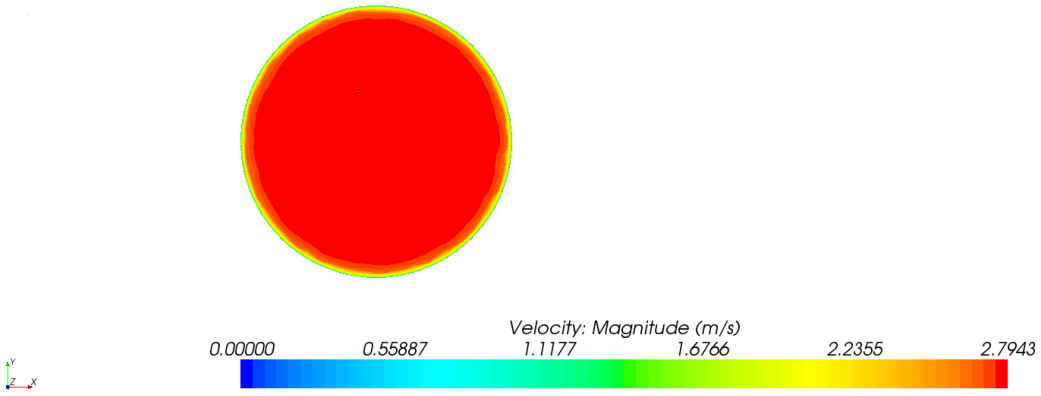

2 m/s

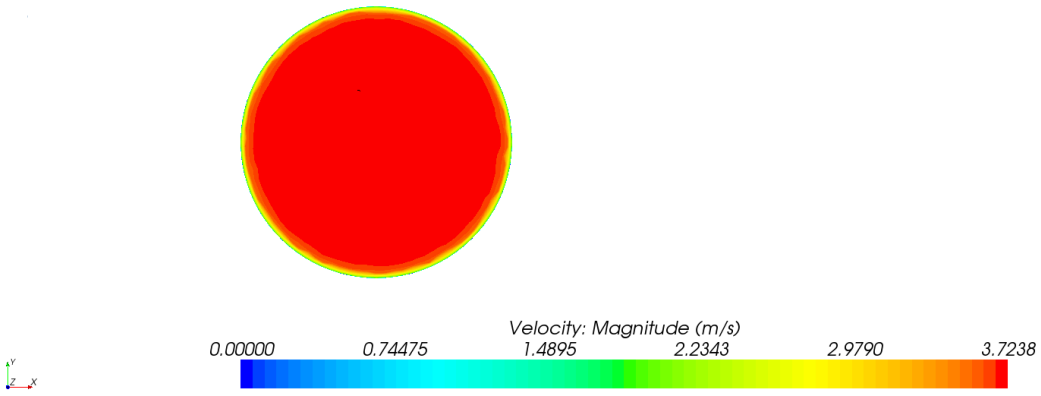

2.4 m/s

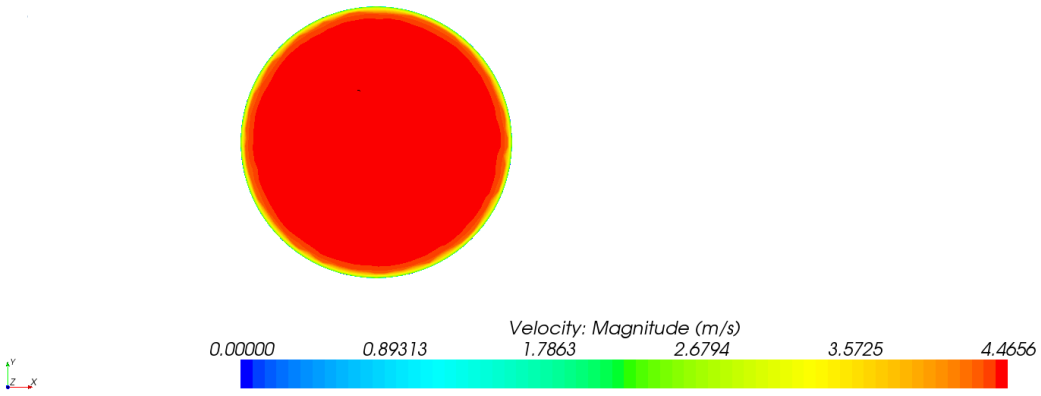

Figure 4.4: CR 2 Model XY Plane Velocity Scalars at Probe Position 1

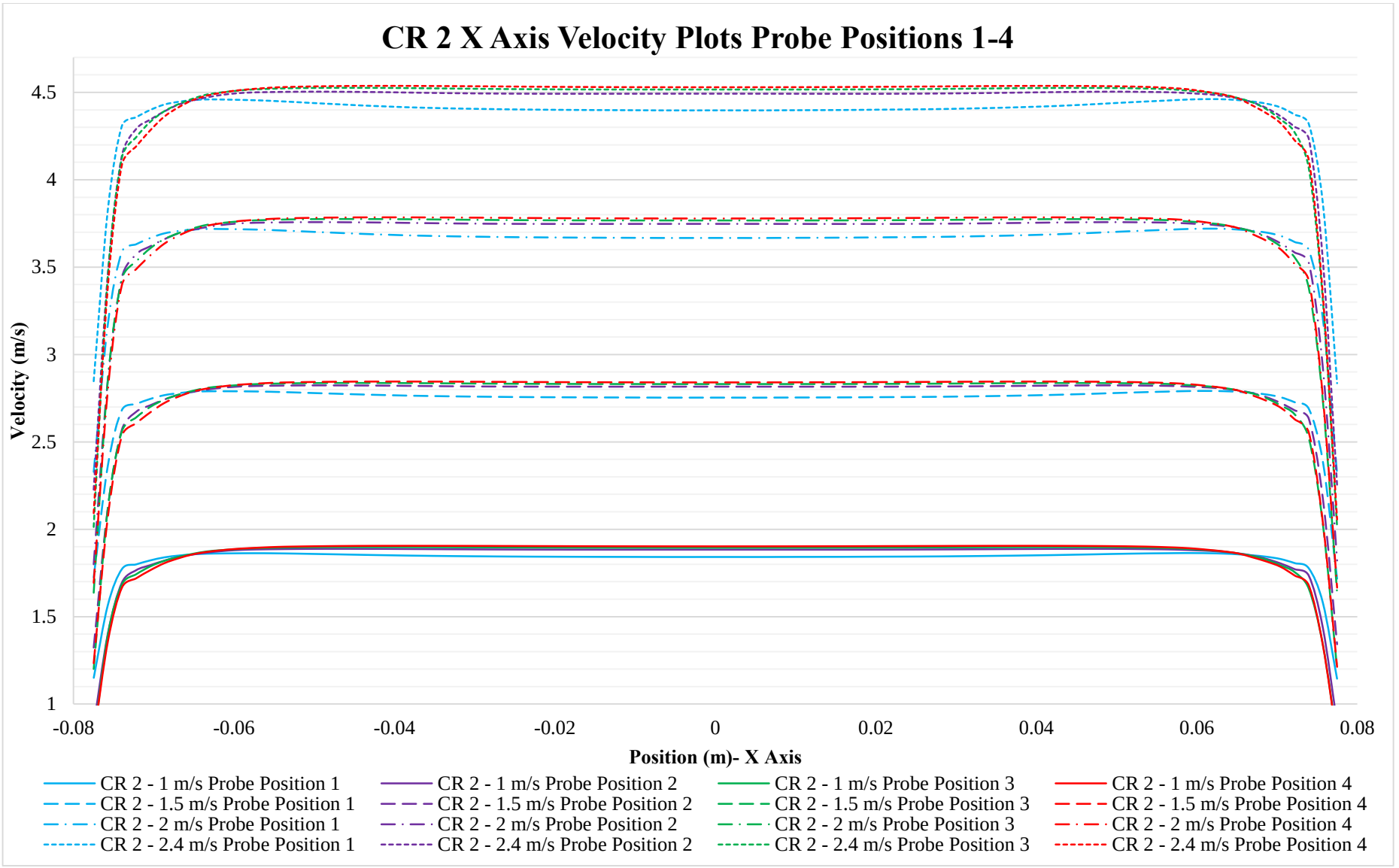

Figure 4.5: CR 2 X Axis Velocity XY Plots Probe Positions 1-4

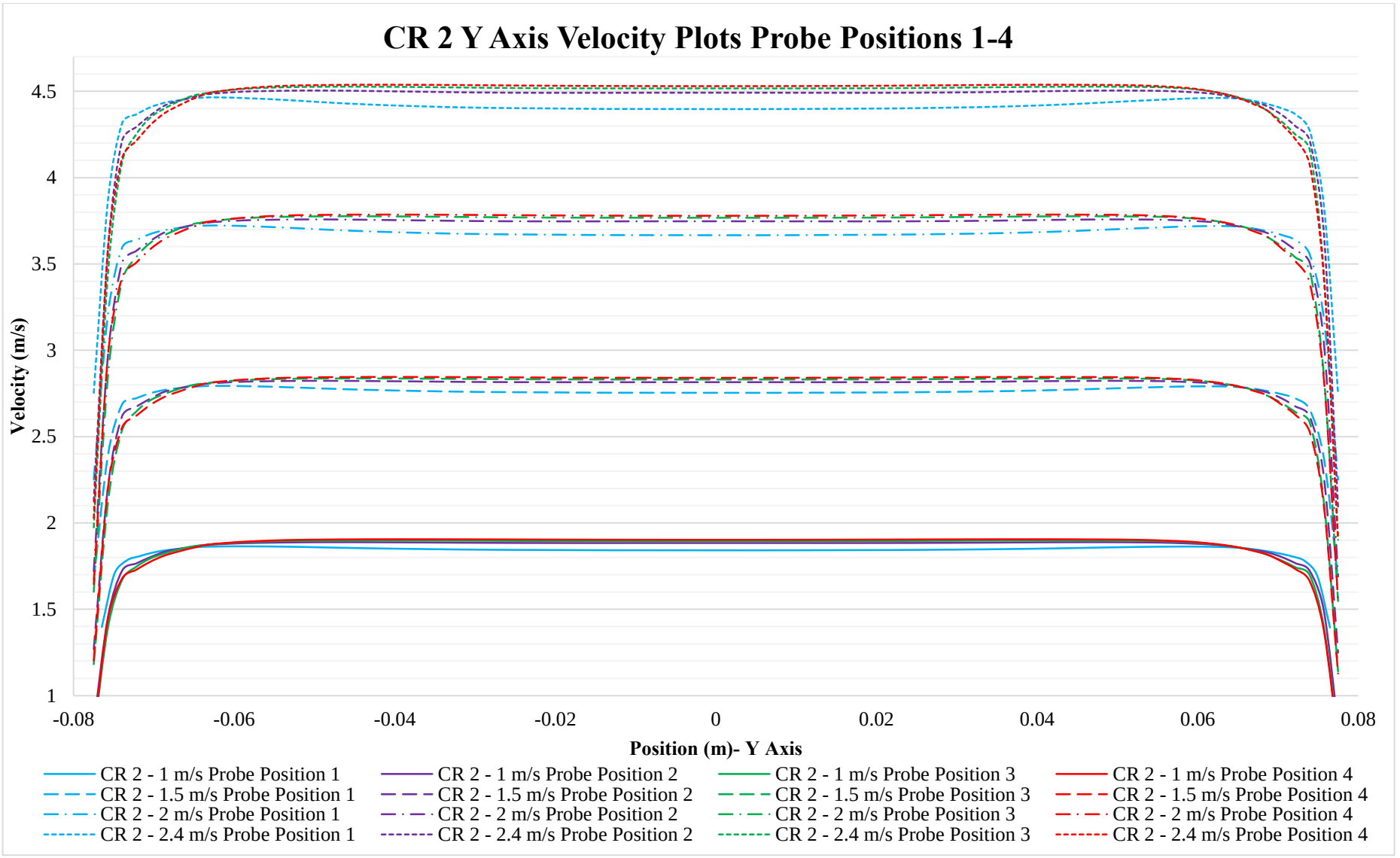

Figure 4.6: CR 2 Y Axis Velocity XY Plots Probe Positions 1-4

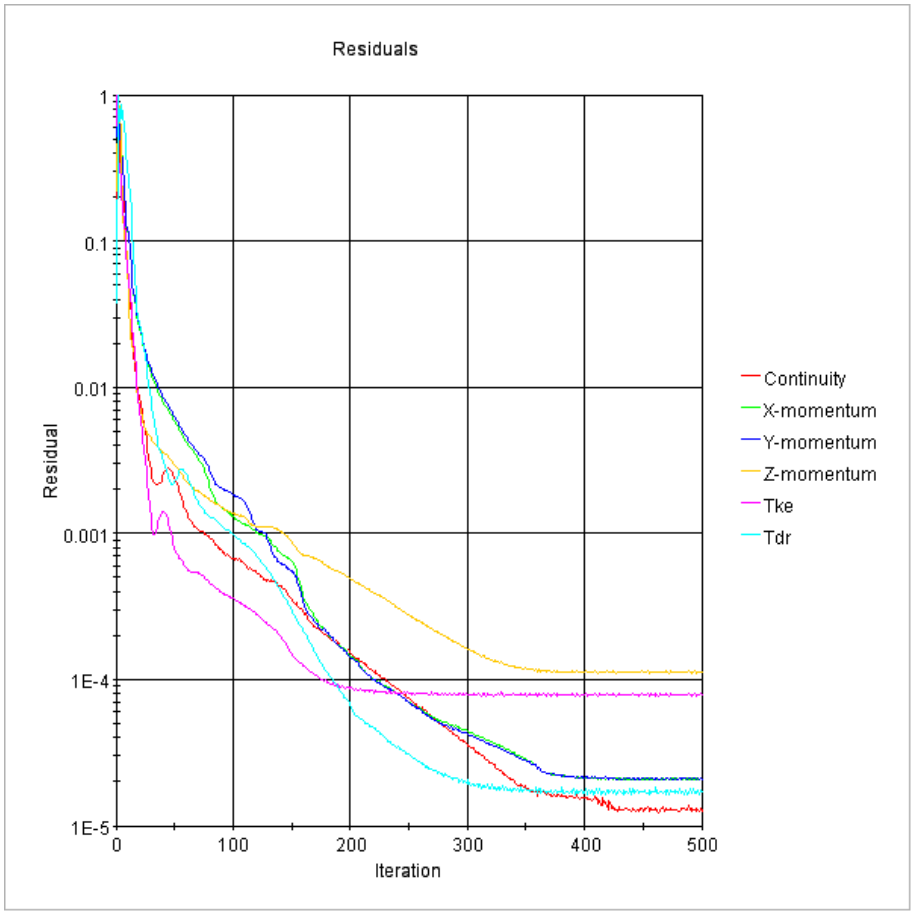

Figure 4.7: CR 2 Simulation Residual Plot – 1m/s Velocity Inlet

4.2.2. CR 2.5 Model Results

The results for the CR 2.5 Model are provided in **Figure 4.8** to **Figure 4.12**. All four of the CR 2.5 simulations were completed with acceptable results within the stopping criteria of 500 iteration steps. The residual plot for the 1m/s simulation is provided in **Figure 4.12**. The velocity distributions are of all four the simulations are presented in **Figure 4.8** and **Figure 4.9**. The velocity distributions on the downstream end of the reducer are fairly uniform with an increase in velocity gradient when compared to the CR 2 Models. **Figure 4.10** and **Figure 4.11** illustrate that the acceleration of flow creates a velocity distribution with acceleration towards the sides of the pipe at Probe Position 1, but this velocity distribution is evened out into a uniform distribution typical of pipe flow at a distance of 1xD2 downstream from the reducer (Probe Position 2). This acceleration is greater than the acceleration experienced with the CR 2 model. The two XY plots reflect the same velocity distributions due to the concentric nature of the reducer and the flow accelerating evenly from all directions.

1 m/s

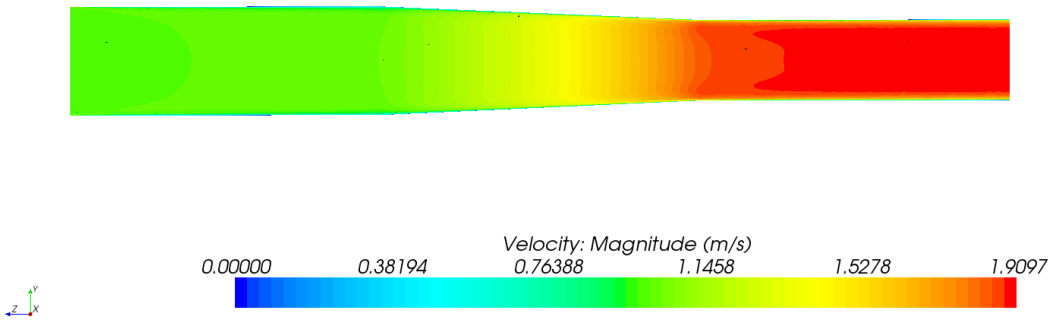

1.5 m/s

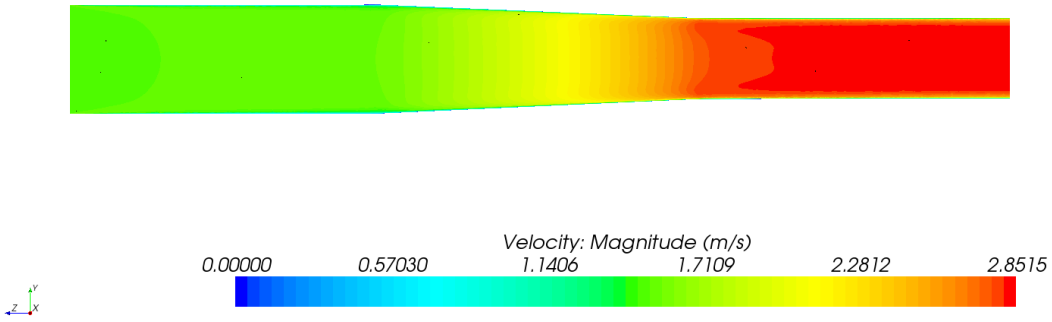

2 m/s

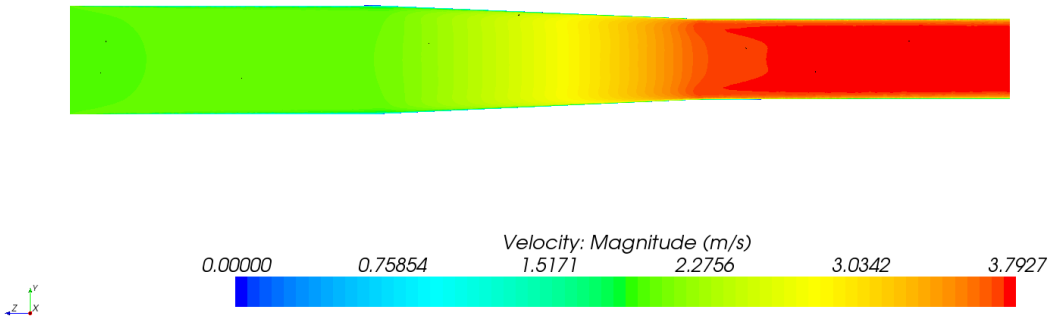

2.4 m/s

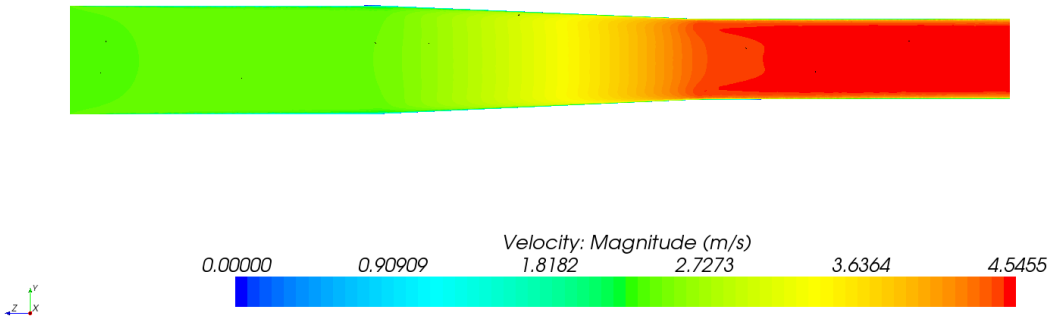

Figure 4.8: CR 2.5 Model YZ Plane Velocity Scalars

1 m/s

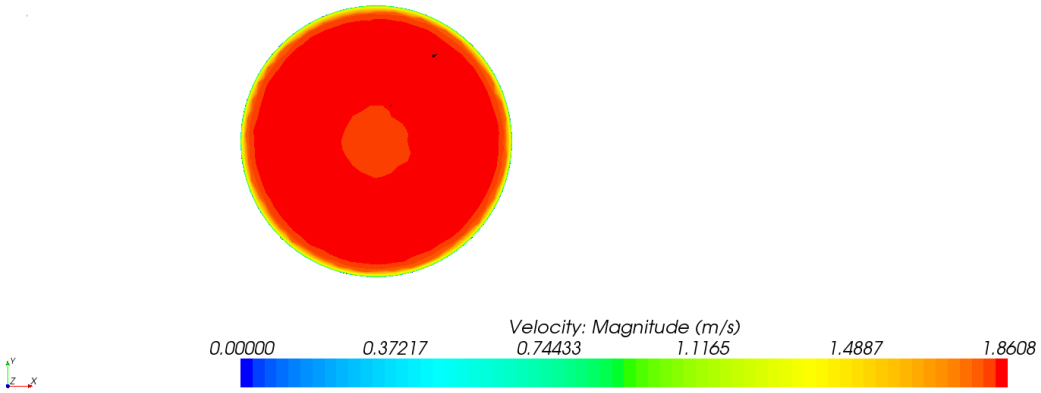

1.5 m/s

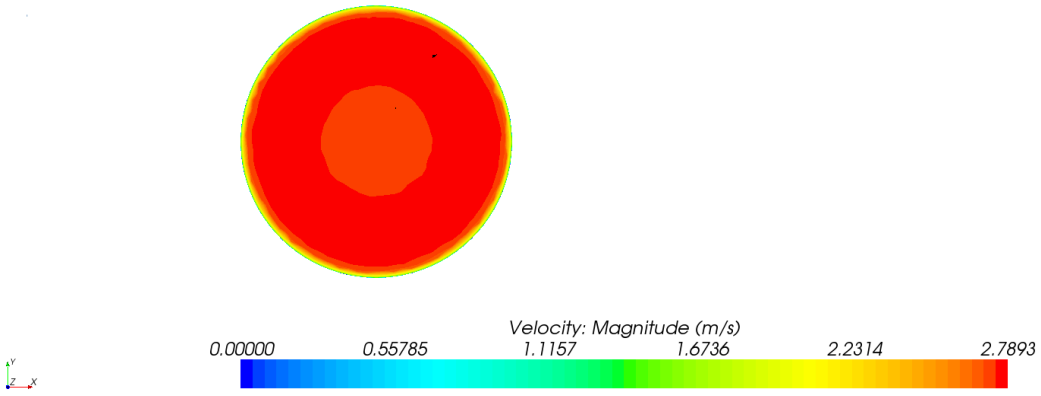

2 m/s

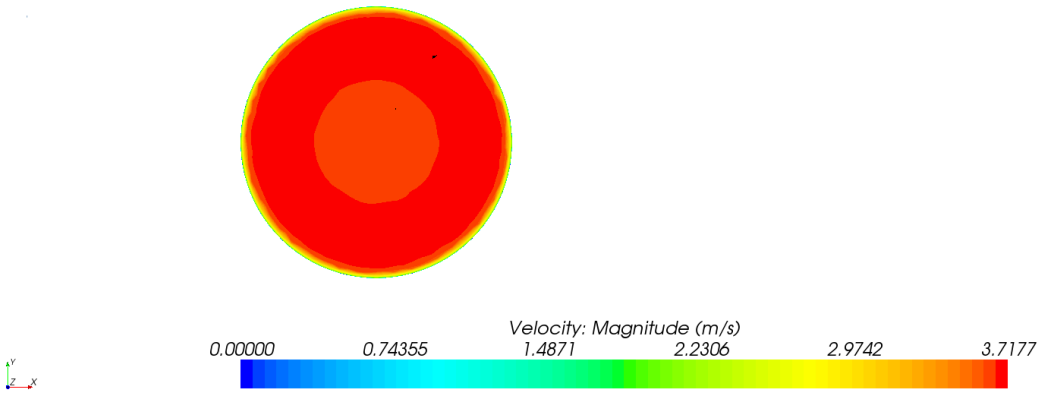

2.4 m/s

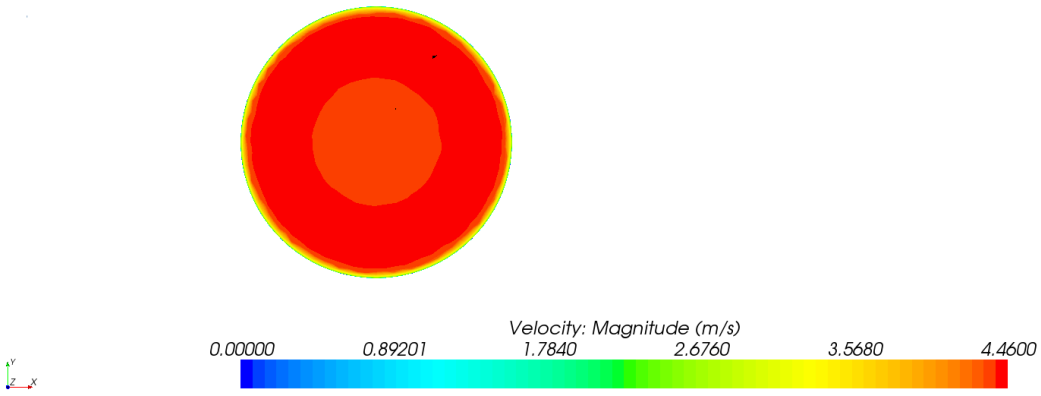

Figure 4.9: CR 2.5 Model XY Plane Velocity Scalars at Probe Position 1

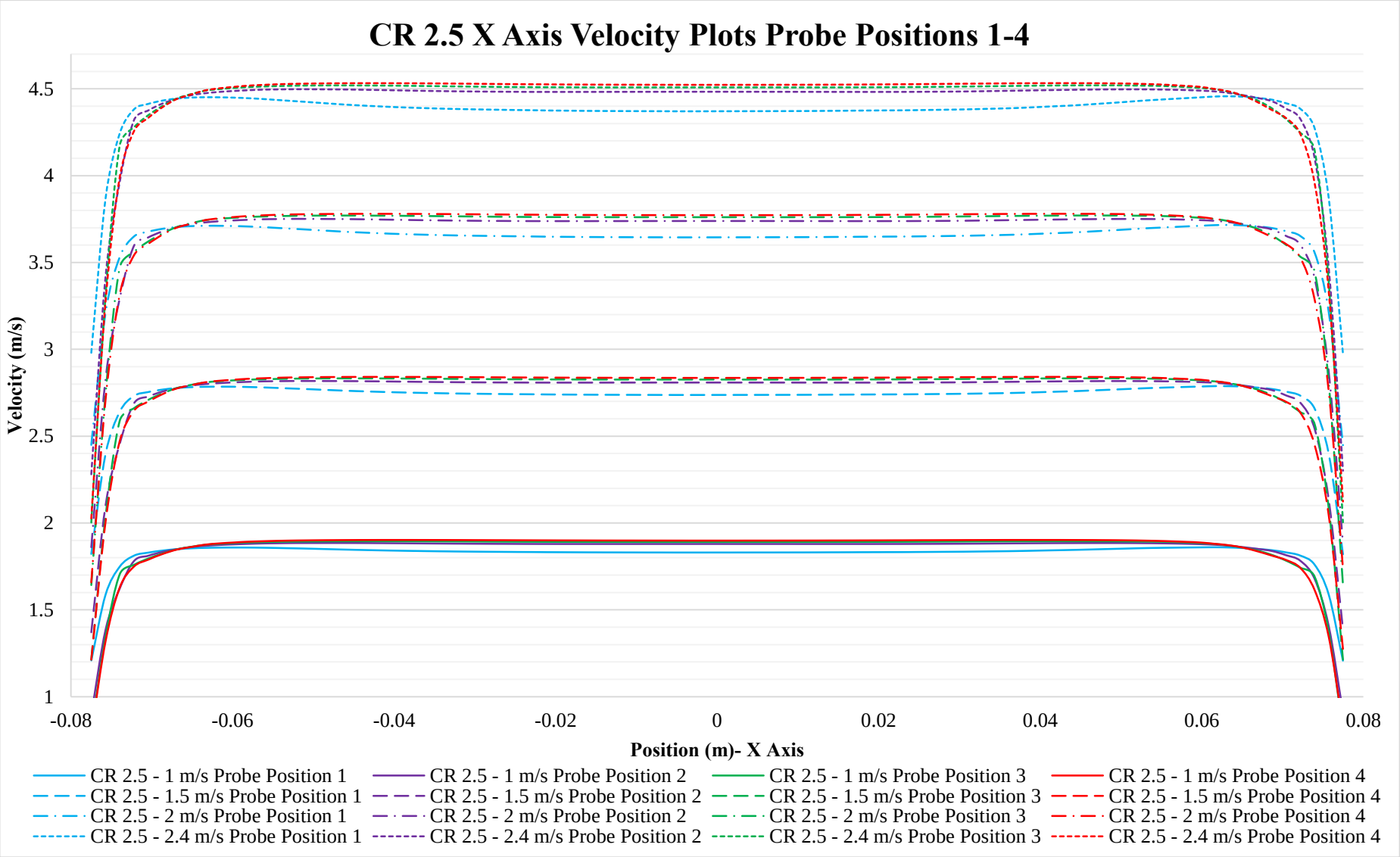

Figure 4.10: CR 2.5 X Axis Velocity XY Plots Probe Positions 1-4

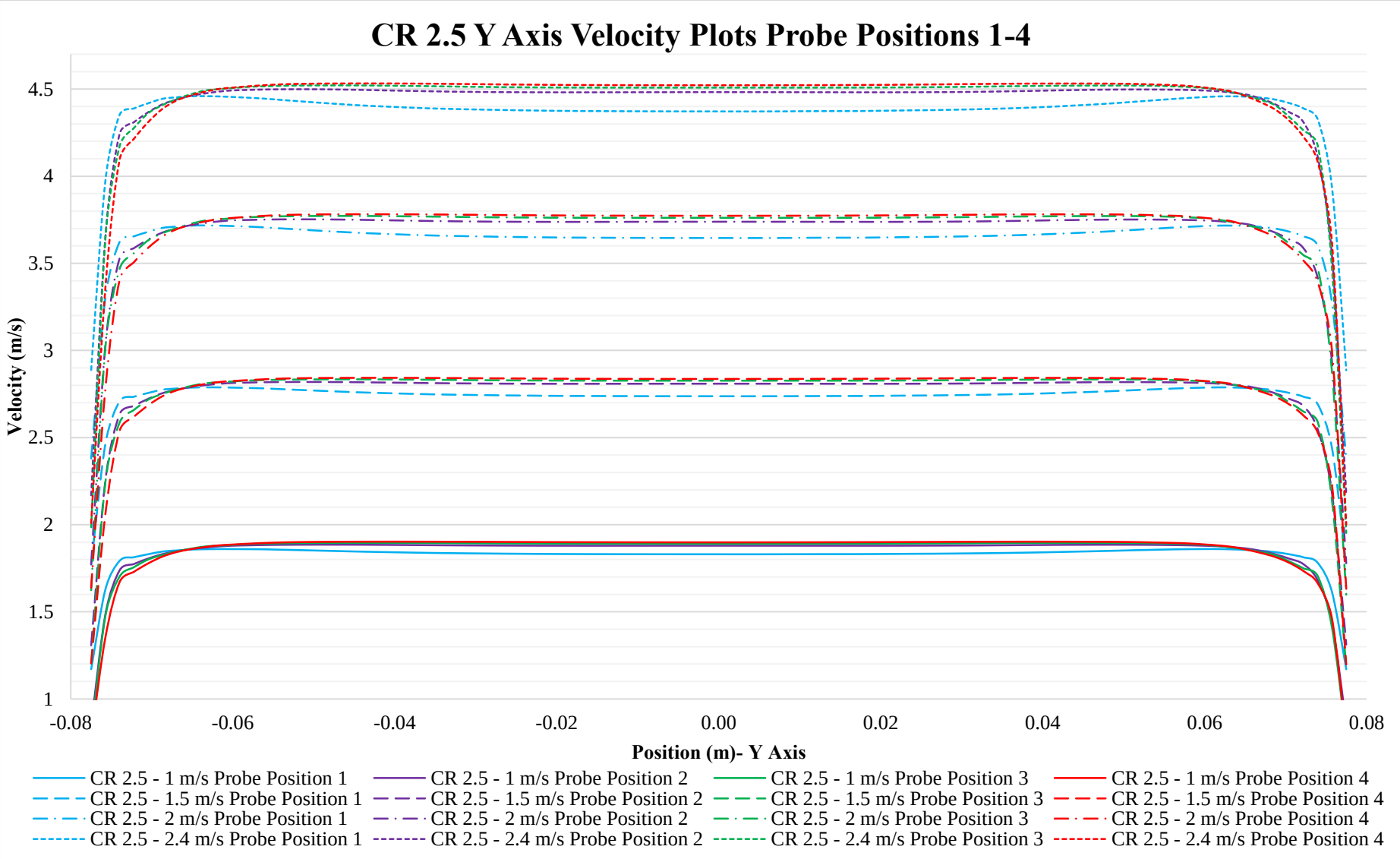

Figure 4.11: CR 2.5 Y Axis Velocity XY Plots Probe Positions 1-4

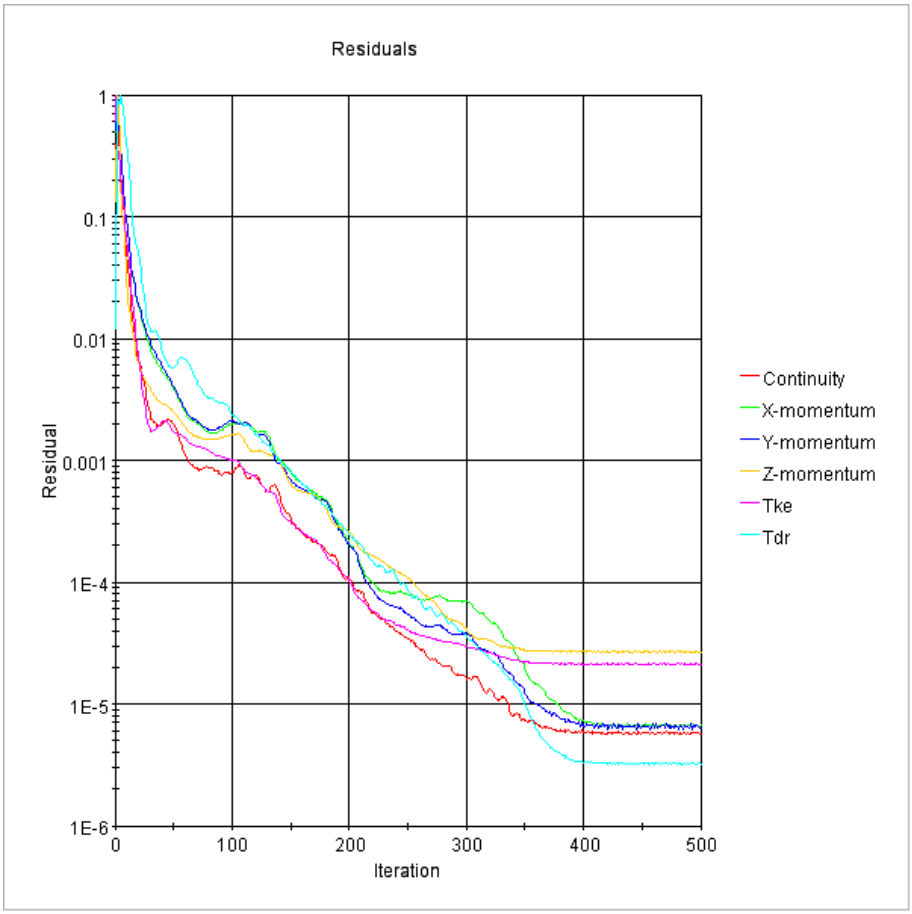

Figure 4.12: CR 2.5 Simulation Residual Plot – 1m/s Velocity Inlet

4.2.3. CR 5 Model Results

The results for the CR 5 Model are provided in **Figure 4.13** to **Figure 4.17**. The velocity distribution has increased for the CR 5 Model when compared to the previous two models due to greater levels of acceleration through the reducer. The velocity acceleration caused by the reducer is now clearly visible in both the scalar plots and the velocity distribution plots. The convergence criteria for the CR 5 models was met within the stopping criteria of 500 iteration steps. The residual plot for the 1 m/s simulation is provided in **Figure 4.17**. The velocity distributions of all the simulations are presented in **Figure 4.13** and **Figure 4.14.** The velocity distribution that was caused by the acceleration of flow through the reducer is present at Probe Position 1, but is once again dissipated into a uniform distribution at the distance of 1xD2 downstream from the reducer, as is shown in **Figure 4.15** and **Figure 4.16**. There is no significant difference in the velocity distribution at the three positions (Probe Positions, 2, 3 and 4) recorded downstream from the reducer. The two XY plots reflect symmetrical velocity distributions due to the concentric nature of the reducer and the flow accelerating evenly from all directions.

1 m/s

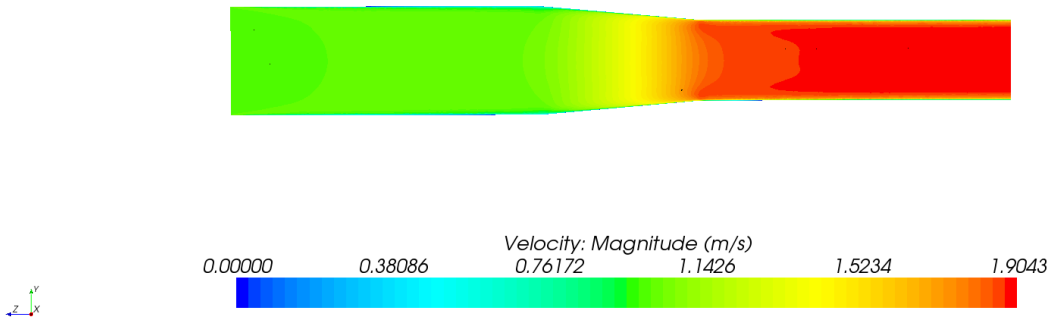

1.5 m/s

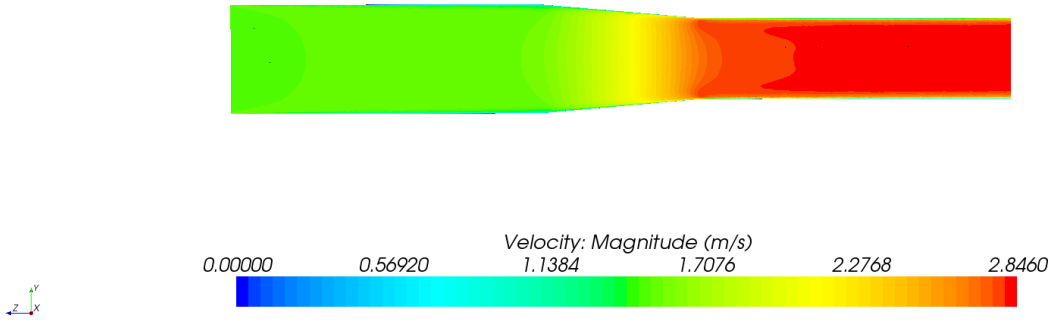

2 m/s

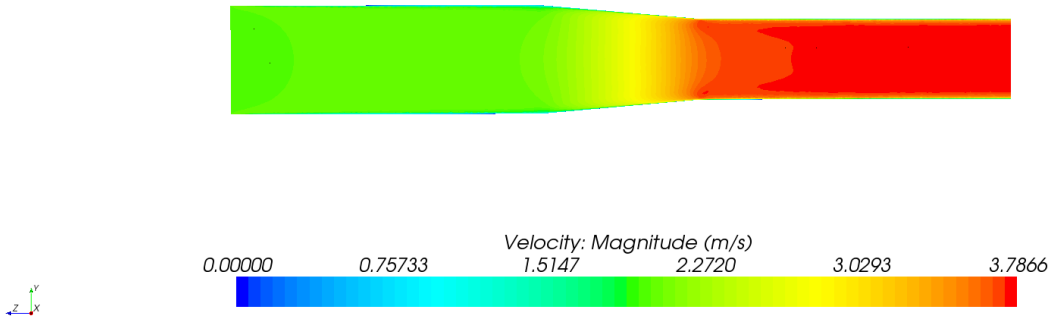

2.4 m/s

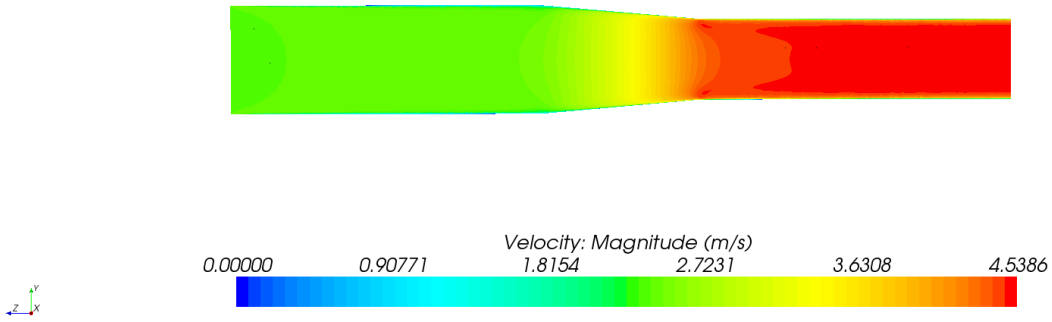

Figure 4.13: CR 5 Model YZ Plane Velocity Scalars

1 m/s

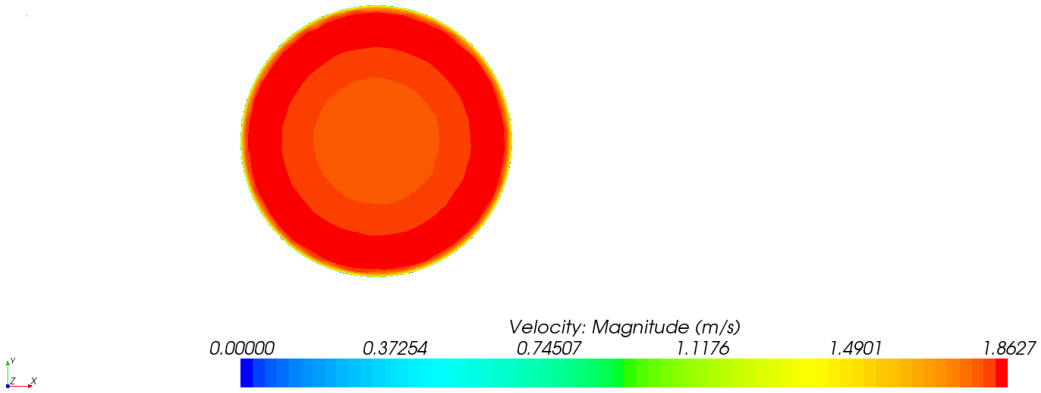

1.5 m/s

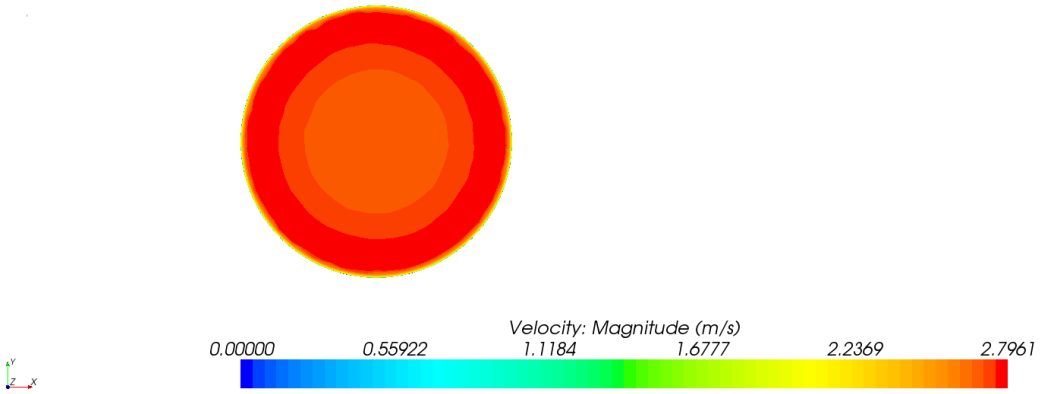

2 m/s

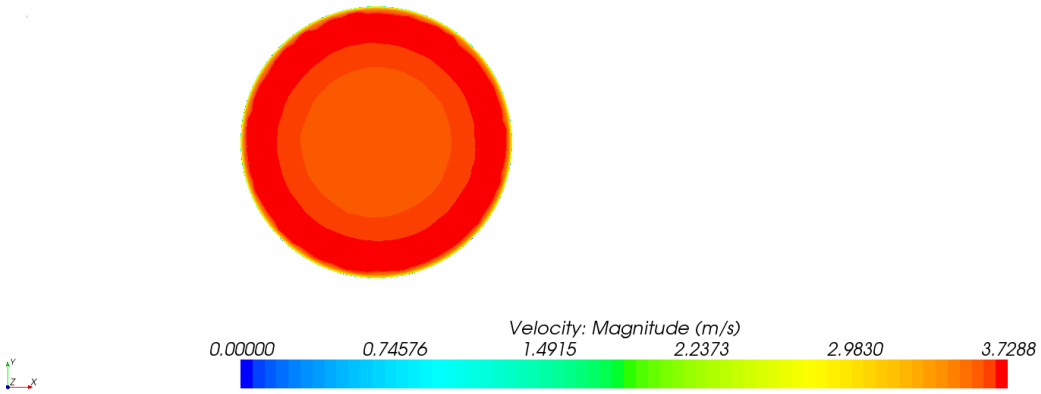

2.4 m/s

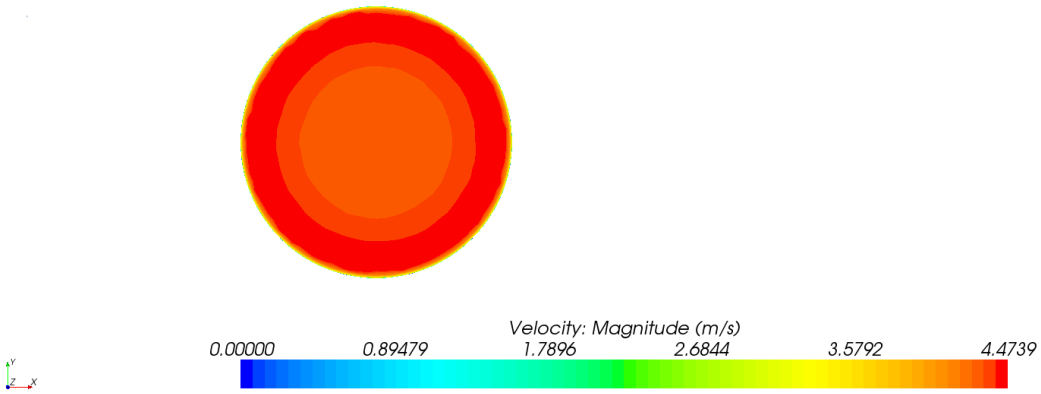

Figure 4.14: CR 5 Model XY Plane Velocity Scalars at Probe Position 1

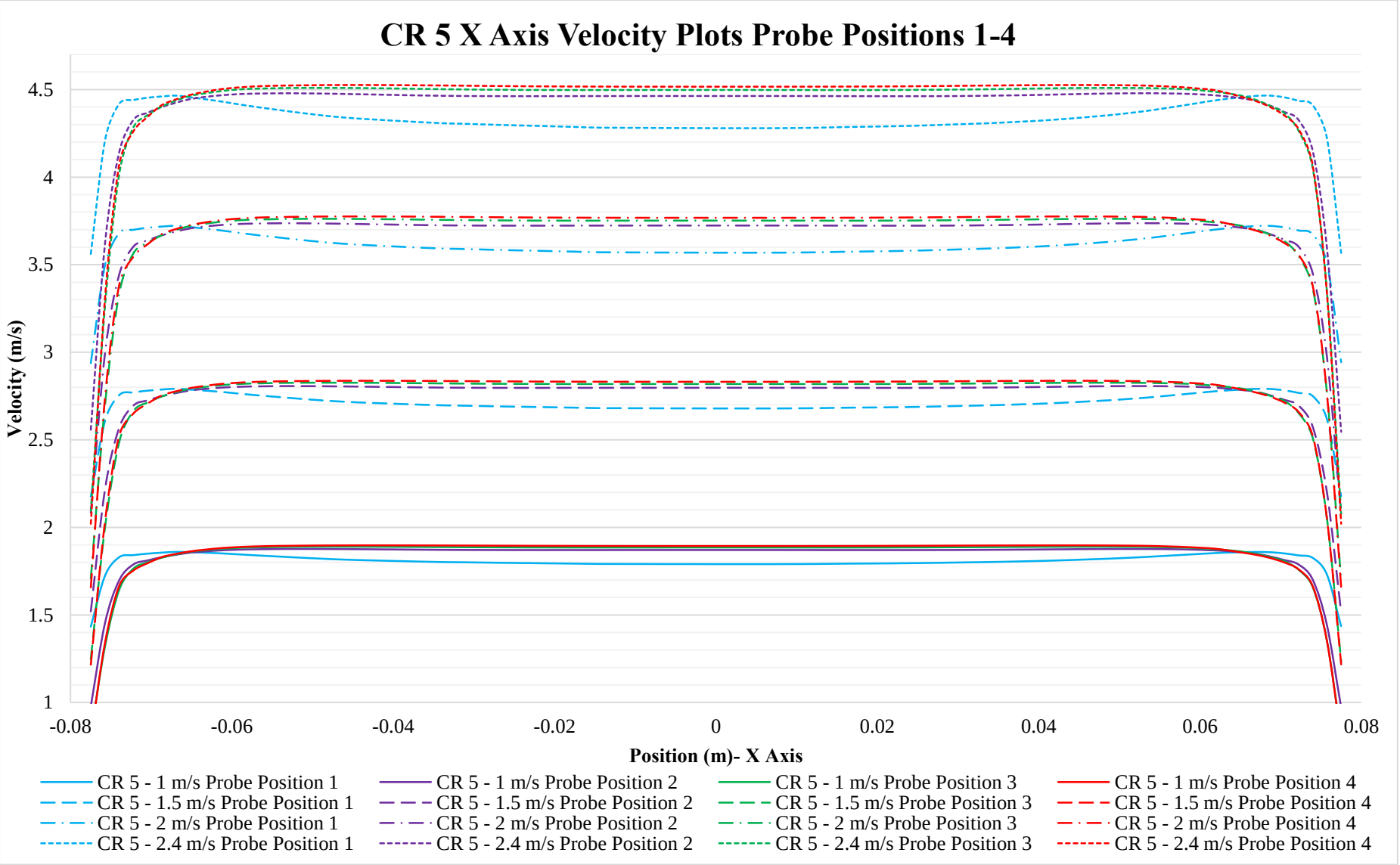

Figure 4.15: CR 5 X Axis Velocity XY Plots Probe Positions 1-4

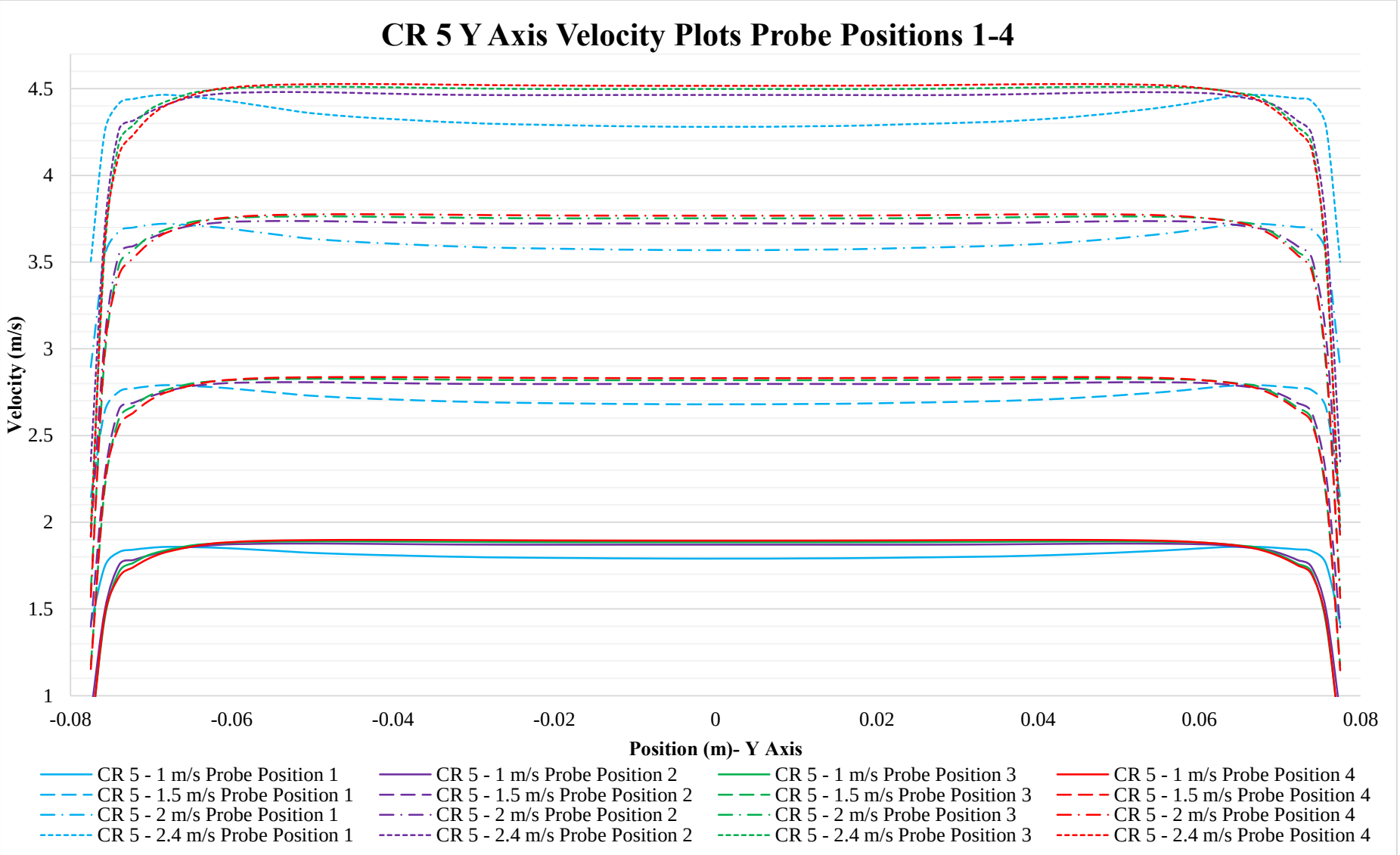

Figure 4.16: CR 5 Y Axis Velocity XY Plots Probe Positions 1-4

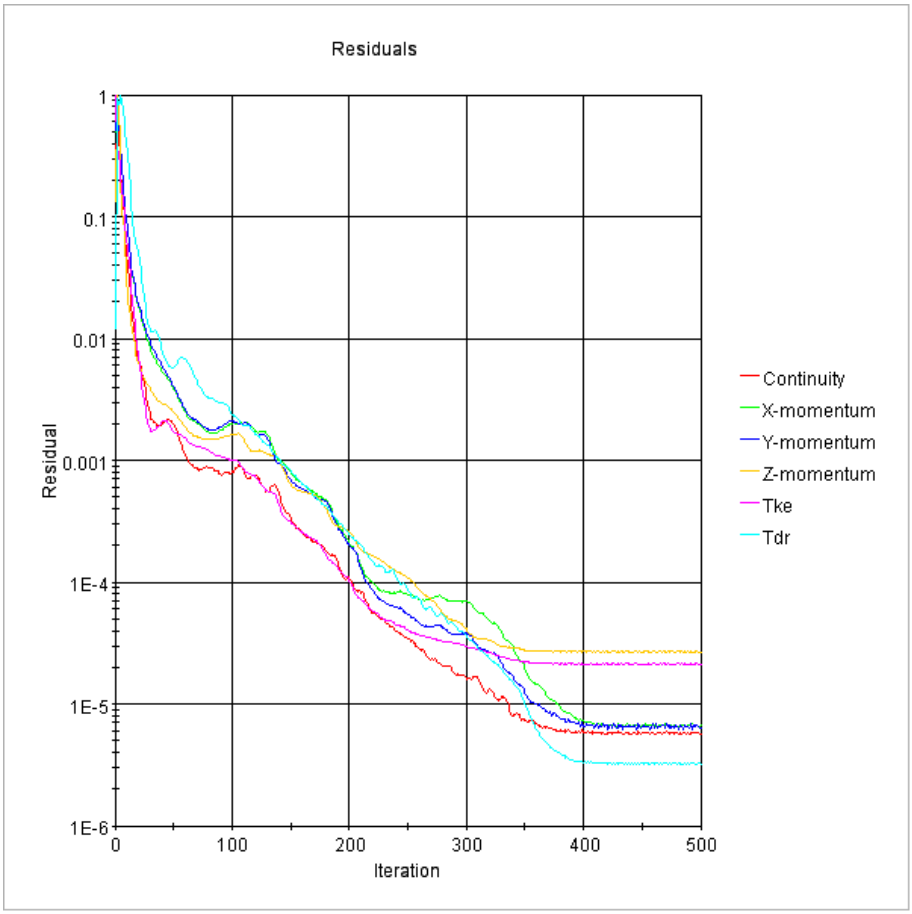

Figure 4.17: CR 5 Simulation Residual Plot – 1m/s Velocity Inlet

4.2.4. CR 10 Model Results

The results for the CR 10 Model are provided in **Figure 4.18** to **Figure 4.22**. All four of the CR 10 Models were completed with acceptable results within the stopping criteria of 500 iteration steps. The residual plot for the 1 m/s simulation is provided in **Figure 4.22**. Noticeable areas of high velocities are present at the position where the reducer returns to a straight pipe at the downstream end of the reducer, illustrated in **Figure 4.18** and **Figure 4.19** and the velocity gradient has increased even further when compared to the models previously discussed. **Figure 4.20** and **Figure 4.21** illustrate that the acceleration of flow through the reducer fitting creates a velocity distribution with acceleration towards the sides of the pipe at Probe Position 1, but this velocity distribution is evened out into a uniform distribution typical of pipe flow at a distance of 1xD2 downstream from the reducer (Probe Position 2). This acceleration is greater than the acceleration experienced with the previous models. The two XY plots reflect symmetrical velocity distributions due to the concentric nature of the reducer and the flow accelerating evenly from all directions.

1 m/s

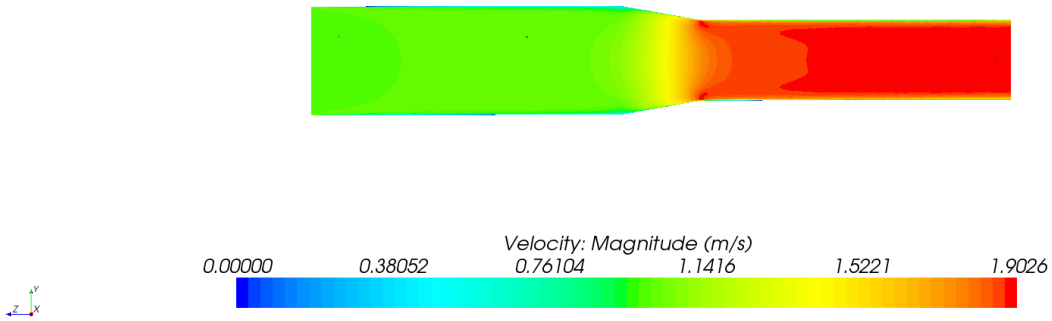

1.5 m/s

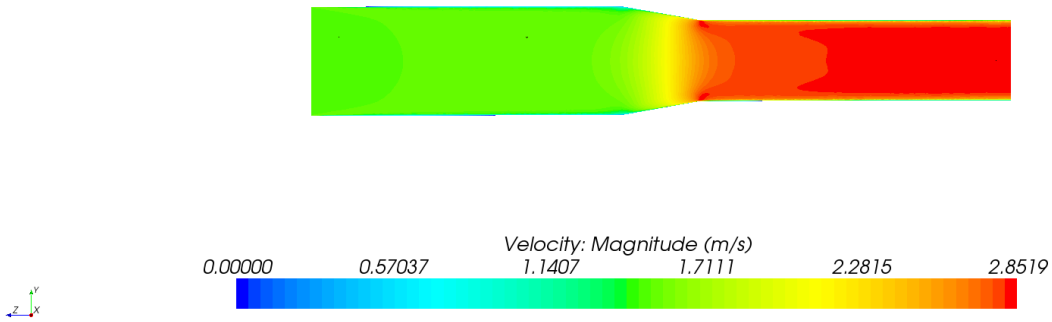

2 m/s

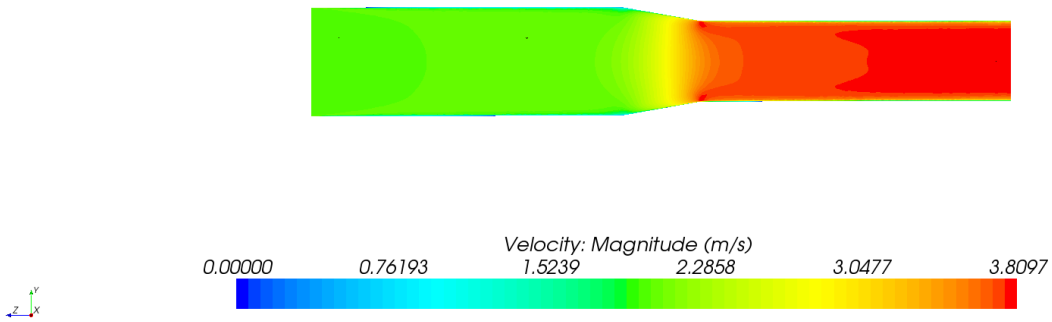

2.4 m/s

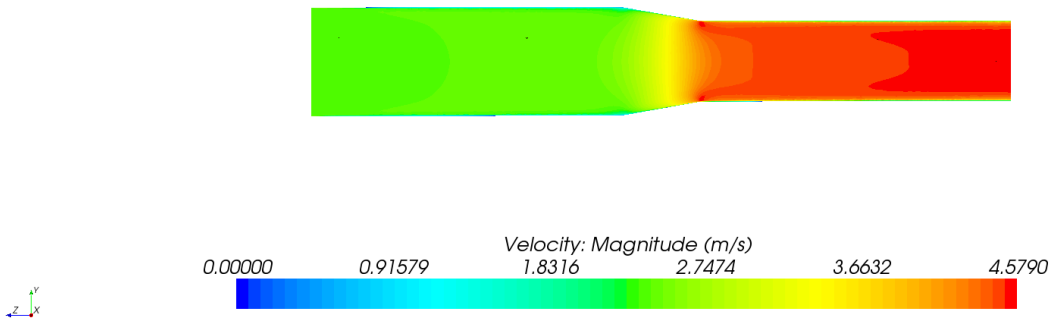

Figure 4.18: CR 10 Model YZ Plane Velocity Scalars

1 m/s

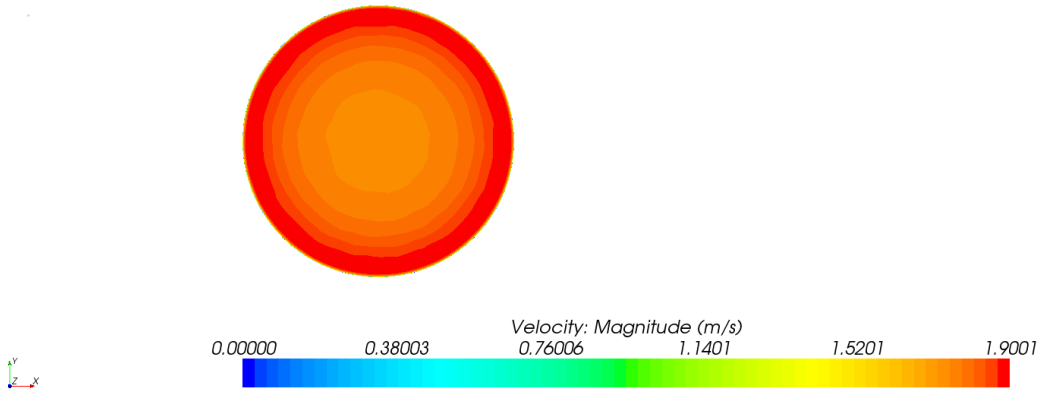

1.5 m/s

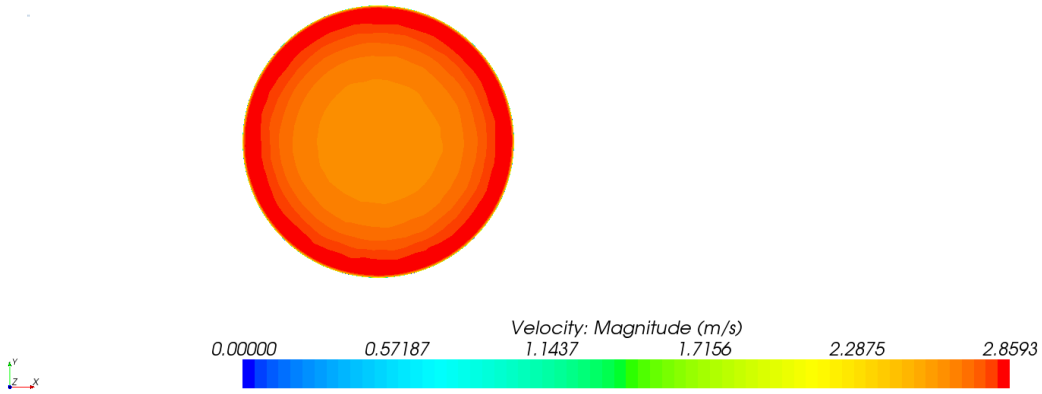

2 m/s

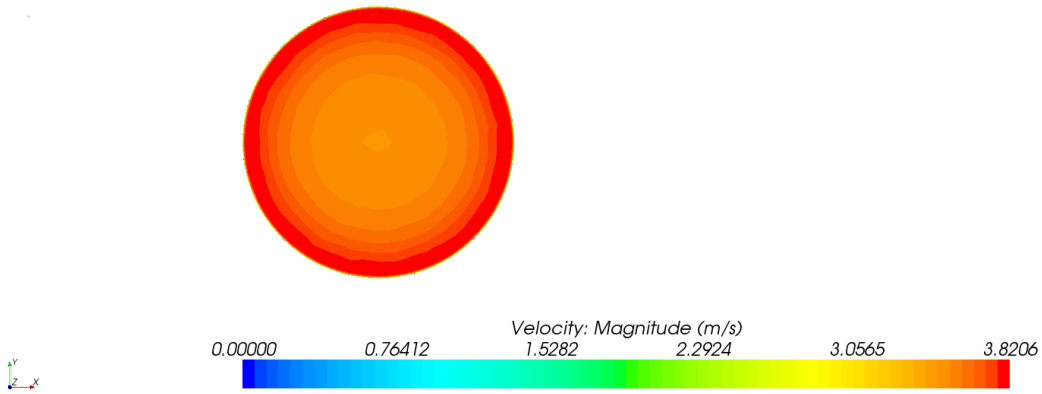

2.4 m/s

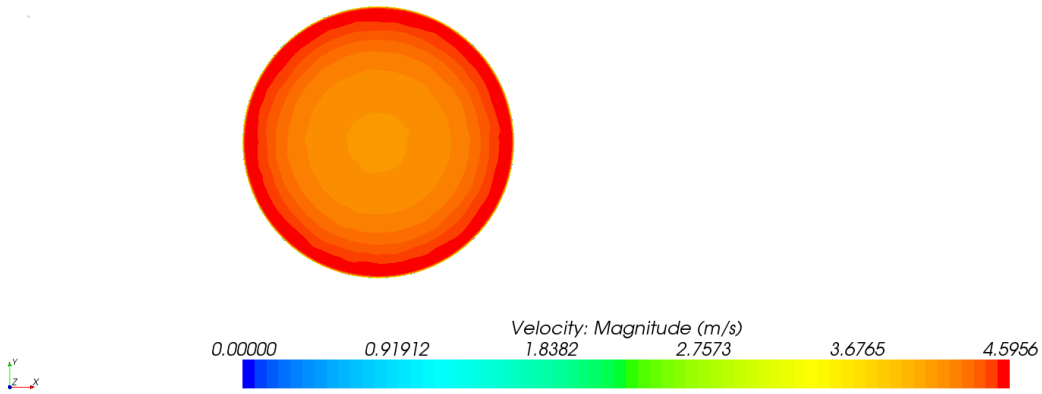

Figure 4.19: CR 10 Model XY Plane Velocity Scalars at Probe Position 1

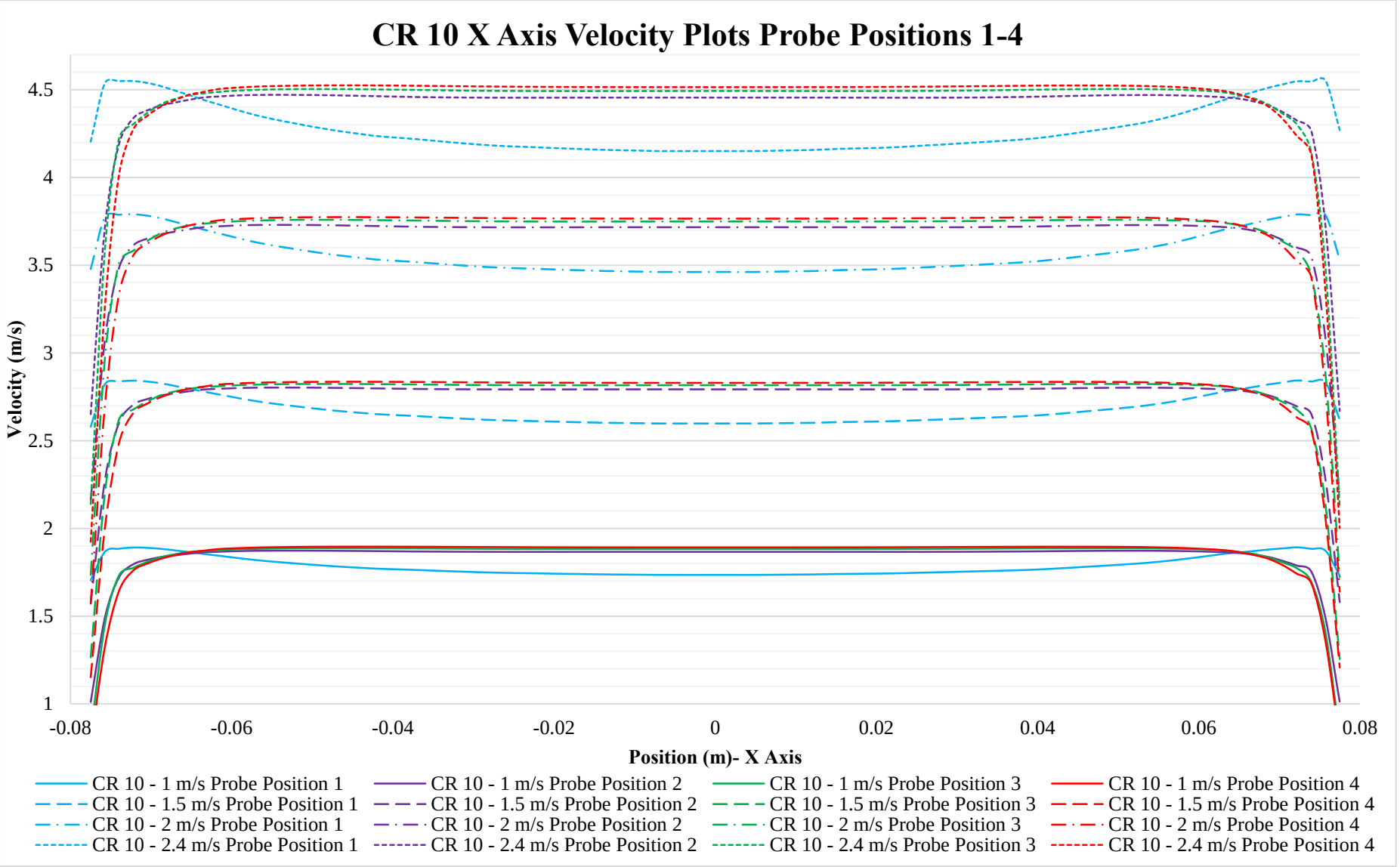

Figure 4.20: CR 10 X Axis Velocity XY Plots Probe Positions 1-4

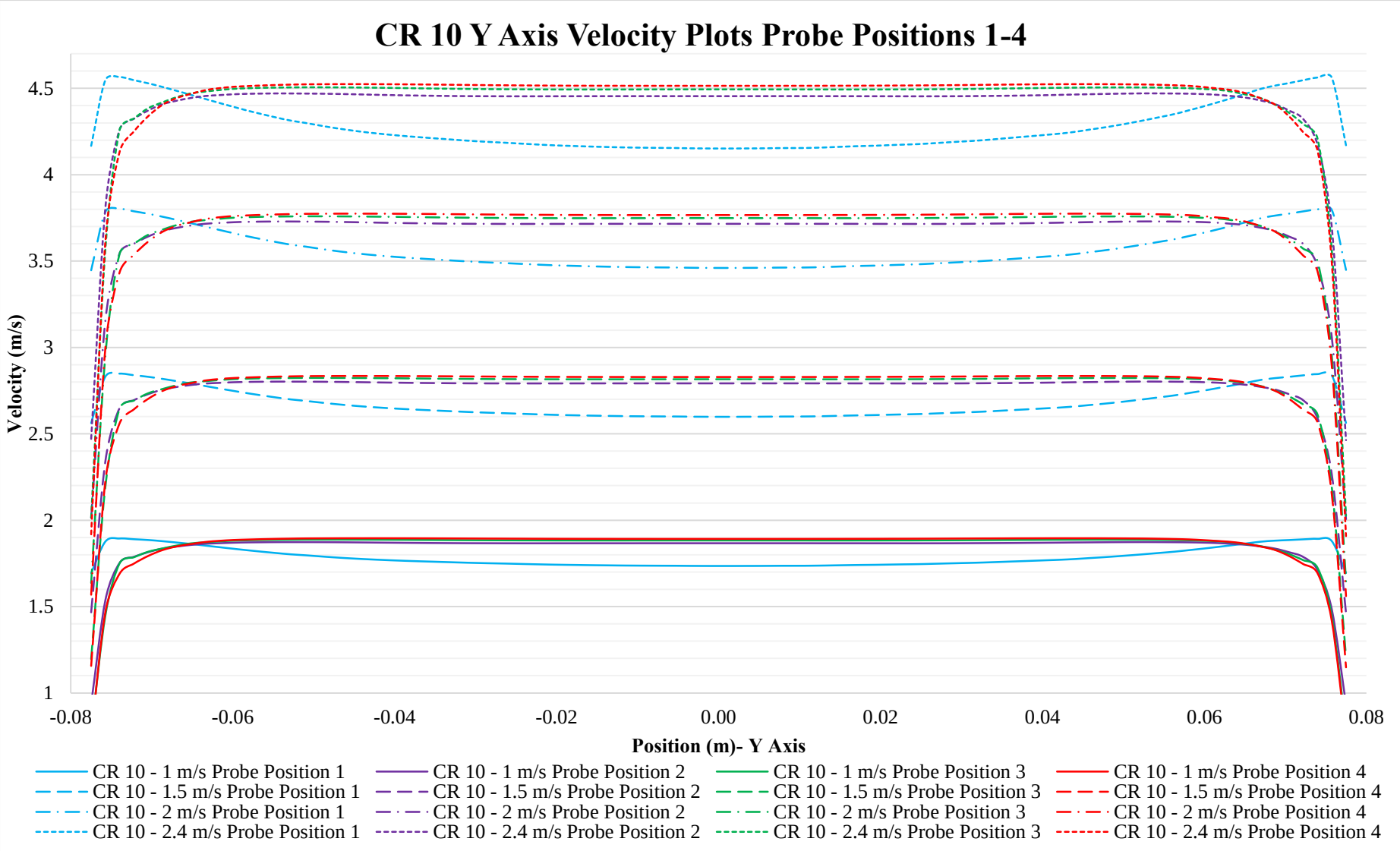

Figure 4.21: CR 10 Y Axis Velocity XY Plots Probe Positions 1-4

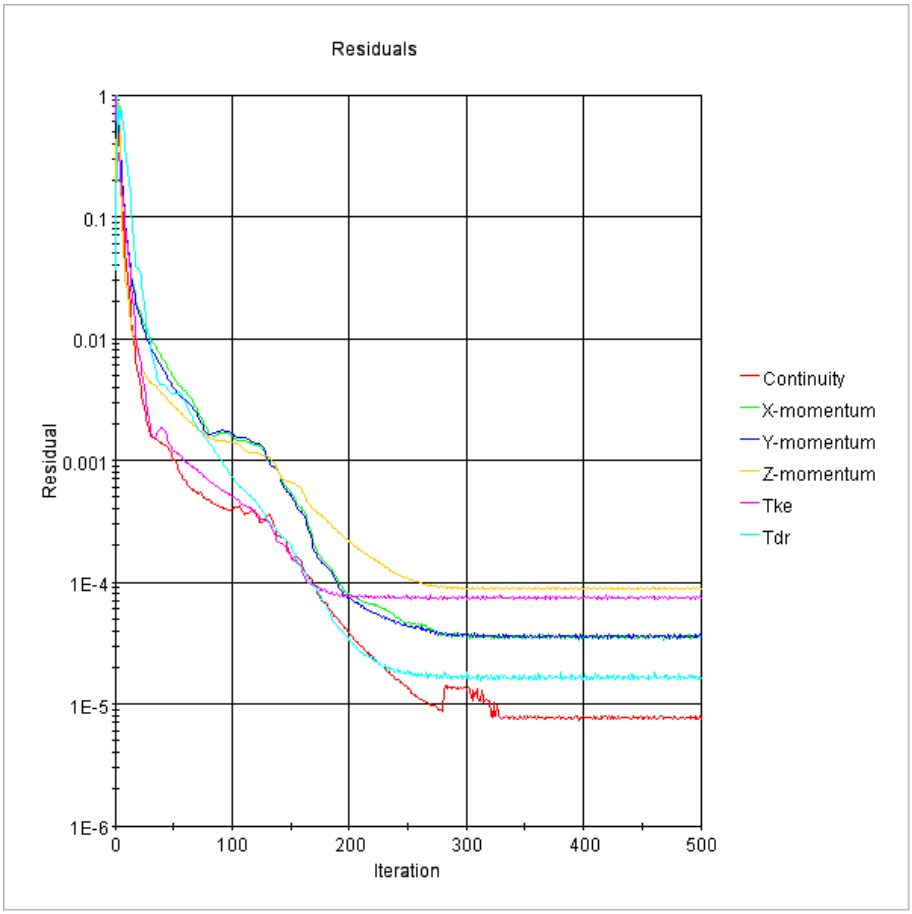

Figure 4.22: CR 10 Simulation Residual Plot – 1m/s Velocity Inlet

4.2.5. CR 15 Model Results

The results for the CR 15 Model are provided in **Figure 4.23** to **Figure 4.27**. All four of the simulations were solved to an acceptable level within the 500 iteration steps. The residual plot for the 1 m/s simulation is provided in **Figure 4.27**. **Figure 4.23** and **Figure 4.24** illustrate the velocity distributions for the CR 15 Models and it is observed that they have significant velocity distributions with high velocities towards the outer areas of the fluid body through the reducer fitting. This velocity distribution however remain symmetrical around the center of the pipe, i.e. the velocity contours are circular in shape. **Figure 4.25** and **Figure 4.26** illustrate that the acceleration of flow through the reducer fitting creates a velocity distribution with acceleration towards the sides of the pipe at Probe Position 1, but this velocity distribution is evened out into a uniform distribution typical of pipe flow at a distance of 1xD2 downstream from the reducer (Probe Position 2). This acceleration is greater than the acceleration experienced with the previous models.

1 m/s

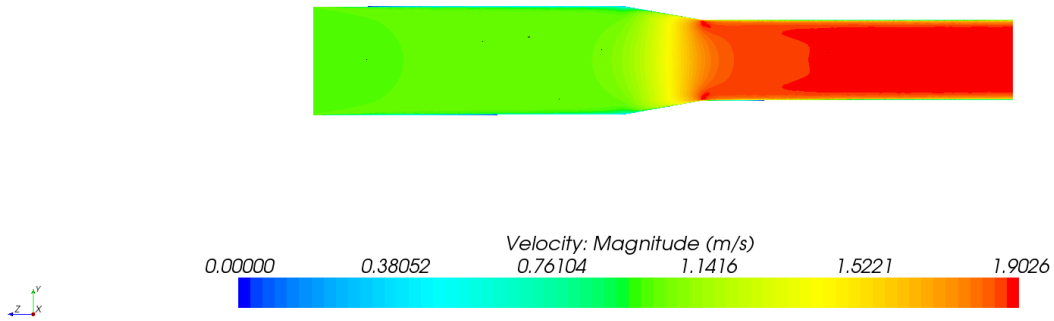

1.5 m/s

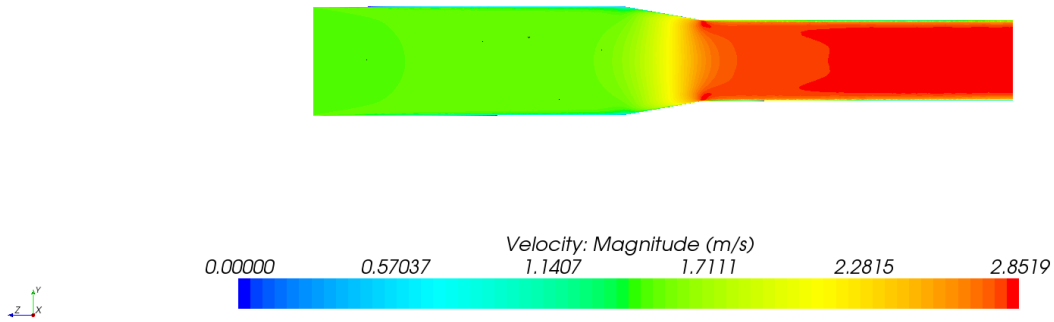

2 m/s

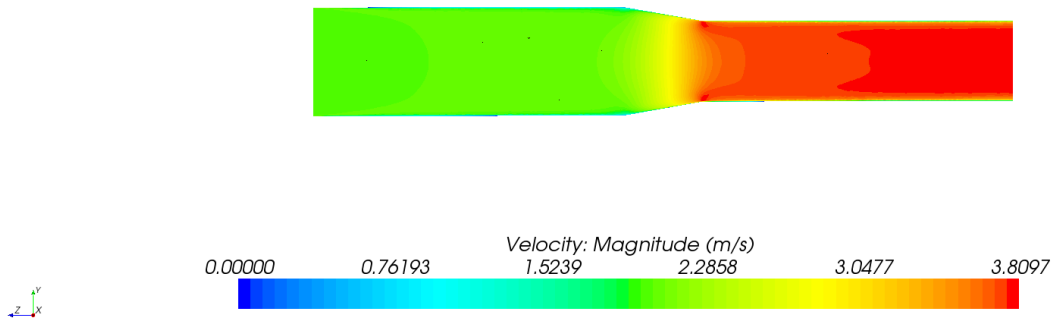

2.4 m/s

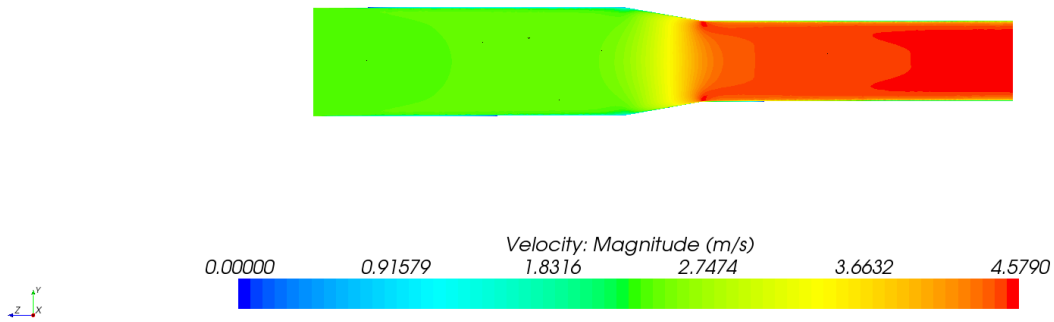

Figure 4.23: CR 15 Model YZ Plane Velocity Scalars

1 m/s

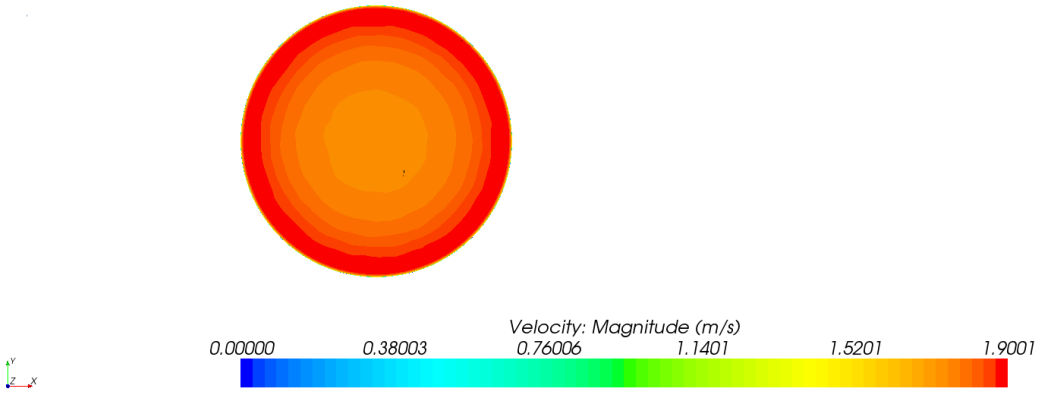

1.5 m/s

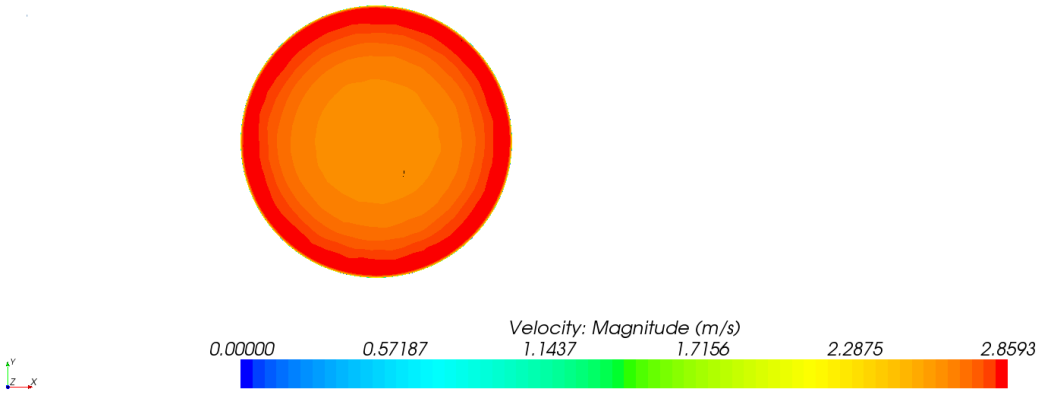

2 m/s

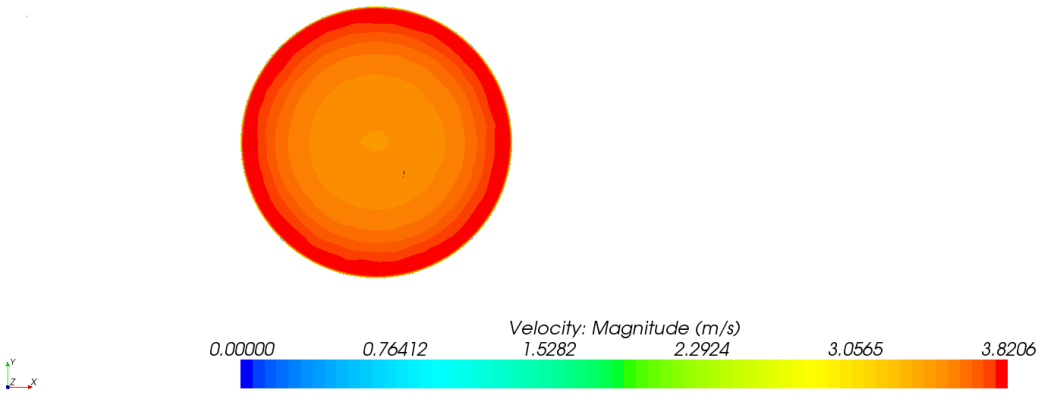

2.4 m/s

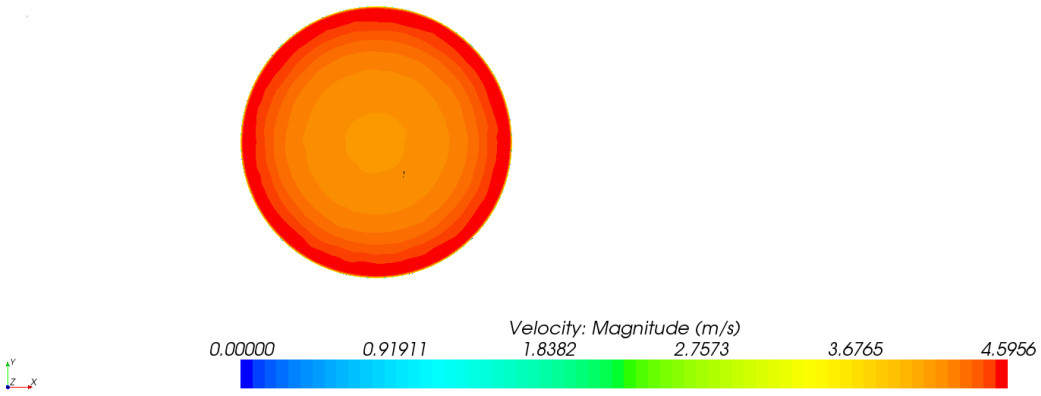

Figure 4.24: CR 15 Model XY Plane Velocity Scalars at Probe Position 1

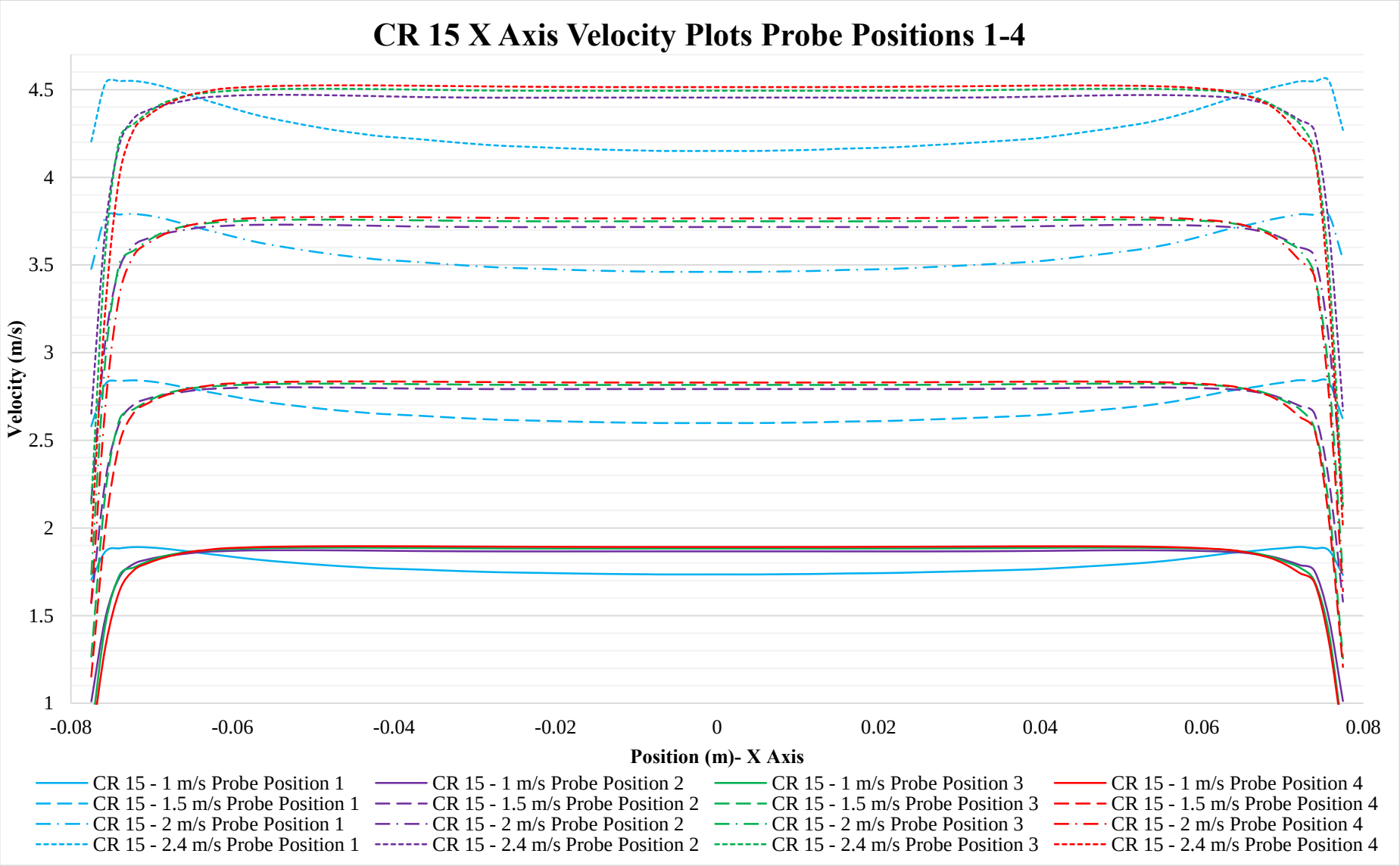

Figure 4.25: CR 15 X Axis Velocity XY Plots Probe Positions 1-4

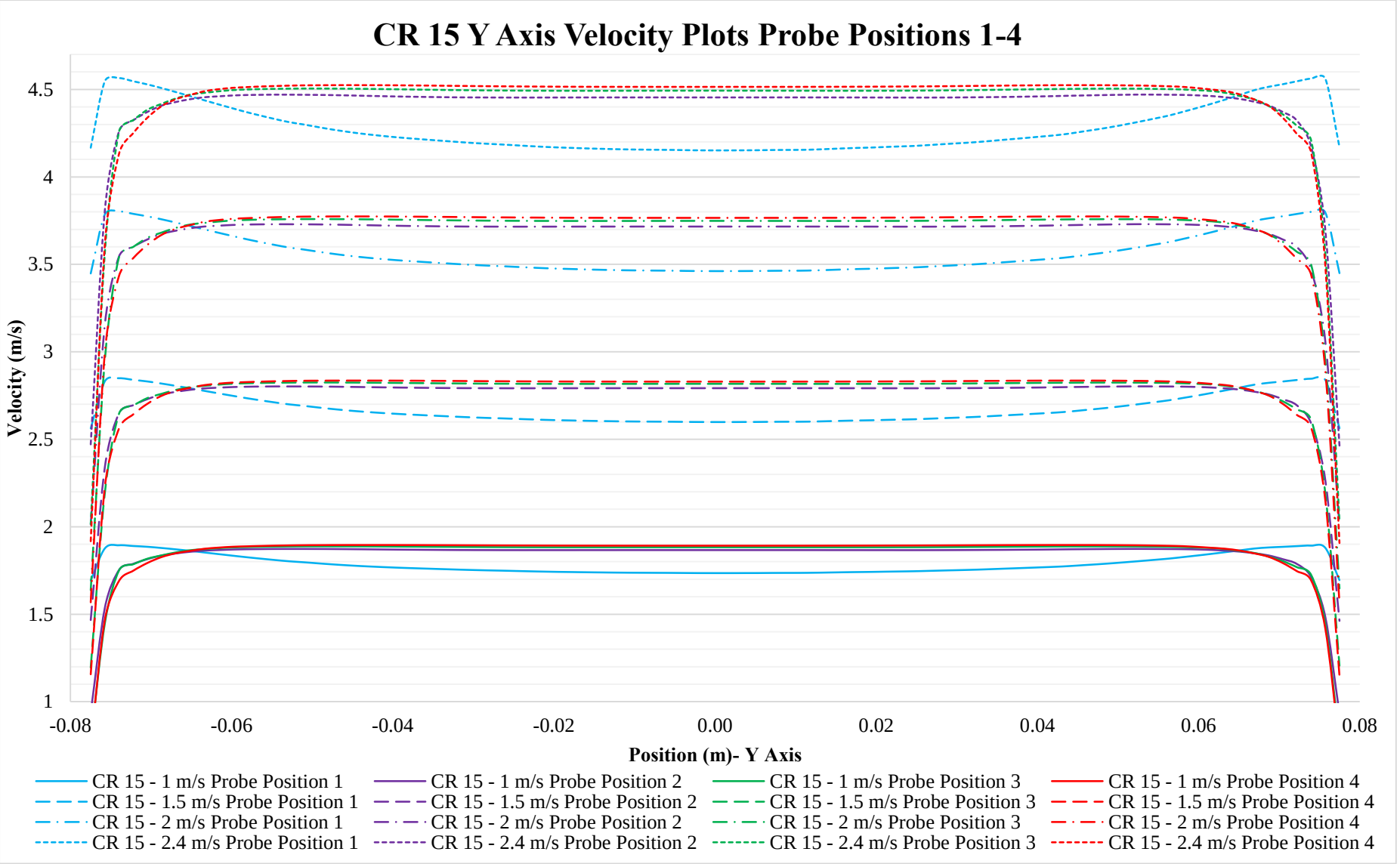

Figure 4.26: CR 15 Y Axis Velocity XY Plots Probe Positions 1-4

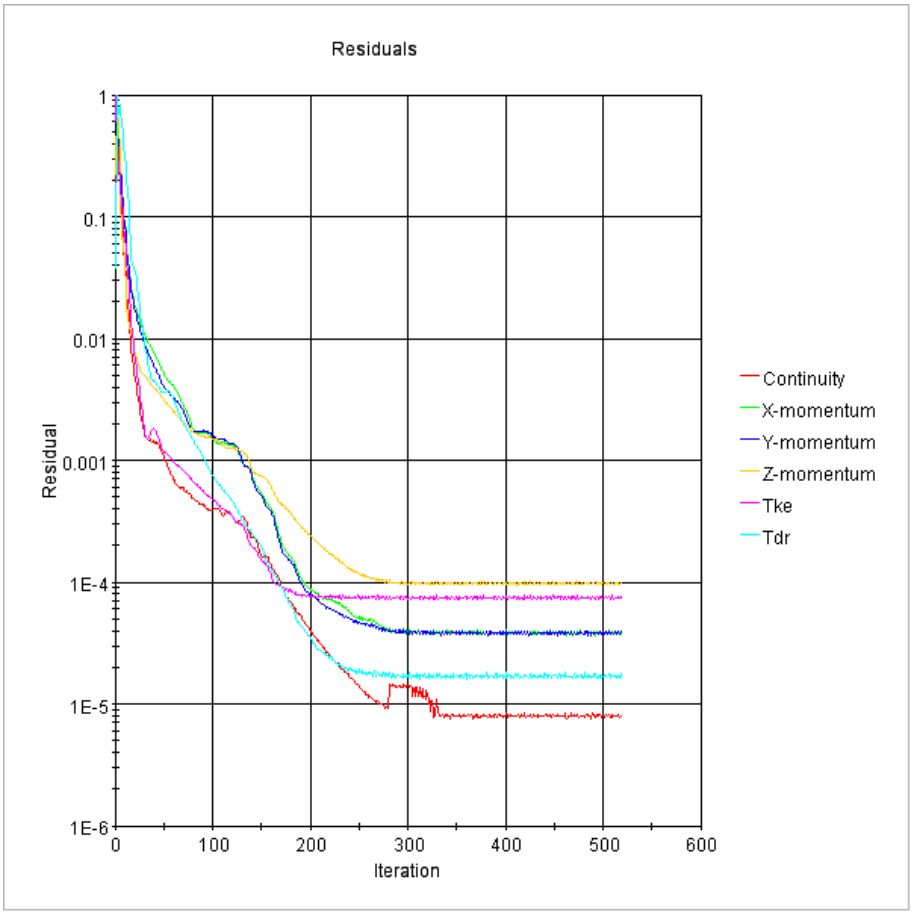

Figure 4.27: CR 15 Simulation Residual Plot – 1m/s Velocity Inlet

4.2.6. CR 20 Model Results

The results for the CR 20 Model are provided in **Figure 4.28** and **Figure 4.32**. All four velocity simulations were solved satisfactorily in the 500 iteration steps. The residual plot for the 1 m/s simulation is provided in **Figure 4.32**. Areas of extreme velocities are resultant of the reducer's steep angles where velocities in excess of 10% of the average velocity through the section are experienced, as is illustrated in **Figure 4.28** and **Figure 4.29**. **Figure 4.30** and **Figure 4.31** illustrate that the acceleration of flow through the reducer fitting creates a velocity distribution with acceleration towards the sides of the pipe at Probe Position 1, but this velocity distribution is evened out into a uniform distribution typical of pipe flow at a distance of 1xD2 downstream from the reducer (Probe Position 2) even with the areas of extreme velocities experienced. This acceleration is greater than the acceleration experienced with the previous models.

1 m/s

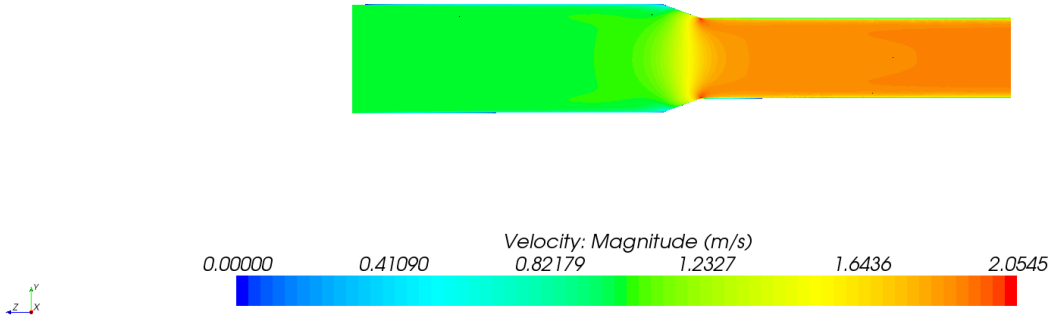

1.5 m/s

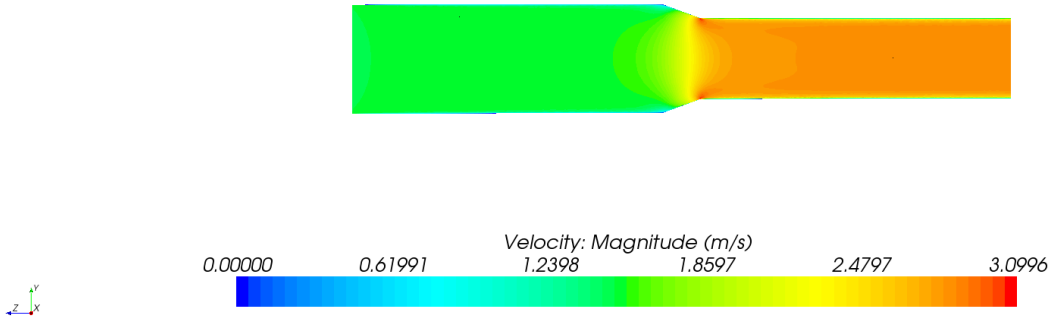

2 m/s

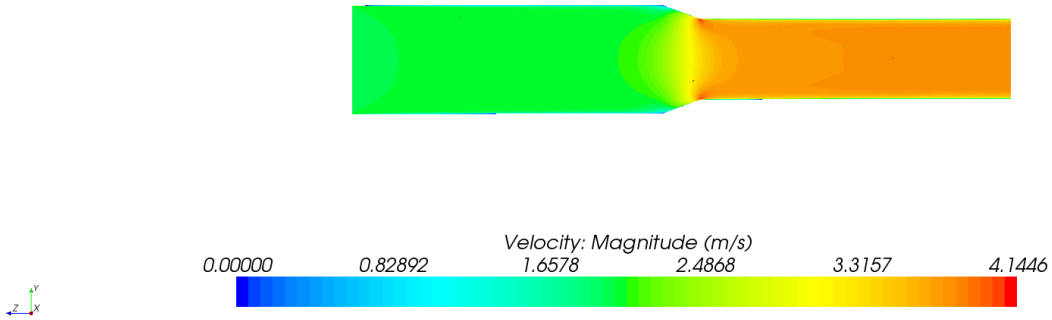

2.4 m/s

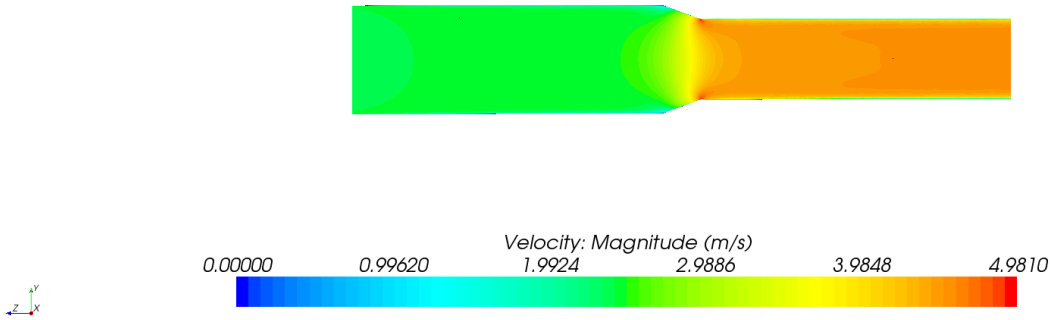

Figure 4.28: CR 20 Model YZ Plane Velocity Scalars

1 m/s

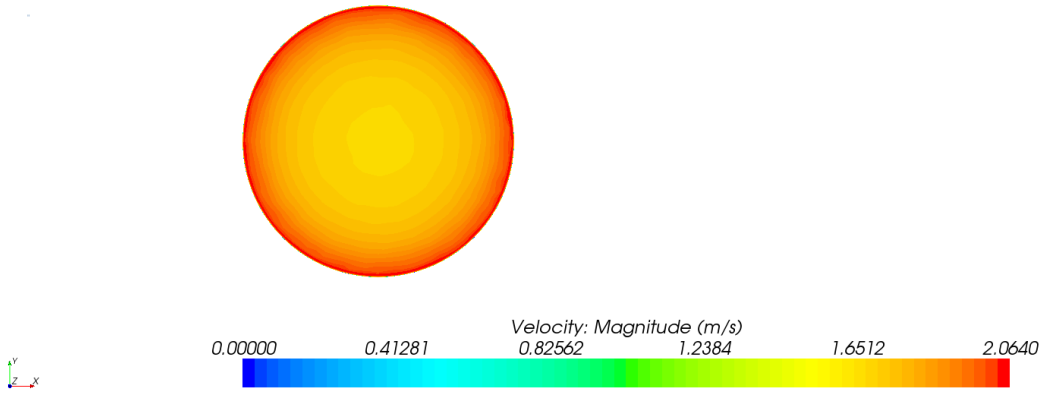

1.5 m/s

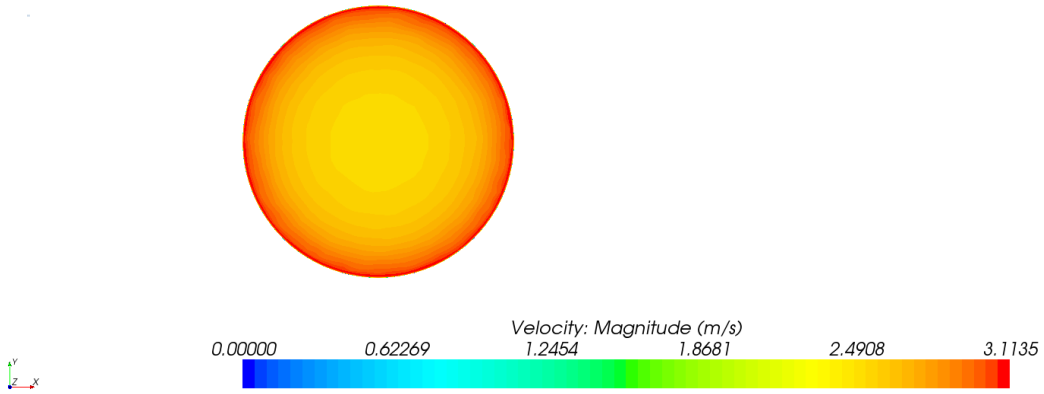

2 m/s

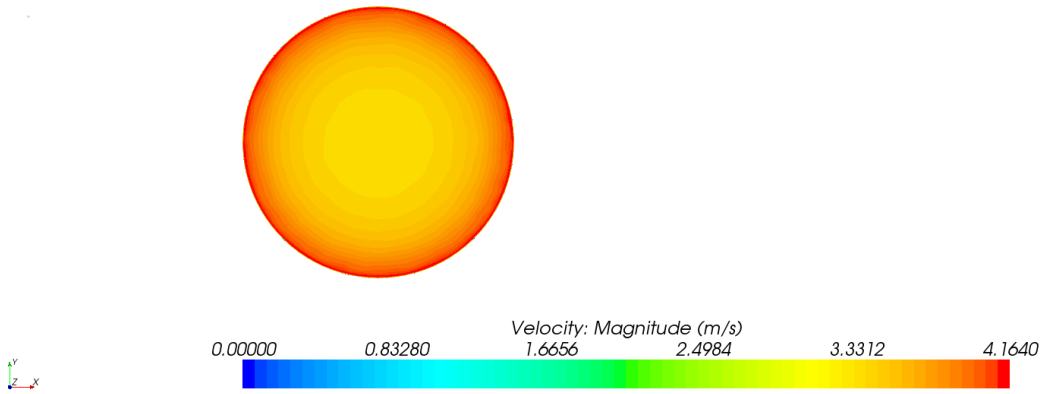

2.4 m/s

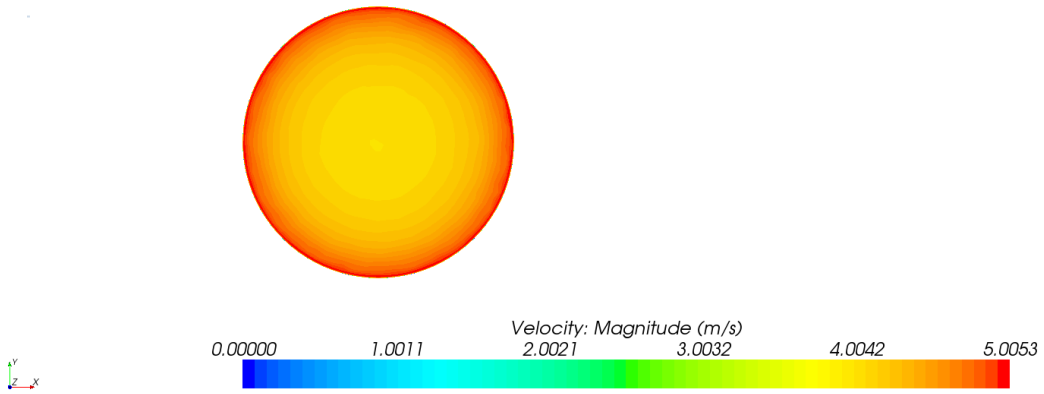

Figure 4.29: CR 20 Model YZ Plane Velocity Scalars at Probe Position 1

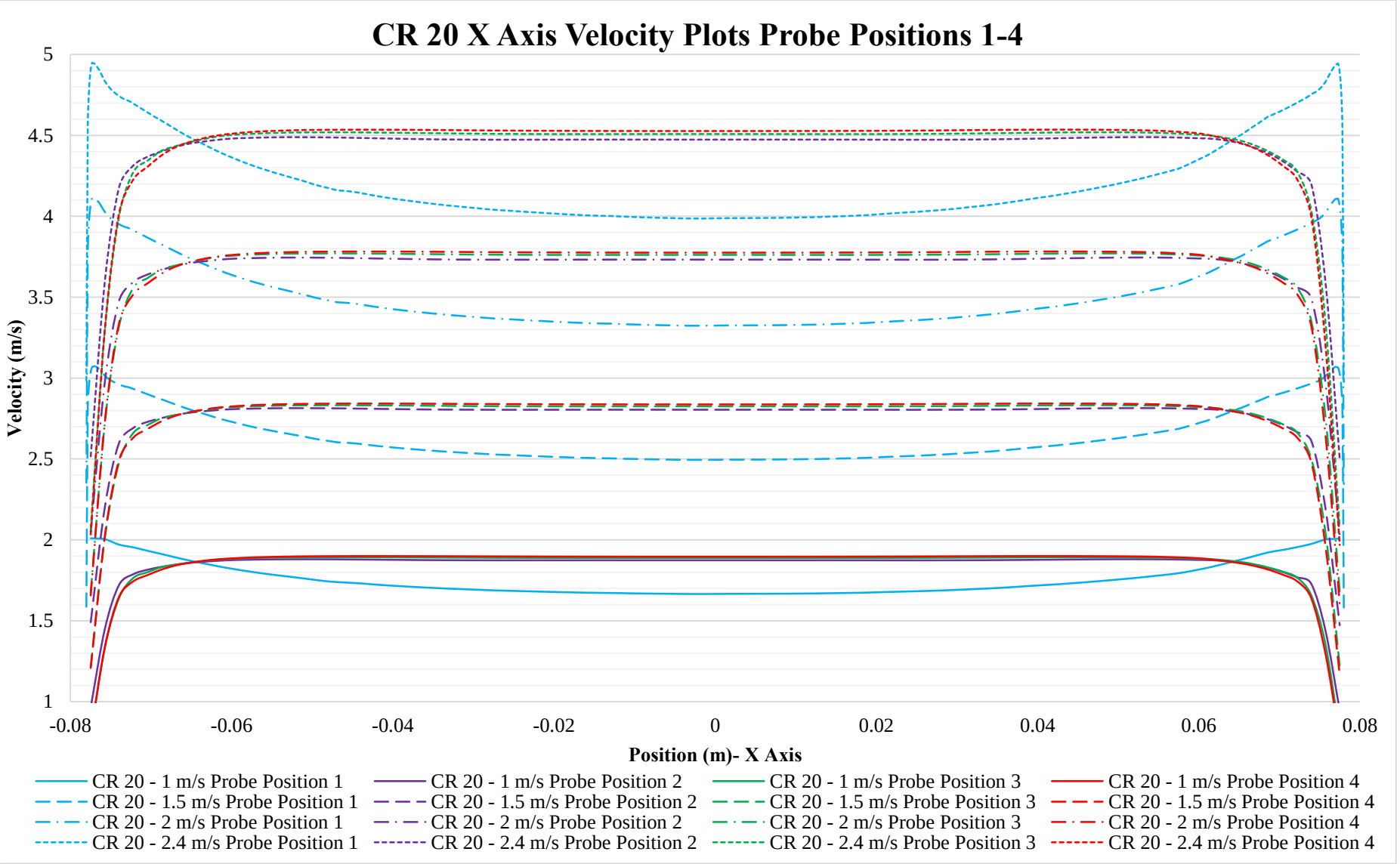

Figure 4.30: CR 20 X Axis Velocity XY Plots Probe Positions 1-4

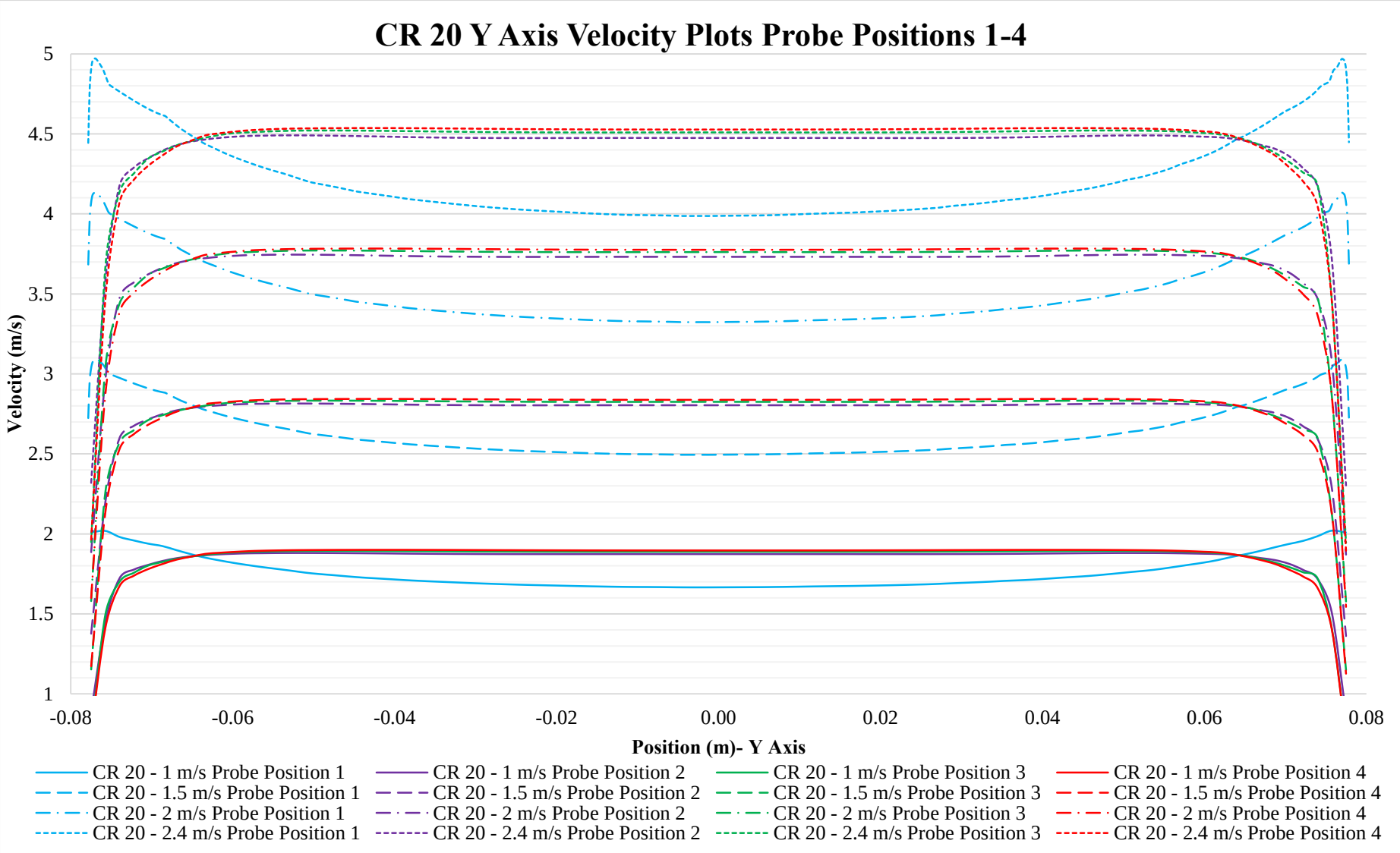

Figure 4.31: CR 20 X Axis Velocity XY Plots Probe Positions 1-4

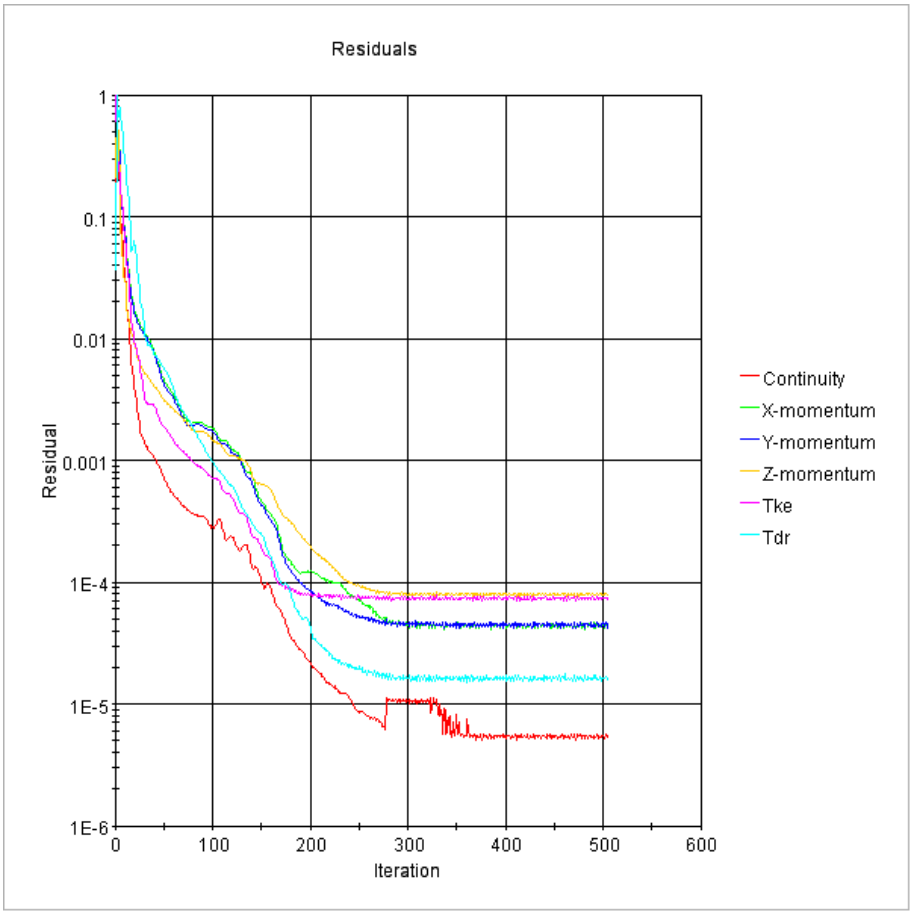

Figure 4.32: CR 20 Simulation Residual Plot – 1m/s Velocity Inlet

4.3. ECCENTRIC REDUCER MODELS SIMULATION RESULTS

4.3.1. ER 2.5 Model Results

The results for the ER 2.5 Model are provided in **Figure 4.33** to **Figure 4.37**. The four flow velocities were applied to the ER 2.5 Model, the simulation for the 2 m/s and 2.4 m/s velocities did not converge to an acceptable level within the 500 iteration steps. The number of iteration steps was increased to 600 for this simulation and then acceptable results were achieved. The ER 2.5 Model did converge within 500 iterations for the 1 m/s and the 1.5 m/s flow velocities. The residual plot for the 2 m/s simulation with 600 iterations is provided in **Figure 4.37** and the remaining residual plots are provided on the ***Supporting Digital Media***.

The velocity distribution for the ER 2.5 model remains fairly uniform, with a slight increase in velocity in the lower portion of the reducer fitting as reflected in **Figure 4.33** and **Figure 4.34**. **Figure 4.35** and **Figure 4.36** illustrate that the acceleration through the reducer is not the same along

the X Axis and the Y Axis at Probe Position 1. The velocity distributions along the X Axis are similar to those of the concentric reducers, but the velocity distribution at Probe Position 1 for the Y Axis shows higher velocities at the bottom, sloped, side. This caused by the acceleration along this bottom side. The velocity distributions even out into a uniform velocity distribution typical of pipe flow at a distance of 1xD2 downstream from the reducer (Probe Position 2). The velocity distributions at Probe Positions 2, 3 and 4 are almost identical for both the X Axis and the Y Axis.

1 m/s

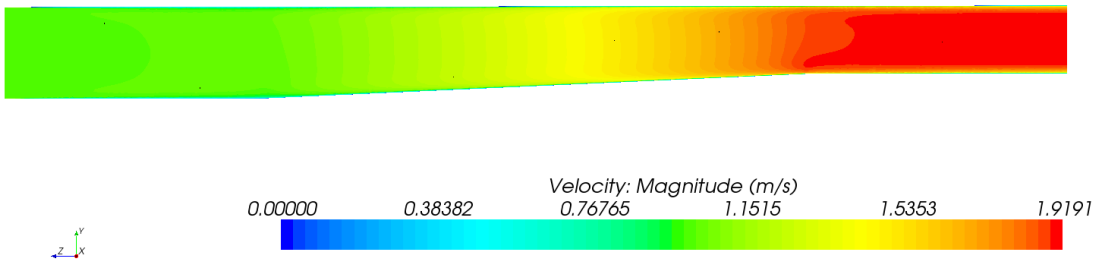

1.5 m/s

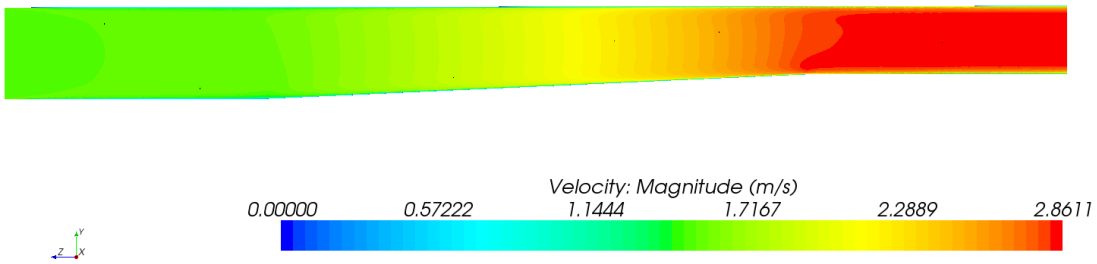

2 m/s

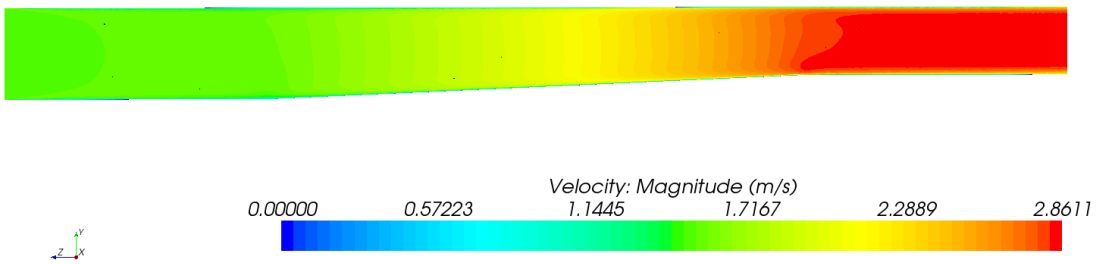

2.4 m/s

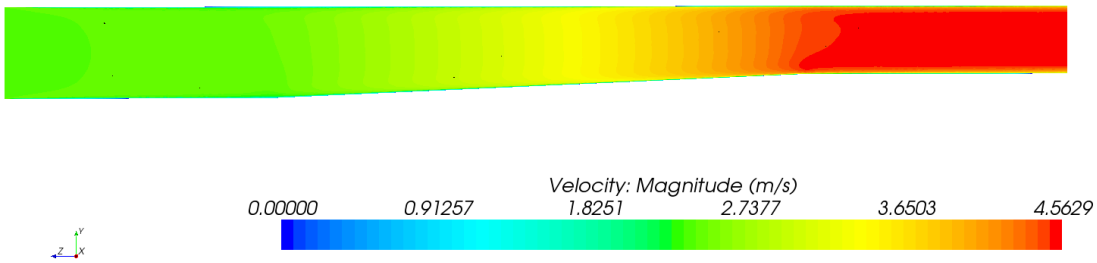

Figure 4.33: ER 2.5 Model YZ Plane Velocity Scalars

1 m/s

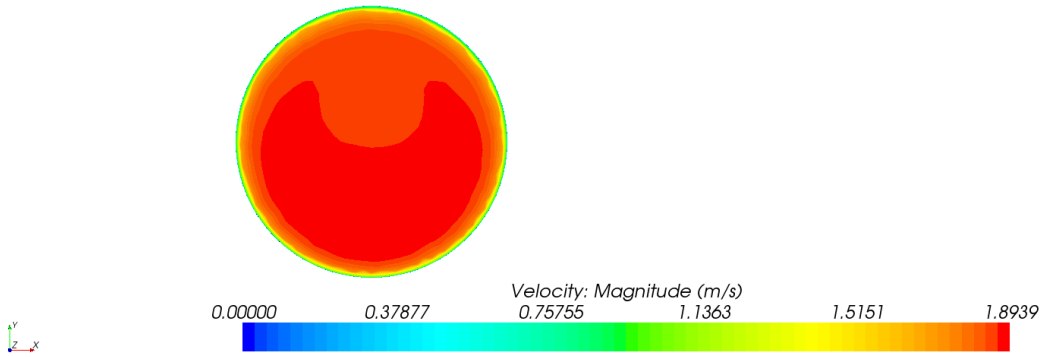

1.5 m/s

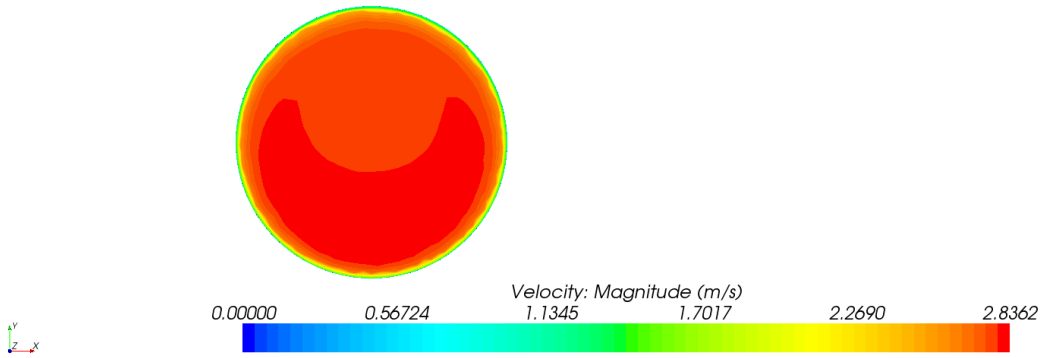

2 m/s

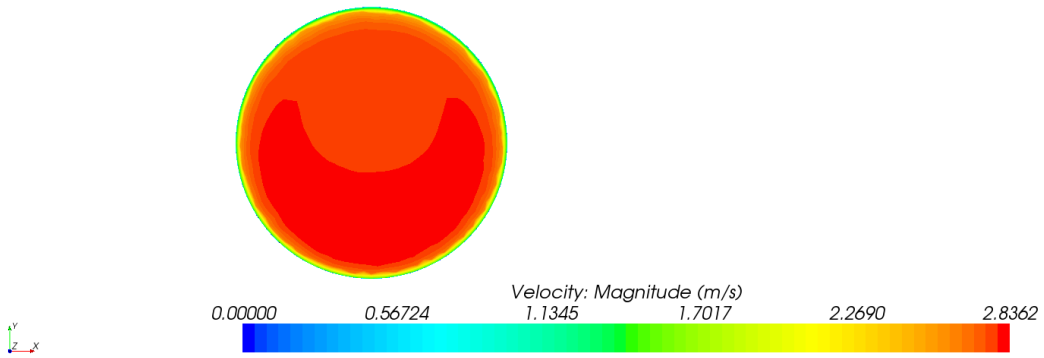

2.4 m/s

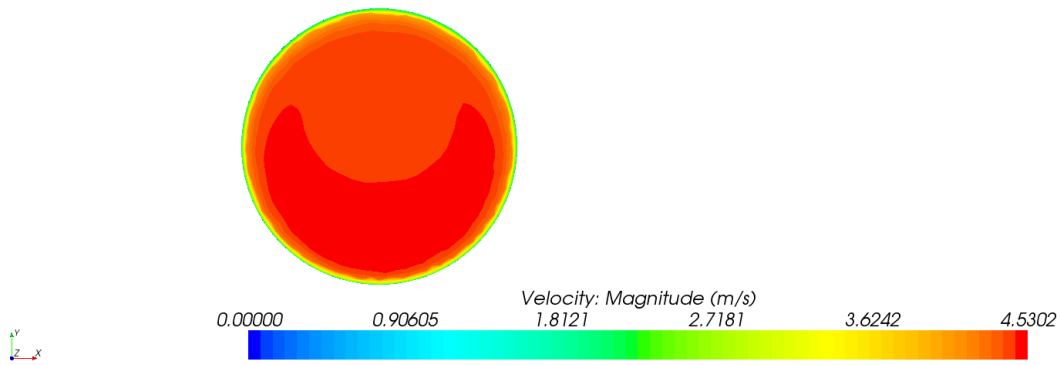

Figure 4.34: ER 2.5 Model XY Plane Velocity Scalars at Probe Position 1

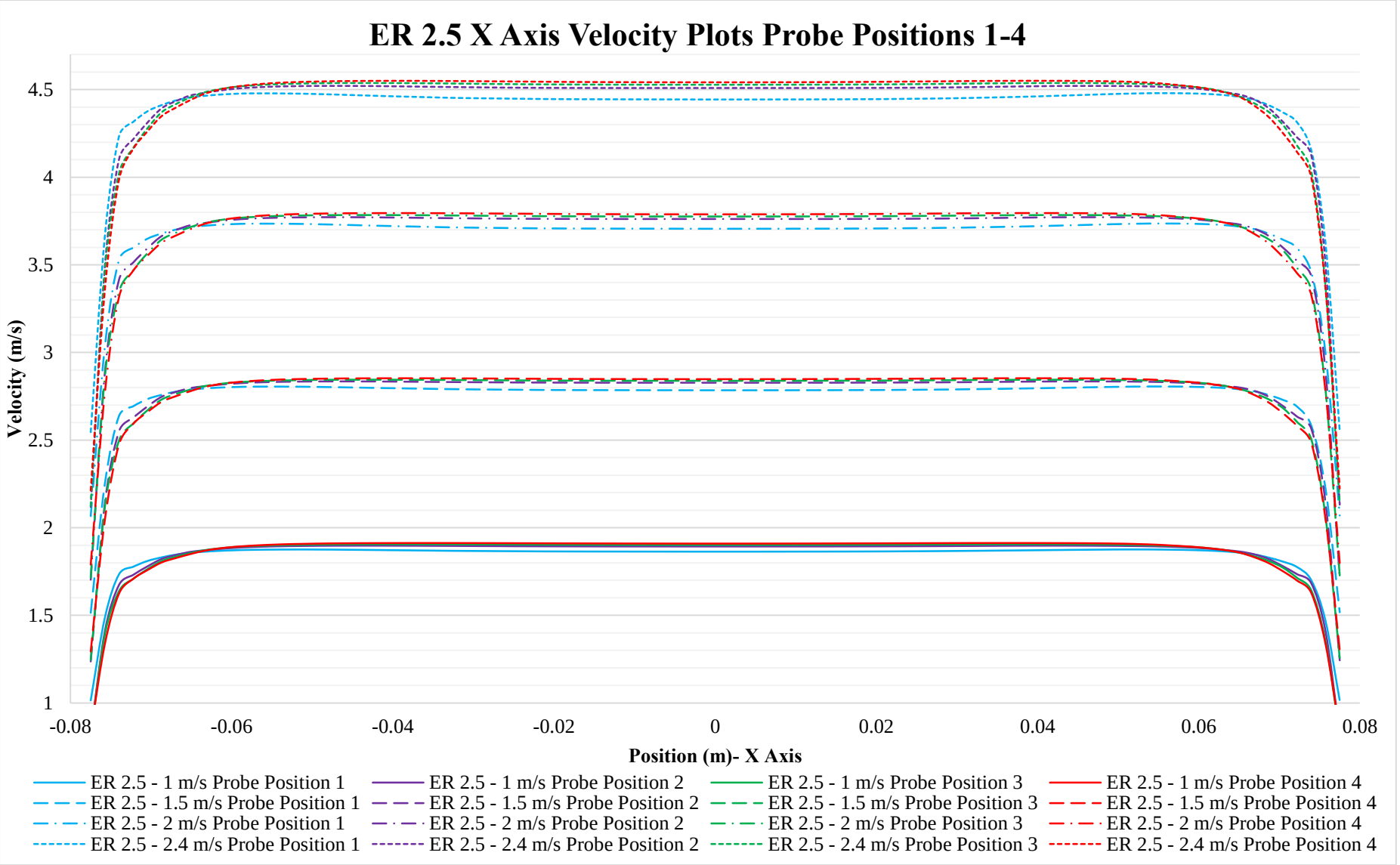

Figure 4.35: ER 2.5 X Axis Velocity XY Plots Probe Positions 1-4

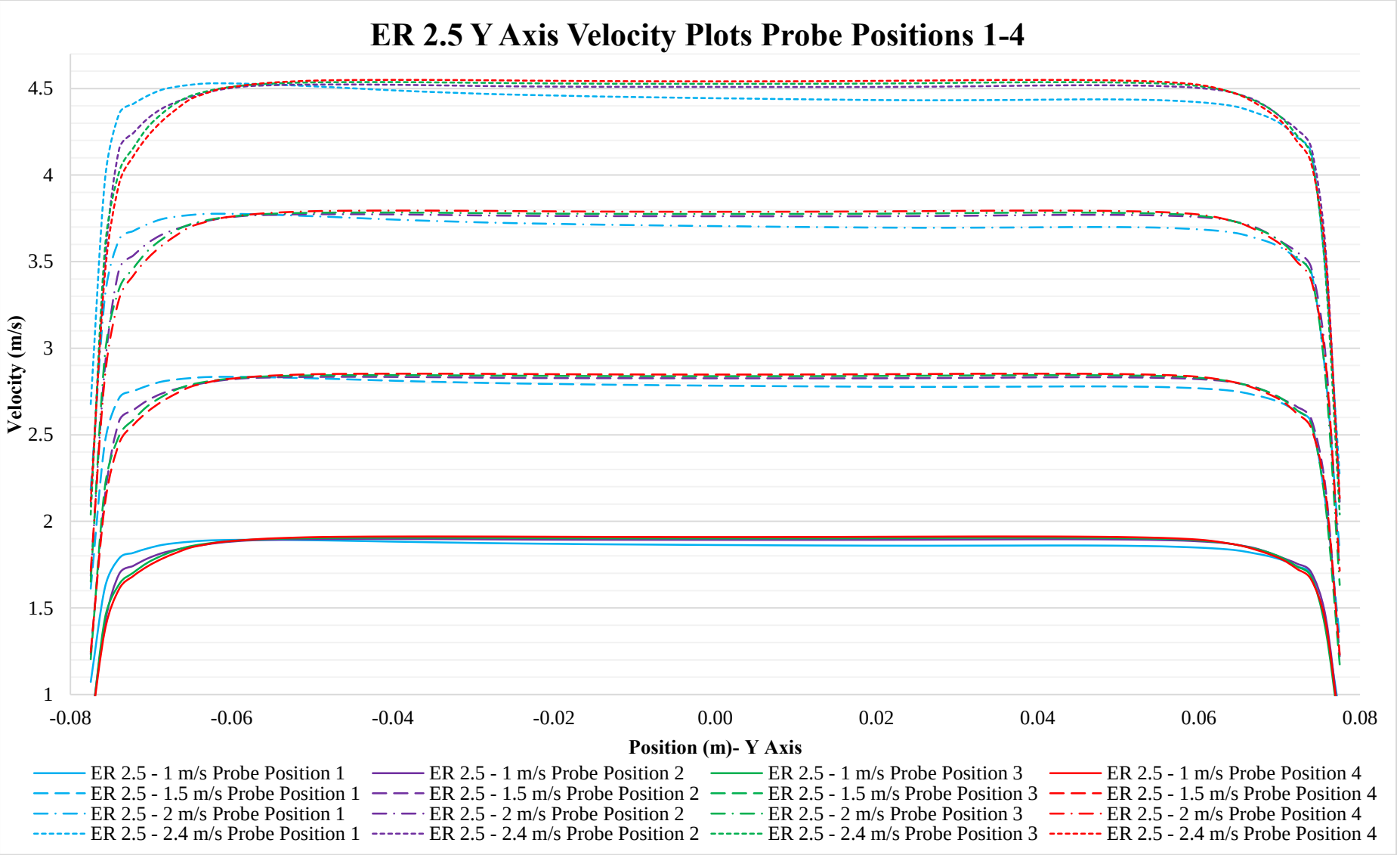

Figure 4.36: ER 2.5 Y Axis Velocity XY Plots Probe Positions 1-4

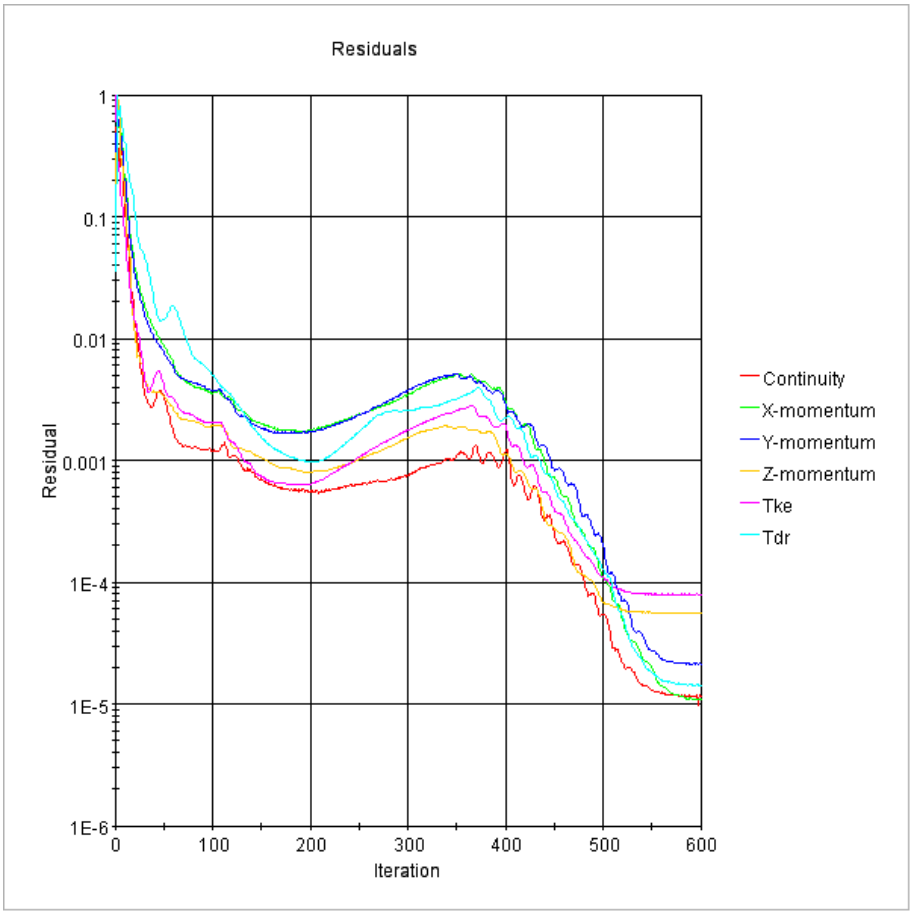

Figure 4.37: ER 2.5 Simulation Residual Plot – 2m/s Velocity Inlet

4.3.2. ER 5 Model Results

The results for the ER 5 Model are provided in **Figure 4.38** to **Figure 4.42**. All four of the ER 5 Models converged to an acceptable level within the stopping criteria of 500 iteration steps. The residual plot for the 1 m/s simulation is provided in **Figure 4.42**. The velocity gradient for the ER 5 Model has increased along the Y Axis, but has remained fairly uniform along the X Axis as reflected in **Figure 4.38** and **Figure 4.39**. The velocity distributions along the X Axis are similar to those of the concentric reducers, but the velocity distribution at Probe Position 1 for the Y Axis shows higher velocities at the bottom, sloped, side. The acceleration of water along the bottom section of the reducer is experienced again as was for the ER 2.5 model, but the amount of acceleration has increased. The velocity distributions however return to a uniform distribution within a distance of 1xD2 downstream for the reducer (Probe Position 2). These two phenomena are illustrated in **Figure 4.40** and **Figure 4.41**.

1 m/s

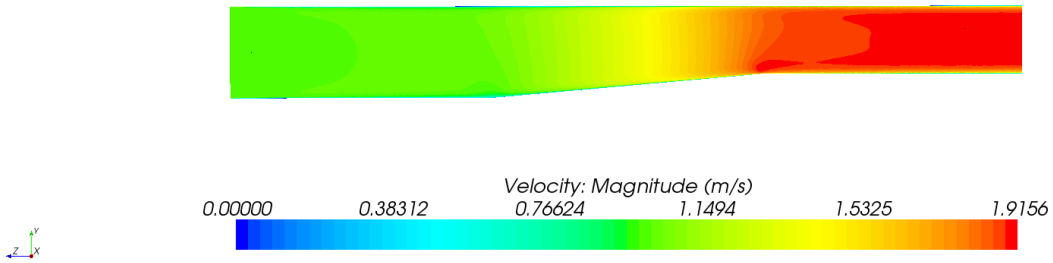

1.5 m/s

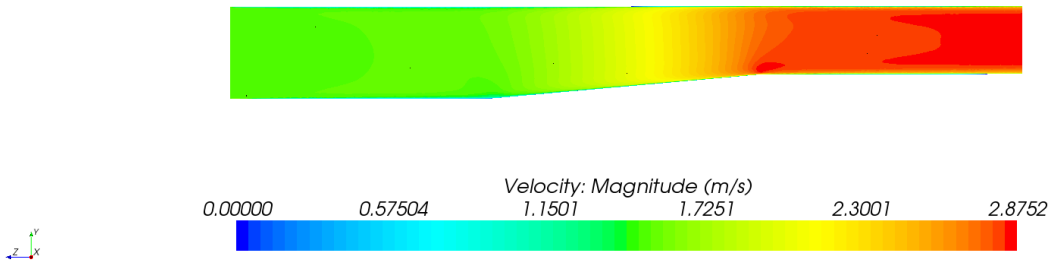

2 m/s

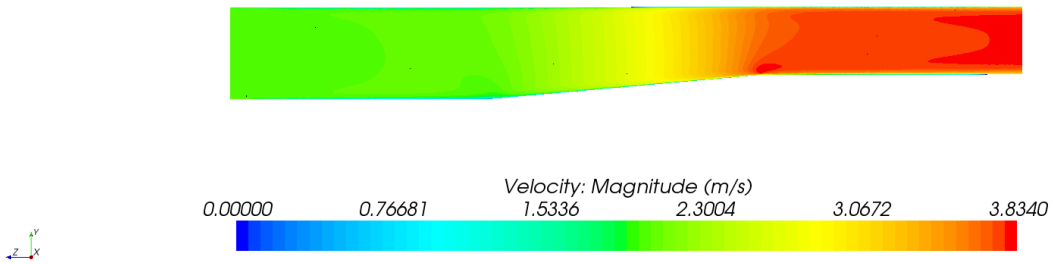

2.4 m/s

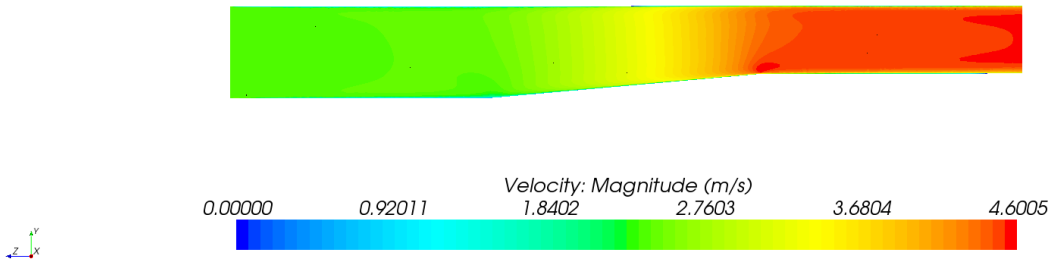

Figure 4.38: ER 5 Model YZ Plane Velocity Scalars

1 m/s

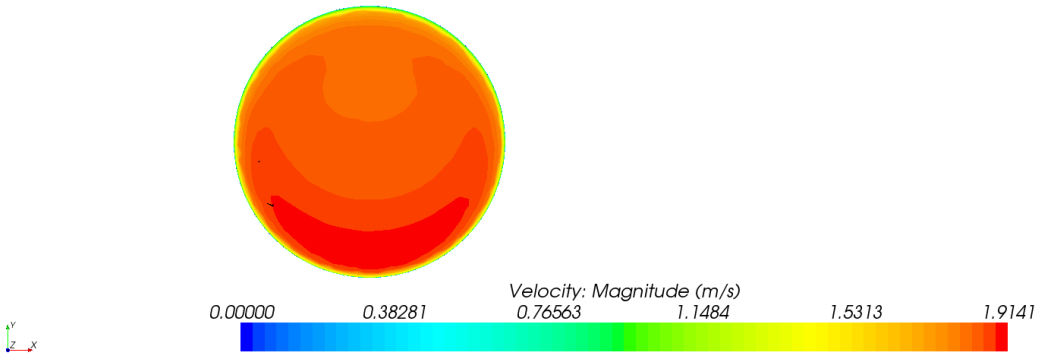

1.5 m/s

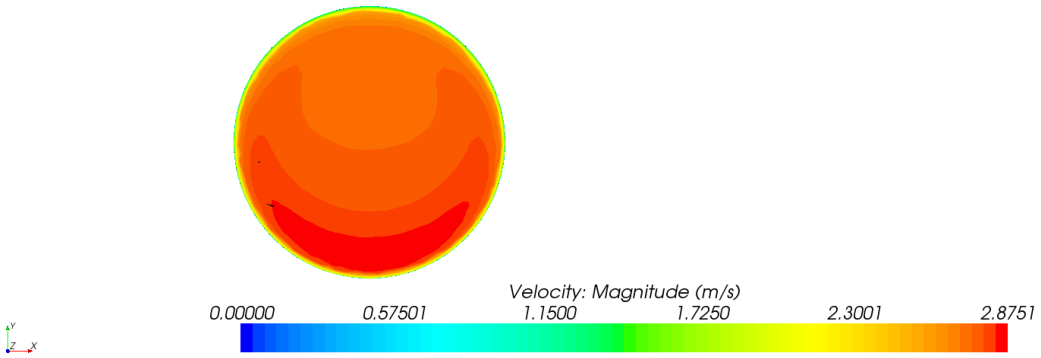

2 m/s

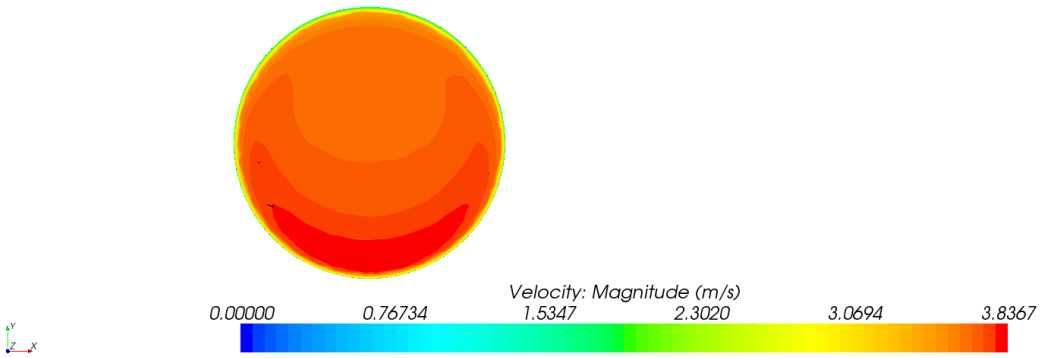

2.4 m/s

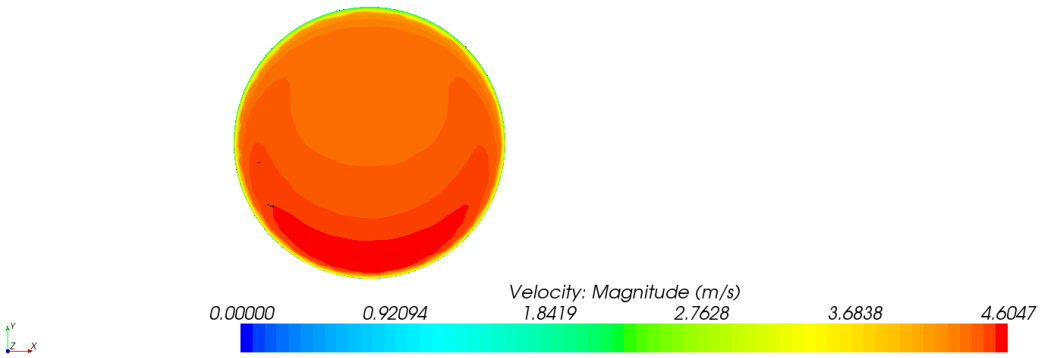

Figure 4.39: ER 5 Model XY Plane Velocity Scalars at Probe Position 1

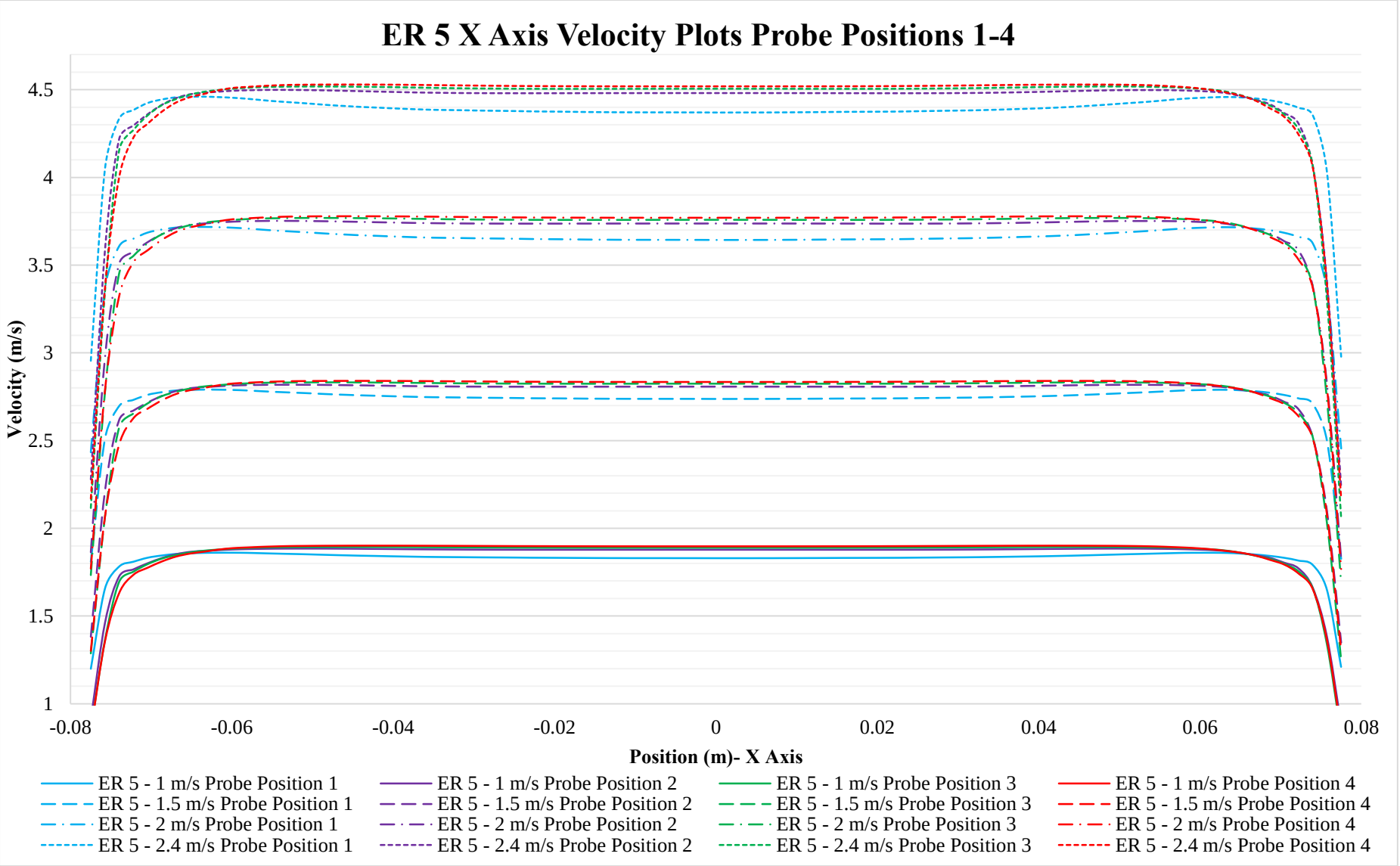

Figure 4.40: ER 5 X Axis Velocity XY Plots Probe Positions 1-4

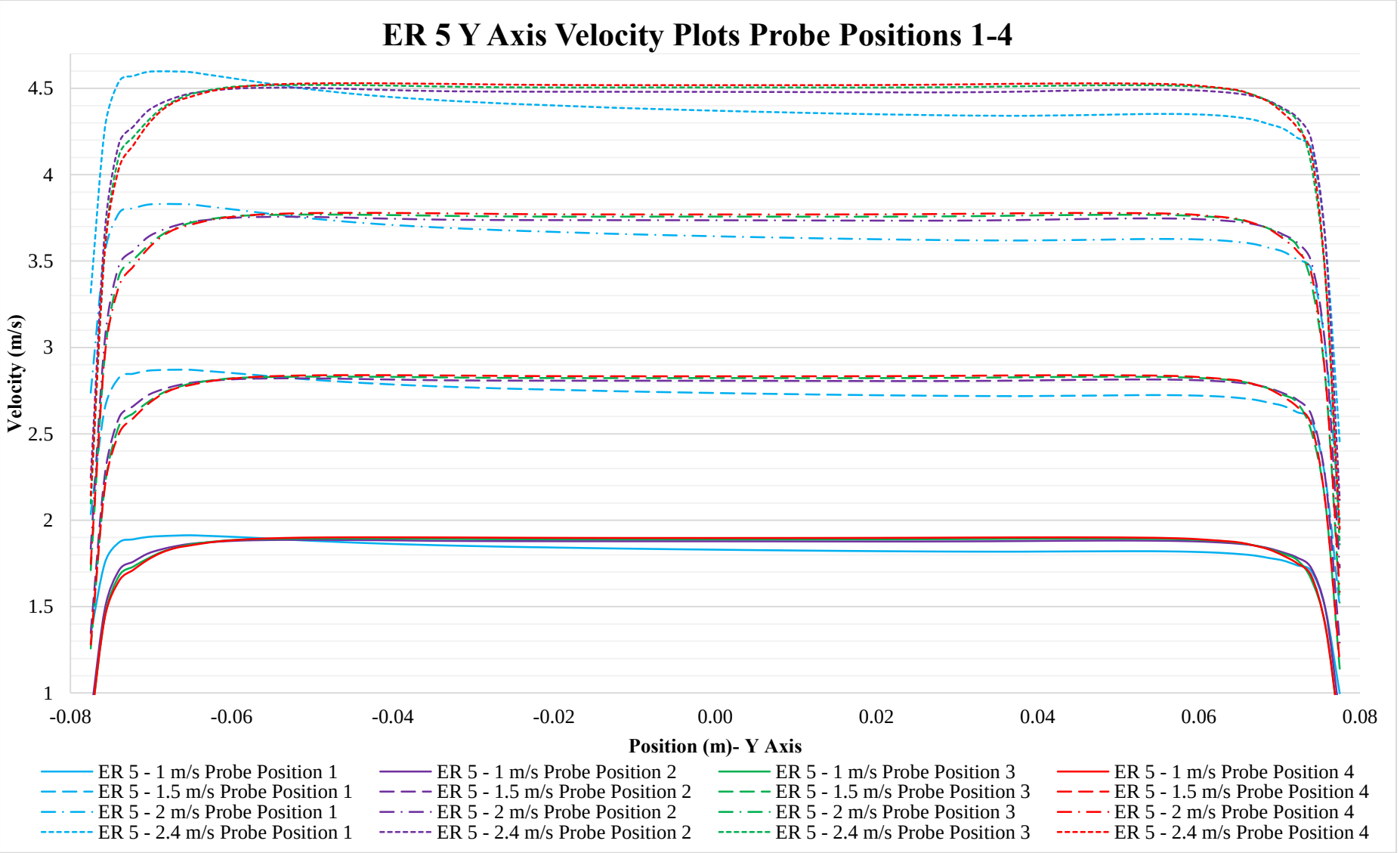

Figure 4.41: ER 5 Y Axis Velocity XY Plots Probe Positions 1-4

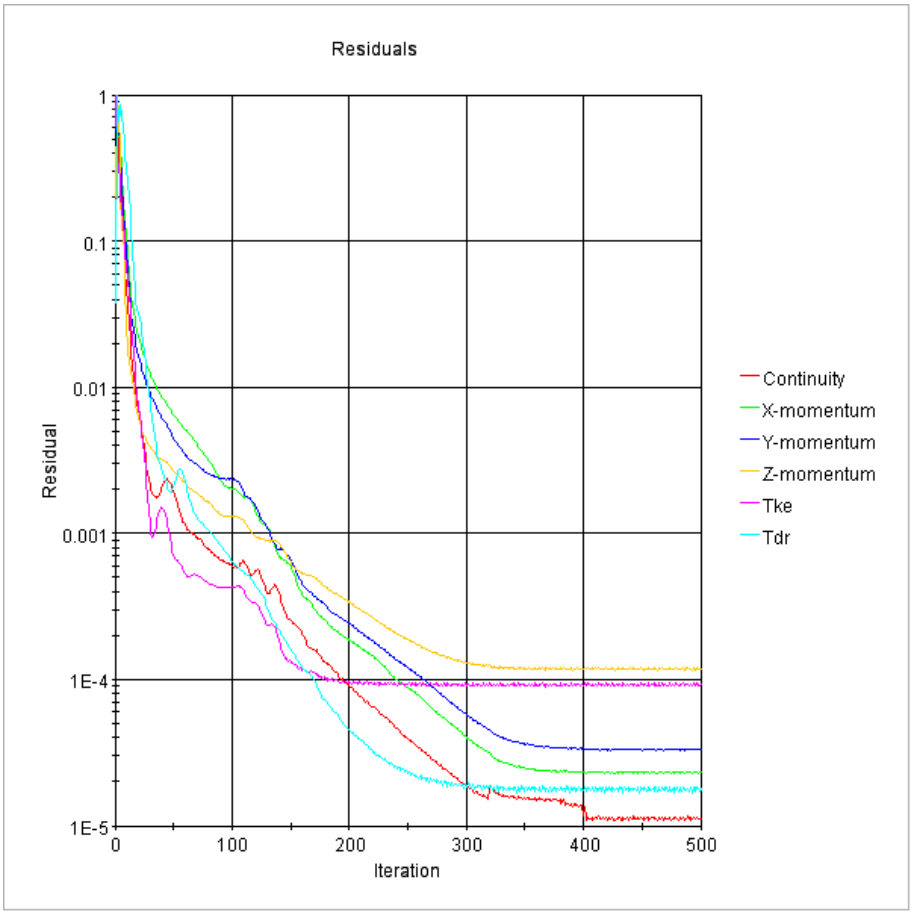

Figure 4.42: ER 5 Simulation Residual Plot – 1m/s Velocity

4.3.3. ER 10 Model Results

The results for the ER 10 model are provided in **Figure 4.43** to **Figure 4.47**. The convergence criteria for all four velocities for the ER 10 Model were met within the stopping criteria of 500 iteration steps. The residual plot for the 1 m/s simulation is provided in **Figure 4.47**. An area of high velocity has developed at the immediate end of the reducer fitting on the lower side, thereby creating a considerable velocity gradient on the Y Axis. The velocity gradient for the X Axis remains fairly uniform when compared to the Y Axis. These velocity gradients are reflected in **Figure 4.43** and **Figure 4.44**. **Figure 4.45** and **Figure 4.46** illustrate the acceleration through the reducer, with acceleration towards both sides along the X Axis and acceleration towards one side for the Y Axis. The velocity distributions however return to a uniform distribution within a distance of 1xD2 downstream for the reducer (Probe Position 2).

1 m/s

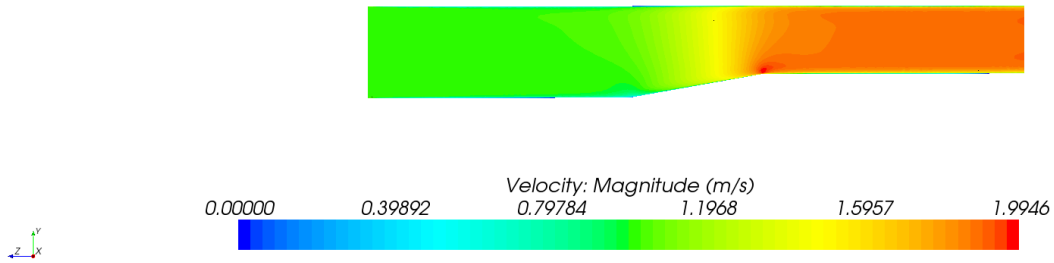

1.5 m/s

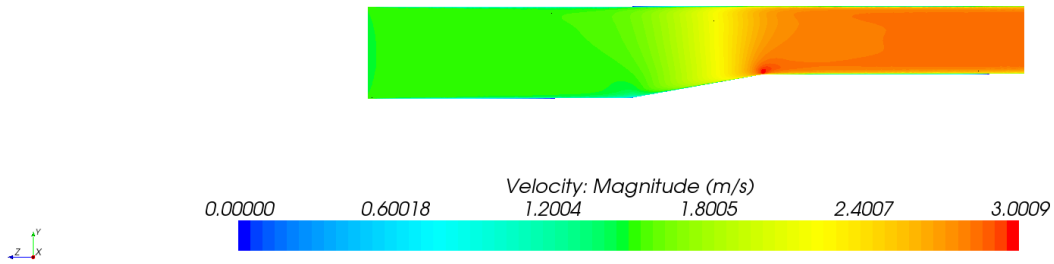

2 m/s

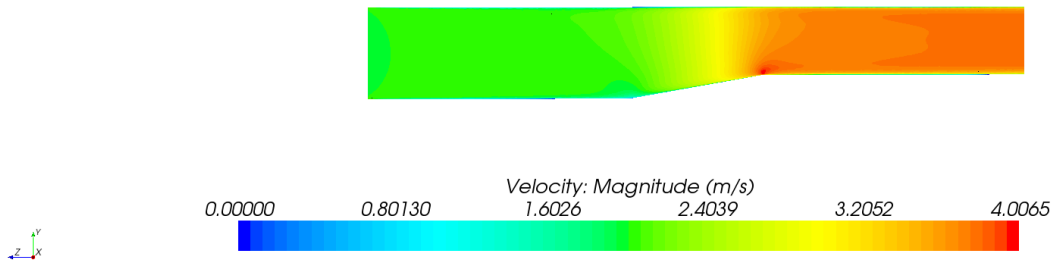

2.4 m/s

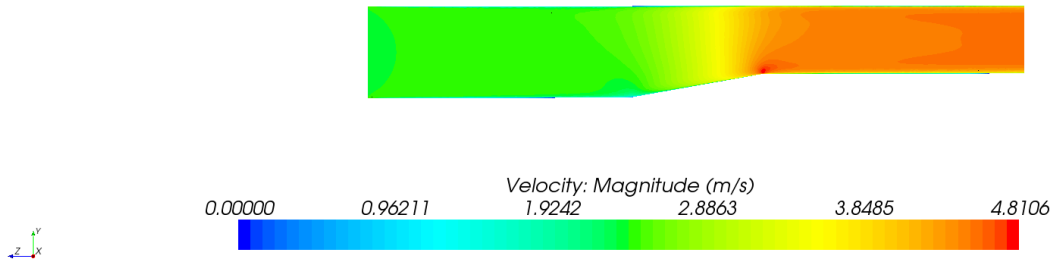

Figure 4.43: ER 10 Model YZ Plane Velocity Scalars

1 m/s

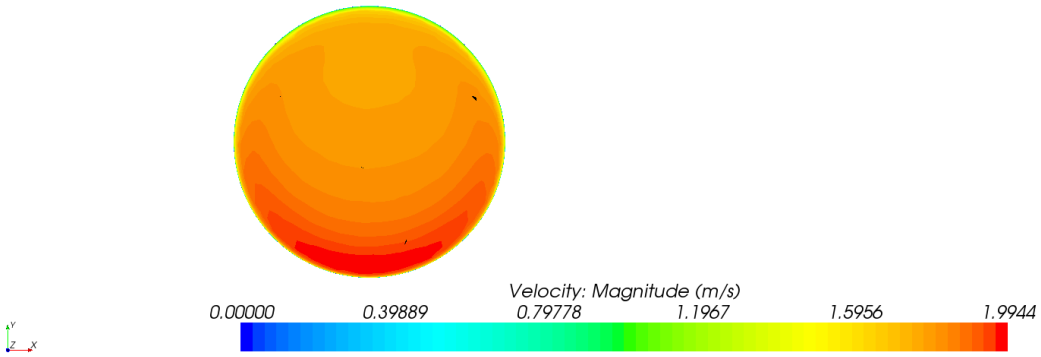

1.5 m/s

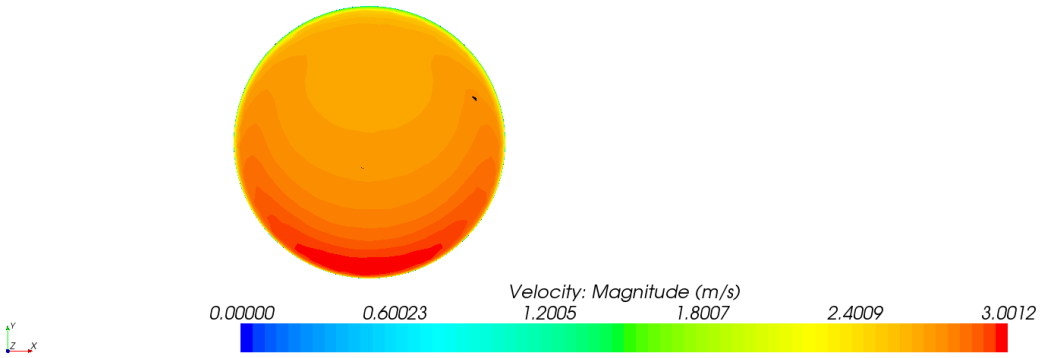

2 m/s

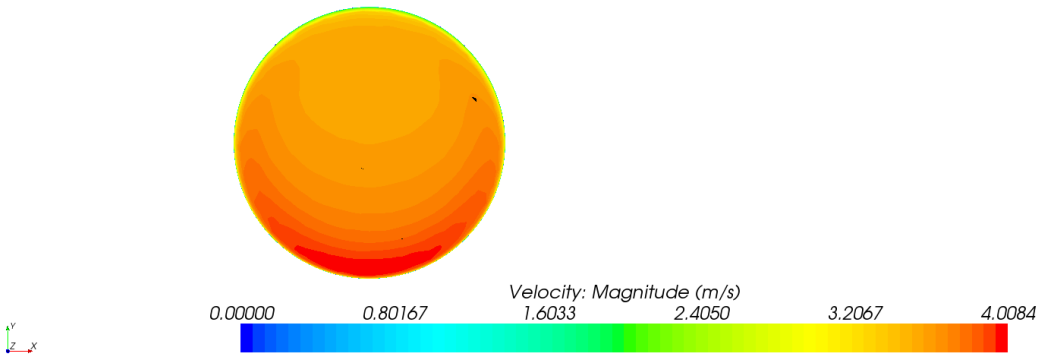

2.4 m/s

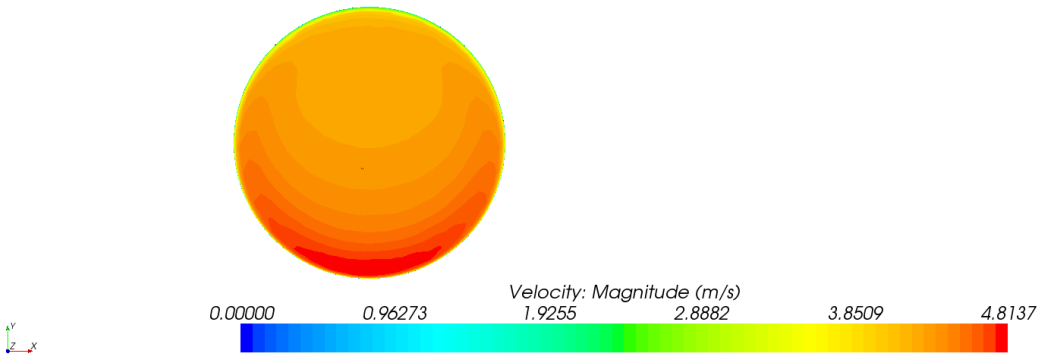

Figure 4.44: ER 10 Model XY Plane Velocity Scalars at Probe Position 1

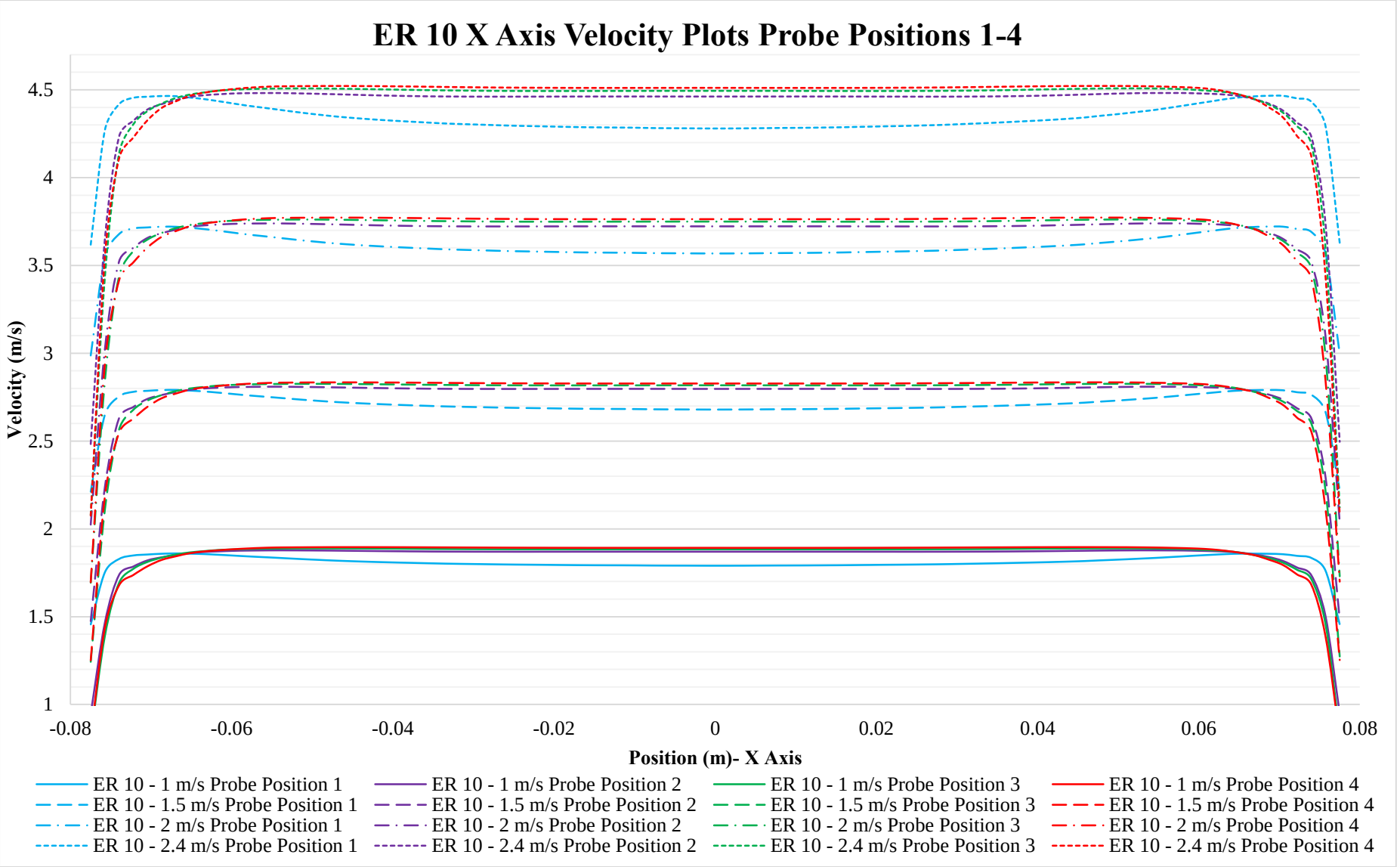

Figure 4.45: ER 10 X Axis Velocity XY Plots Probe Positions 1-4

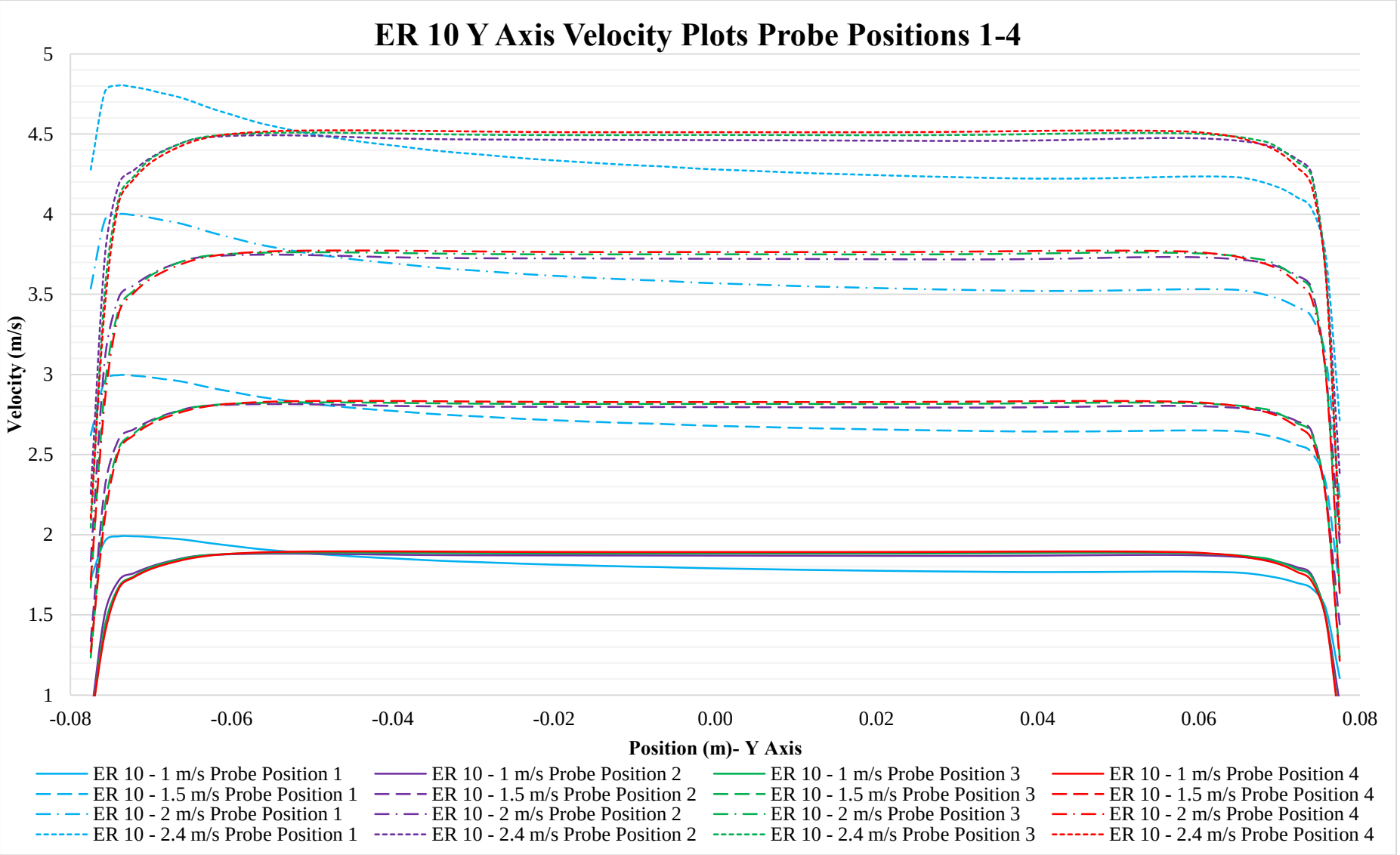

Figure 4.46: ER 10 Y Axis Velocity XY Plots Probe Positions 1-4

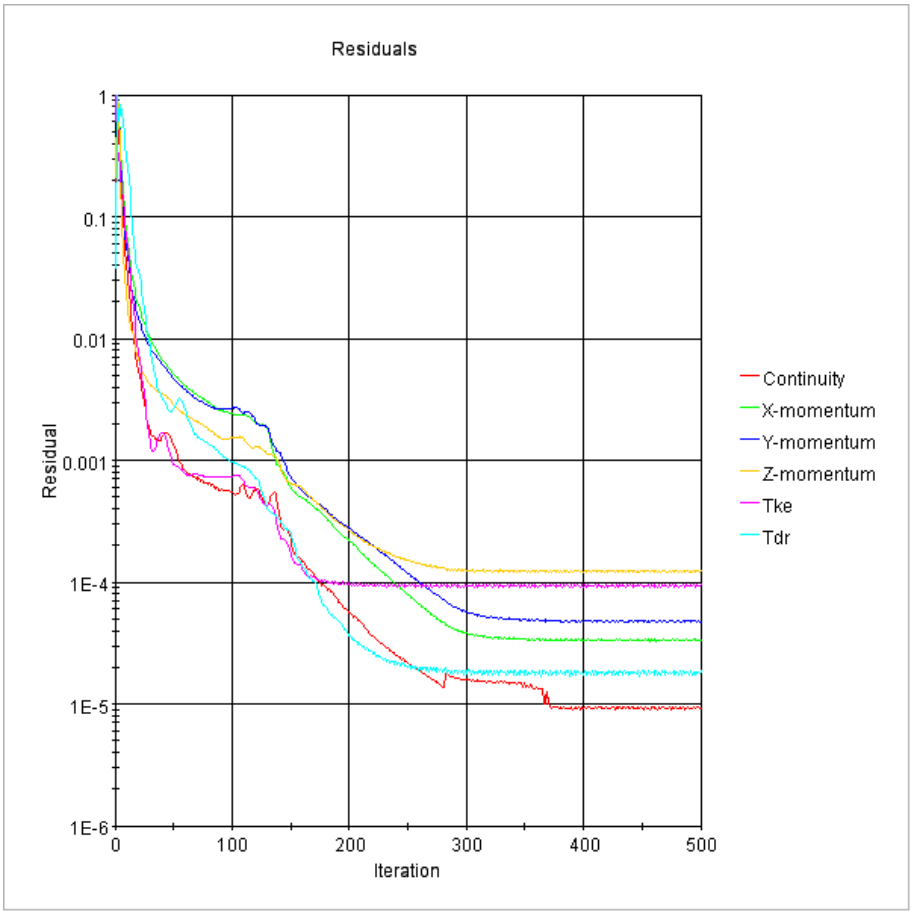

Figure 4.47: ER 10 Simulation Residual Plot – 1m/s Velocity

4.3.4. ER 15 Model Results

The results for the ER 15 Model are provided in **Figure 4.48** and **Figure 4.52**. All four of the ER 15 simulations were solved to the required levels within the 500 iteration steps. The residual plot for the 1 m/s simulation is provided in **Figure 4.47**. The significant velocity gradients on the Y Axis for the ER 15 models have increased further compared to ER 10 models whilst the velocity gradient on the X Axis remains relatively constant, this reflected in **Figure 4.48** and **Figure 4.49**. **Figure 4.50** and **Figure 4.51** illustrate the acceleration toward the bottom side of the reducer along the Y Axis and acceleration towards both sides along the X Axis. The velocity distributions along both axes at the three probe positions downstream form the reducer present uniform flow conditions typical of pipe flow.

1 m/s

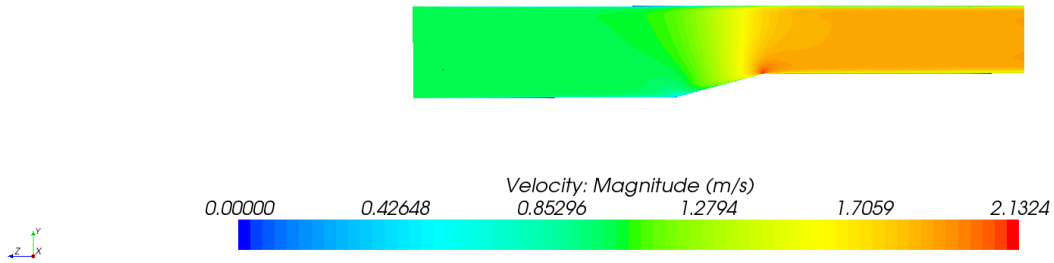

1.5 m/s

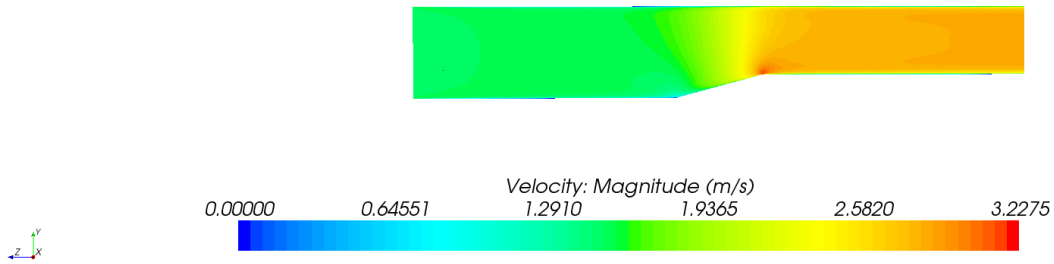

2 m/s

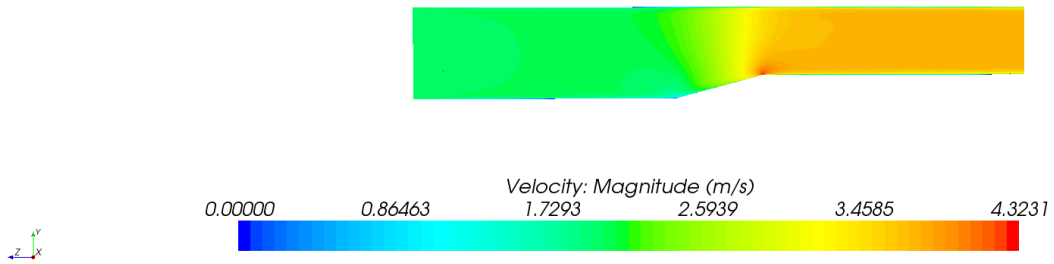

2.4 m/s

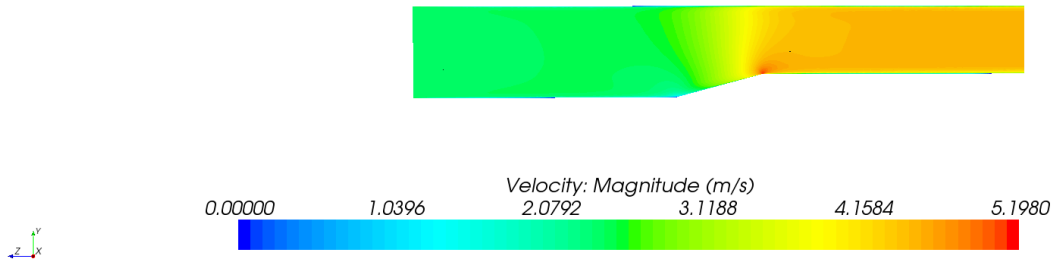

Figure 4.48: ER 15 Model YZ Plane Velocity Scalars

1 m/s

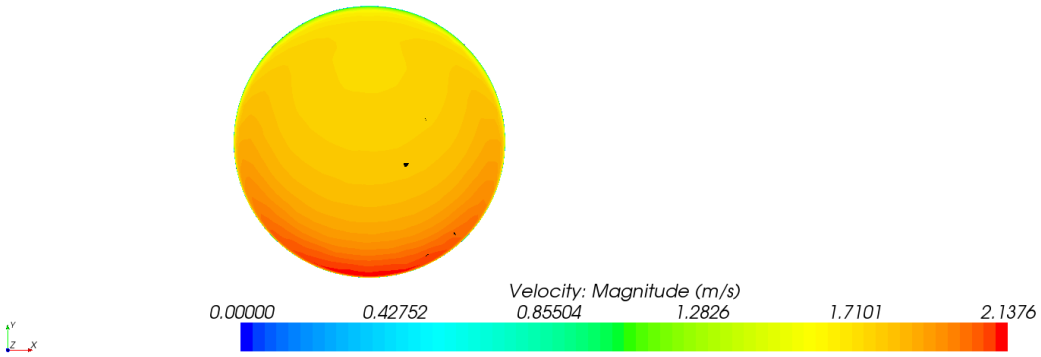

1.5 m/s

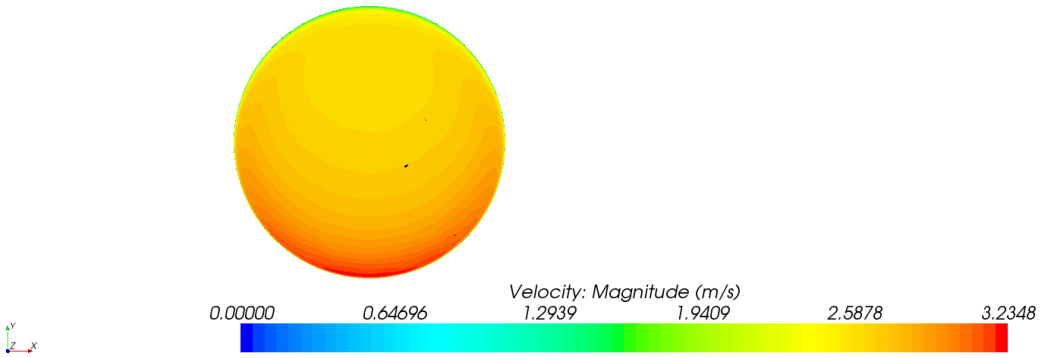

2 m/s

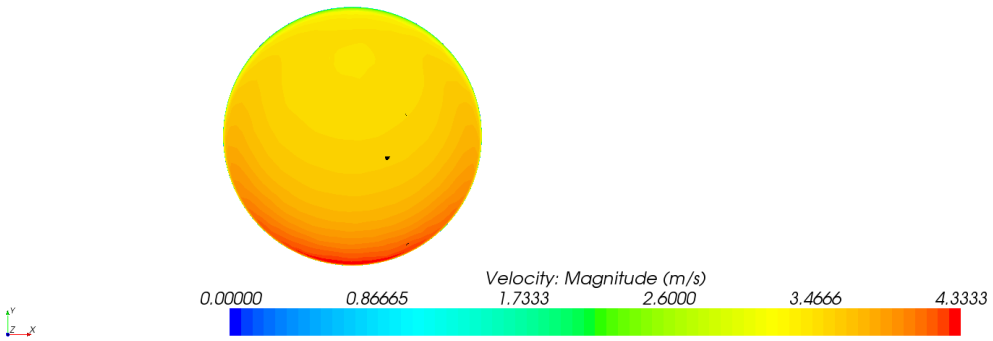

2.4 m/s

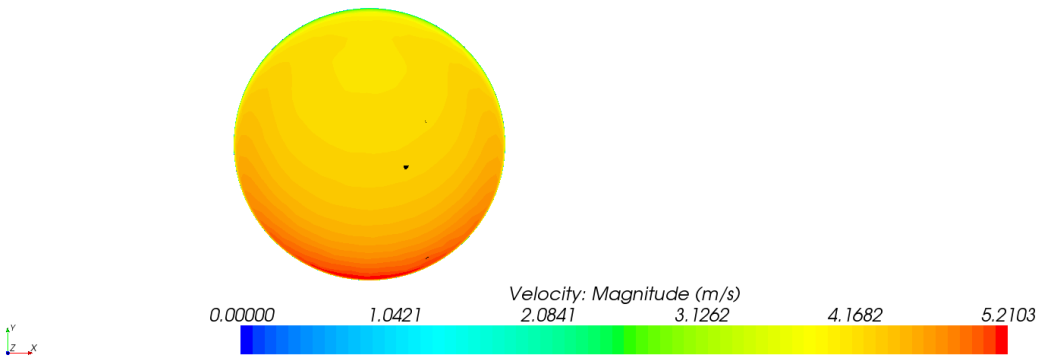

Figure 4.49: ER 15 Model XY Plane Velocity Scalars at Probe Position 1

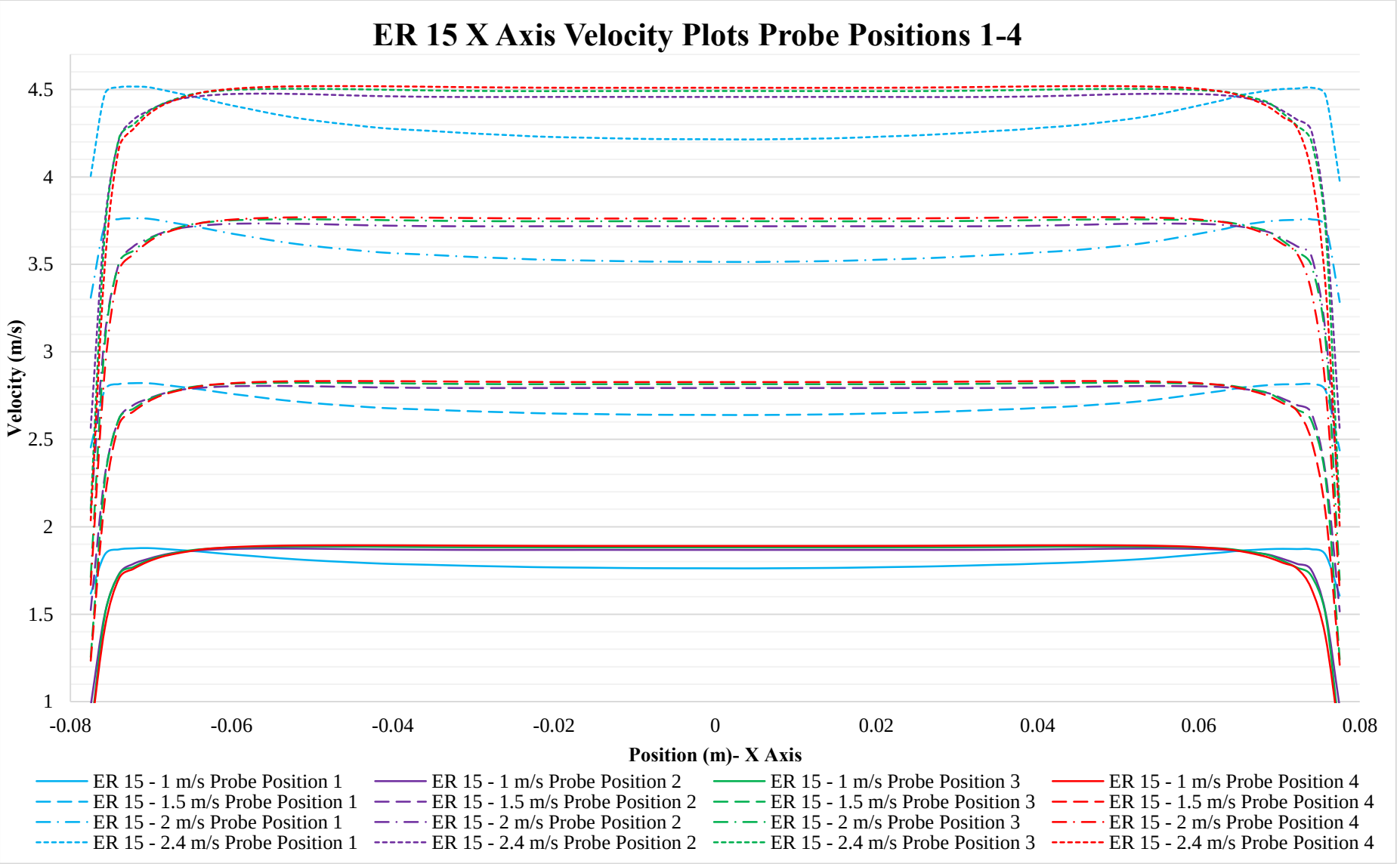

Figure 4.50: ER 15 X Axis Velocity XY Plots Probe Positions 1-4

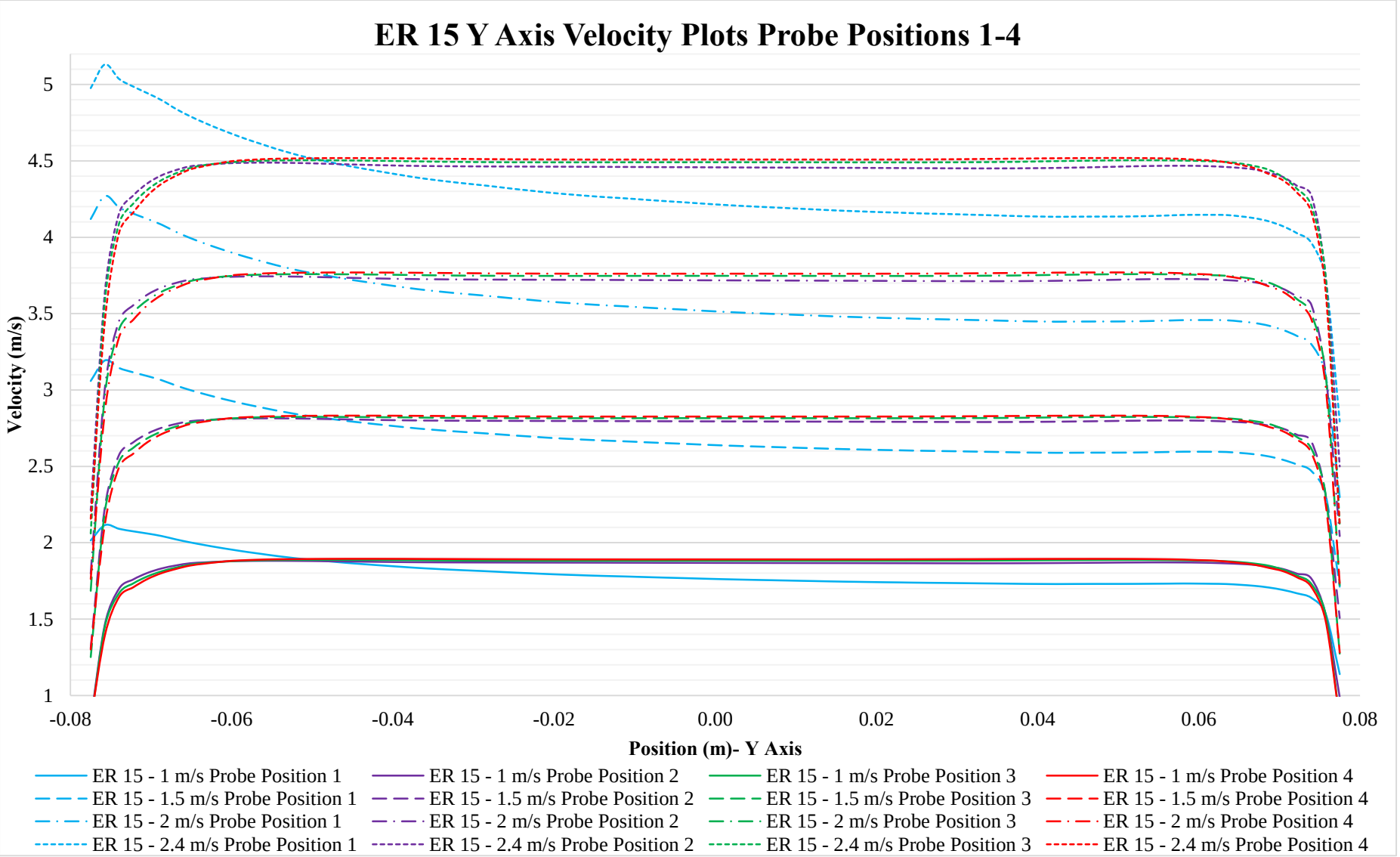

Figure 4.51: ER 15 Y Axis Velocity XY Plots Probe Positions 1-4

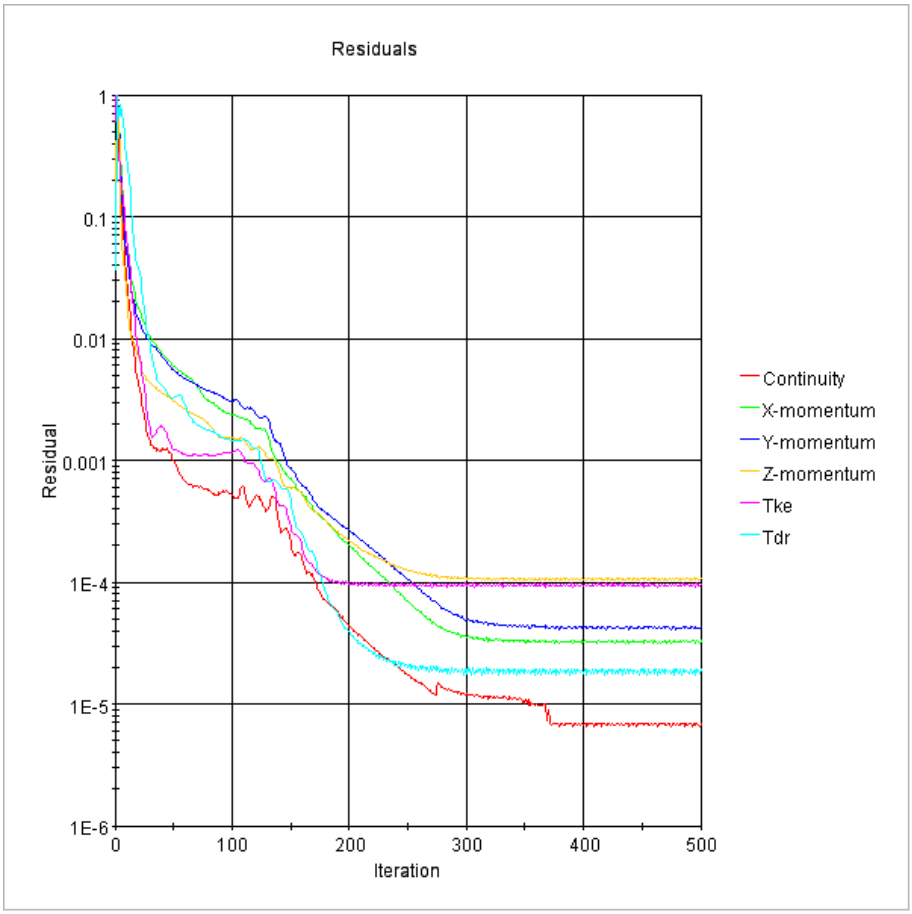

Figure 4.52: ER 15 Simulation Residual Plot – 1m/s Velocity

4.3.5. ER 20 Model Results

The results for the ER 20 Model are provided in **Figure 4.53** to **Figure 4.57**. All four of the ER 20 simulations satisfied the convergence criteria within the 500 iteration steps. The residual plot for the 1 m/s is provided in **Figure 4.57**. **Figure 4.53** and **Figure 4.54** illustrate that the velocities along the bottom side of the reducer are in excess of 10% of the average velocity through the reducer. **Figure 4.55** and **Figure 4.56** illustrate that the acceleration of flow creates a velocity distribution with acceleration towards the bottom side of the reducer along the Y Axis at Probe Position 1 and acceleration towards both sides of the reducer along the X Axis at Probe Position 1. This velocity distribution does however even out at a distance of 1xD2 downstream of the reducer (Probe Position 2).

1 m/s

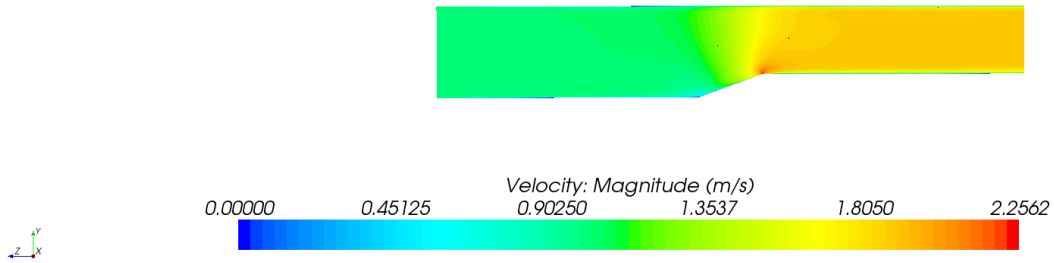

1.5 m/s

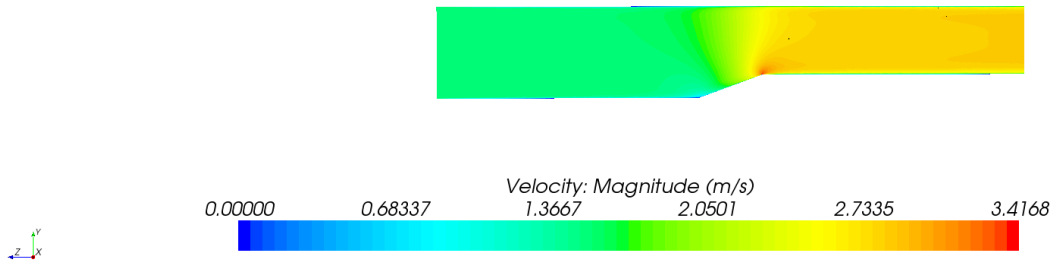

2 m/s

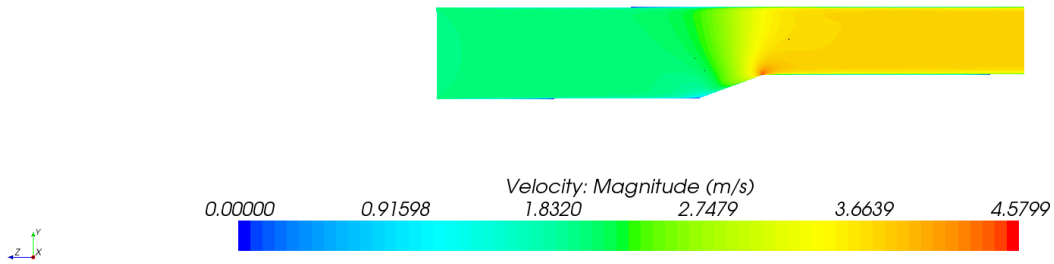

2.4 m/s

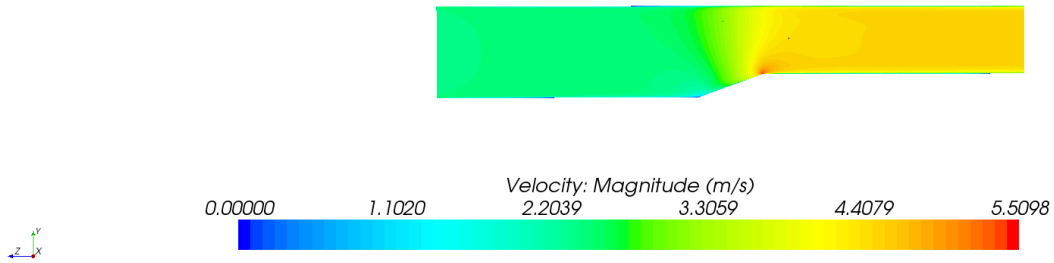

Figure 4.53: ER 20 Model YZ Plane Velocity Scalars

1 m/s

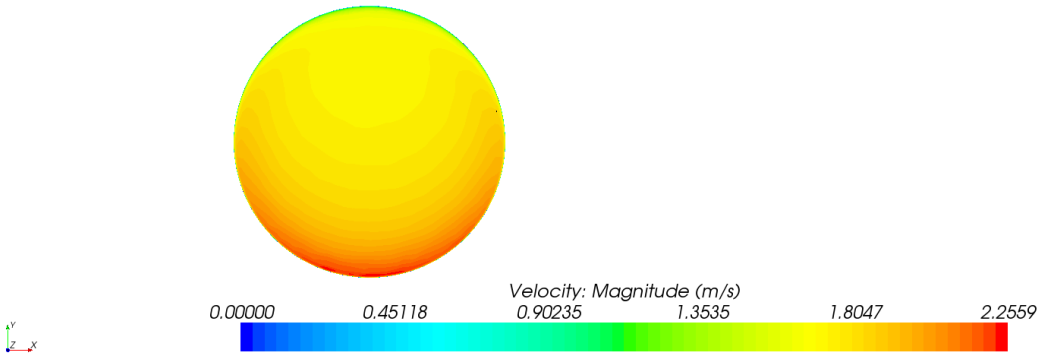

1.5 m/s

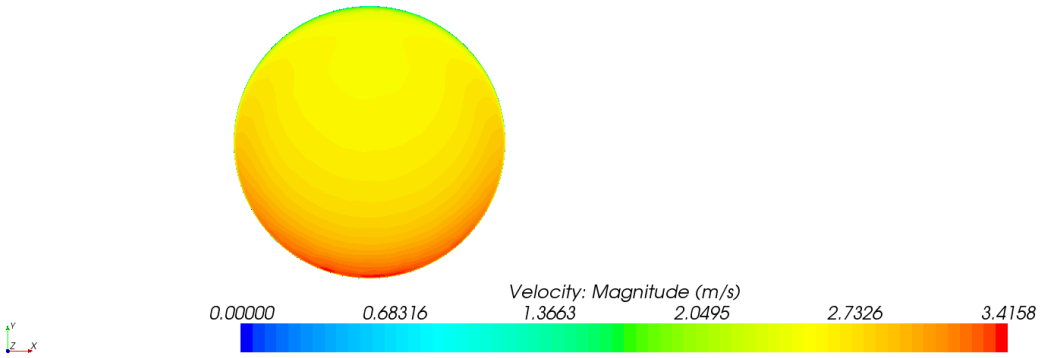

2 m/s

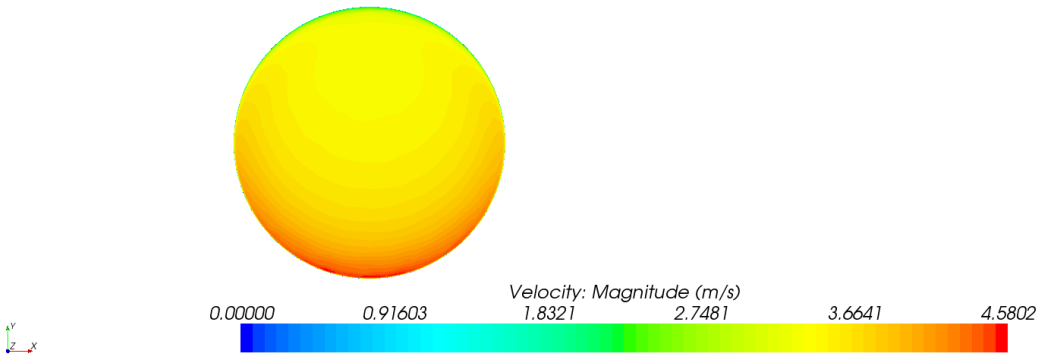

2.4 m/s

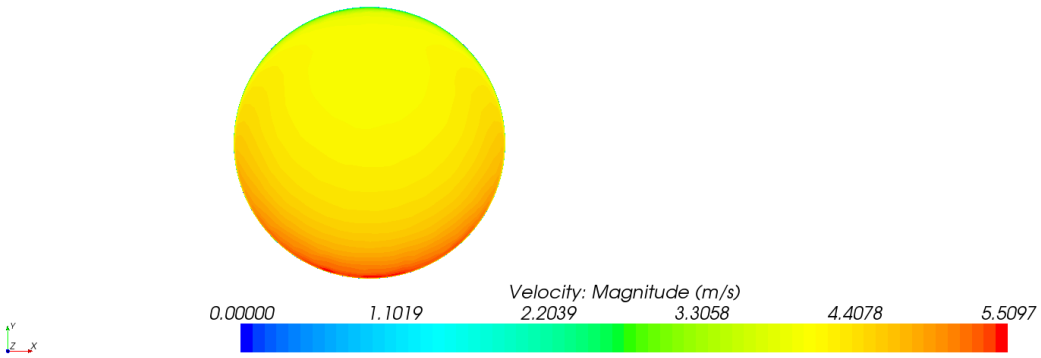

Figure 4.54: ER 20 Model XY Plane Velocity Scalars at Probe Position 1

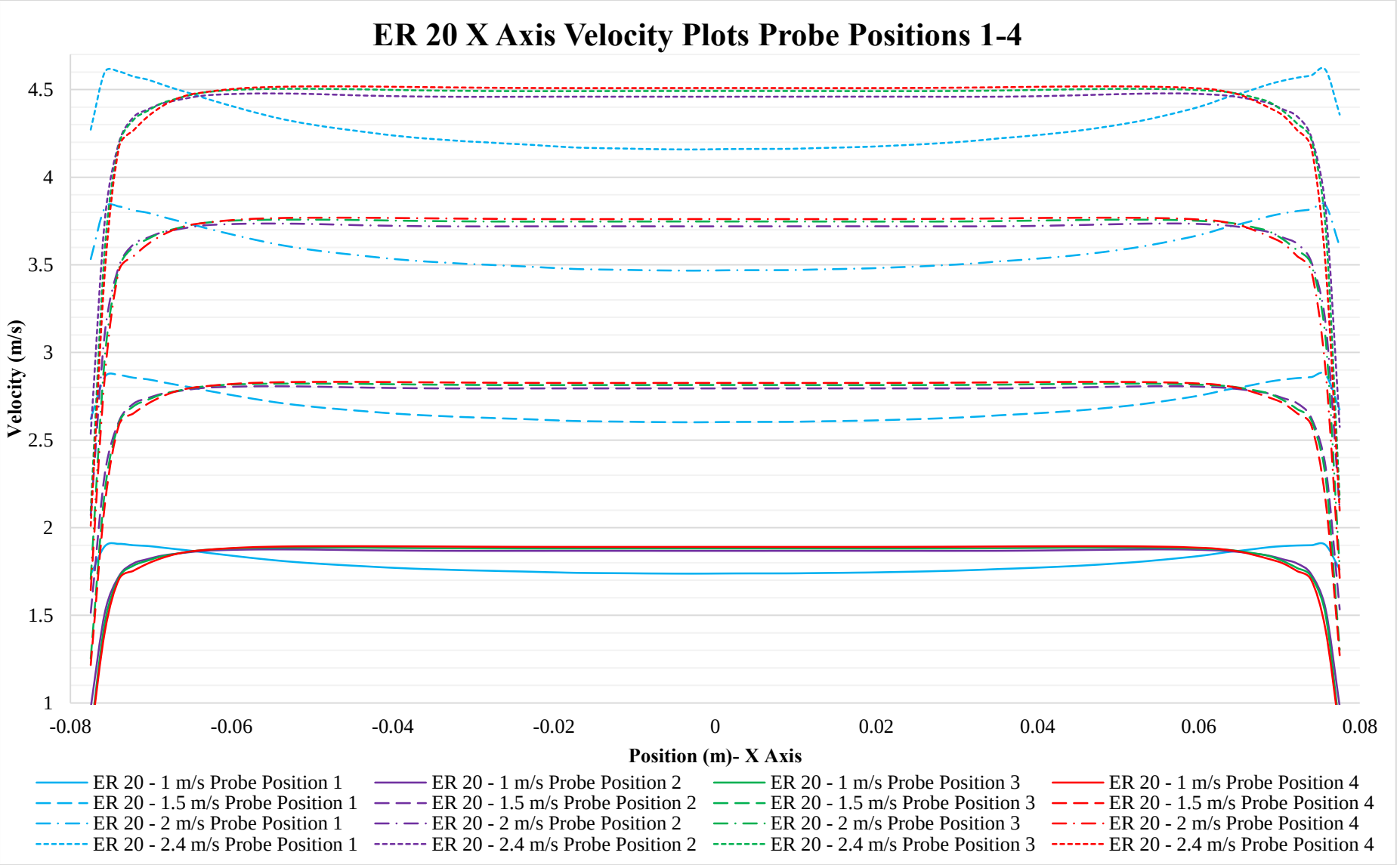

Figure 4.55: ER 20 X Axis Velocity XY Plots Probe Positions 1-4

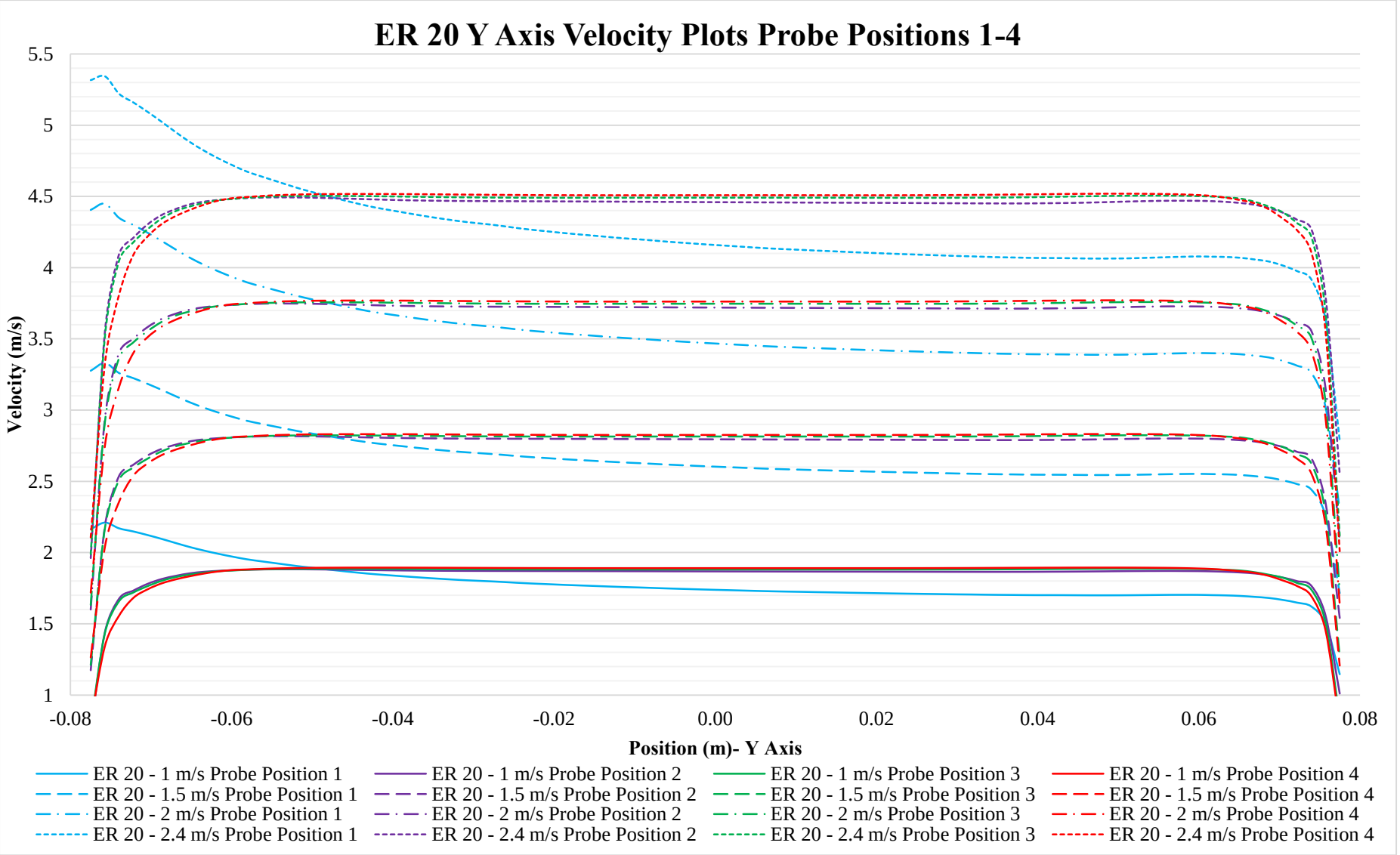

Figure 4.56: ER 20 Y Axis Velocity XY Plots Probe Positions 1-4

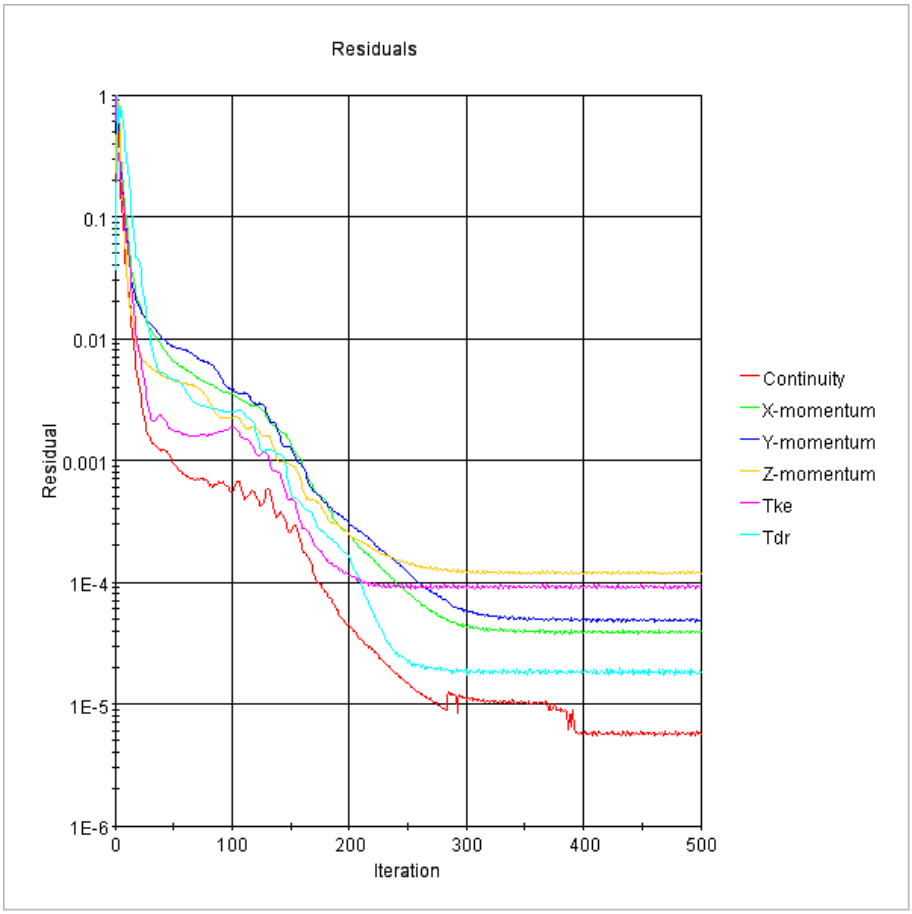

Figure 4.57: ER 20 Simulation Residual Plot – 1m/s Velocity

4.3.6. ER 30 Model Results

The results for the ER 30 Model are provided in **Figure 4.58** to **Figure 4.62**. All four velocity simulations were solved satisfactorily in the 500 iteration steps. The residual plot for the 1m/s simulation is provided in **Figure 4.62**. Excessively high velocities result from the ER 30 Model, with velocities in the range of 6 m/s for the 2.4 m/s inlet velocity model (2.5 times the inlet velocity) are reflected in **Figure 4.58** and **Figure 4.59**. **Figure 4.60** and **Figure 4.61** illustrate that this excessive distribution is not only experienced on the Y Axis, but on the X Axis as well, although not at such high velocities. The velocity distribution still however returns to a uniform velocity distribution at a distance of 1xD2 from the reducer and this velocity distribution remains relatively constant through the distances 2xD2 and 3xD2 downstream from the reducer.

1 m/s

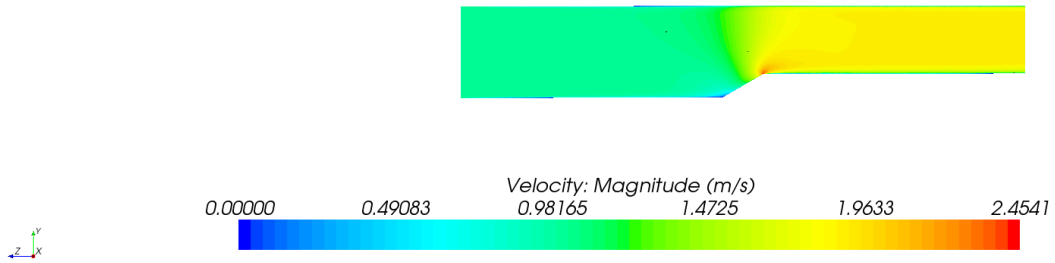

1.5 m/s

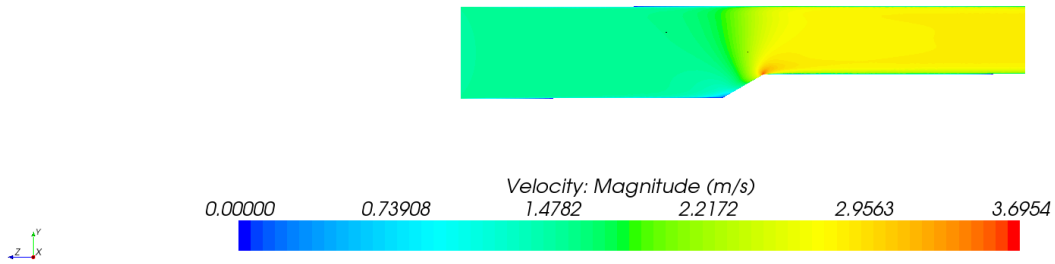

2 m/s

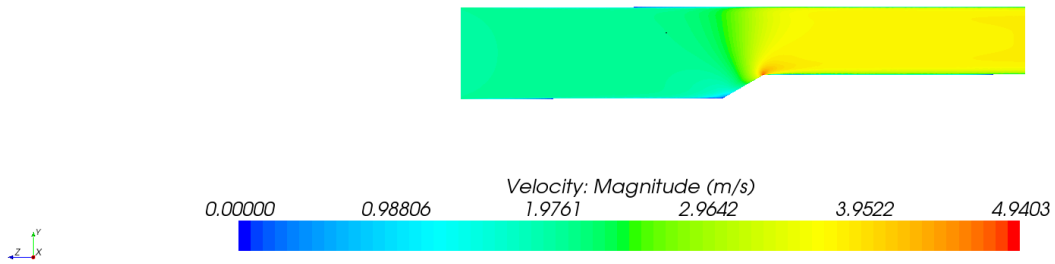

2.4 m/s

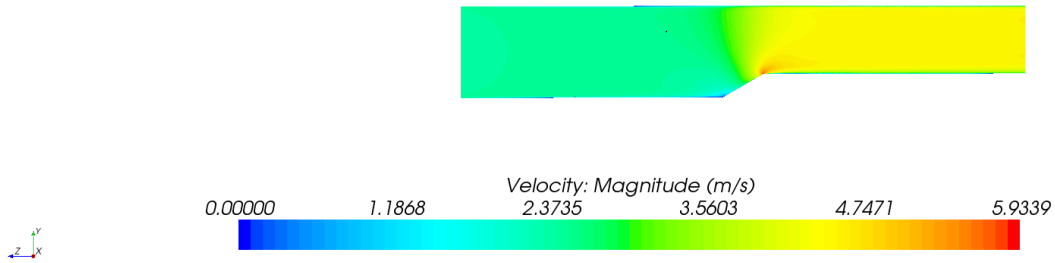

Figure 4.58: ER 30 Model YZ Plane Velocity Scalars

1 m/s

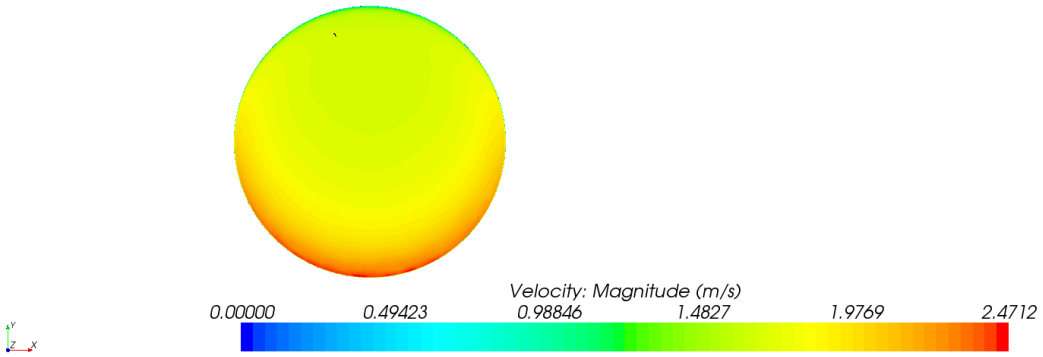

1.5 m/s

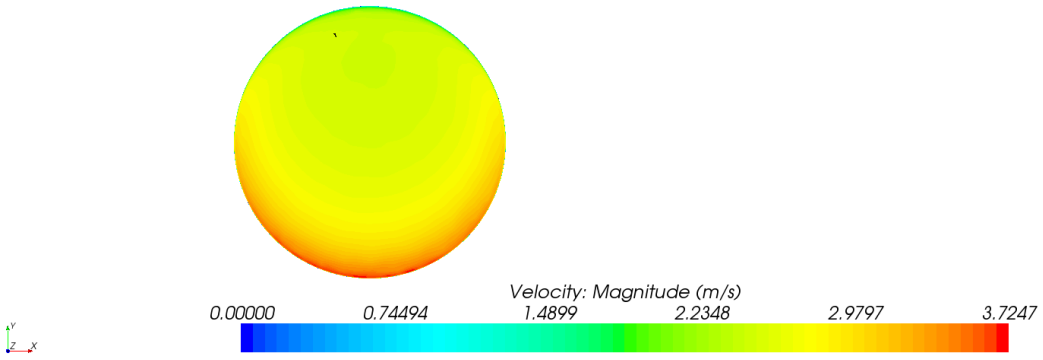

2 m/s

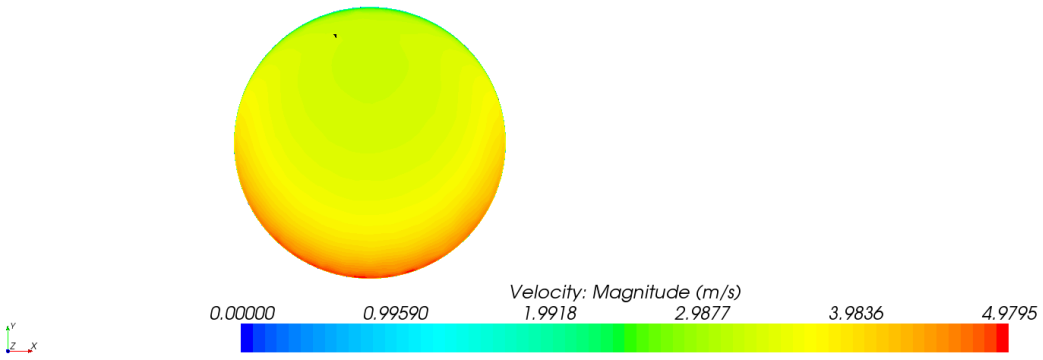

2.4 m/s

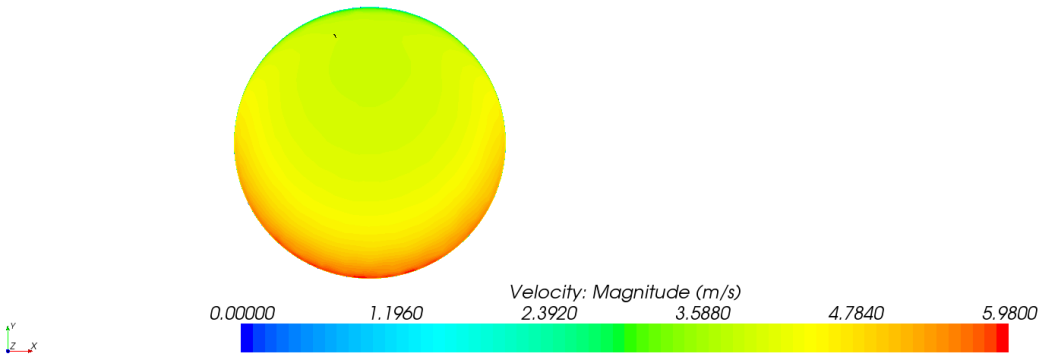

Figure 4.59: ER 30 Model YZ Plane Velocity Scalars at Probe Position 1

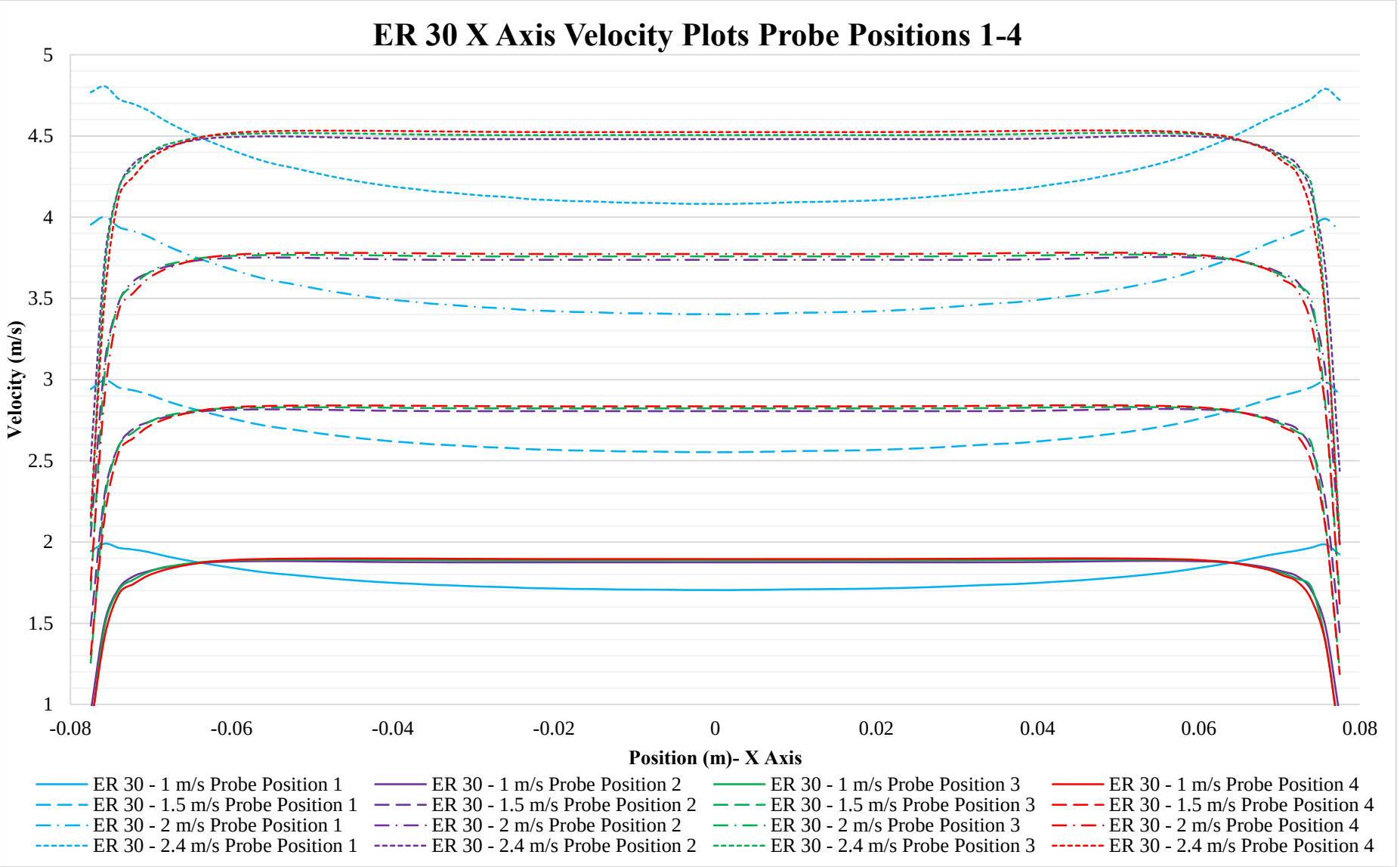

Figure 4.60: ER 30 X Axis Velocity Plots Probe Positions 1-4

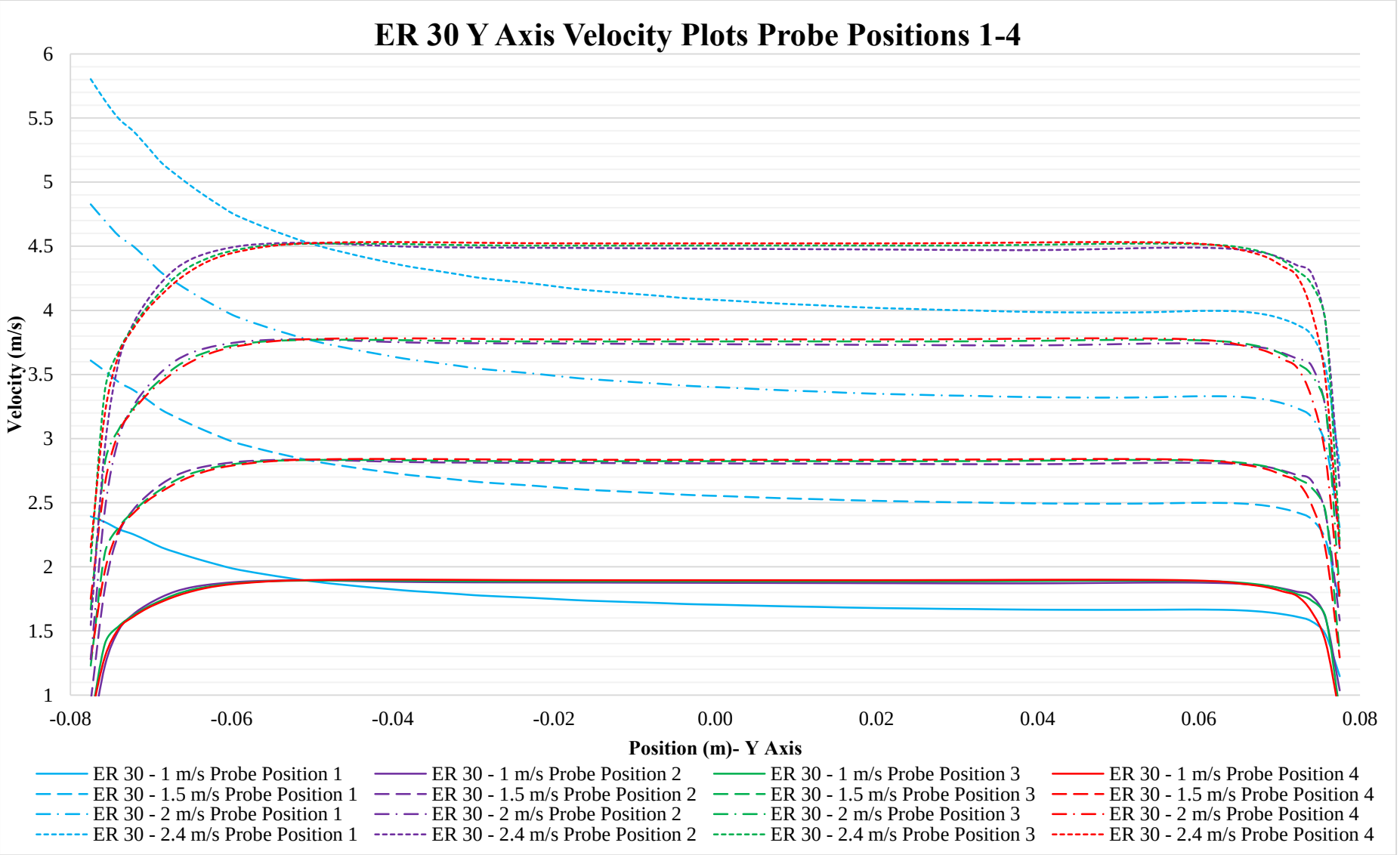

Figure 4.61: ER 30 Y Axis Velocity Plots Probe Positions 1-4

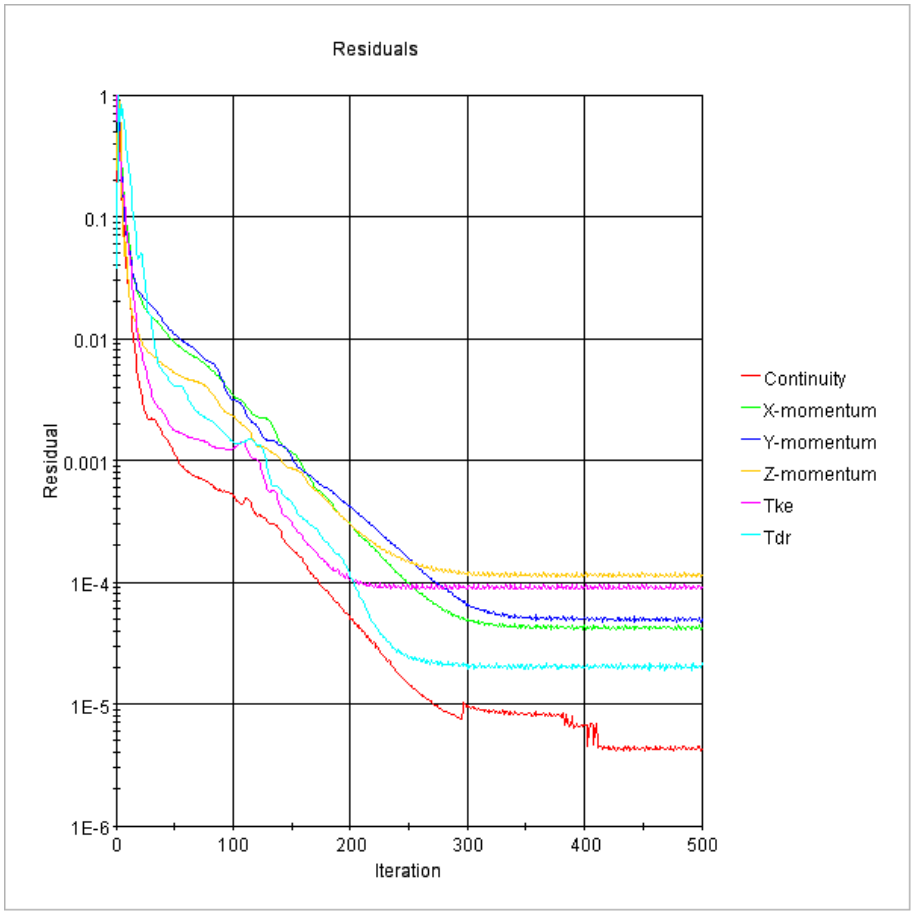

Figure 4.62: ER 30 Simulation Residual Plot – 1m/s Velocity

4.4. OBSERVATIONS

The main observations made from the numerical simulation results presented in this chapter can be summarized as follows:

- The simulations typically reached the required level of convergence within 500 iteration steps, with the exception of two of the ER 2.5 Models which reached the requirement in 600 iteration steps;
- The flow distribution evens out rapidly and presents a typical uniform distribution by the time it reaches a distance of 1xD2 from the reducer (Probe Position 2);
- The concentric reducers produce velocity distributions that are symmetrical around the center of the pipe, i.e. the velocity contours are circular in shape;
- The eccentric reducers produce velocity distributions with areas of high velocities towards the bottom side of the reducer (the side that is at angle);
- Areas of high velocities are generated around the perimeter of the downstream end for the concentric reducer, whereas these areas are only on the one side for the eccentric reducers;
- The magnitude of velocity distributions increases with an increase in reducer angle; and
- The cases of the reducers with larger angles, the resulting velocities may be of such a nature that they will fall outside of the acceptance criteria discussed in ***Paragraph 2.2***.

A more detailed assessment into the criteria and the velocity distributions for each velocity with the various reducer angles is provided in the next chapter (***Chapter 5***) to assess which reducers produce velocity distributions that are acceptable.

5. RESULTS ASSESSMENT AND DISCUSSION

5.1. ASSESSMENT CRITERIA

The criteria according to which the velocity distributions will be assessed are the pump inlet requirements from HR Wallingford (Sinotech CC 2005) described in ***Paragraph 2.2.*** These guidelines are as follows:

- Criteria 1: Velocity variation along line ABCD (placed vertically along the center line of the pipe) is less than 10% of the average velocity (see **Figure 2.2** and **Figure 5.1**); and
- Criteria 2: Maximum velocity variation along a circle AEDF is ± 5% of the average velocity (see **Figure 2.2** and **Figure 5.1**).

These guidelines from HR Wallingford expand on the guidelines provided by ANSI/HI (2000), Jones et al (eds. 2008) and Ninham Shand Consulting Services (2007) where the requirement for the time averaged velocities at the pump suction is to be within 10% of the cross-sectional area average velocity (***Paragraph 2.2.***). Flow disturbances such as fittings and valves may create a velocity distribution that is skewed to one side, therefore the average velocity along an arbitrary line through the cross section of the pipe, dividing the cross into two equal halves (such as line ABCD), may not equal the cross-sectional area average velocity. An additional criteria, Criteria 3, has been included in addition to the HR Wallingford criteria (Criteria 1 and 2) to assess the cross-sectional area average velocity (to be less than 10% of the average velocity). There are however only probe lines along the X Axis and the Y Axis at the four probe positions that can be used to assess acceptance according to Criteria 3. Criteria 3 has therefore been divided into sub criteria: Criteria 3 X Axis and Criteria 3 Y Axis.

The criteria provided by HR Wallingford do not provide the locations of points A, B, C and D on the Y Axis and E and F on the X Axis (see **Figure 2.2**). The locations are however required to complete the assessment for Criteria 2. Therefore two locations were defined to complete this assessment, namely: circles, AEDF (HRW 1) and BGCH (HRW 2). **Two circles were defined to assess if the location of the circle affects the acceptance of a velocity distribution or not**. The locations are described in **Figure 5.1**. Further to the location of the circles, HR Wallingford does not discretely state what average velocities are to be used in the assessment. For this study it was interpreted that the average velocities are to be the average of the velocities along the line of the circle on which the assessment is being completed. The definitions of the three acceptance criteria and a reference to the paragraph under which the results are discussed are summarised in **Table 5.1**.

Table 5.1: Summary of the Assessment Criteria and Definitions of the Average Velocity

Criteria	Definition of Average Velocity	Acceptance Criteria	Paragraph Reference
Criteria 1	Average velocity along line ABCD	Velocity variation along line ABCD is less than 10% of the Defined Average Velocity	Paragraph 5.2
Criteria 2 HRW 1	Average velocity along circle AEDF	Velocity variation along circle AEDF is less than 5% of the Defined Average Velocity	Paragraph 5.3
Criteria 2 HRW 2	Average velocity along circle BGCH	Velocity variation along circle BGCH is less than 5% of the Defined Average Velocity	Paragraph 5.3
Criteria 3 X Axis	Cross-sectional area average velocity	Velocity variation along line EGHF (X Axis) is less than 10% of the Defined Average Velocity	Paragraph 5.4
Criteria 3 Y Axis	Cross-sectional area average velocity	Velocity variation along line ABCD (Y Axis) is less than 10% of the Defined Average Velocity	Paragraph 5.2

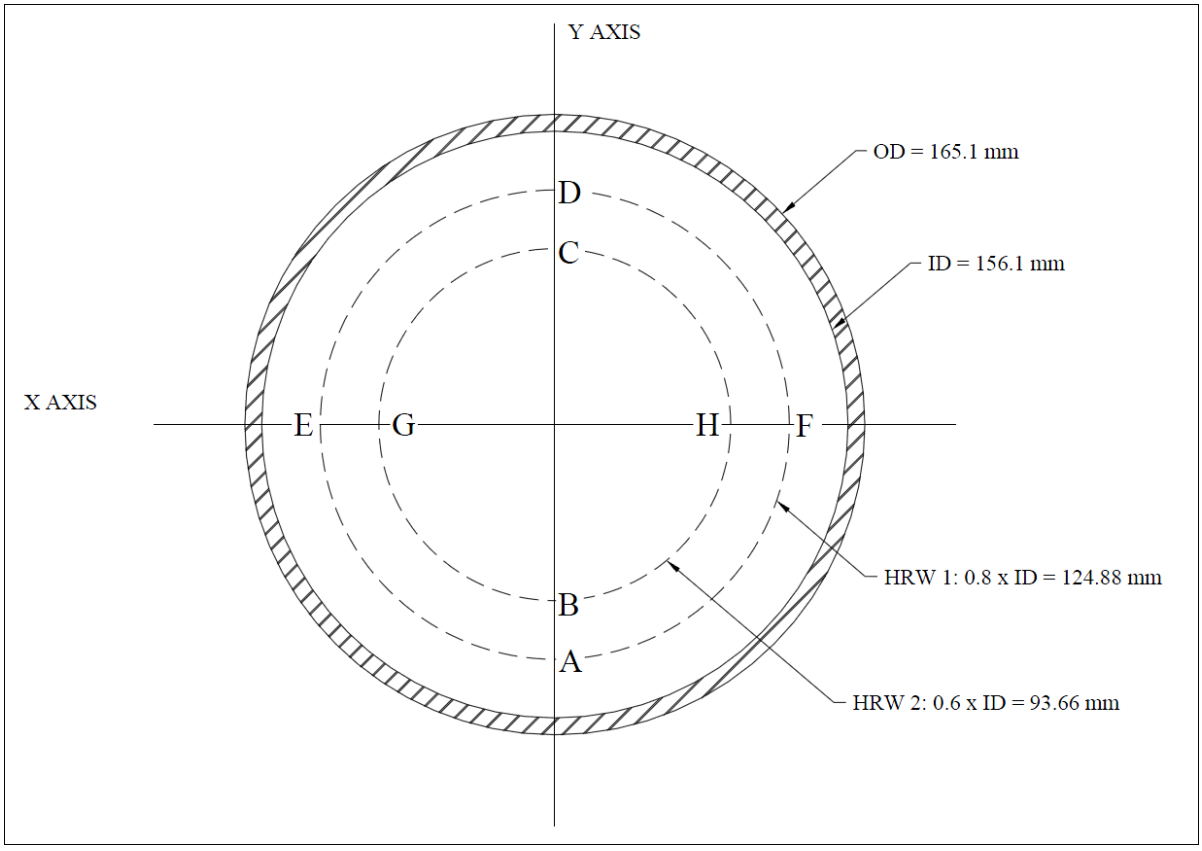

Figure 5.1: Section View of the Pipeline for the Review of Velocity Distribution

In order to apply the criteria defined by ANSI/HI (2000), Jones et al (eds. 2008) and Ninham Shand Consulting Services (2007) (Criteria 3) the average velocity at the plane in question is required. This average velocity can be calculated by the flow rate equation (Equation 3-1) and the principle of

continuity of mass i.e. the mass flow entering the model = the mass flow exiting the model. The average velocities at the downstream end of the reducer (at ID D2 = 156.1 mm) were calculated and are provided in **Table 5.2**. The average velocities along line ABCD, the Y Axis at Probe Position 1, were calculated for all the simulations run and the results are presented in **Table 5.3**.These average velocities are within 0.04 m/s per second of the average velocity. Therefore Criteria 1 and the Criteria 3 Y Axis are assumed to be equal for the assessment and the assessment is conducted on the cross-sectional area average velocity.

Table 5.2: DS Average Flow Velocities

US Flow Velocity (m/s)	ID D1 (mm)	Flow Rate (m^3/s)	ID D2 (mm)	DS Flow Velocity (m/s)
1	210.1	0.034669	156.1	1.81
1.5	210.1	0.052004	156.1	2.72
2	210.1	0.069338	156.1	3.62
2.4	210.1	0.083206	156.1	4.35

Table 5.3: Averages Velocities for the Y Axis Calculated at Probe Position 1

Model	Input Velocity 1 (m/s)	Input Velocity 1.5 (m/s)	Input Velocity 2 (m/s)	Input Velocity 2.4 (m/s)
CR 2	1.83	2.73	3.64	4.37
CR 2.5	1.82	2.73	3.63	4.36
CR 5	1.80	2.70	3.60	4.32
CR 10	1.78	2.67	3.56	4.27
CR 15	1.78	2.67	3.56	4.27
CR 20	1.76	2.63	3.51	4.21
ER 2.5	1.83	2.74	3.65	4.38
ER 5	1.82	2.72	3.63	4.36
ER 10	1.81	2.71	3.60	4.32
ER 15	1.80	2.69	3.59	4.30
ER 20	1.79	2.68	3.57	4.28
ER 30	1.77	2.65	3.54	4.24
Average	1.80	2.69	3.59	4.31

In addition to the three criteria described above the critical velocities for the hydraulic transportation of air through the concentric reducers will be calculated in order to assess if a trapped air pocket will be able to be transported through the concentric reducer. The hydraulic transportation of air equations provided in ***Paragraph 2.4*** will be used to calculate the critical velocities. It is accepted that air will travel through the eccentric reducer irrespective of the positive velocity of the water.

A matrix summarising the acceptance or failure per reducer size for each velocity according to the four criteria is provided ***Paragraph 5.5***.

5.2. ASSESSMENT OF REDUCERS TO CRITERIA 1 AND CRITERIA 3 Y AXIS

Refer to **Figure 5.1** for the position of the reference lines. Criteria 1 requires the velocity variation along line ABCD to be less than 10% of the average velocity along line ABCD. Criteria 3 Y Axis requires the velocity variation along line ABCD (Y Axis) to be less than 10% of the cross-sectional average velocity. It was shown in **Table 5.2** and **Table 5.3** that the average along line ABCD and the cross-sectional average velocity are approximately equal, therefore the two criteria are assessed together. The XY Plots for the velocity in the direction of the Y Axis were combined into individual plots for each velocity, together with lines representing the acceptance envelope for Criteria 1 and Criteria 3 Y Axis (Upper Limits and Lower Limits). The velocity relationships for the input velocities (1, 1.5, 2, 2.4 m/s), the outlet velocities (downstream end of the reducer) and the upper and lower limit velocities are provided in **Table 5.4**. The results for the position at Probe Position 1 are provided in this paragraph, **Figure 5.2** to **Figure 5.5,** one chart for each velocity modelled. The results for Probe Positions 2, 3 and 4 are not provided due to the uniformity in the velocity distribution at these positions, as was demonstrated in ***Paragraph 4.2***.

Table 5.4: Inlet and Outlet Velocity Relationships

Inlet Velocity at D1 – Model Velocity (m/s)	Outlet Velocity at D2 - V_{Avg} (m/s)	Upper Limit (at D2) – V_{Avg} + 0.1 *x* V_{Avg} (m/s)	Lower Limit (at D2) - V_{Avg} - 0.1 *x* V_{Avg} (m/s)
1	1.81	1.99	1.63
1.5	2.72	2.99	2.45
2	3.62	3.99	3.26
2.4	4.35	4.78	3.91

The upper end of the eccentric reducers, (ER 15, ER 20 and ER 30) and the CR 20 model concentric extend past the upper limit of the acceptance envelope and therefore do not pass acceptance Criteria 1 and Criteria 3 Y Axis. ER 10 is on the limit of the acceptance Criteria 1 and Criteria 3 Y Axis, but has been judged to pass the criteria. The remaining concentric reducers (CR2, CR 2.5, CR 5, CR 10 and CR 15) and eccentric reducers (ER 2.5, ER 5 and ER 10) all fall within Criteria 1 and Criteria 3 Y Axis.

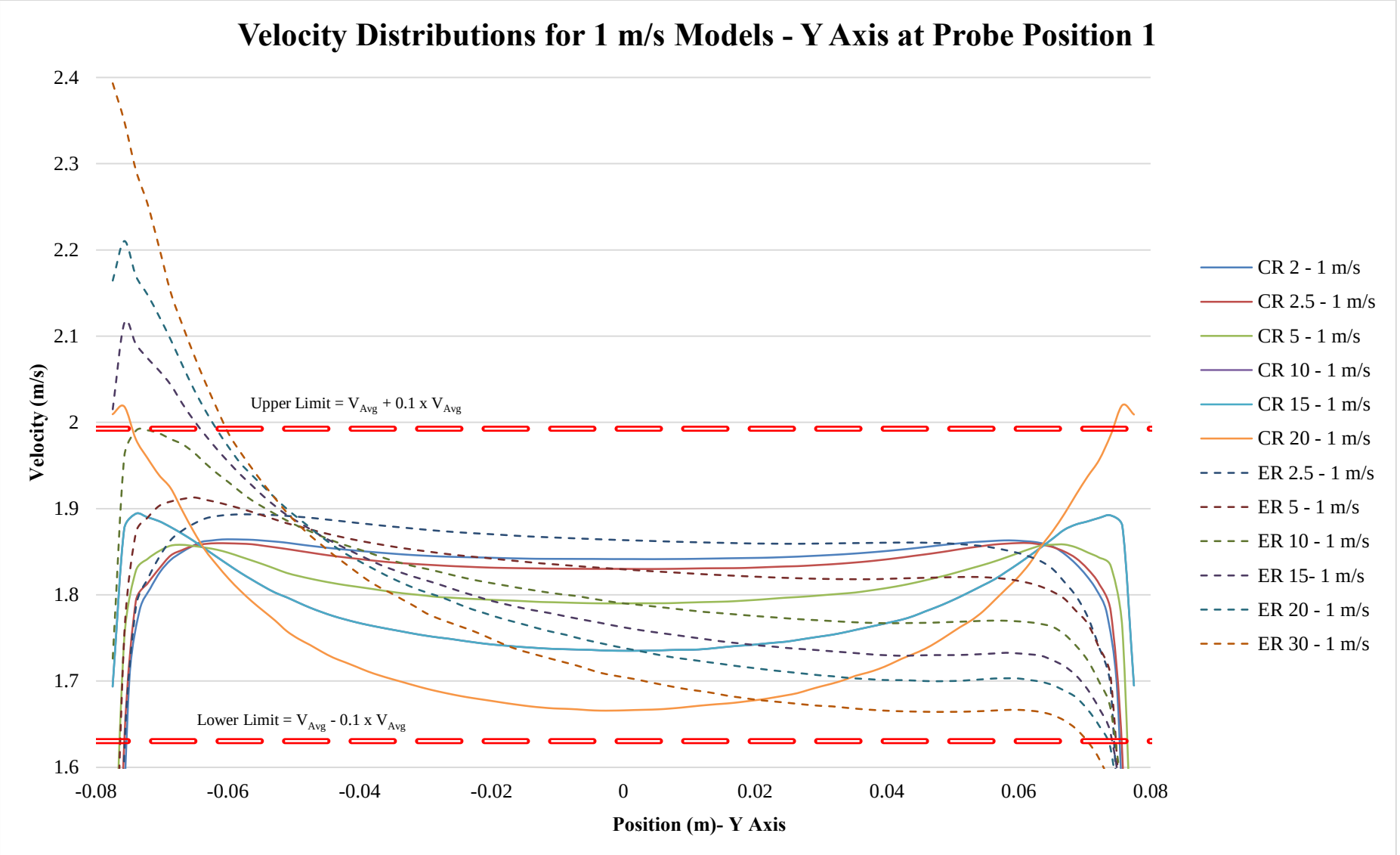

Figure 5.2: Velocity Distributions for 1 m/s Models – Y Axis at Probe Position 1

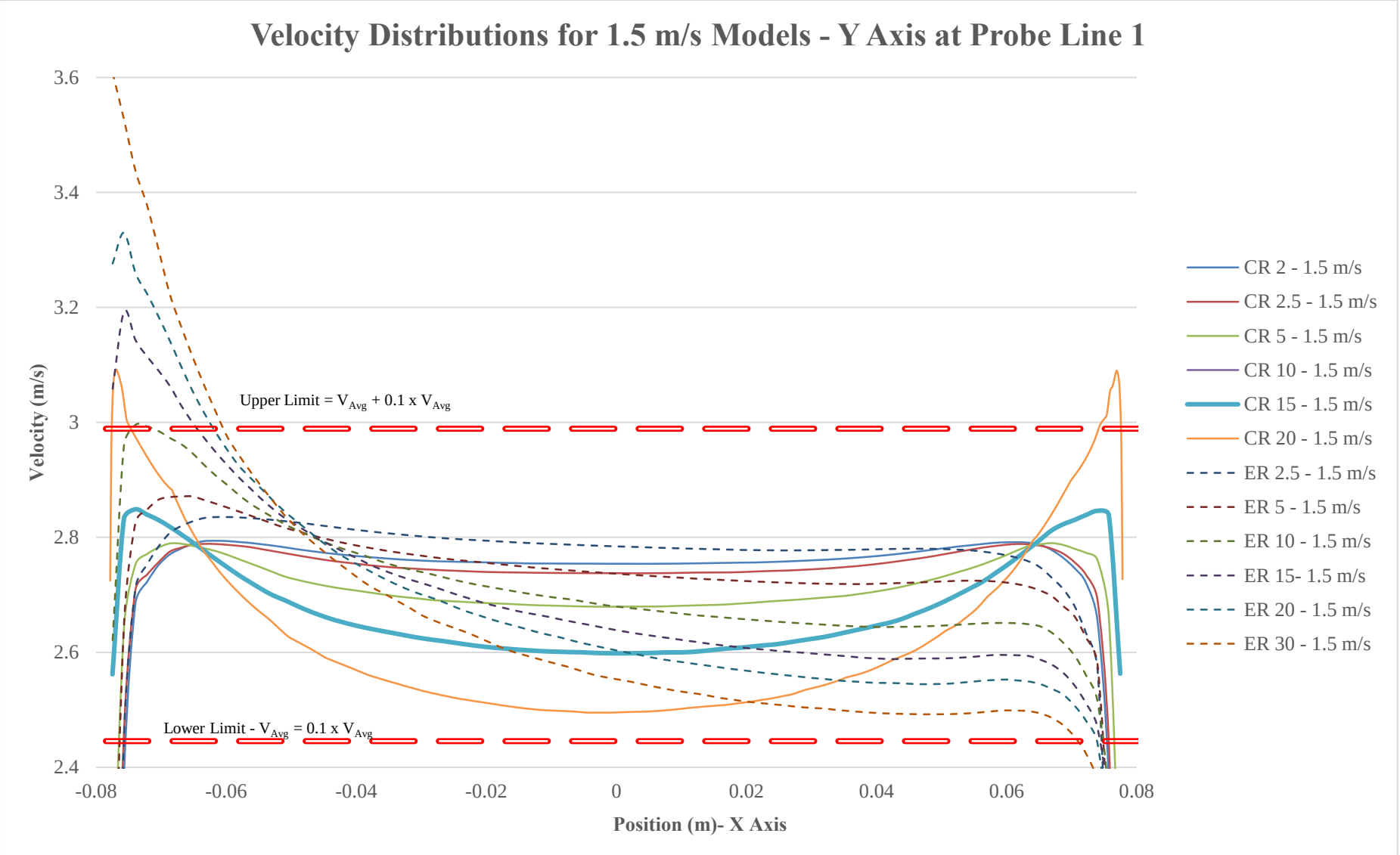

Figure 5.3: Velocity Distributions for 1.5 m/s Models – Y Axis at Probe Position 1

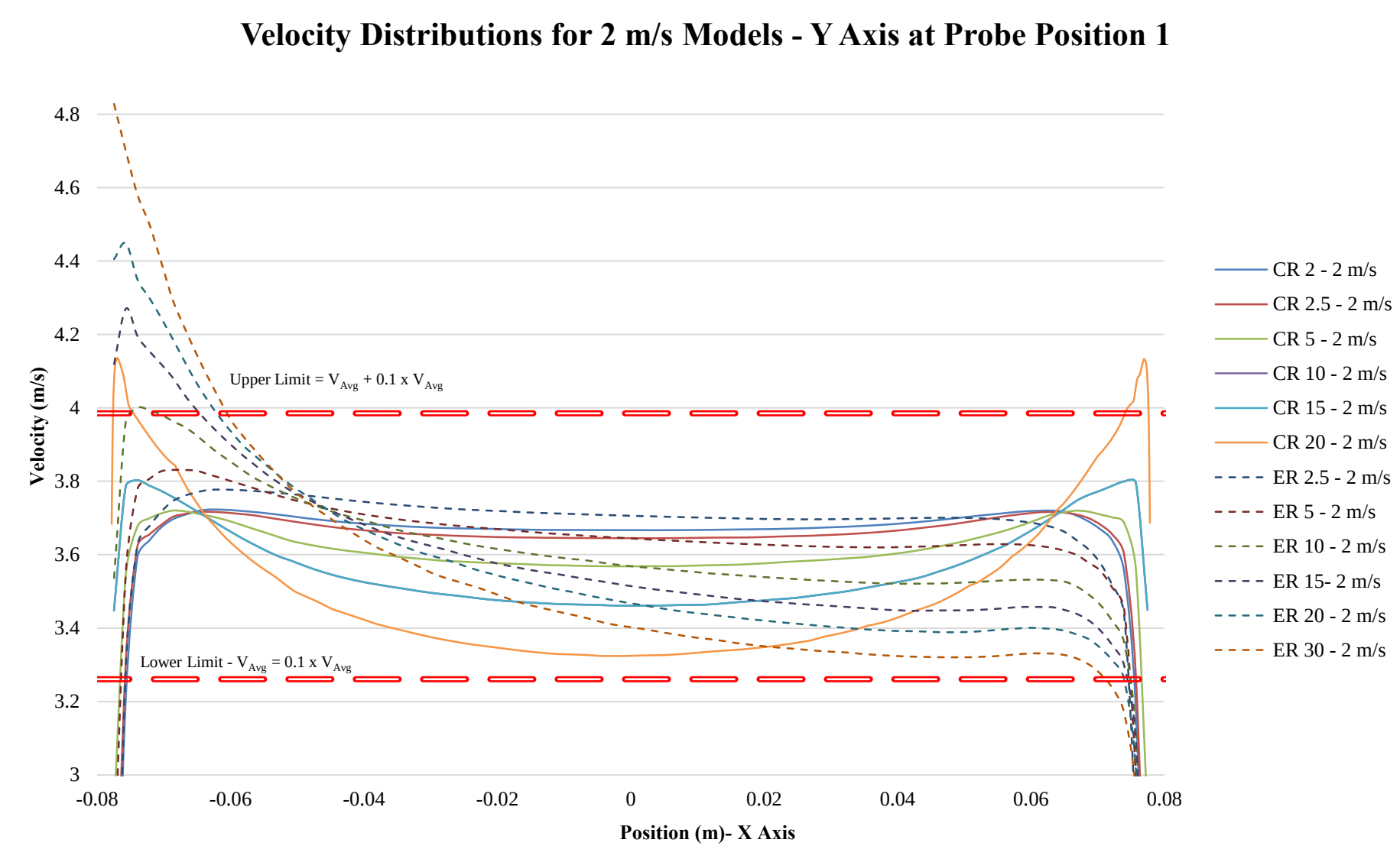

Figure 5.4: Velocity Distributions for 2 m/s Models – Y Axis at Probe Position 1

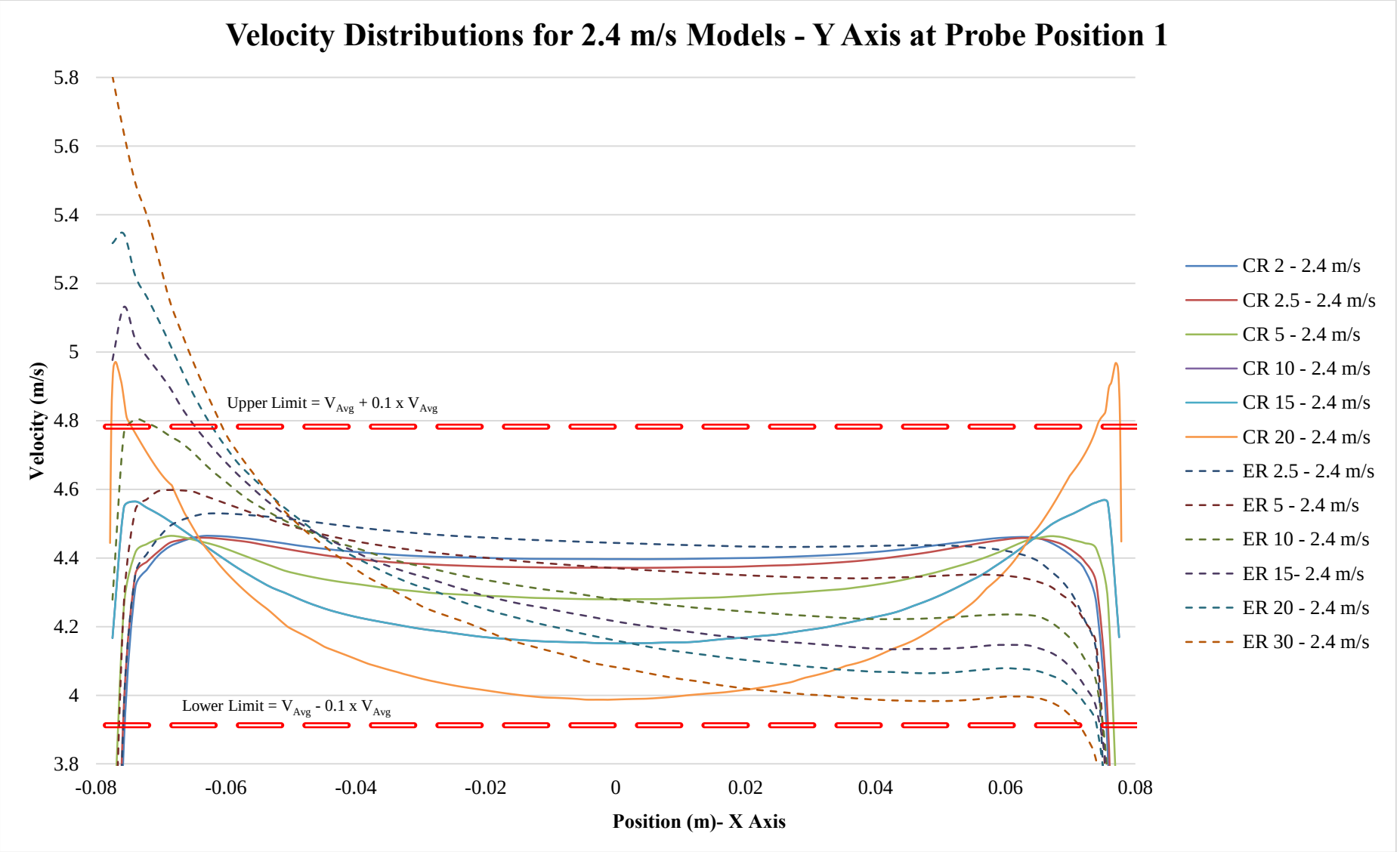

Figure 5.5: Velocity Distributions for 2.4 m/s Models – Y Axis at Probe Position 1

5.3. ASSESSMENT OF ECCENTRIC REDUCERS TO CRITERIA 2

Refer to **Figure 5.1** for the position of the reference circles. Criteria 2 HRW1 requires the velocity variation along circle AEDF to be less than 5% of the average velocity along line AEDF and Criteria 2 HRW2 requires the velocity variation along circle BGCH to be less than 5% of the average velocity along line BGCH. In order to assess Criteria 2, cylindrical data plots on a new defined co-ordinate systems with their origins at the centre of downstream end of the reducers were created in addition to the various CFD reporting and visualisation outputs described in ***Paragraph 3.6***. These cylindrical data plots were only created at Probe Position 1. The results for Probe Positions 2, 3 and 4 were not plotted due to the uniformity in the velocity distribution at these positions, as was demonstrated in ***Paragraph 4.2.*** The concentric reducers were not assessed according to Criteria 2 as their velocity distributions are symmetrical around the centre of the pipe, i.e. the velocity contours are circular in shape and will produce results that will fall within the acceptance envelope.

Two cylinders were created: HRW 1 and HRW 2 (see **Figure 5.1**). The cylinders have diameters of 124.88 mm (HRW 1) and 93.66 mm (HRW 2). The velocities along the circumference of the cylinder are plotted on the Y Axis and an angle relating to the position of the cylinder is plotted on the X Axis. This angle is a component of the new defined co-ordinate system, illustrated in **Figure 5.6**, and allows for the data to be presented on a XY chart.

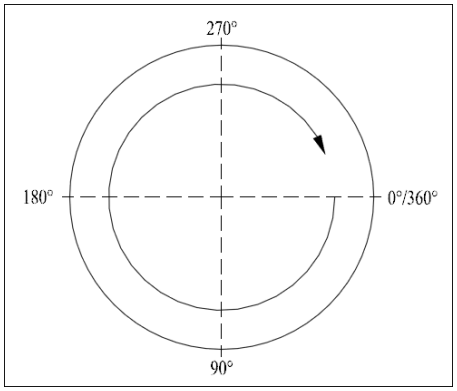

Figure 5.6: Section View of Pipeline Illustrating the Defined Angular Co-ordinate System

The average velocity for each cylinder was calculated and the 5% acceptance envelope for Criteria 2 was calculated from this average velocity. The acceptance envelope together with the average velocity for each velocity modelled was plotted for both circle HRW 1 and circle HRW 2. Examples of these

plots are provided in **Figure 5.7** and **Figure 5.8** below. **Figure 5.7** is the plot for the ER 2.5 Model with a 1 m/s input velocity and the results for both cylinders fall within the acceptance criteria. **Figure 5.8** is the plot for the ER 15 Model with a 1 m/s input velocity and the results for the HRW 1 cylinder fall outside of the acceptance envelope while the results for the HRW 2 cylinder fall within the acceptance envelope. **This highlights that position of the HR Wallingford Criteria 2 circles has an effect on the outcomes of the results.** The remainder of the results are provided in ***Appendix D***.

Models ER 20 and ER 30 fall outside both the HRW 1 and HRW 2 cylinders and the ER 15 Model falls outside the HRW 1 cylinder. Therefore ER 15, ER 20 and ER 30 do not pass acceptance Criteria 2. The remainder of the eccentric reducers (ER 2.5, ER 5 and ER 10) are within the acceptance envelope for Criteria 2.

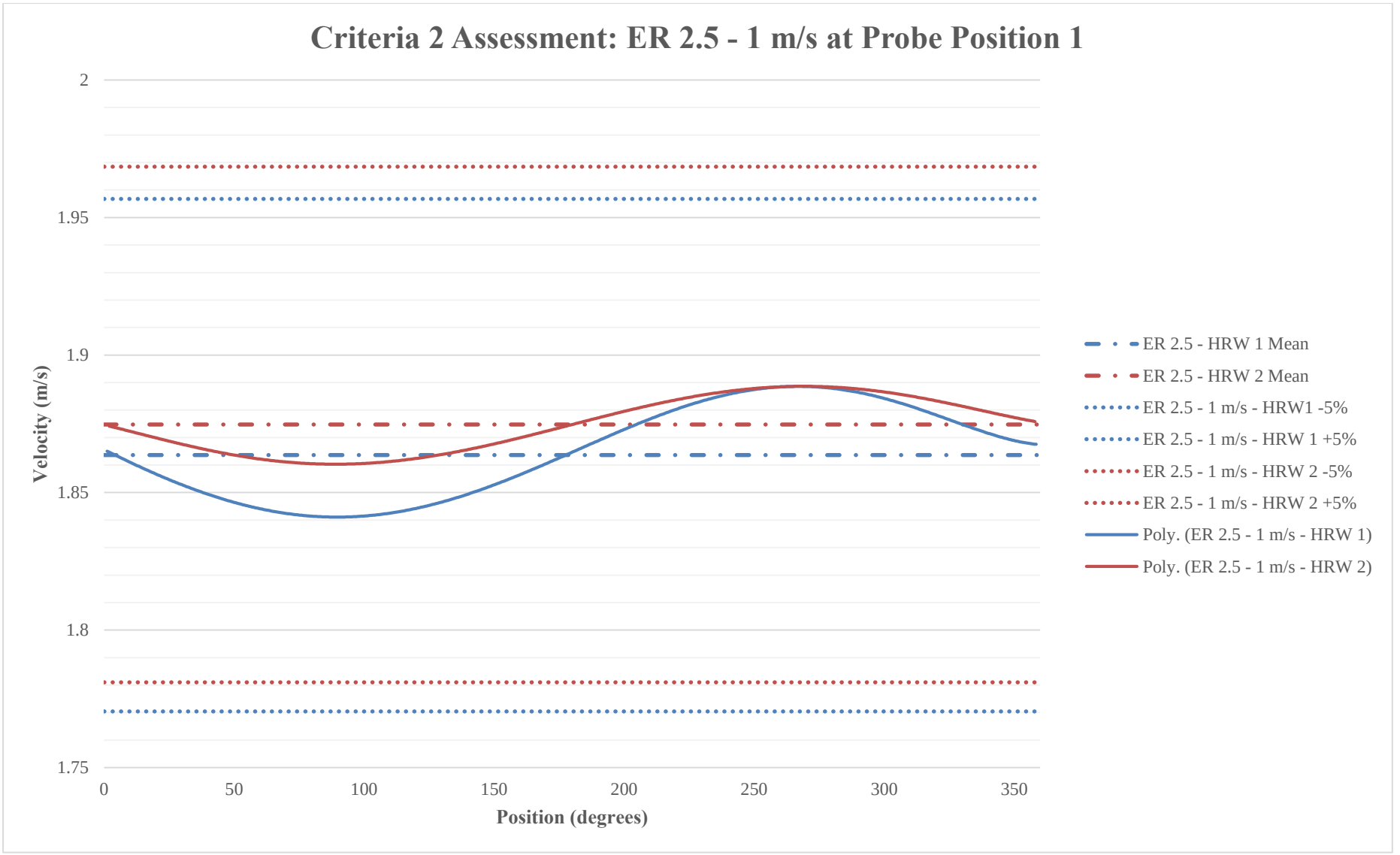

Figure 5.7: Criteria 2 Assessment: ER 2.5 – 1 m/s at Probe Position 1

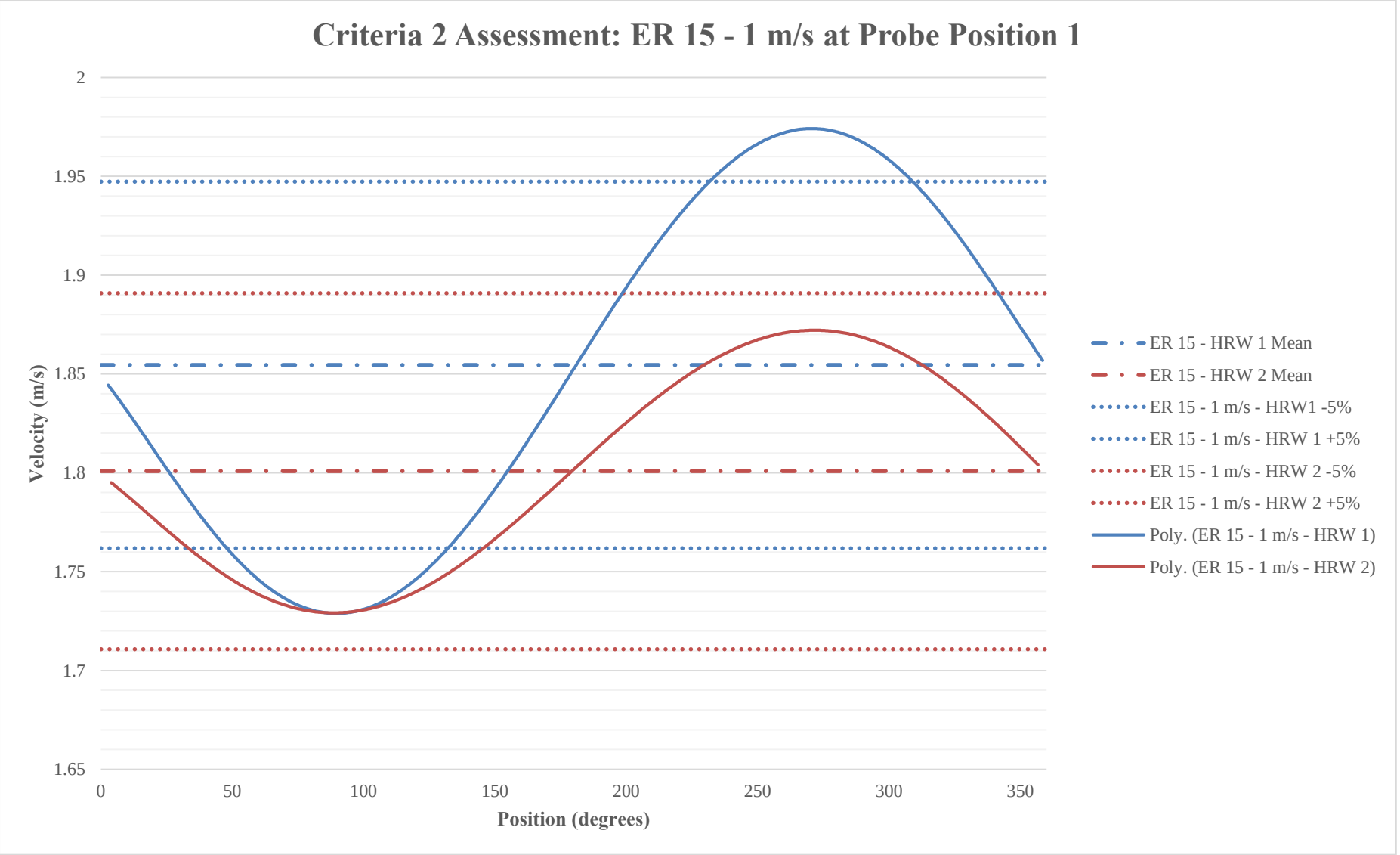

Figure 5.8: Criteria 2 Assessment: ER 15 – 1 m/s at Probe Position 1

5.4. ASSESSMENT OF REDUCERS TO CRITERIA 3 X AXIS

Refer to **Figure 5.1** for the position of the reference lines. Criteria 3 X Axis requires the velocity variation along line EGHF (X Axis) to be less than 10% of the cross-sectional average velocity. The XY plots for velocity in the direction of the X Axis were combined into individual plots for each velocity, together with lines representing the acceptance envelope for Criteria 3. The results for the position at Probe Position 1 together with the lower and upper limits are provided in this paragraph, **Figure 5.9** to **Figure 5.12**, one chart for each velocity modelled. The velocity relationships for the input velocities (1, 1.5, 2, 2.4 m/s), the outlet velocities (downstream end of the reducer) and the upper and lower limit velocities are provided in **Table 5.4**. The results for Probe Positions 2, 3 and 4 are not provided due to the uniformity in the velocity distribution at these positions, as was demonstrated in ***Paragraph 4.2***.

The CR 20 Model falls outside of acceptance Criteria 3 X Axis for all four flow velocities and the ER 30 Model falls outside of acceptance Criteria 3 Axis for the 1.5 m/s, 2 m/s and 2.4 m/s velocities and falls within the criteria for the 1 m/s velocity. The ER 30 Model is the only model that is affected in the acceptance criteria by the input velocity, where the **general trend of acceptance is not affected by the input velocity**. The remainder of the models (CR 2, CR 2.5, CR 5, CR 10, CR 15, ER 2.5, ER 5, ER 10, ER 15 and ER 20) all fall within the Criteria 3 X Axis acceptance envelopes.

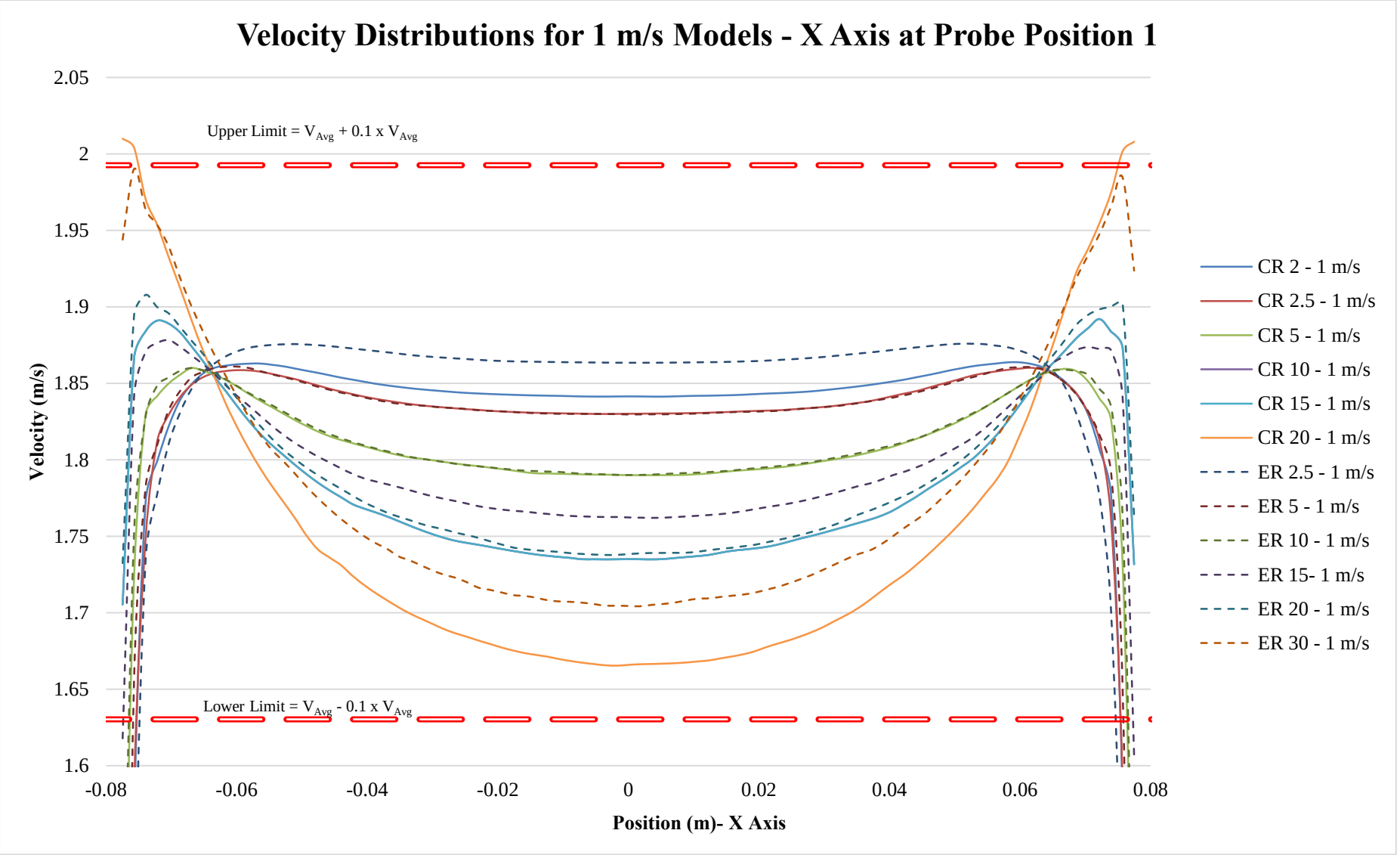

Figure 5.9: Velocity Distributions for 1 m/s Models – X Axis at Probe Position 1

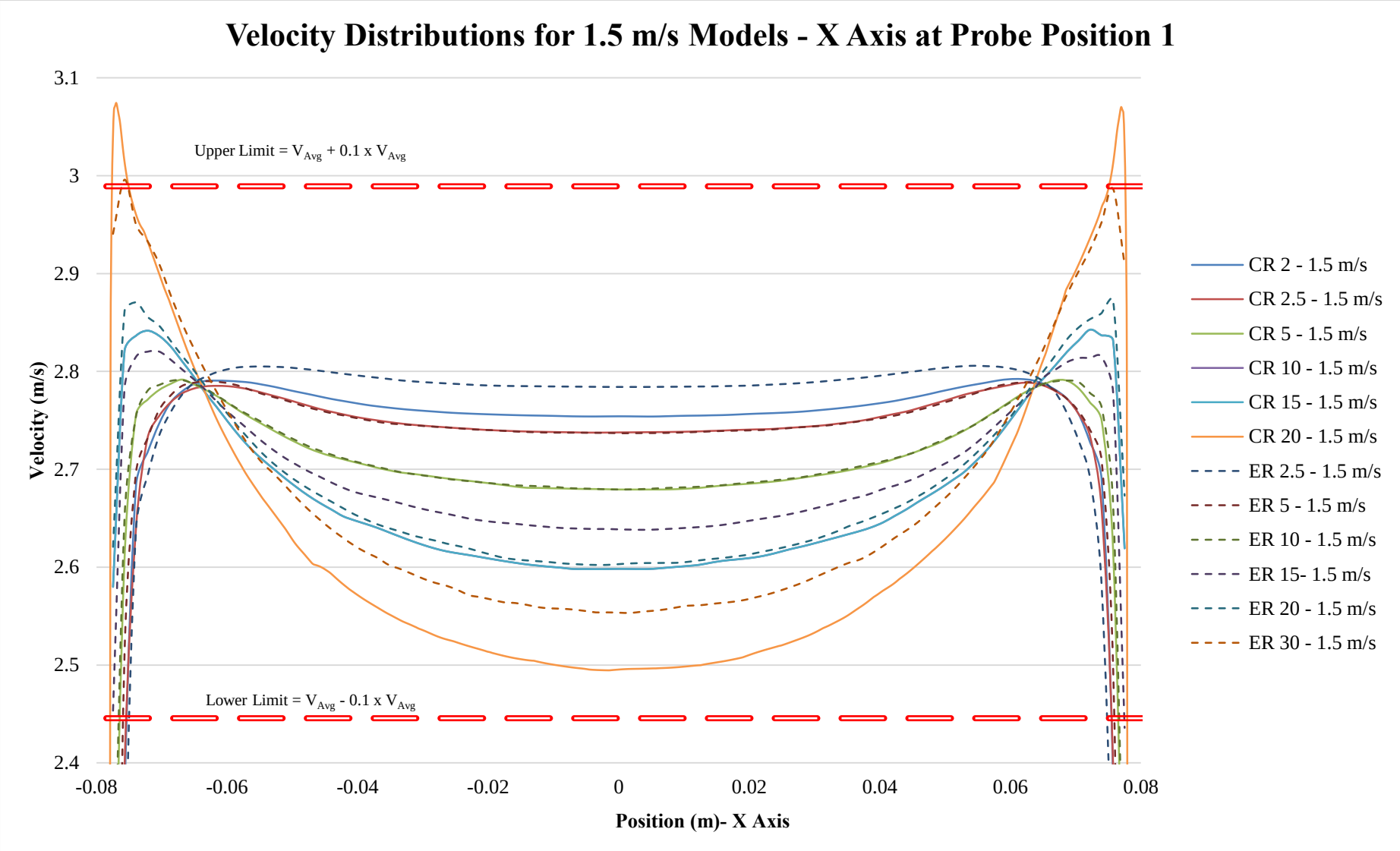

Figure 5.10: Velocity Distributions for 1.5 m/s Models – X Axis at Probe Position 1

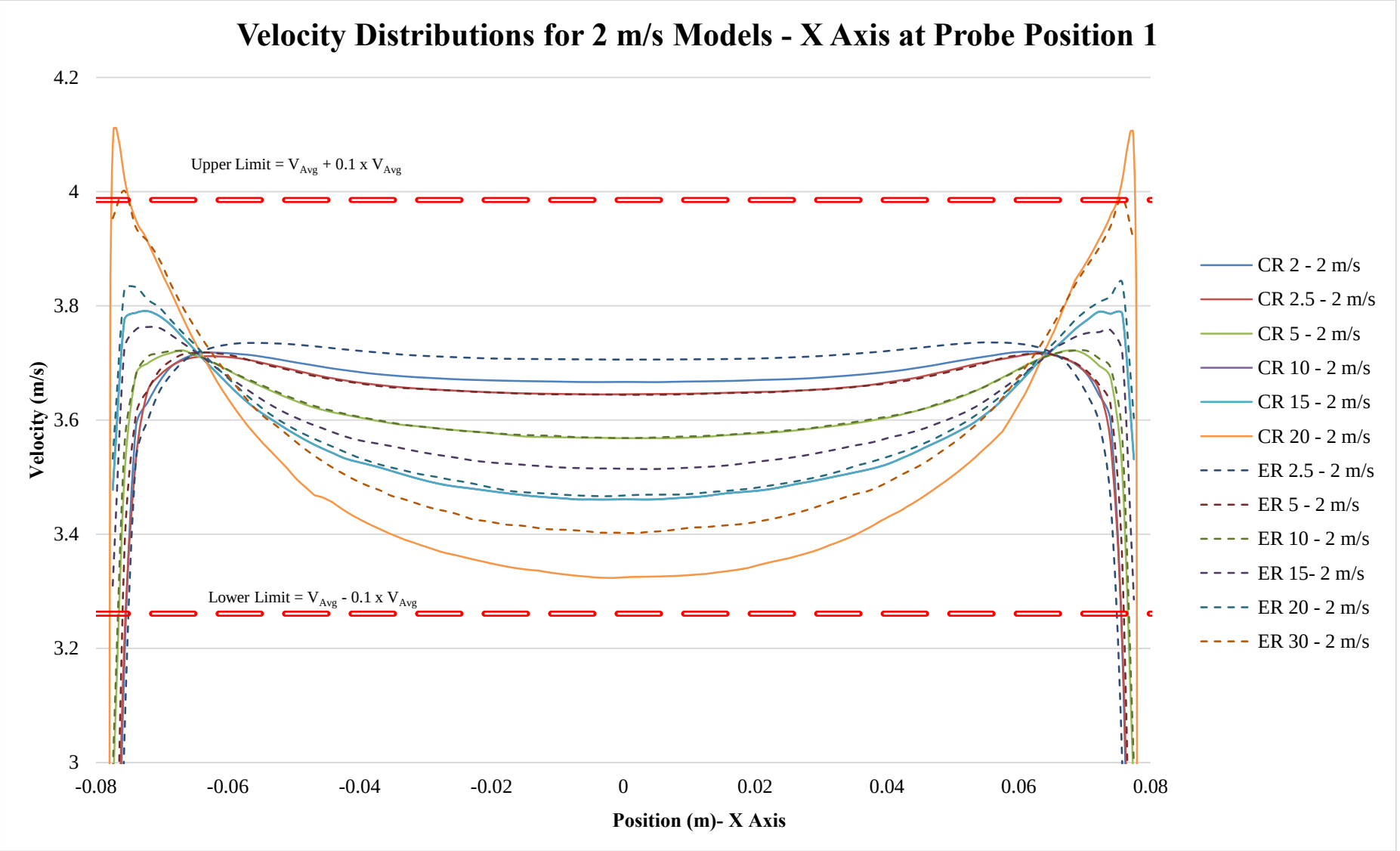

Figure 5.11: Velocity Distributions for 2 m/s Models – X Axis at Probe Position 1

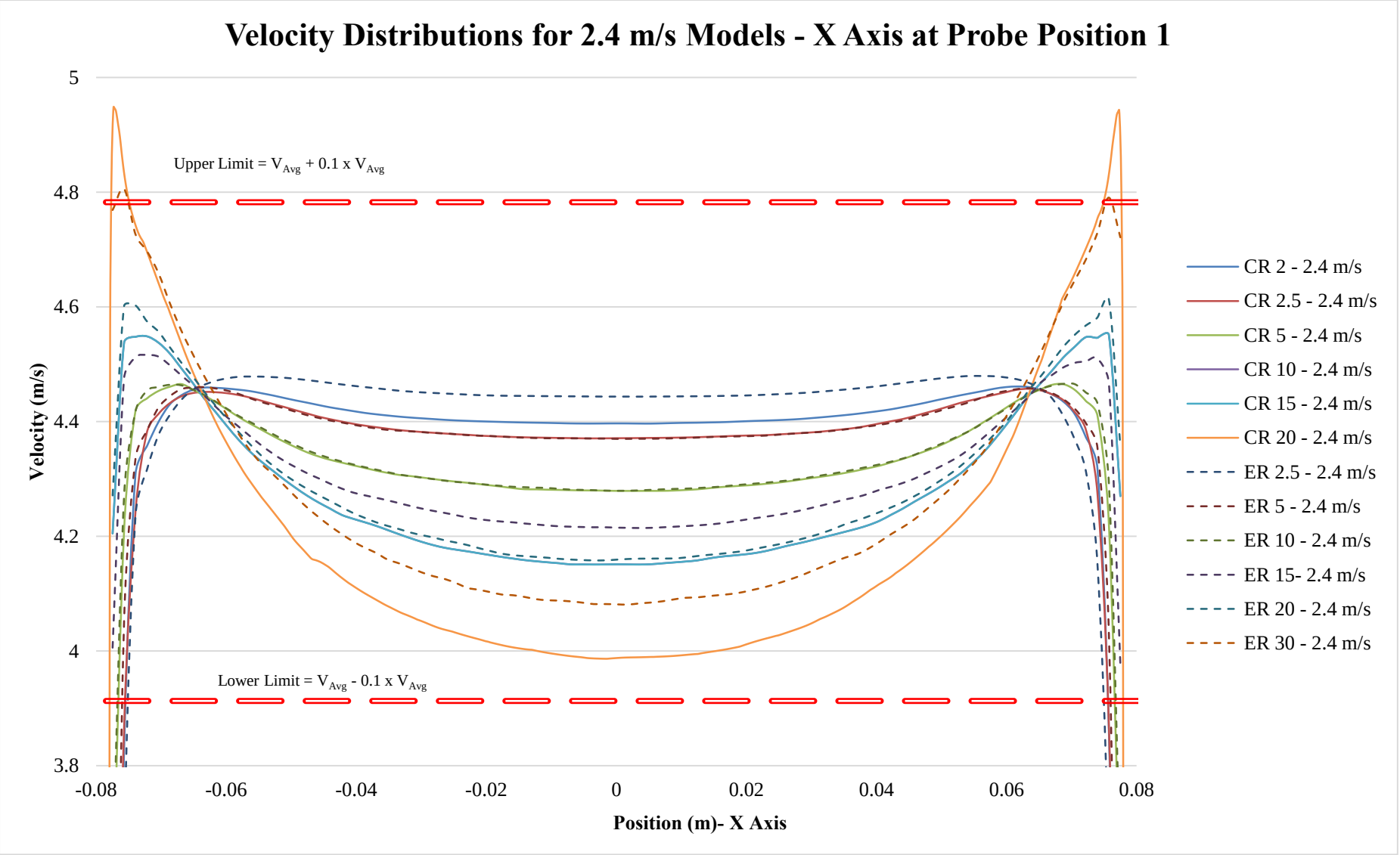

Figure 5.12: Velocity Distributions for 2.4 m/s Models – X Axis at Probe Position 1

5.5. ASSESSMENT OF THE HYDRAUILIC TRANSPORTATION OF AIR

The critical velocity for each of the concentric reducers was calculated with the upstream (larger) diameter as the input diameter in the calculation as the velocity increases through the reducer thereby increasing the capacity to hydraulically transport the air. The calculated critical velocities are provided in **Table 5.5**. The values calculated with Equation 2-2 (Kalinske and Bliss) and Equation 2-4 (Van Vuuren, Van Dijk and Steenkamp) are representative of one another, however the values calculated with Equation 2-3 (Wisener, Mohsen and Kouwen) are not representative (this is due to the addition of a constant of 0.825 x $(gD)^{0.5}$ that effects the equation at low velocities). Only the values obtained with Equation 2-2 and Equation 2-4 were utilised to assess the hydraulic transportation of air through the models. The only model where air could not be hydraulically transported through it is the CR 20 Model at 1m/s. This model however also fails Criteria 1 and Criteria 3 as well.

Table 5.5: Critical Velocities for the Concentric Reducer Models

Model	Pipe Slope - Θ (°)	Diameter of Pipe (m)	Critical Velocity (Eq 2-2)	Critical Velocity (Eq 2-3)	Critical Velocity (Eq 2-4)
CR 2	2	0.2191	0.293	1.278	0.422
CR 2.5	2.5	0.2191	0.328	1.259	0.451
CR 5	5	0.2191	0.463	1.290	0.596
CR 10	10	0.2191	0.654	1.334	0.787
CR 15	15	0.2191	0.798	1.367	0.925
CR 20	20	0.2191	0.918	1.394	1.038

5.6. RESULTS MATRIX

The final assessment of the success or failure of all 48 Models simulated with CFD according to the four criteria, Criteria 1, Criteria 2, Criteria 3 and Hydraulic Transportation of Air, is provided in **Table 5.7**. Concentric reducers CR 2, CR 2.5, CR 5, CR 10 and CR 15 and eccentric reducers ER 2, ER 5 and ER 10 all produce velocity distributions that fall within all four of the acceptance criteria at all four flow rates modelled. The CR 20 concentric reducer and eccentric reducers ER 15, ER 20 and ER 30 all fail one or more of the assessment criteria.

The lengths of the reducers producing the reducer angles utilised in this study are summarised below in **Table 5.6** and greater detail on the geometries is provided in **Table 3.1**. The shortest acceptable concentric reducer is the CR 15 measuring 101 mm, whereas the shortest acceptable eccentric reducer is the ER 10 measuring 306 mm. This saving in length not only applies to cost of the reducer, but to the entire pump station foot print and can be applied to any diameter reduction. ***The results from this study are however dimensionless*** as reducer angles were modelled and not reducer lengths and this above statement and table below is provided as an example of the possible effect on the selection of the correct reducer.

Table 5.6: Study's Reducer Length Summary

Geometry Name	Angle (°)	L (mm)
ER 30	30	94
ER 20	20	148
ER 15	15	202
ER 10	10	306
ER 5	5	617
ER 2.5	2.5	1237
CR 20	20	74
CR 15	15	101
CR 10	10	153
CR 5	5	309
CR 2.5	2.5	618
CR 2	2	773

Figure 3.3 presents a chart illustrating the standard reducer sizes, containing the sizes both from AWWA C208 and the fitting manufacturers. This figure has been separated into two new charts, one for the concentric reducers and one for the eccentric reducers, the acceptance criteria has also been added to these charts. These charts are provided in **Figure 5.13** and **Figure 5.14**. From these charts it is observed that ***various standard size reducer fittings fall outside of the acceptance criteria and for the eccentric reducers this includes the AWWA C208 standard***.

Table 5.7: Final Acceptance Matrix

	Acceptance	CR 2	CR 2.5	CR 5	CR 10	CR 15	CR 20	ER 2.5	ER 5	ER 10	ER 15	ER 20	ER 30
1 m/s Velocity	Criteria 1	✓	✓	✓	✓	✓	×	✓	✓	✓	×	×	×
	Criteria 2 HRW 1	N/A	N/A	N/A	N/A	N/A	N/A	✓	✓	✓	×	×	×
	Criteria 2 HRW 2	N/A	N/A	N/A	N/A	N/A	N/A	✓	✓	✓	✓	×	×
	Criteria 3 X	✓	✓	✓	✓	✓	×	✓	✓	✓	✓	✓	✓
	Criteria 3 Y	✓	✓	✓	✓	✓	×	✓	✓	✓	×	×	×
	Air Transport	✓	✓	✓	✓	✓	×	✓	✓	✓	✓	✓	✓
1.5 m/s Velocity	Criteria 1	✓	✓	✓	✓	✓	×	✓	✓	✓	×	×	×
	Criteria 2 HRW 1	N/A	N/A	N/A	N/A	N/A	N/A	✓	✓	✓	×	×	×
	Criteria 2 HRW 2	N/A	N/A	N/A	N/A	N/A	N/A	✓	✓	✓	✓	×	×
	Criteria 3 X	✓	✓	✓	✓	✓	×	✓	✓	✓	✓	✓	×
	Criteria 3 Y	✓	✓	✓	✓	✓	×	✓	✓	✓	×	×	×
	Air Transport	✓	✓	✓	✓	✓	×	✓	✓	✓	✓	✓	✓
2 m/s Velocity	Criteria 1	✓	✓	✓	✓	✓	×	✓	✓	✓	×	×	×
	Criteria 2 HRW 1	N/A	N/A	N/A	N/A	N/A	N/A	✓	✓	✓	×	×	×
	Criteria 2 HRW 2	N/A	N/A	N/A	N/A	N/A	N/A	✓	✓	✓	✓	×	×
	Criteria 3 X	✓	✓	✓	✓	✓	×	✓	✓	✓	✓	✓	×
	Criteria 3 Y	✓	✓	✓	✓	✓	×	✓	✓	✓	×	×	×
	Air Transport	✓	✓	✓	✓	✓	×	✓	✓	✓	✓	✓	✓
2.4 m/s Velocity	Criteria 1	✓	✓	✓	✓	✓	×	✓	✓	✓	×	×	×
	Criteria 2 HRW 1	N/A	N/A	N/A	N/A	N/A	N/A	✓	✓	✓	×	×	×
	Criteria 2 HRW 2	N/A	N/A	N/A	N/A	N/A	N/A	✓	✓	✓	✓	×	×
	Criteria 3 X	✓	✓	✓	✓	✓	×	✓	✓	✓	✓	✓	×
	Criteria 3 Y	✓	✓	✓	✓	✓	×	✓	✓	✓	×	×	×
	Air Transport	✓	✓	✓	✓	✓	×	✓	✓	✓	✓	✓	✓

✓ Simulation Passes the Criterion	× Simulation Fails the Criterion	N/A Criterion not applicable

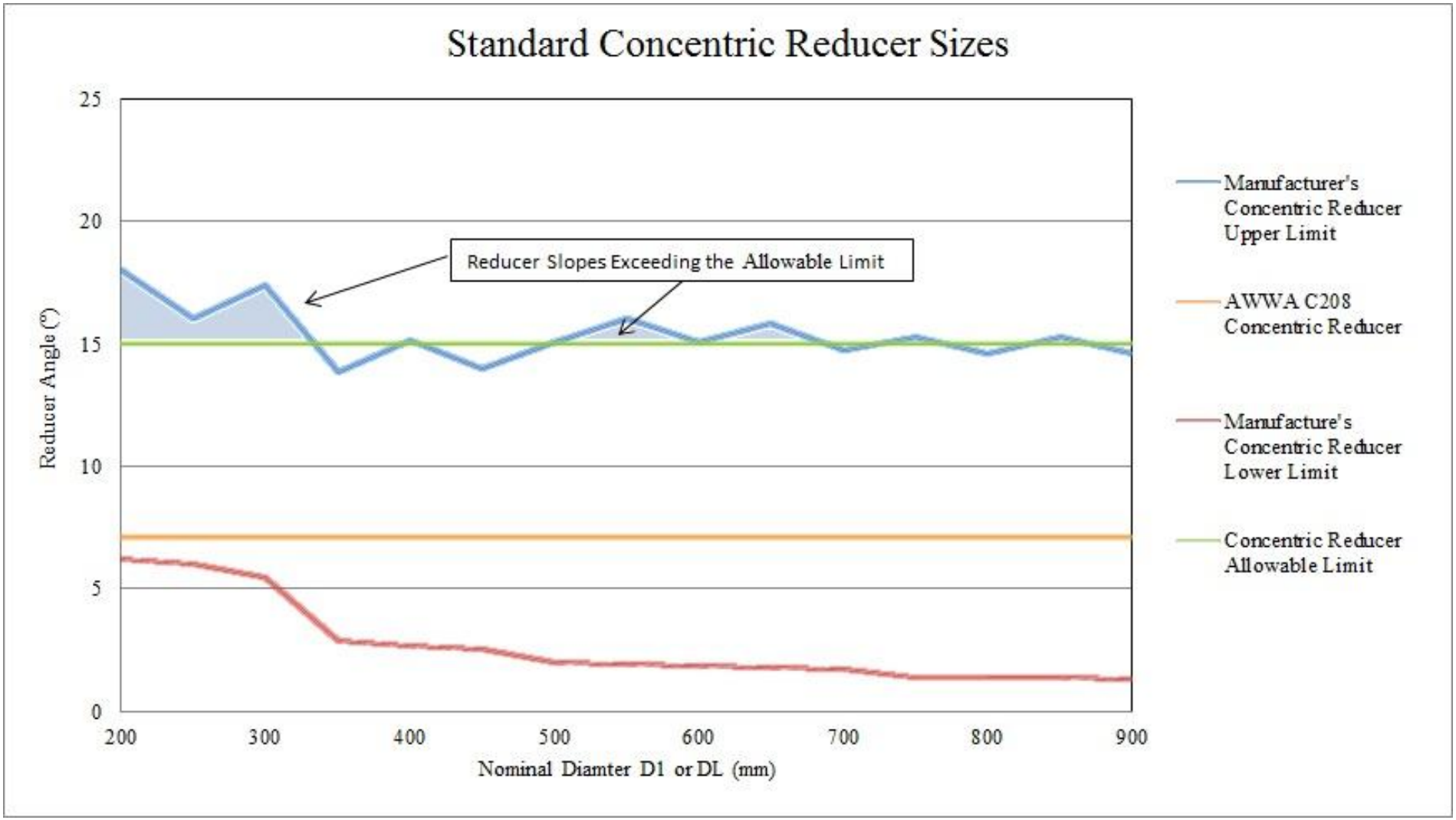

Figure 5.13: Standard Concentric Reducer Sizes with Allowable Concentric Reducers Limits

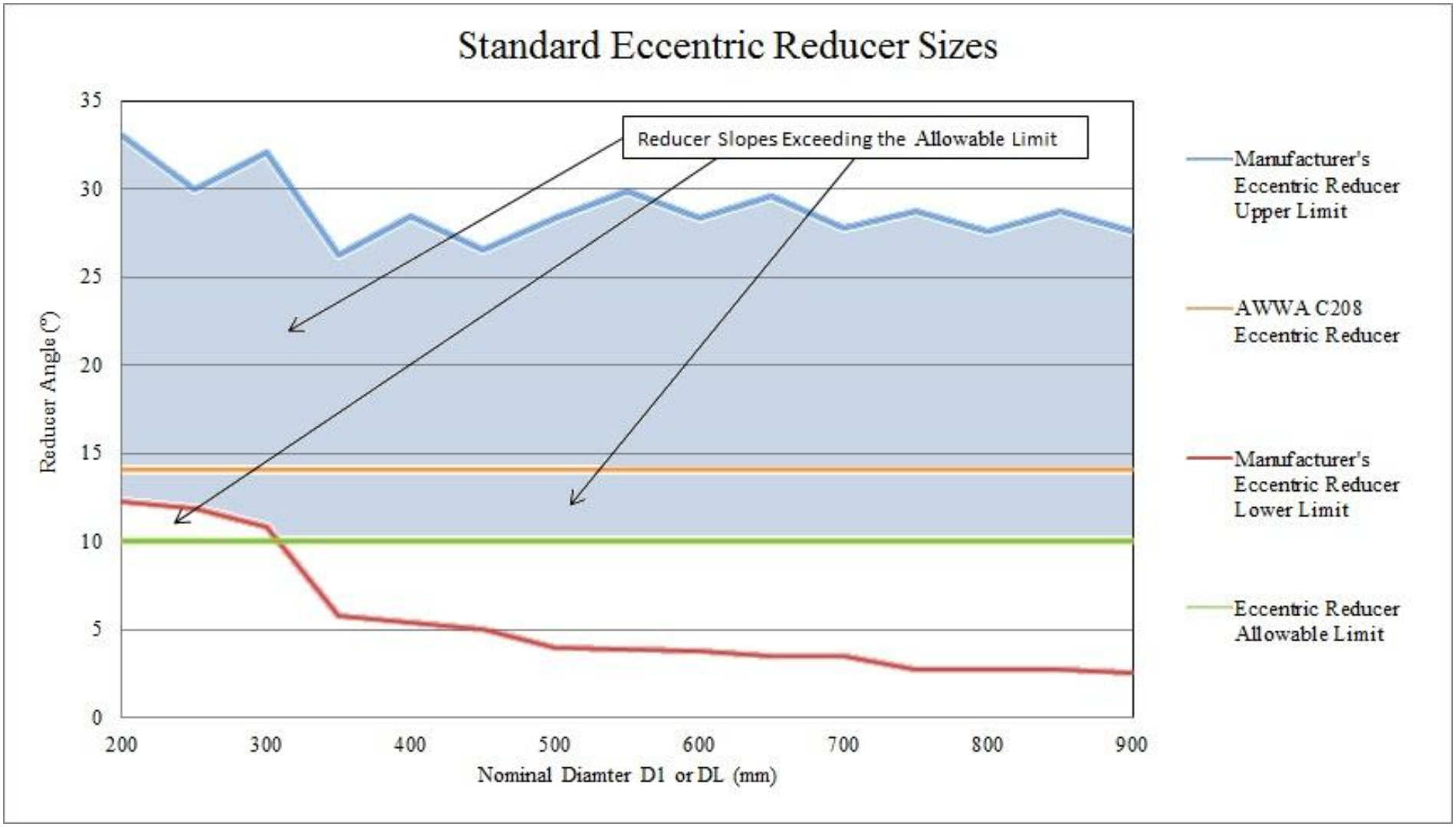

Figure 5.14: Standard Eccentric Reducer Sizes with Allowable Eccentric Reducers Limits

6. CONCLUSIONS AND RECOMMENDATIONS

6.1. CONCLUSIONS

The objective of this study was to review the pump inlet design guidelines and standards, with the focus being on the selection of the correct reducer type. It was proposed to utilise CFD to analyse various reducer geometries in combination with various flow rates.

The concept of eccentric and concentric reducers was introduced and their application in pump suction pipe work was explored. All the design guidelines favour eccentric reducers with the flat section on top to allow for transportation of air through the reducer. Together with the design guidelines, criteria were reported whereby inlet conditions into pumps can be assessed.

The theory behind the hydraulic transportation of air was investigated and it was shown that air can be hydraulically transported through pipes, even though the pipe has a negative slope. This transportation depends on the flow rate, pipe diameter and pipe slope.

Various case studies were presented where it was highlighted that the incorrect selection of reducer type may lead to premature pump failure due to unbalanced loads acting on the pump impeller.

From the theory and case studies described above it was questioned that whether **a correctly designed concentric reducer will not only provide a more uniform pressure/velocity distribution in comparison to an eccentric reducer, but will allow air to be hydraulically transported through the reducer to the pump.**

Twelve geometric models (six concentric reducers and six eccentric reducers) were defined to represent the range of standard reducer fitting dimensions typically available. Four flow velocities were identified to be applied to the models ranging from a velocity of 1 m/s to a velocity of 2.4 m/s. Therefore a total of 48 CFD models were simulated. The CFD models were set up and run in the commercial software STAR-CCM+ and the results were recorded in various formats.

The results were assessed according to four criteria identified in the Literature Review:

i) Criteria 1 – HR Wallingford: Velocity variation along line ABCD is less than 10% of the average velocity;
ii) Criteria 2 – HR Wallingford: Maximum velocity variation along a circle AEDF is ±5% of the average velocity;
iii) Criteria 3 – ANSI, Jones et al and Ninham Shand Consulting Services: Time averaged velocity is to be within 10% of the cross-sectional area average velocity; and
iv) Hydraulic Transportation of Air – Air must be able to be hydraulically transported through the reducer.

Following from the assessment it was found that concentric reducers CR2, CR 2.5, CR 5, CR 10 and CR 15 and eccentric reducers ER 2, ER 5 and ER 10 all produce velocity distributions that fall within all four of the acceptance criteria at all four flow rates modelled. The CR 20 concentric reducer and eccentric reducers ER 15, ER 20 and ER 30 all fail one or more of the assessment criteria. **The maximum allowable angles of concentric reducer CR 15 and eccentric reducer ER 10 infers various standard size reducer fittings fall outside of the acceptance criteria and for the eccentric reducers, this includes the AWWA C208 standard.**

It was also observed that the velocity distributions for all the reducers return to an acceptable distribution at a length of 1xD2 downstream from the reducer. Therefore if the hydraulic transport of air remains a concern and there is space available in the pumping station, the addition of a straight length of pipe on the downstream end of the reducer will serve to provide a desirable pump inlet velocity distribution.

CFD was used to review the pump inlet design guidelines and standards, with the focus being on the selection of the correct reducer type. And the posed question can be answered: **Yes a correctly designed concentric reducer (angle less or equal to 15°) will not only provide a more uniform pressure/velocity distribution in comparison to an eccentric reducer, but will allow air to be hydraulically transported through the reducer to the pump.**

6.2. LIMITATIONS

In the analyses uniform flow conditions were provided at the inlet of the geometry, in engineering applications this may seldom be the case. These non-uniform flow conditions may influence the velocity distribution in such a way that a concentric or eccentric reducer within the recommended range may produce a velocity distribution that is outside of the acceptance criteria.

The range of angles modelled is representative of a wide range of reducers, separated by large increments in order to keep the sample group manageable (i.e. ER 2.5, ER 5, ER 10 and not ER 1, ER 2, ER 3, etc). The reducers that have been listed for the maximum allowable angles (CR 15 and ER 10) may be conservative. For example a concentric reducer of 16° may still provide acceptable results as the angles is less than the CR 20 reducer that did not pass the various criteria.

Two of the three hydraulic transportation of air equations were utilised while the third equation was discarded as it did not relate to the other two equations. This third equation may represent the air transport correctly with the remaining two equations being incorrect. This will require a higher velocity (>1.2 m/s) to transport the air through the concentric reducer. This inability to hydraulically transport air may be increased if the velocities in the suction pipe work is less than 1 m/s, which may be the case for pump stations with various pump operating configurations (i.e. only one out of three operating under low dam levels and two out of three pumps operating under high dam levels) and oversized pump suction pipe work to minimise suction head losses and thereby increase available NPSH. The ability to hydraulically transport air through the reducer must therefore always be assessed when selecting the reducer type.

The fluid being pumped that was the focus of this study is water. Pumping applications extend to a wide variety of other fluids. Air is typically not of a concern in the petrochemical industry (i.e. there are no air valves on petroleum pipelines) and pumping velocities are typically much higher. The petrochemical design standards were not reviewed and assessed in this study. Additionally the application of concentric reducers in slurry pumping application may not be desirable as solids may accumulate at the slope change on the bottom side of the reducer if the velocity of the liquid is not large enough to hydraulically transport it through the reducer and therefore an eccentric reducer with the horizontal surface at the bottom may be desirable.

6.3. RECOMMENDATIONS FOR PUMP INLET REQUIREMENTS

The pump inlet requirements reviewed did not explicitly state where the criteria are to be measured and what average velocities are to be used. The following list provides a proposed alternative set of criteria whereby pump inlet conditions can be assessed (see **Figure 6. 1**):

i) Criteria 1: Velocity variation along line ABCD is less than ±10% of the average velocity along line ABCD;
ii) Criteria 2: Velocity variation along line EGHF is less than ±10% of the average velocity along line EGHF;
iii) Criteria 3: Maximum velocity variation along a circle AEDF is ±5% of the average velocity along circle AEDF, the diameter of circle AEDF is 0.8 x ID;
iv) Criteria 4: Maximum velocity variation along a circle BGCH is ±5% of the average velocity along circle BHCG, the diameter of circle BGCH is 0.6 x ID;
v) Criteria 5: Time averaged velocity at any point is to be within ±10% of the cross-sectional area average velocity; and
vi) Criteria 6: Air must be able to be hydraulically transported through the reducer.

This proposed alternative set of criteria provides an assessment that will produce uniform results due to the location of set measuring points and defined average velocities. These alternative proposed criteria also allow for the case where the velocity is distributed along the X Axis (due to an upstream bend or other fitting) and not only along the Y Axis as it was for the original Criteria 1. This proposed alternative set of criteria will need to be evaluated in further studies to establish their application in industry. These further studies are discussed in the following paragraph.

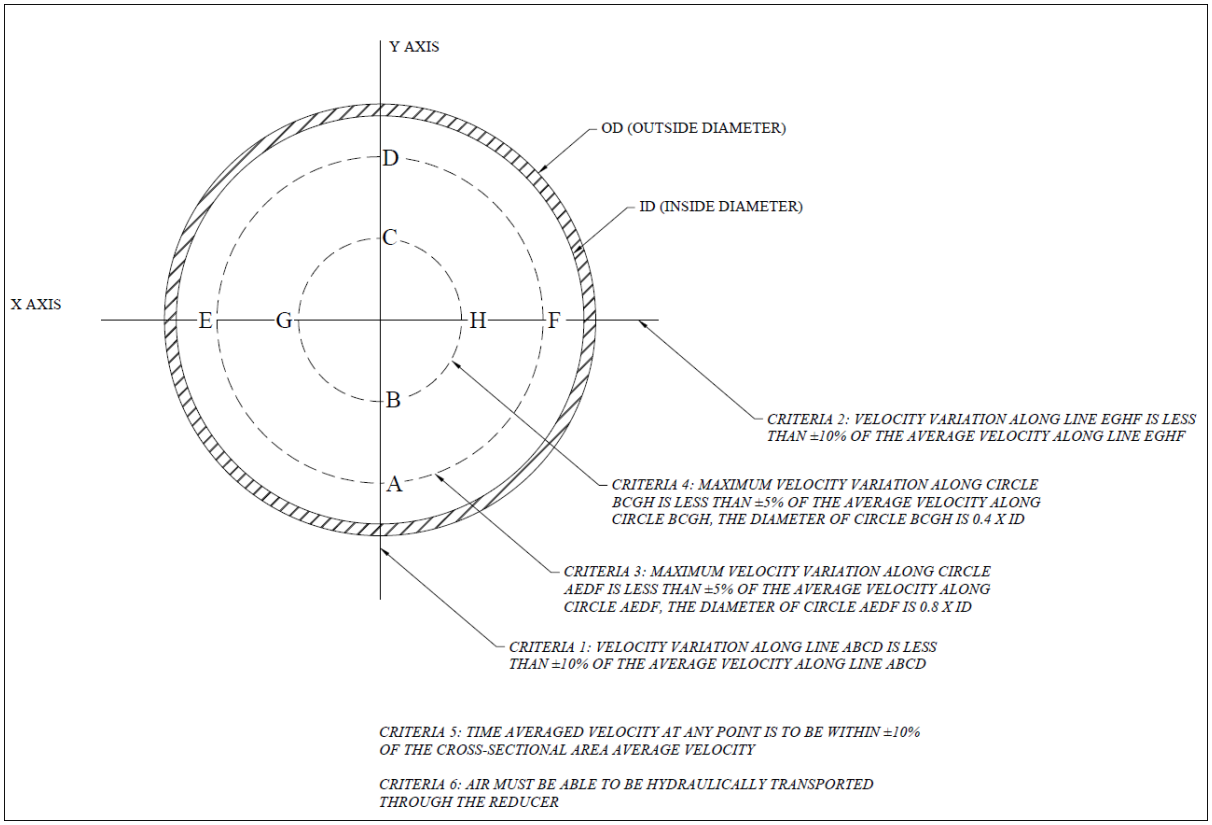

Figure 6. 1: Proposed Set of Pump Inlet requirements for Reducers – Section View

6.4. PROPOSED FUTURE RESEARCH

It is recommended that:

- The results from this study are to be confirmed with an independent CFD study and/or with a physical model study;
- Additional models with various bends, elbows, sweep tees typically found in pump inlet pipe work that could possibly create swirl or non-uniform flow conditions entering into the suction reducers are to be modeled With this information guidelines on typical suction manifold and suction pipework can be developed; and
- Additional CFD modeling and/or physical model studies where the hydraulic transport of air through the concentric reducer is explored to assess which of the hydraulic transport of air equations best suits this problem.

7. REFERENCE LIST

1. ABEYLA TRADING. 2008. *Pipes fittings flanges fabrication.* Abeyla Trading: as author.

2. AEROTHERM. 2011. *Computational fluid dynamic analysis of the Mokolo Pump Station pipe network*. Unpublished Technical Report. Report No ATPN-2011-15-00143. Available at Mokolo Crocodile Consultants.

3. ANSI/AWWA. 2008. *ANSI/AWWA C208-07 Dimensions for fabricated steel water pipe fittings.* American Water Works Association, Denver.

4. ANSI/HI. 2000. *ANSI/HI 9.8-1998 American National Standard for pump intake design*. Hydraulic Institute, New Jersey.

5. ANSI/HI. 2009. *ANSI/HI 9.6.6-2009 American National Standard for rotodynamic pumps for pump piping.* Hydraulic Institute, New Jersey.

6. AWWA. 2004. *AWWA M11 Steel pipe – a guide for design and installation.* American Water Works Association, Denver.

7. BARBA, L. 2010. 'Lecture 20 Part 1: Introduction to CFD; the basic ingredients (model, discretization, analysis, solution)' *Fluid Mechanics – ENG ME303 Videos*. Boston University. Available on: iTunes u.

8. BASSON, M.S., VAN NIEKERK, P.H. and VAN ROOYEN, J.A. 1997. *Overview of water resources availability and utilisation in South Africa.* South Africa. Department of Water Affairs and Forestry Report P RSA/00/0197. CTP Book Printers, Cape Town.

9. BLOCH, H.P. 2010. 'Eccentric reducers and straight runs of pipe at pump suction', *Hydrocarbon Processing.* September 2010, p. 9.

10. BLOCH, H.P. and BUDRIS, A.R. 2010. *Pump User's Handbook Life Extension,* 3rd ed. The Fairmont Press, Lilburn.

11. CD-ADAPCO. 2012. *USER GUIDE STAR-CCM+ Version 7.04.006*

12. CHADWICK, A., MORFETT, J. and BORTHWICK, M. 2004. *Hydraulics in Civil and Environmental Engineering.* Spon Press: London. 4th ed. Spon Press: London.

13. DWA: DEPARTMENT OF WATER AFFAIRS. 1986. *Bestuur van die waterhulpbronne van die Republiek van Suid-Afrika* [Management of the water resources of the Republic of South Africa]. CTP Book Printers, Cape Town.

14. HALL LONGMORE. 1989. *Men of steel*. 3rd ed. Hall Longmore: as author.

15. HIRSCH, C. 2007. *Numerical Computation of Internal and External Flows. Fundamentals of Computational Fluid Dynamics*, 2nd ed. Butterworth-Heinemann, Oxford.

16. WALLINGFORD, H.R. and BARR, D.I.H. 2006. *Tables for the hydraulic design of pipes, sewers and channels volume ii*, 8th ed. Thomas Telford, London.

17. HYDRAULIC INSTITUTE. 2001. *Pump life cycle costs: A guide to LCC analysis for pumping systems. Executive summary*. [Accessed 21 May 2012]. Available at <http://www.pumps.org/WorkArea/DownloadAsset.aspx?id=5652>

18. JONES, G.M., SANKS, R.L., TCHOBANOGLOUS, G and BOSSERMAN II, B.E. (eds.) 2008. *Pumping Station Design.* Pumps: Intake Design, Selection, and Installation. 3rd ed. Butterworth-Heinemann, Burlington

19. KSB. 2012. *Operating Instructions ETA Centrifugal Pump (A,B,C,D Pedestals).* [Accessed 12/04/2012].
<http://www.ksbpumps.co.za//products/eta-c-&-d/eta-c-d_operating_instructions.pdf.>

20. MACKAY, R. 2004. *Practical Pump Handbook.* Elsevier Advanced Technology, Oxford.

21. MINING PRESSURE SYSTEMS n.d. *Technical manual*. Mining Pressure Systems: as author.

22. NINHAM SHAND CONSULTING SERVICES. 2007. *Computational Fluid Dynamics Analysis for Eastford Pumpstation.* Unpublished Technical Report. Report No 4316/401608. Available at Aurecon Knowledge Centre.

23. POTHOF, I.W.M. and F.H.L.R. CLEMENS (2011). Experimental study of air-water flow in downward sloping pipes. *International Journal of Multiphase Flow*. No. 37, pp. 278-292.

24. SOUTH AFRICAN BUREAU OF STANDARDS. 2011. *Electric welded low carbon steel pipes for aqueous fluids (large bore).* (SANS 719: 2011). SABS Standards Division, Pretoria.

25. SOUTH AFRICAN BUREAU OF STANDARDS. 2013. *Steel Pipes. Part 2: Screwed pieces and pipe fitting of nominal size not exceeding 150 mm*. (SANS 62-2: 2011). SABS Standards Division, Pretoria.

26. SOUTH AFRICAN PUMP MANUFACTURERS ASSOCIATION (SAPMA). 2002. *Pumps Principles & Practice.* 4th ed. K Myles and Associates, Johannesburg.

27. SINOTECH CC. 2005. *CFD Modelling of the Pipe Work on the inlet side of the Abstraction Works.* Unpublished Technical Report. Available at Sinotech CC.

28. STURM, T.W. 2010. Water, water everywhere. *Journal of Hydraulic Engineering.* January, pp. 1-2.

29. SULZER PUMPS LTD. 2010. *Centrifugal Pump Handbook*. 3rd ed. Butterworth-Heinemann, Oxford.

30. TU, J., YEOH, G.H. and LIU, C. 2008. *Computational fluid dynamics- a practical approach.* Butterworth-Heinemann, Oxford.

31. UNIVERSITY OF PRETORIA. 2011. 'Standards for Sumps, Pumps and Pipe Work.' *SHW 795 – Pump Station Design Course Notes*, 2011. University of Pretoria, School of Civil Engineering.

32. VAN DER WESTHUIZEN, W. 2011. 'Case study: Inlet conditions leading to problems – Knysna.' *SHW 795 – Pump Station Design*, 2011. University of Pretoria, School of Civil Engineering.

33. VAN VUUREN, S.J., VAN DIJK, M and STEENKAMP, J.N. 2004. *Guidelines for effective de-aeration.* WRC Report No. 1177/2/04. Water Research Commission, Pretoria.

APPENDIX A

REDUCER TYPE SELECTION REFERENCE DRAWINGS

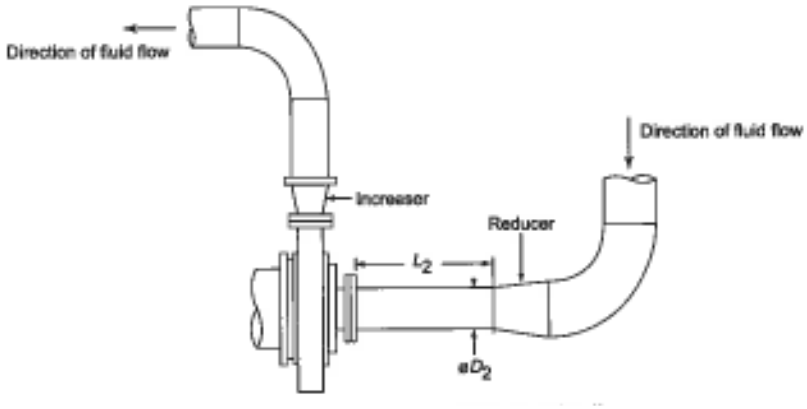

Figure A-1: Straight Pipe Lengths and Reducers Required (ANSI/HI 2009)

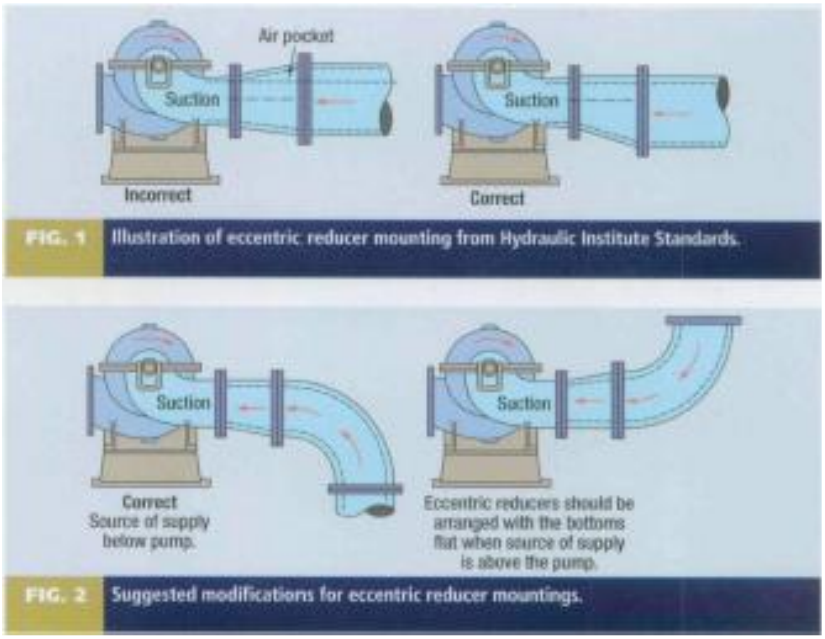

Figure A-2: Reducer Type and Installation Requirements (Bloch 2010)

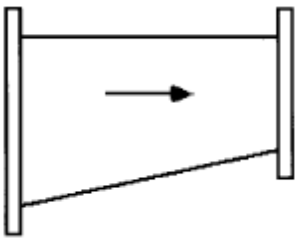

Figure A-3: Reducer Type and Installation Requirements (Mackay 2004)

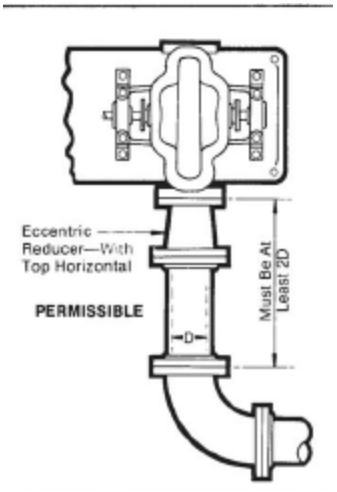

Figure A-4: Reducer and straight pipe length requirements (Bloch and Budris 2010)

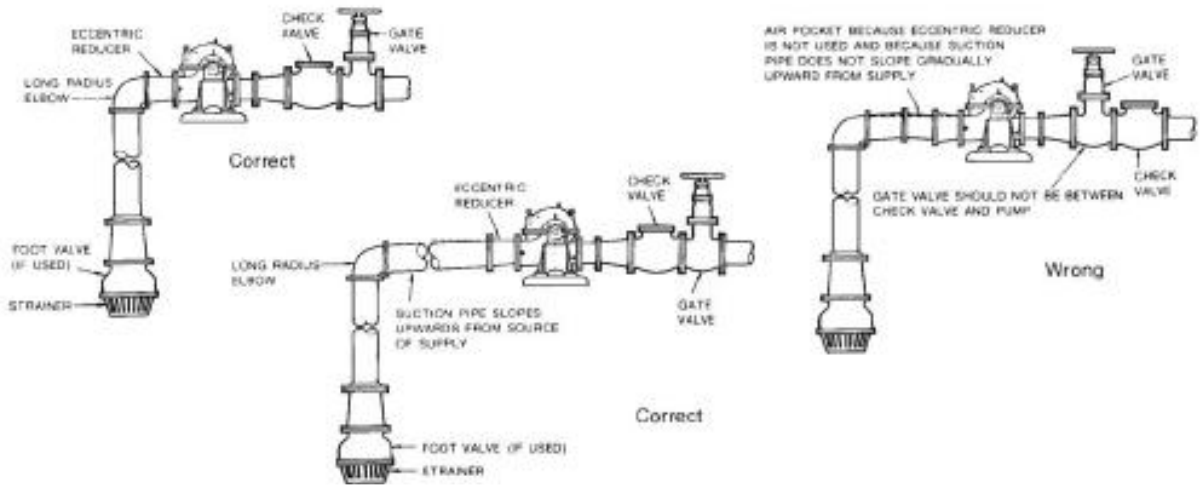

Figure A-5: Reducer selection and piping design (Bloch and Budris 2010)

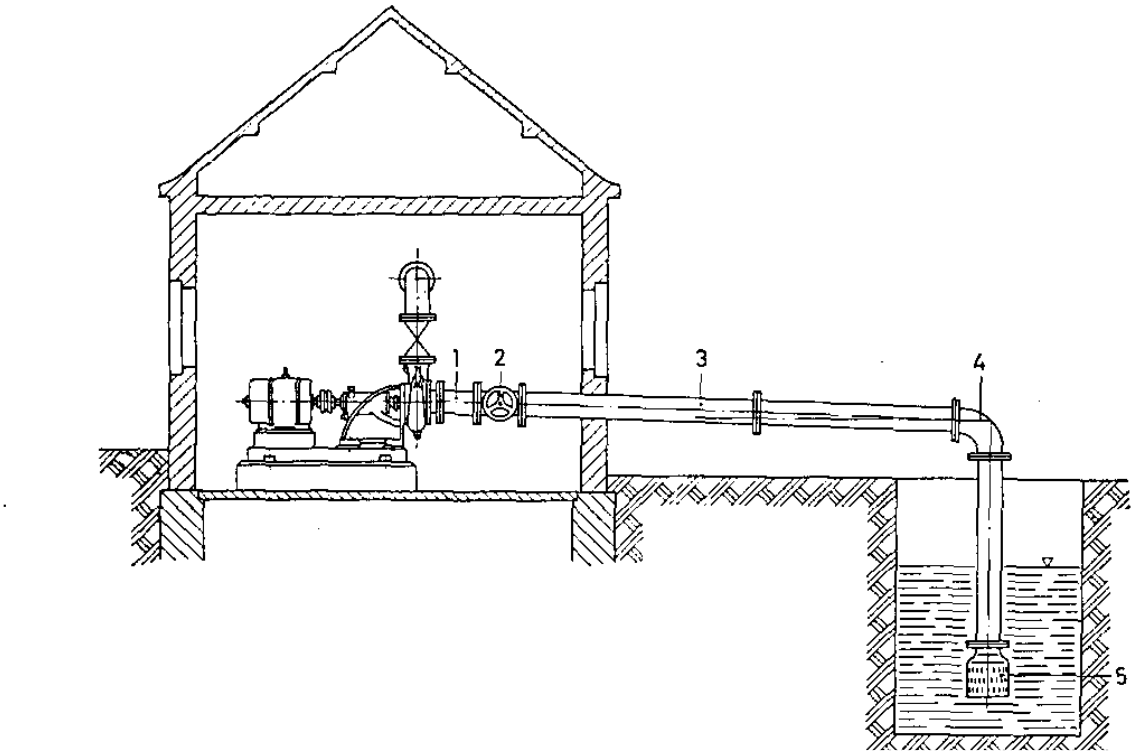

Figure A-6: Reducer selection and piping design (KSB 2012)

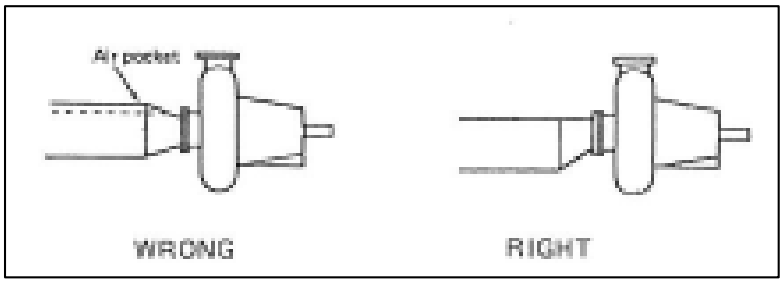

Figure A-7: Reducer Selection (SAPMA 2002)

APPENDIX B

CALCULATIONS

Table B.1: Critical Velocity Comparison Calculation

van Vuuren, van Dijk and Steenkamp						Kalinske and Bliss						Wisener, Mohsen and Kouwen					
DN 200 (Eq 2-4)		DN 600 (Eq 2-4)		DN 900 (Eq 2-4)		DN 200 (Eq 2-2)		DN 600 (Eq 2-2)		DN 900 (Eq 2-2)		DN 200 (Eq 2-3)		DN 600 (Eq 2-3)		DN 900 (Eq 2-3)	
θ (°)	V_c (m/s)	θ (°)	V_c (m/s)	θ (°)	V_c (m/s)	θ (°)	V_c (m/s)	θ (°)	V_c (m/s)	θ (°)	V_c (m/s)	θ (°)	V_c (m/s)	θ (°)	V_c (m/s)	θ (°)	V_c (m/s)
0.5	0.242	0.5	0.403	0.5	0.494	0.5	0.147	0.5	0.245	0.5	0.300	0.5	1.244	0.5	2.075	0.5	2.541
1	0.319	1	0.533	1	0.652	1	0.207	1	0.346	1	0.424	1	1.258	1	2.098	1	2.570
1.5	0.376	1.5	0.627	1.5	0.767	1.5	0.254	1.5	0.424	1.5	0.519	1.5	1.269	1.5	2.116	1.5	2.592
2	0.422	2	0.703	2	0.861	2	0.293	2	0.489	2	0.599	2	1.278	2	2.132	2	2.611
2.5	0.461	2.5	0.769	2.5	0.942	2.5	0.328	2.5	0.547	2.5	0.670	2.5	1.286	2.5	2.145	2.5	2.627
3	0.496	3	0.827	3	1.013	3	0.359	3	0.599	3	0.734	3	1.293	3	2.157	3	2.642
3.5	0.527	3.5	0.880	3.5	1.078	3.5	0.388	3.5	0.647	3.5	0.792	3.5	1.300	3.5	2.169	3.5	2.656
4	0.556	4	0.928	4	1.137	4	0.415	4	0.691	4	0.847	4	1.306	4	2.179	4	2.669
4.5	0.583	4.5	0.973	4.5	1.192	4.5	0.440	4.5	0.733	4.5	0.898	4.5	1.312	4.5	2.189	4.5	2.681
5	0.609	5	1.015	5	1.243	5	0.463	5	0.773	5	0.947	5	1.318	5	2.198	5	2.692
5.5	0.632	5.5	1.055	5.5	1.292	5.5	0.486	5.5	0.811	5.5	0.993	5.5	1.323	5.5	2.207	5.5	2.703
6	0.655	6	1.092	6	1.337	6	0.507	6	0.846	6	1.037	6	1.328	6	2.215	6	2.713
6.5	0.676	6.5	1.128	6.5	1.381	6.5	0.528	6.5	0.881	6.5	1.079	6.5	1.333	6.5	2.223	6.5	2.723
7	0.696	7	1.162	7	1.423	7	0.548	7	0.914	7	1.119	7	1.337	7	2.231	7	2.732
7.5	0.716	7.5	1.194	7.5	1.463	7.5	0.567	7.5	0.946	7.5	1.158	7.5	1.342	7.5	2.238	7.5	2.741
8	0.735	8	1.225	8	1.501	8	0.586	8	0.977	8	1.196	8	1.346	8	2.246	8	2.750
8.5	0.753	8.5	1.256	8.5	1.538	8.5	0.603	8.5	1.007	8.5	1.233	8.5	1.350	8.5	2.253	8.5	2.759
9	0.770	9	1.285	9	1.573	9	0.621	9	1.035	9	1.268	9	1.354	9	2.259	9	2.767
9.5	0.787	9.5	1.313	9.5	1.608	9.5	0.638	9.5	1.064	9.5	1.303	9.5	1.358	9.5	2.266	9.5	2.775
10	0.803	10	1.340	10	1.641	10	0.654	10	1.091	10	1.336	10	1.362	10	2.272	10	2.783
10.5	0.819	10.5	1.366	10.5	1.674	10.5	0.670	10.5	1.118	10.5	1.369	10.5	1.366	10.5	2.278	10.5	2.791
11	0.835	11	1.392	11	1.705	11	0.686	11	1.144	11	1.401	11	1.370	11	2.285	11	2.798
11.5	0.850	11.5	1.417	11.5	1.736	11.5	0.701	11.5	1.169	11.5	1.432	11.5	1.373	11.5	2.290	11.5	2.805

van Vuuren, van Dijk and Steenkamp						Kalinske and Bliss						Wisener, Mohsen and Kouwen					
DN 200 (Eq 2-4)		DN 600 (Eq 2-4)		DN 900 (Eq 2-4)		DN 200 (Eq 2-2)		DN 600 (Eq 2-2)		DN 900 (Eq 2-2)		DN 200 (Eq 2-3)		DN 600 (Eq 2-3)		DN 900 (Eq 2-3)	
12	0.864	12	1.442	12	1.766	12	0.716	12	1.194	12	1.462	12	1.377	12	2.296	12	2.812
12.5	0.879	12.5	1.465	12.5	1.795	12.5	0.730	12.5	1.218	12.5	1.492	12.5	1.380	12.5	2.302	12.5	2.819
13	0.892	13	1.489	13	1.823	13	0.744	13	1.242	13	1.521	13	1.383	13	2.307	13	2.826
13.5	0.906	13.5	1.511	13.5	1.851	13.5	0.758	13.5	1.265	13.5	1.549	13.5	1.387	13.5	2.313	13.5	2.833
14	0.919	14	1.533	14	1.878	14	0.772	14	1.288	14	1.577	14	1.390	14	2.318	14	2.839
14.5	0.932	14.5	1.555	14.5	1.905	14.5	0.785	14.5	1.310	14.5	1.604	14.5	1.393	14.5	2.323	14.5	2.846
15	0.945	15	1.576	15	1.931	15	0.798	15	1.332	15	1.631	15	1.396	15	2.329	15	2.852
15.5	0.958	15.5	1.597	15.5	1.956	15.5	0.811	15.5	1.353	15.5	1.658	15.5	1.399	15.5	2.334	15.5	2.858
16	0.970	16	1.618	16	1.981	16	0.824	16	1.375	16	1.683	16	1.402	16	2.338	16	2.864
16.5	0.982	16.5	1.638	16.5	2.006	16.5	0.836	16.5	1.395	16.5	1.709	16.5	1.405	16.5	2.343	16.5	2.870
17	0.994	17	1.658	17	2.030	17	0.849	17	1.416	17	1.734	17	1.408	17	2.348	17	2.876
17.5	1.005	17.5	1.677	17.5	2.054	17.5	0.861	17.5	1.436	17.5	1.758	17.5	1.410	17.5	2.353	17.5	2.882
18	1.017	18	1.696	18	2.077	18	0.873	18	1.455	18	1.782	18	1.413	18	2.357	18	2.887
18.5	1.028	18.5	1.715	18.5	2.100	18.5	0.884	18.5	1.475	18.5	1.806	18.5	1.416	18.5	2.362	18.5	2.893
19	1.039	19	1.733	19	2.123	19	0.896	19	1.494	19	1.830	19	1.419	19	2.366	19	2.898
19.5	1.050	19.5	1.751	19.5	2.145	19.5	0.907	19.5	1.513	19.5	1.853	19.5	1.421	19.5	2.371	19.5	2.904
20	1.061	20	1.769	20	2.167	20	0.918	20	1.531	20	1.875	20	1.424	20	2.375	20	2.909
20.5	1.071	20.5	1.787	20.5	2.188	20.5	0.929	20.5	1.549	20.5	1.898	20.5	1.426	20.5	2.379	20.5	2.914
21	1.082	21	1.804	21	2.209	21	0.940	21	1.567	21	1.919	21	1.429	21	2.383	21	2.919
21.5	1.092	21.5	1.821	21.5	2.230	21.5	0.950	21.5	1.585	21.5	1.941	21.5	1.431	21.5	2.388	21.5	2.924
22	1.102	22	1.838	22	2.251	22	0.961	22	1.602	22	1.963	22	1.434	22	2.392	22	2.929
22.5	1.112	22.5	1.855	22.5	2.271	22.5	0.971	22.5	1.620	22.5	1.984	22.5	1.436	22.5	2.396	22.5	2.934
23	1.122	23	1.871	23	2.291	23	0.981	23	1.636	23	2.004	23	1.439	23	2.400	23	2.939
23.5	1.131	23.5	1.887	23.5	2.311	23.5	0.991	23.5	1.653	23.5	2.025	23.5	1.441	23.5	2.404	23.5	2.944
24	1.141	24	1.903	24	2.331	24	1.001	24	1.670	24	2.045	24	1.443	24	2.407	24	2.948

van Vuuren, van Dijk and Steenkamp						Kalinske and Bliss						Wisener, Mohsen and Kouwen					
DN 200 (Eq 2-4)		DN 600 (Eq 2-4)		DN 900 (Eq 2-4)		DN 200 (Eq 2-2)		DN 600 (Eq 2-2)		DN 900 (Eq 2-2)		DN 200 (Eq 2-3)		DN 600 (Eq 2-3)		DN 900 (Eq 2-3)	
24.5	1.150	24.5	1.919	24.5	2.350	24.5	1.011	24.5	1.686	24.5	2.065	24.5	1.446	24.5	2.411	24.5	2.953
25	1.160	25	1.935	25	2.369	25	1.020	25	1.702	25	2.084	25	1.448	25	2.415	25	2.958
25.5	1.169	25.5	1.950	25.5	2.388	25.5	1.030	25.5	1.718	25.5	2.104	25.5	1.450	25.5	2.419	25.5	2.962
26	1.178	26	1.965	26	2.407	26	1.039	26	1.733	26	2.123	26	1.452	26	2.422	26	2.967
26.5	1.187	26.5	1.980	26.5	2.425	26.5	1.048	26.5	1.749	26.5	2.142	26.5	1.454	26.5	2.426	26.5	2.971
27	1.196	27	1.995	27	2.443	27	1.058	27	1.764	27	2.160	27	1.456	27	2.429	27	2.975
27.5	1.205	27.5	2.010	27.5	2.462	27.5	1.067	27.5	1.779	27.5	2.179	27.5	1.459	27.5	2.433	27.5	2.980
28	1.214	28	2.024	28	2.479	28	1.075	28	1.794	28	2.197	28	1.461	28	2.436	28	2.984
28.5	1.222	28.5	2.039	28.5	2.497	28.5	1.084	28.5	1.808	28.5	2.215	28.5	1.463	28.5	2.440	28.5	2.988
29	1.231	29	2.053	29	2.514	29	1.093	29	1.823	29	2.233	29	1.465	29	2.443	29	2.992
29.5	1.239	29.5	2.067	29.5	2.532	29.5	1.101	29.5	1.837	29.5	2.250	29.5	1.467	29.5	2.446	29.5	2.996
30	1.248	30	2.081	30	2.549	30	1.110	30	1.851	30	2.267	30	1.469	30	2.450	30	3.000
30.5	1.256	30.5	2.095	30.5	2.566	30.5	1.118	30.5	1.865	30.5	2.284	30.5	1.471	30.5	2.453	30.5	3.004
31	1.264	31	2.109	31	2.583	31	1.126	31	1.879	31	2.301	31	1.473	31	2.456	31	3.008
31.5	1.272	31.5	2.122	31.5	2.599	31.5	1.135	31.5	1.892	31.5	2.318	31.5	1.474	31.5	2.459	31.5	3.012
32	1.280	32	2.136	32	2.616	32	1.143	32	1.906	32	2.334	32	1.476	32	2.463	32	3.016
32.5	1.288	32.5	2.149	32.5	2.632	32.5	1.150	32.5	1.919	32.5	2.350	32.5	1.478	32.5	2.466	32.5	3.020
33	1.296	33	2.162	33	2.648	33	1.158	33	1.932	33	2.366	33	1.480	33	2.469	33	3.023
33.5	1.304	33.5	2.175	33.5	2.664	33.5	1.166	33.5	1.945	33.5	2.382	33.5	1.482	33.5	2.472	33.5	3.027
34	1.312	34	2.188	34	2.680	34	1.174	34	1.958	34	2.398	34	1.484	34	2.475	34	3.031
34.5	1.320	34.5	2.201	34.5	2.696	34.5	1.181	34.5	1.970	34.5	2.413	34.5	1.485	34.5	2.478	34.5	3.034
35	1.327	35	2.214	35	2.711	35	1.189	35	1.983	35	2.428	35	1.487	35	2.481	35	3.038

Table B.2: Reducer Angle Calculation

D1			D2		L	Concentric Reducer (Manufacturers)		Eccentric Reducer (Manufacturers)		Concentric Reducer AWWA C208	Eccentric Reducer AWWA C208
Nominal Diameter (mm) i	Nominal Diameter (mm) ii	Outside Diameter (mm)	Nominal Diameter (mm) i	Nominal Diameter (mm) ii	Reducer Length (mm)	Pipe Slope i°	Pipe Slope ii°	Pipe Slope i°	Pipe Slope ii°	Pipe Slope°	Pipe Slope°
200	200	219.1	102	180	180	18.02	6.20	33.05	12.26	7.13	14.04
250	250	273.1	155	230	205	16.07	6.00	29.95	11.87	7.13	14.04
300	300	323.9	180	280	230	17.37	5.45	32.03	10.81	7.13	14.04
350	350	355.6	230	330	255	13.84	2.87	26.22	5.73	7.13	14.04
400	400	406.4	255	380	280	15.13	2.70	28.40	5.39	7.13	14.04
450	450	457	305	430	305	13.99	2.53	26.49	5.06	7.13	14.04
500	500	508	330	485	330	15.09	2.00	28.34	3.99	7.13	14.04
550	550	559	355	535	355	16.03	1.94	29.88	3.87	7.13	14.04
600	600	610	405	585	380	15.10	1.88	28.35	3.76	7.13	14.04
650	650	660	430	635	405	15.85	1.77	29.59	3.53	7.13	14.04
700	700	711	485	685	430	14.72	1.73	27.73	3.46	7.13	14.04
750	750	762	510	740	460	15.32	1.37	28.72	2.74	7.13	14.04
800	800	813	560	790	485	14.62	1.36	27.55	2.72	7.13	14.04
850	850	864	585	840	510	15.30	1.35	28.68	2.69	7.13	14.04
900	900	914	635	890	535	14.61	1.28	27.54	2.57	7.13	14.04

APPENDIX C

CFD INPUT PARAMETERS

Summary Report: CR 10 Model

Session Summary

Date	Sep 4, 2013 4:59:36 PM
Simulation	F:\RM Working\Final CR 10 Models\CR 10 Model.sim
File size	53 MB
Number of Partitions	1
Number of Restored Partitions	3

Software Summary

Version	BuildArch: win64 BuildEnv: intel12.1 ReleaseDate: Mon Jun 3 13:40:43 UTC 2013 ReleaseNumber: 8.04.007

Hardware Summary

Hosts	Controller: PTAL003494.aurecon.info Number of Workers: 0

Simulation Properties

1 CR 10 Model
+-1 Tags
+-2 Contacts
+-3 Filters
+-4 3D-CAD Models
+-5 Parts

`-1 Solid1	Region	Solid1
	Contacts	[]
	Descriptions	[Ljava.lang.String;@141430f3
	Face count	716
	Index	1
	Tags	[]
	Meta Data	{}
+-1 Surfaces		
+-1 DS End - Pressure Outlet	Tags	[]
	Meta Data	{}
	Boundary	Solid1: DS End - Pressure Outlet
+-2 Fluid Wall	Tags	[]
	Meta Data	{}
	Boundary	Solid1: Fluid Wall
`-3 US End - Velocity Inlet	Tags	[]
	Meta Data	{}
	Boundary	Solid1: US End - Velocity Inlet
`-2 Curves		
`-1 Edges	Tags	[]
	Feature Curve	Solid1:Default Feature Curve

+-6 Operations

+-7 Descriptions	Number of children	1
`-1 Root	Described Parts	[Ljava.lang.String;@67646de5
+-8 Continua	Continua	2
+-1 Mesh 1	Enable Parallel Meshing	false
	Verbose Output	false
	OOC translation	false
	Per-Region Meshing	false

Interpolation Option	Nearest neighbor
Interfaces	[]
Regions	[Solid1]

Models

Generalized Cylinder

Polyhedral Mesher

Enable Mesh Expansion Control	false
Run Optimizer	true
Include Refinement	false
Optimization Cycles	1
Quality Threshold	0.4

Prism Layer Mesher

Stretching Function	Geometric Progression
Stretching Mode	Stretch Factor
Gap Fill Percentage	25.0
Minimum Thickness Percentage	10.0
Layer Reduction Percentage	50.0
Boundary March Angle	50.0
Concave Angle Limit	0.0
Convex Angle Limit	360.0
Near Core Layer Aspect Ratio	0.0
Generate Standard Cells Only	false
Improve Subsurface Quality	true

Surface Remesher

Do curvature refinement	true
Do proximity refinement	true
Do compatibility refinement	false
Retain geometric features	true
Create aligned meshes	true
Minimum Face Quality	0.05
Enable automatic surface repair	true

Reference Values

Base Size	
Value	0.0050 m
Automatic Surface Repair	
Connected surface count limit	None
Connected surface size limits	None
Minimum Proximity	
Minimum Proximity	0.05
Minimum Quality	
Minimum Quality	0.01
CAD Projection	
Project to CAD	true
Number of Prism Layers	
Number of Prism Layers	10
Prism Layer Stretching	
Prism Layer Stretching	1.5
Prism Layer Thickness	
Size type	Relative to base
Relative Size	
Percentage of Base	33.3
Absolute Size	0.0016649999999999998 m
Surface Curvature	
Enable curvature deviation distance	false
Basic Curvature	
# Pts/circle	36.0
Surface Growth Rate	
Surface Growth Rate	1.3
Surface Proximity	
# Points in gap	2.0
Enable Search Ceiling	false
Search Floor	0.0 m
Surface Size	
Relative/Absolute	Relative to base
Size Method	Min and Target
Relative Minimum Size	
Percentage of Base	25.0
Absolute Size	0.00125 m
Relative Target Size	
Percentage of Base	100.0
Absolute Size	0.0050 m
Tet/Poly Density	
Density	1.0
Growth Factor	1.0
Tet/Poly Volume Blending	
Blending Factor	1.0

Volumetric Controls

Physics 1

Interfaces	[]

	Regions	[Solid1]
+-1 Models		
| +-1 Constant Density		
| +-2 Gradients	Verbose	false
| |	Gradient Method	Hybrid Gauss-LSQ
| |	Limiter Method	Venkatakrishnan
| |	Least-Squares Quality Criterion	true
| |	Flat Cells Curvature Criterion	true
| |	Cell Skewness Criterion	true
| |	Chevron-Cell Criterion	true
| |	Least-Squares Tensor Minimum Eigenvalues Ratio	0.1
| |	Normalized Flat Cells Curvature Factor	1.0
| |	Maximum safe (positive) skewness angle (deg.)	75.0
| |	Minimum unsafe (positive) skewness angle (deg.)	88.0
| |	Use TVB Gradient Limiting	false
| |	Acceptable Field Variation (Factor)	0.05
| +-3 K-Epsilon Turbulence		
| +-4 Liquid		
| | `-1 H2O	Database Material	H2O (Water) [Standard/Liquids]
| | `-1 Material Properties		
| | +-1 Density	Method	Constant
| | | `-1 Constant	Value	997.561 kg/m^3
| | `-2 Dynamic Viscosity	Method	Constant
| | `-1 Constant	Value	8.8871E-4 Pa-s
| +-5 Realizable K-Epsilon Two-Layer	Two-Layer Type	Shear Driven (Wolfstein)
| |	Normal Stress Term	false
| |	Two-Layer ReY*	60.0
| |	Two-Layer Delta ReY	10.0
| |	Secondary Gradients	On
| |	Convection	2nd-order
| |	Buoyancy Production of Dissipation	Boundary Layer Orientation
| |	Cmu	0.09
| |	C1e	1.44
| |	C2e	1.9
| |	Ct	1.0
| |	Sigma_k	1.0
| |	Sigma_e	1.2
| |	Sarkar	2.0
| |	Tke Minimum	1.0E-10
| |	Tdr Minimum	1.0E-10
| +-6 Reynolds-Averaged Navier-Stokes		
| +-7 Segregated Flow	Minimum Absolute Pressure	1000.0 Pa
| |	Flow Boundary Diffusion	true
| |	Secondary Gradients	On
| |	Convection	2nd-order
| |	Delta-V Dissipation	Off
| +-8 Steady		
| +-9 Three Dimensional		
| +-10 Turbulent		
| `-11 Two-Layer All y+ Wall Treatment	Iterative Ustar	false
+-2 Reference Values		
| +-1 Minimum Allowable Wall	Value	1.0E-6 m

Distance		
| | `-2 Reference Pressure	Value	101325.0 Pa
| `-3 Initial Conditions		
| +-1 Pressure	Method	Constant
| | `-1 Constant	Value	150000.0 Pa
| +-2 Turbulence Intensity	Method	Constant
| | `-1 Constant	Value	0.01
| +-3 Turbulence Specification	Method	Intensity + Viscosity Ratio
| +-4 Turbulent Velocity Scale	Method	Constant
| | `-1 Constant	Value	1.0 m/s
| +-5 Turbulent Viscosity Ratio	Method	Constant
| | `-1 Constant	Value	10.0
| `-6 Velocity	Coordinate System	Laboratory
| |	Method	Constant
| `-1 Constant	Value	[0.0, 0.0, -1.5] m/s
+-9 Regions	Regions	1
| `-1 Solid1	Index	0
| |	Physics Continuum	Physics 1
| |	Type	Fluid Region
| |	Mesh Continuum	Mesh 1
| |	Parts	[Solid1]
| +-1 Boundaries	Boundaries	3
| | +-1 DS End - Pressure Outlet	Index	3
| | | |	Type	Pressure Outlet
| | | |	Interfaces	
| | | |	Part Surfaces	[Solid1.DS End - Pressure Outlet]
| | | +-1 Mesh Conditions		
| | | | +-1 Custom Surface Curvature	Custom curvature	Use Continuum Values
| | | | +-2 Custom Surface Proximity	Custom proximity	Use Continuum Values
| | | | +-3 Custom Surface Size	Custom surface size	Disabled
| | | | +-4 Customize Prism Mesh	Customize Prism Mesh	Use Default Values
| | | | +-5 Customize Surface Remeshing	Disable surface remeshing	Disabled
| | | | `-6 Generalized Cylinder Extrusion Type	Extrusion law	None
| | | +-2 Physics Conditions		
| | | | +-1 Backflow Direction Specification	Method	Boundary-Normal
| | | | +-2 Pressure Jump Option	Option	None
| | | | +-3 Pressure Specification	Pressure specification	Environmental
| | | | +-4 Target Mass Flow Option	Target Mass Flow Option	Disabled
| | | | `-5 Turbulence Specification	Method	Intensity + Viscosity Ratio
| | | `-3 Physics Values		
| | | +-1 Pressure	Method	Constant
| | | | `-1 Constant	Value	150000.0 Pa
| | | +-2 Turbulence Intensity	Method	Constant
| | | | `-1 Constant	Value	0.01
| | | `-3 Turbulent Viscosity Ratio	Method	Constant
| | | `-1 Constant	Value	10.0
| | +-2 Fluid Wall	Index	1
| | | |	Type	Wall
| | | |	Interfaces	
| | | |	Part Surfaces	[Solid1.Fluid Wall]
| | | +-1 Mesh Conditions		

| | | | +-1 Custom Surface Curvature	Custom curvature	Use Continuum Values
| | | | +-2 Custom Surface Proximity	Custom proximity	Use Continuum Values
| | | | +-3 Custom Surface Size	Custom surface size	Disabled
| | | | +-4 Customize Prism Mesh	Customize Prism Mesh	Use Default Values
| | | | +-5 Customize Surface Remeshing	Disable surface remeshing	Disabled
| | | | `-6 Generalized Cylinder Extrusion Type	Extrusion law	Constant
| | | +-2 Mesh Values		
| | | | `-1 Generalized Cylinder Parameters	Number of Layers	70
| | | +-3 Physics Conditions		
| | | | +-1 Shear Stress Specification	Method	No-Slip
| | | | +-2 Tangential Velocity Specification	Method	None
| | | | |	Reference Frame	Relative To Mesh
| | | | `-3 Wall Surface Specification	Method	Rough
| | | `-4 Physics Values		
| | | +-1 Blended Wall Function	E	9.0
| | | |	Kappa	0.42
| | | +-2 Roughness Height	Method	Constant
| | | | `-1 Constant	Value	6.0E-5 m
| | | `-3 Wall Roughness Parameters	B	0.0
| | |	C	0.253
| | |	RplusSmooth	2.25
| | |	RplusRough	90.0
| | |	Roughness Limiter	true
| | `-3 US End - Velocity Inlet	Index	2
| | |	Type	Velocity Inlet
| | |	Interfaces	
| | |	Part Surfaces	[Solid1.US End - Velocity Inlet]
| | +-1 Mesh Conditions		
| | | +-1 Custom Surface Curvature	Custom curvature	Use Continuum Values
| | | +-2 Custom Surface Proximity	Custom proximity	Use Continuum Values
| | | +-3 Custom Surface Size	Custom surface size	Disabled
| | | +-4 Customize Prism Mesh	Customize Prism Mesh	Use Default Values
| | | +-5 Customize Surface Remeshing	Disable surface remeshing	Disabled
| | | `-6 Generalized Cylinder Extrusion Type	Extrusion law	None
| | +-2 Physics Conditions		
| | | +-1 Flow Direction Specification	Method	Boundary-Normal
| | | +-2 Reference Frame Specification	Option	Lab Frame
| | | +-3 Turbulence Specification	Method	Intensity + Viscosity Ratio
| | | `-4 Velocity Specification	Method	Magnitude + Direction
| | `-3 Physics Values		
| | +-1 Turbulence Intensity	Method	Constant
| | | `-1 Constant	Value	0.01
| | +-2 Turbulent Viscosity Ratio	Method	Constant

| | | `-1 Constant	Value	10.0
| | `-3 Velocity Magnitude	Method	Constant
| | `-1 Constant	Value	1.5 m/s
| +-2 Feature Curves	Feature Curves	1
| | `-1 Default Feature Curve	Part Curves	[Solid1.Edges]
| | `-1 Mesh Conditions		
| | `-1 Custom Surface Size	Custom surface size	Disabled
| +-3 Mesh Conditions		
| | +-1 Customize Prism Mesh	Customize Prism Mesh	Use Default Values
| | `-2 Customize Tet/Poly Density	Customize Tet/Poly Density	Disabled
| +-4 Physics Conditions		
| | +-1 Initial Condition Option	Option	Use Continuum Values
| | +-2 Mass Source Option	Mass Source Option	Disabled
| | +-3 Momentum Source Option	Momentum Source Option	None
| | `-4 Turbulence Source Option	Turbulence Source Option	None
| `-5 Physics Values		
| +-1 Axis	Direction	[0.0, 0.0, 1.0]
| |	Coordinate System	Laboratory
| |	Origin	[0.0, 0.0, 0.0] m
| `-2 Motion Specification	Motion	Stationary
|	Reference Frame	Lab Reference Frame
+-10 Derived Parts	Derived Parts	4
| +-1 plane section	Coordinate System	Laboratory
| | |	Origin	[0.0, 0.0, 0.0] m,m,m
| | |	Normal	[1.0, 0.0, 0.0] m,m,m
| | |	Section Mode	Single Section
| | |	Displayed Index	-1
| | |	Parts	[Solid1]
| | `-1 Single section	Offset	0.0 m
| +-2 plane section 2	Coordinate System	Laboratory
| | |	Origin	[0.0, 0.0, 0.0] m,m,m
| | |	Normal	[0.0, 0.0, 1.0] m,m,m
| | |	Section Mode	Single Section
| | |	Displayed Index	-1
| | |	Parts	[Solid1]
| | `-1 Single section	Offset	0.0 m
| +-3 X Axis line-probe	CoordinateSystem	Laboratory
| |	Point 1	[-0.07805, 0.07805, 0.0] m,m,m
| |	Point 2	[0.07805, 0.07805, 0.0] m,m,m
| |	Resolution	100
| |	Parts	[Solid1]
| `-4 Y Axis line-probe 2	CoordinateSystem	Laboratory
|	Point 1	[0.0, 0.0, 0.0] m,m,m
|	Point 2	[0.0, 0.1561, 0.0] m,m,m
|	Resolution	100
|	Parts	[Solid1]
+-11 Solvers		
| +-1 Partitioning	Partitioning method	Per-Region
| |	Solver Frozen	false
| +-2 Wall Distance	Verbosity	0
| |	Parallel memory optimization scaling factor	1.0
| |	Solver Frozen	false
| +-3 Segregated Flow	Reconstruction Frozen	false
| | |	Reconstruction Zeroed	false
| | |	Temporary Storage Retained	false
| | |	Solver Frozen	false

+-1 Velocity	Under-Relaxation Factor	0.7
+-1 Under-Relaxation Factor Ramp	Ramp Method	No Ramp
`-2 AMG Linear Solver	Verbosity	None
	Max Cycles	30
	Parallel Migration Limit	25
	Subdomain coarsening enabled	true
	Enable direct-solver	false
	Maximum direct-solver equations	32
	Convergence Tolerance	0.1
	Epsilon	0.0
	Cycle Type	Flex Cycle
	Group Size Control	Auto
	Group Size	4
	Relaxation Scheme	Gauss-Seidel
	Acceleration method	None
	Scaling	Disabled
`-1 Flex Cycle	Restriction Tolerance	0.9
	Prolongation Tolerance	0.5
	Sweeps	1
`-2 Pressure	Under-Relaxation Factor	0.3
	Pressure Reference Location	Automatic Selection
+-1 Under-Relaxation Factor Ramp	Ramp Method	No Ramp
`-2 AMG Linear Solver	Verbosity	None
	Max Cycles	30
	Parallel Migration Limit	25
	Subdomain coarsening enabled	true
	Enable direct-solver	false
	Maximum direct-solver equations	32
	Convergence Tolerance	0.1
	Epsilon	0.0
	Cycle Type	V Cycle
	Group Size Control	Auto
	Group Size	4
	Relaxation Scheme	Gauss-Seidel
	Acceleration method	Conjugate Gradient
	Scaling	Auto
`-1 V Cycle	Pre-Sweeps	1
	Post-Sweeps	1
	Max Levels	50
+-4 K-Epsilon Turbulence	Under-Relaxation Factor	0.8
	Reconstruction Frozen	false
	Reconstruction Zeroed	false
	Temporary Storage Retained	false
	Solver Frozen	false
+-1 Under-Relaxation Factor Ramp	Ramp Method	No Ramp
`-2 AMG Linear Solver	Verbosity	None
	Max Cycles	30
	Parallel Migration Limit	25
	Subdomain coarsening enabled	true
	Enable direct-solver	false
	Maximum direct-solver equations	32
	Convergence Tolerance	0.1
	Epsilon	0.0
	Cycle Type	Flex Cycle
	Group Size Control	Auto

Group Size	4
Relaxation Scheme	Gauss-Seidel
Acceleration method	None
Scaling	Disabled
Restriction Tolerance	0.9
Prolongation Tolerance	0.5
Sweeps	1
Under-Relaxation Factor	1.0
Maximum Ratio	100000.0
Solver Frozen	false

+-12 Stopping Criteria

Maximum Steps	1000
Enabled	true
Criterion Satisfied	true
Logical Rule	Or
Stop Inner Iterations	true
Path	ABORT
Enabled	true
Criterion Satisfied	false
Logical Rule	Or

+-13 Solution Histories

+-14 Solution Views

Solution Time	0.0
Iteration	1000
Time Step	0

+-15 Reports

Reports	0

+-16 Monitors

Monitors	8
Monitors To Print	[Continuity, X-momentum, Y-momentum, Z-momentum, Tke, Tdr]
Output Direction	Horizontal
Heading Print Frequency	10
Maximum Plot Samples	5000
Maximum Plot Samples	5000

+-17 Representations

+-1 Geometry

+-2 Initial Surface

Faces	716
Edges	366

`-1 Regions

`-1 Solid1

Faces	716
Edges	366

+-1 Boundaries

Faces	88
Faces	540
Faces	88

+-1 DS End - Pressure Outlet

+-2 Fluid Wall

`-3 US End - Velocity Inlet

`-2 Feature Curves

Edges	366

`-1 Default Feature Curve

+-3 Remeshed Surface

Faces	82760
Edges	1116

`-1 Regions

`-1 Solid1

Faces	82760
Edges	1116

+-1 Boundaries

Faces	1856
Faces	77178
Faces	3726

+-1 DS End - Pressure Outlet

+-2 Fluid Wall

`-3 US End - Velocity Inlet

| | `-2 Feature Curves		
| | `-1 Default Feature Curve	Edges	1116
| `-4 Volume Mesh	Cells	223468
| |	Interior Faces	790365
| |	Vertices	361128
| +-1 Finite Volume Regions		
| | `-1 Solid1	Cells	223468
| | |	Interior Faces	790365
| | |	Vertices	361128
| | `-1 Finite Volume Boundaries		
| | +-1 DS End - Pressure Outlet	Faces	2733
| | +-2 Fluid Wall	Faces	9156
| | `-3 US End - Velocity Inlet	Faces	3723
| `-2 Cell Sets		
+-18 Tables	Tables	0
+-19 Units	Preferred System	Systeme Internationale
+-20 Coordinate Systems		
| `-1 Laboratory		
| `-1 Local Coordinate Systems		
+-21 Field Functions		
+-22 Volume Shapes		
+-23 Update Events	Event Count	0
|	Event Names	
+-24 Data Set Functions	Data Directory	function_data
+-25 User Code		
+-26 Layouts		
| `-1 default		
+-27 Data Mappers		
+-28 Motions		
| `-1 Stationary		
+-29 Reference Frames		
| `-1 Lab Reference Frame		

Solution

Accumulated CPU Time over all processes (s)	1438.7889999999932
Elapsed Time (s)	479.56807000000845
Iterations	1000

Summary Report: CR 10 - Attempt 2

Session Summary

Date	Sep 4, 2013 5:00:51 PM
Simulation	F:\RM Working\Final CR 10 Models\CR 10 - Attempt 2.sim
File size	2.5e+02 MB
Number of Partitions	1
Number of Restored Partitions	3

Software Summary

Version	BuildArch: win64 BuildEnv: intel12.1 ReleaseDate: Mon Jun 3 13:40:43 UTC 2013 ReleaseNumber: 8.04.007

Hardware Summary

Hosts	Controller: PTAL003494.aurecon.info Number of Workers: 0

Simulation Properties

1 **CR 10 - Attempt 2**
+-1 Tags
+-2 Contacts
+-3 Filters
+-4 3D-CAD Models
+-5 Parts

`-1 **Solid1**

Region	Solid1
Contacts	[]
Descriptions	[Ljava.lang.String;@6189076
Face count	716
Index	1
Tags	[]
Meta Data	{}

+-1 Surfaces

+-1 **DS End - Pressure Outlet**

Tags	[]
Meta Data	{}
Boundary	Solid1: DS End - Pressure Outlet

+-2 **Fluid Wall**

Tags	[]
Meta Data	{}
Boundary	Solid1: Fluid Wall

`-3 **US End - Velocity Inlet**

Tags	[]
Meta Data	{}
Boundary	Solid1: US End - Velocity Inlet

`-2 Curves

`-1 **Edges**

Tags	[]
Feature Curve	Solid1:Default Feature Curve

+-6 Operations
+-7 Descriptions

`-1 Root

Number of children	1
Described Parts	[Ljava.lang.String;@b920c51

+-8 Continua

+-1 **Mesh 1**

Continua	2
Enable Parallel Meshing	false
Verbose Output	false
OOC translation	false
Per-Region Meshing	false

Interpolation Option	Nearest neighbor
Interfaces	[]
Regions	[Solid1]

+-1 Models

+-1 Polyhedral Mesher

Enable Mesh Expansion Control	false
Run Optimizer	true
Include Refinement	false
Optimization Cycles	1
Quality Threshold	0.4

+-2 Prism Layer Mesher

Stretching Function	Geometric Progression
Stretching Mode	Stretch Factor
Gap Fill Percentage	25.0
Minimum Thickness Percentage	10.0
Layer Reduction Percentage	50.0
Boundary March Angle	50.0
Concave Angle Limit	0.0
Convex Angle Limit	360.0
Near Core Layer Aspect Ratio	0.0
Generate Standard Cells Only	false
Improve Subsurface Quality	true

`-3 Surface Remesher

Do curvature refinement	true
Do proximity refinement	true
Do compatibility refinement	false
Retain geometric features	true
Create aligned meshes	true
Minimum Face Quality	0.05
Enable automatic surface repair	true

+-2 Reference Values

+-1 Base Size

Value	0.0050 m

+-2 Automatic Surface Repair

Connected surface count limit	None
Connected surface size limits	None

+-1 Minimum Proximity

Minimum Proximity	0.05

`-2 Minimum Quality

Minimum Quality	0.01

+-3 CAD Projection

Project to CAD	true

+-4 Number of Prism Layers

Number of Prism Layers	10

+-5 Prism Layer Stretching

Prism Layer Stretching	1.5

+-6 Prism Layer Thickness

Size type	Relative to base

`-1 Relative Size

Percentage of Base	33.3
Absolute Size	0.0016649999999999998 m

+-7 Surface Curvature

Enable curvature deviation distance	false

`-1 Basic Curvature

# Pts/circle	36.0

+-8 Surface Growth Rate

Surface Growth Rate	1.3

+-9 Surface Proximity

# Points in gap	2.0
Enable Search Ceiling	false
Search Floor	0.0 m

+-10 Surface Size

Relative/Absolute	Relative to base
Size Method	Min and Target

+-1 Relative Minimum Size

Percentage of Base	25.0
Absolute Size	0.00125 m

`-2 Relative Target Size

Percentage of Base	100.0
Absolute Size	0.0050 m

+-11 Tet/Poly Density

Density	1.0
Growth Factor	1.0

`-12 Tet/Poly Volume Blending

Blending Factor	1.0

`-3 Volumetric Controls

`-2 **Physics 1**

Interfaces	[]
Regions	[Solid1]

+-1 Models	
| +-1 Constant Density	
| +-2 Gradients	
| |	Verbose: false
| |	Gradient Method: Hybrid Gauss-LSQ
| |	Limiter Method: Venkatakrishnan
| |	Least-Squares Quality Criterion: true
| |	Flat Cells Curvature Criterion: true
| |	Cell Skewness Criterion: true
| |	Chevron-Cell Criterion: true
| |	Least-Squares Tensor Minimum Eigenvalues Ratio: 0.1
| |	Normalized Flat Cells Curvature Factor: 1.0
| |	Maximum safe (positive) skewness angle (deg.): 75.0
| |	Minimum unsafe (positive) skewness angle (deg.): 88.0
| |	Use TVB Gradient Limiting: false
| |	Acceptable Field Variation (Factor): 0.05
| +-3 K-Epsilon Turbulence	
| +-4 Liquid	
| | `-1 **H2O**	Database Material: H2O (Water) [Standard/Liquids]
| | | `-1 Material Properties	
| | | +-1 Density	Method: Constant
| | | | `-1 Constant	Value: 997.561 kg/m^3
| | | `-2 Dynamic Viscosity	Method: Constant
| | | `-1 Constant	Value: 8.8871E-4 Pa-s
| +-5 Realizable K-Epsilon Two-Layer	Two-Layer Type: Shear Driven (Wolfstein)
| |	Normal Stress Term: false
| |	Two-Layer ReY*: 60.0
| |	Two-Layer Delta ReY: 10.0
| |	Secondary Gradients: On
| |	Convection: 2nd-order
| |	Buoyancy Production of Dissipation: Boundary Layer Orientation
| |	Cmu: 0.09
| |	C1e: 1.44
| |	C2e: 1.9
| |	Ct: 1.0
| |	Sigma_k: 1.0
| |	Sigma_e: 1.2
| |	Sarkar: 2.0
| |	Tke Minimum: 1.0E-10
| |	Tdr Minimum: 1.0E-10
| +-6 Reynolds-Averaged Navier-Stokes	
| +-7 Segregated Flow	Minimum Absolute Pressure: 1000.0 Pa
| |	Flow Boundary Diffusion: true
| |	Secondary Gradients: On
| |	Convection: 2nd-order
| |	Delta-V Dissipation: Off
| +-8 Steady	
| +-9 Three Dimensional	
| +-10 Turbulent	
| `-11 Two-Layer All y+ Wall Treatment	Iterative Ustar: false
+-2 Reference Values	
| +-1 Minimum Allowable Wall Distance	Value: 1.0E-6 m

`-2 Reference Pressure	Value	101325.0 Pa
`-3 Initial Conditions		
+-1 Pressure	Method	Constant
`-1 Constant	Value	150000.0 Pa
+-2 Turbulence Intensity	Method	Constant
`-1 Constant	Value	0.01
+-3 Turbulence Specification	Method	Intensity + Viscosity Ratio
+-4 Turbulent Velocity Scale	Method	Constant
`-1 Constant	Value	1.0 m/s
+-5 Turbulent Viscosity Ratio	Method	Constant
`-1 Constant	Value	10.0
`-6 Velocity	Coordinate System	Laboratory
	Method	Constant
`-1 Constant	Value	[0.0, 0.0, -1.5] m/s
+-9 Regions	Regions	1
`-1 **Solid1**	Index	0
	Physics Continuum	Physics 1
	Type	Fluid Region
	Mesh Continuum	Mesh 1
	Parts	[Solid1]
+-1 Boundaries	Boundaries	3
+-1 **DS End - Pressure Outlet**	Index	3
	Type	Pressure Outlet
	Interfaces	
	Part Surfaces	[Solid1.DS End - Pressure Outlet]
+-1 Mesh Conditions		
+-1 Custom Surface Curvature	Custom curvature	Use Continuum Values
+-2 Custom Surface Proximity	Custom proximity	Use Continuum Values
+-3 Custom Surface Size	Custom surface size	Disabled
+-4 Customize Prism Mesh	Customize Prism Mesh	Use Default Values
`-5 Customize Surface Remeshing	Disable surface remeshing	Disabled
+-2 Physics Conditions		
+-1 Backflow Direction Specification	Method	Boundary-Normal
+-2 Pressure Jump Option	Option	None
+-3 Pressure Specification	Pressure specification	Environmental
+-4 Target Mass Flow Option	Target Mass Flow Option	Disabled
`-5 Turbulence Specification	Method	Intensity + Viscosity Ratio
`-3 Physics Values		
+-1 Pressure	Method	Constant
`-1 Constant	Value	150000.0 Pa
+-2 Turbulence Intensity	Method	Constant
`-1 Constant	Value	0.01
`-3 Turbulent Viscosity Ratio	Method	Constant
`-1 Constant	Value	10.0
+-2 **Fluid Wall**	Index	1
	Type	Wall
	Interfaces	
	Part Surfaces	[Solid1.Fluid Wall]
+-1 Mesh Conditions		
+-1 Custom Surface Curvature	Custom curvature	Use Continuum Values
+-2 Custom Surface	Custom proximity	Use Continuum Values

Proximity		
+-3 Custom Surface Size	Custom surface size	Disabled
+-4 Customize Prism Mesh	Customize Prism Mesh	Use Default Values
`-5 Customize Surface Remeshing	Disable surface remeshing	Disabled
+-2 Physics Conditions		
+-1 Shear Stress Specification	Method	No-Slip
+-2 Tangential Velocity Specification	Method	None
	Reference Frame	Relative To Mesh
`-3 Wall Surface Specification	Method	Rough
`-3 Physics Values		
+-1 Blended Wall Function	E	9.0
	Kappa	0.42
+-2 Roughness Height	Method	Constant
`-1 Constant	Value	6.0E-5 m
`-3 Wall Roughness Parameters	B	0.0
	C	0.253
	RplusSmooth	2.25
	RplusRough	90.0
	Roughness Limiter	true
`-3 **US End - Velocity Inlet**	Index	2
	Type	Velocity Inlet
	Interfaces	
	Part Surfaces	[Solid1.US End - Velocity Inlet]
+-1 Mesh Conditions		
+-1 Custom Surface Curvature	Custom curvature	Use Continuum Values
+-2 Custom Surface Proximity	Custom proximity	Use Continuum Values
+-3 Custom Surface Size	Custom surface size	Disabled
+-4 Customize Prism Mesh	Customize Prism Mesh	Use Default Values
`-5 Customize Surface Remeshing	Disable surface remeshing	Disabled
+-2 Physics Conditions		
+-1 Flow Direction Specification	Method	Boundary-Normal
+-2 Reference Frame Specification	Option	Lab Frame
+-3 Turbulence Specification	Method	Intensity + Viscosity Ratio
`-4 Velocity Specification	Method	Magnitude + Direction
`-3 Physics Values		
+-1 Turbulence Intensity	Method	Constant
`-1 Constant	Value	0.01
+-2 Turbulent Viscosity Ratio	Method	Constant
`-1 Constant	Value	10.0
`-3 Velocity Magnitude	Method	Constant
`-1 Constant	Value	1.5 m/s
+-2 Feature Curves	Feature Curves	1
`-1 **Default Feature Curve**	Part Curves	[Solid1.Edges]
`-1 Mesh Conditions		
`-1 Custom Surface Size	Custom surface size	Disabled
+-3 Mesh Conditions		
+-1 Customize Prism Mesh	Customize Prism Mesh	Use Default Values

`-2 Customize Tet/Poly Density	Customize Tet/Poly Density: Disabled
+-4 Physics Conditions	
+-1 Initial Condition Option	Option: Use Continuum Values
+-2 Mass Source Option	Mass Source Option: Disabled
+-3 Momentum Source Option	Momentum Source Option: None
`-4 Turbulence Source Option	Turbulence Source Option: None
`-5 Physics Values	
+-1 Axis	Direction: [0.0, 0.0, 1.0]
	Coordinate System: Laboratory
	Origin: [0.0, 0.0, 0.0] m
`-2 Motion Specification	Motion: Stationary
	Reference Frame: Lab Reference Frame
+-10 Derived Parts	Derived Parts: 4
+-1 **plane section**	Coordinate System: Laboratory
	Origin: [0.0, 0.0, 0.0] m,m,m
	Normal: [1.0, 0.0, 0.0] m,m,m
	Section Mode: Single Section
	Displayed Index: -1
	Parts: [Solid1]
`-1 Single section	Offset: 0.0 m
+-2 **plane section 2**	Coordinate System: Laboratory
	Origin: [0.0, 0.0, 0.0] m,m,m
	Normal: [0.0, 0.0, 1.0] m,m,m
	Section Mode: Single Section
	Displayed Index: -1
	Parts: [Solid1]
`-1 Single section	Offset: 0.0 m
+-3 **X Axis line-probe**	CoordinateSystem: Laboratory
	Point 1: [-0.07805, 0.07805, 0.0] m,m,m
	Point 2: [0.07805, 0.07805, 0.0] m,m,m
	Resolution: 100
	Parts: [Solid1]
`-4 **Y Axis line-probe 2**	CoordinateSystem: Laboratory
	Point 1: [0.0, 0.0, 0.0] m,m,m
	Point 2: [0.0, 0.1561, 0.0] m,m,m
	Resolution: 100
	Parts: [Solid1]
+-11 Solvers	
+-1 Partitioning	Partitioning method: Per-Region
	Solver Frozen: false
+-2 Wall Distance	Verbosity: 0
	Parallel memory optimization scaling factor: 1.0
	Solver Frozen: false
+-3 Segregated Flow	Reconstruction Frozen: false
	Reconstruction Zeroed: false
	Temporary Storage Retained: false
	Solver Frozen: false
+-1 Velocity	Under-Relaxation Factor: 0.7
+-1 Under-Relaxation Factor Ramp	Ramp Method: No Ramp
`-2 AMG Linear Solver	Verbosity: None
	Max Cycles: 30
	Parallel Migration Limit: 25
	Subdomain coarsening enabled: true
	Enable direct-solver: false
	Maximum direct-solver equations: 32

Convergence Tolerance	0.1
Epsilon	0.0
Cycle Type	Flex Cycle
Group Size Control	Auto
Group Size	4
Relaxation Scheme	Gauss-Seidel
Acceleration method	None
Scaling	Disabled
Restriction Tolerance	0.9
Prolongation Tolerance	0.5
Sweeps	1
Under-Relaxation Factor	0.3
Pressure Reference Location	Automatic Selection
Ramp Method	No Ramp
Verbosity	None
Max Cycles	30
Parallel Migration Limit	25
Subdomain coarsening enabled	true
Enable direct-solver	false
Maximum direct-solver equations	32
Convergence Tolerance	0.1
Epsilon	0.0
Cycle Type	V Cycle
Group Size Control	Auto
Group Size	4
Relaxation Scheme	Gauss-Seidel
Acceleration method	Conjugate Gradient
Scaling	Auto
Pre-Sweeps	1
Post-Sweeps	1
Max Levels	50
Under-Relaxation Factor	0.8
Reconstruction Frozen	false
Reconstruction Zeroed	false
Temporary Storage Retained	false
Solver Frozen	false
Ramp Method	No Ramp
Verbosity	None
Max Cycles	30
Parallel Migration Limit	25
Subdomain coarsening enabled	true
Enable direct-solver	false
Maximum direct-solver equations	32
Convergence Tolerance	0.1
Epsilon	0.0
Cycle Type	Flex Cycle
Group Size Control	Auto
Group Size	4
Relaxation Scheme	Gauss-Seidel
Acceleration method	None
Scaling	Disabled
Restriction Tolerance	0.9
Prolongation Tolerance	0.5
Sweeps	1
Under-Relaxation Factor	1.0
Maximum Ratio	100000.0

	Solver Frozen	false
+-12 Stopping Criteria		
| +-1 **Maximum Steps**	Maximum Steps	1000
| |	Enabled	true
| |	Criterion Satisfied	true
| |	Logical Rule	Or
| `-2 **Stop File**	Stop Inner Iterations	true
|	Path	ABORT
|	Enabled	true
|	Criterion Satisfied	false
|	Logical Rule	Or
+-13 Solution Histories		
+-14 Solution Views		
| `-1 **Current Solution**	Solution Time	0.0
|	Iteration	1000
|	Time Step	0
+-15 Reports	Reports	0
+-16 Monitors	Monitors	8
| |	Monitors To Print	[Continuity, X-momentum, Y-momentum, Z-momentum, Tke, Tdr]
| |	Output Direction	Horizontal
| |	Heading Print Frequency	10
| +-1 **Iteration**	Maximum Plot Samples	5000
| +-2 **Physical Time**	Maximum Plot Samples	5000
+-17 Representations		
| +-1 **Geometry**		
| +-2 **Initial Surface**	Faces	716
| | |	Edges	366
| | `-1 Regions		
| | `-1 Solid1	Faces	716
| | |	Edges	366
| | +-1 Boundaries		
| | | +-1 DS End - Pressure Outlet	Faces	88
| | | +-2 Fluid Wall	Faces	540
| | | `-3 US End - Velocity Inlet	Faces	88
| | `-2 Feature Curves		
| | `-1 Default Feature Curve	Edges	366
| +-3 **Remeshed Surface**	Faces	82760
| | |	Edges	1116
| | `-1 Regions		
| | `-1 Solid1	Faces	82760
| | |	Edges	1116
| | +-1 Boundaries		
| | | +-1 DS End - Pressure Outlet	Faces	1856
| | | +-2 Fluid Wall	Faces	77178
| | | `-3 US End - Velocity Inlet	Faces	3726
| | `-2 Feature Curves		
| | `-1 Default Feature Curve	Edges	1116
| `-4 **Volume Mesh**	Cells	703634
| |	Interior Faces	3737927
| |	Vertices	2683724
| +-1 Finite Volume Regions		
| | `-1 Solid1	Cells	703634
| | |	Interior Faces	3737927
| | |	Vertices	2683724

| | `-1 Finite Volume Boundaries		
| | +-1 DS End - Pressure Outlet	Faces	1871
| | +-2 Fluid Wall	Faces	39576
| | `-3 US End - Velocity Inlet	Faces	3743
| `-2 Cell Sets		
+-18 Tables	Tables	0
+-19 Units	Preferred System	Systeme Internationale
+-20 Coordinate Systems		
| `-1 **Laboratory**		
| `-1 Local Coordinate Systems		
+-21 Field Functions		
+-22 Volume Shapes		
+-23 Update Events	Event Count	0
|	Event Names	
+-24 Data Set Functions	Data Directory	function_data
+-25 User Code		
+-26 Layouts		
| `-1 default		
+-27 Data Mappers		
+-28 Motions		
| `-1 **Stationary**		
+-29 Reference Frames		
| `-1 **Lab Reference Frame**		

Solution

Accumulated CPU Time over all processes (s)	15744.947999999975
Elapsed Time (s)	5248.187093999819
Iterations	1000

APPENDIX D

CRITERIA 2: VELOCITY DISTRIBUTION PLOTS